
**UNIVERSIDADE TÉCNICA DE LISBOA**

**INSTITUTO SUPERIOR TÉCNICO**

# Magnetoresistive biochips:

## Detection of biomolecular recognition and On-chip transport of magnetically labeled biomolecules

**Hugo Alexandre Teixeira Duarte Ferreira**

**(Licenciado)**

**Dissertação para a obtenção do Grau de Doutor em Física**

**Orientador: Doutor Paulo Jorge Peixeiro de Freitas**

**Co-Orientador: Doutor Joaquim Manuel Sampaio Cabral**

**Júri**

**Presidente: Reitor da Universidade Técnica de Lisboa**

**Vogais: Doutor Hubert Brückl**

**Doutor Leo Van Ijzendoorn**

**Doutor Joaquim Manuel Sampaio Cabral**

**Doutor Paulo Jorge Peixeiro de Freitas**

**Doutor João Pedro Estrela Rodrigues Conde**

**Doutor Luís Humberto Viseu Melo**

**Julho 2007**

O Sonho de Pigmaleão

Surgiste-me bela e misteriosa,
difusa como a luz de um dia enevoado.
Olhei-te de alto a baixo,
sustendo a respiração ...
prestando atenção a todos os pormenores ...
Vi que os outros também te procuravam,
pareciam perceber-te ...
e contigo trocavam palavras de amor.
Suspirei ...
Também eu queria admirar-te.
Moldar-te com os meus lábios.
Suavizar o traço dos teus olhos.
Colorir as maçãs do teu rosto.
Entender o teu sorriso.
Fazer-te também minha.
Tornar-te mais bela,
e depois ...

Fazes-me sonhar,
O Sonho de Pigmaleão.

# Abstract

In this thesis, magnetic field based chips were developed for the detection of biomolecular recognition using magnetic particles as biomolecular labels. Chips were designed and fabricated using different magnetoresistive sensors such as planar Hall sensors; spin valves and magnetic tunnel junctions, in order to assess their performance.

On the other hand, magnetic particles of different compositions and sizes, from micrometers down to nanometers, and with distinct surface functionalities were also investigated for their suitability as biomolecular labels.

In addition, on-chip metal line structures based on tapered and u-shape designs were developed and integrated with the sensors for transport and focusing of the magnetic labels. These structures were later used to promote the rate at which biomolecular recognition events happen at the chip surface, overcoming passive diffusion limits and enabling the detection of hybridization between complementary DNA strands in less than 5 minutes for low sample concentrations.

In early stages, the developed platform was used to demonstrate biomolecular recognition using several biological models, ranging from biotin-streptavidin binding to antibody-ligand recognition and DNA hybridization. Later on, starting from these proof-of-concept studies, biosensing systems started to be developed toward two applications: the diagnostics of cystic fibrosis, a genetic disease, and the detection of waterborne pathogens.

Finally, and effort was also done and is still on going towards the development of an integrated Lab-on-a-Chip system, for full sample treatment and analysis.



# Keywords

Magnetoresistive sensors; Magnetic Nanoparticles; Biochips; Biosensors; DNA-chips; Protein-Chips; Lab-on-a-Chip

## Resumo

Durante esta tese foram desenvolvidos biochips magnéticos para a detecção do reconhecimento biomolecular usando partículas magnéticas como marcadores. Os chips foram desenhados e fabricados usando diferentes sensores magnetoresistivos, tais como: sensores de efeito Hall planar, sensores válvula de spin e junções de efeito túnel magnéticas, de modo a analizar a suas características e performances.

Por outro lado, diversas partículas magnéticas de diferentes composições químicas, tamanhos da ordem dos nanómetros a micrómetros e com grupos funcionais distintos à superfície, foram investigadas como marcadores biomoleculares.

Em adição, estruturas metálicas baseadas em designs afunilados e em forma de U foram fabricadas on-chip e integradas com os transdutores para transportar e focar os marcadores magnéticos em regiões específicas do chip. Estas estruturas foram mais tarde usadas para promover a interacção entre as biomoléculas imobilizadas na superfície do chip e as em solução, permitindo a detecção de hibridação de cadeias de ADN em menos de 5 minutos para baixas concentrações de amostra.

A plataforma desenvolvida foi inicialmente utilizada para a demonstração da detecção do reconhecimento biomolecular usando diversos modelos biológicos, entre os quais: biotina-estreptavidina; anticorpo-ligando e hibridação de ADN. Posteriormente, partindo destas provas de conceito, começou-se a desenvolver o bio-sistema para duas aplicações particulares: o diagnóstico da doença genética fibrose quística e a detecção de microorganismos patogénicos na água para consumo.

Finalmente, foi feito um esforço, que ainda decorre presentemente, para desenvolver um sistema Lab-on-a-Chip para o tratamento da amostra e detecção integradas.



## Palavras-Chave

Sensores Magnetoresistivos; Nanopartículas Magnéticas; Biochips; Biosensores; Chips de DNA; Chips de Proteína; Lab-on-a-Chip

# Acknowledgments and Support

The work presented in this thesis is not the production of a person alone, but rather of a team of people with various skills and personalities. Of course none of the work would be possible without the infrastructural, human and financial support of several institutions and entities.

I start by thanking the financial support from the Portuguese Foundation of Science and Technology, which paid my doctoral tuition and helped me cover everyday life expenses, through the scholarship SFRH/5031/BD/2001. I also would like to thank Prof. Paulo Freitas and INESC – Microsystems and Nanotechnologies for financial support during these last 6 months, enabling me to put all the PhD work on paper.

I thank also INESC – MN for the human and infrastructural conditions offered for pursuing this work, and for being my home since the summer of 1999. Acknowledgments go also to Prof. Joaquim Sampaio Cabral and the Bioengineering Research Group at Instituto Superior Técnico that provided support related to some of the biochemistry work of this thesis. In addition, I would like to thank the Physics Department of IST that enabled me to choose the PhD curricula I wanted, which encompassed both nanotechnology and biotechnology courses, and regarded valuable for this work.

I would like to especially thank my supervisor, Prof. Paulo Freitas for accepting me in is research group and for investing and trusting in me for all these years that we have worked together. His role was just more than a scientific supervisor or teacher, but over the years he also taught me important issues on leadership, resource management and commitment. I hope, this liaison between us can endure and result in fruitful future endeavors together.

I thank also my co-supervisor, Prof. Joaquim Sampaio Cabral, for is support in everything I needed to pursue my PhD work and more.

I want to give a great thanks to my colleague and friend Dr. Daniel Graham, whose role in this work was pivotal. He was a mentor to me, and taught me plenty about life and biochemistry. Whilst I was the physical and engineering part of the work, he complemented it with chemistry and biology. Only an interdisciplinary team, and good working team, could accomplish what is written throughout these pages. I rightfully share the success of this work with him.

Next, I would like to thank all INESC-MN technicians, Fernando Silva, José Bernardo and Virgínia Soares, with whom I learned a great amount of things and who help me a lot with chip fabrication.

A special thanks to Sr. Faustino, who always cheerfully assembled our chips, helped in early measurement setups, suggested a number of useful things and was always supportive of our biochip work. He is rightfully also a member of the team.

Next I would like to acknowledge the various project and PhD students that have worked more directly with me in this work: Pedro Parracho, Verónica Martins, Nuno Feliciano, Cristina Carias, Daniel Vidal, Filipe Cardoso, Joana Loureiro, José Germano and Pedro Nunes. Their contribution was and still is of utmost importance and I hope their involvement will keep the project alive.

More or less directly other persons have contributed for this work, ranging from scientific support, processing, teaching, or simply discussion of ideas, these include INESC-MN directors, Prof. João Pedro Conde, Dr. Virginia Chu, and Prof. José Luís Martins, and all my colleagues at INESC-MN. To all I extend my thank you.

I just want to acknowledge in particular to Susana Cardoso and Ricardo Ferreira. Although this work was not their research focus, they always helped me when required, to them my sincere thanks.

Not least important, I would like to give a special thanks to Natércia and Cristina for the everyday help with secretary and administrative affairs.

This work and its context involved a great number of people and institutions, places and times, during the almost 7 years I have been at INESC-MN. A list of persons longer than these pages deserves to be included here, but for all of those that had not their names written here, bear in mind that they are not forgotten, and to all of them my greatest thanks.

Finally, I would like to thank my family and my closest friends, whose support was essential to survive the ups and downs of the PhD process.

A very special thanks is sent to my wife Catarina. Of all of the people involved she was the one that suffered and sacrificed the most. I haven't given her the time or the attention she surely deserved due to my involvement in work and studying. She was the one that embraced me when I was down, and the first who rejoiced my successes. Thank you for being my wife and for giving me the love I long waited. This work is also yours …

And thank you also for giving me my precious thing, our baby César … He is the most beautiful thing I have ever seen and is for sure my greatest and most successful "experiment" … in fact he as already helped me writing this thesis … ☺

# Motivation

In 1999, in the end of my 3rd year of studies in the Licenciatura in Technological Physics Engineering at Instituto Superior Técnico I did a summer internship at the Solid-State Technology Group of the Systems and Computer Engineering Institute (INESC), under the supervision of Prof. Paulo Freitas. It was amazing what you could do in the clean-room of the institute: having an idea, you could study its theoretical physical principles and then you could design it, and build-it at the microscale. It is something quite rewarding when you start from an idea or wish and turn it into something touchable, material and with substance. That was my first incursion into the Micro and Nanotechnologies.

In the following semester, now in the 4th year I took a course on Microtechnologies, again with Prof. Freitas. Besides learning the microprocessing techniques and equipments, a microdevice was supposed to be fabricated during the course. At the time, a researcher working at the Bioengineering Research Group under the supervision of Prof. Sampaio Cabral was put into contact with Prof. Freitas. Dr. Daniel Graham's idea was using magnetic particles, traditionally used in separation of biomolecules, as labels for the detection of biomolecular interaction. Prof. Freitas mentioned this idea in classes and purposed it as a project for fabricating a device during the course.

Immediately I grabbed and cherished the idea as if it were my own. I had always liked both physics and biology, as early as I remember in primary school, and this project fulfilled my passions in an interesting and appealing way. Furthermore, I recognized the potential within the idea and started projecting what this technology could help others and perhaps change the world. By the end of the Microtechnologies' course, together with a colleague I fabricated a device, which incorporated magnetic field sensors and on-chip current line structures to attract magnetic particles onto the sensing sites. I was yet able to focus the particles over the sensors before the end of the course but their detection remained to be attempted.

Later that summer, in 2000, did another summer internship at INESC, this time to work on the magnetic biosensor platform. At the time and with a Belgium student from

Interunivesitair Micro-Elektronica Centrum (IMEC), Roel-Wirix Speetjens, a new design for the current line structures was made and a new chip was fabricated. Curiously, this chip was the starting point for both our senior projects, which in the end resulted in a collaborative paper.

During that summer, I also participated in a Board of European Students of Technology (BEST) course for 2 weeks. This course was entitled Microsystems and Nanotechnology and was held at the Institut for Mikro- og Nanoteknologi (MIC) of the Danmarks Tekniske Universitet (DTU) of Denmark. That course further opened my mind for new ideas and possibilities, new technologies, the valorization of science and technology and entrepreneurship. Curiously I met two Portuguese students Filipa Fixe and Dina Gonçalves that later on became my colleagues at INESC, and presently, we are together undertaking a new endeavor. I had also the privilege to later on work in collaboration with Prof. Aric Menon's group at MIC, namely with Louise Ejsing, and later last year (2005) I had the opportunity to return to MIC, this time to give a lecture on my thesis work.

In late 2000 I started working on my senior thesis, at the time the project was like a curiosity, but the independent idea of Dr. Graham of magnetic detection of biomolecular recognition found the feasibility proof from a seminal paper from David Baselt working at the time at the Naval Research Laboratory (NRL) in the U.S. The 1998 paper sent by fax by Dr. Jo de Boeck from IMEC (Roel Wirix-Speetens) gave support to the preparation of the first research project proposition (a national project).

In the beginning of 2001, Dr. Graham joined Prof. Freitas group at INESC and we started working together until the end of 2004. By the summer of 2001, we had shown the detection and on-chip manipulation of magnetically-labeled enzymes, further we showed single magnetic microsphere detection. Our approach was distinct from the one of NRL in the sense that we used magnetic transport of biomolecules onto higher sensitivity sensors, and this promised an interesting biosensing platform.

In 2002, I officially started my PhD work at Solid-State Technology Group of INESC, now renamed INESC – Microsystems and Nanotechnologies (INESC-MN), and from there on I had the privilege to work with and learn with other people in the scope of a

national and an European projects. This latter one focused on the development of a magnetoresistive biosensing platform for cystic fibrosis diagnostics.

I would like to emphasize the work with did more directly with Prof. Sampaio Cabral, Prof. Luís Fonseca and Verónica Martins from the Bioengineering Research Group at IST (Verónica Martins is now a PhD student working on the application of the biochip platform to the detection of pathogens in water); Prof. Margarida Amaral and Dr. Luka Clarke from the Chemistry and Biochemistry Department of the Faculty of Sciences of the University of Lisbon; the group of Dr. Paul Galvin at the Tyndall Institute at Ireland, where I helped assembling the magnetic detection setup system; and Liesbet Lagae and Roel Wirix-Speetjens from IMEC, with to whom some sensor wafers were supplied, some biofunctionalization procedures were tried and finally, an electronics board was tested with our chip platform.

This thesis is the result of the work a number of people, which directly and indirectly, contributed to its success. In this biochip project, we had the contributions of a number of senior year project students, which like me found the appeal and potential of this work, namely Pedro Parracho, who started the work on microfluidics, Nuno Feliciano, who worked on magnetic sensing and magnetic label on-chip transport, Cristina Carias who focused her attention on planar Hall sensors and more recently, Daniel Vidal, who studied on-chip heat generation. Also, Filipe Cardoso, who worked on matrix based biochip architecture and fabrication, and finally Joana Loureiro, who restarted the interest on fluidic devices.

Finally, as it has always been my deepest desire of make meaning and give something back to society, I started developing the idea of making a company based on this work. Since the very start, I found that spintronic biochips could be a disruptive technology and that they could find better uses in the community rather than closed in a drawer of a lab.

The development of these biochips was a hard and quite sometimes down-turning quest. Nevertheless, its potential was and still is terribly inspiring and, overall, the work was fun. This thesis and the future to come is my contribution to change the world and hopefully turning it into a better place.

# Contents

# 1. Introduction

The future is being made now … Millions of men and women are contributing everyday to the advancement of science and technology … I hope I am contributing my share to the Human effort of going further beyond …

Last century has witnessed a dramatic and profound change in the world. The way of living changed more in 100 years than from the uprising of *Homo sapiens sapiens* 100,000 years ago.

Great advances in medicine enabled us to live better and longer and a deeper understanding of matter and energy enabled us to control and manipulate the world in means never thought possible by our ancestors.

The XX$^{th}$ century is the century of information technology. The Transistor, invented in the beginning of the 1950's (http://www.lucent.com/minds/transistor), is the rightful hallmark of this century. Advances in condensed matter physics and engineering have enabled the fabrication of integrated circuits, processors and computers. Further advances have reduced the size of the transistor elements and with that a continuous size miniaturization has been sustained until today. World has changed from a predominantly bucolic rural and bulky industrial and closed landscape into a fast-moving, mobile and knowledge-based globalized world.

The miniaturization has proceeded not only in a steady pace, as given by Moore's law (http://www.intel.com), but also it has moved into other fields of knowledge. Physics, Chemistry, and Biology are meeting at the nanoscale creating an interdisciplinary and high-potential field which promises to revolutionize the world: Nanotechnology, has prophesized by Richard Feynman in his "There's Plenty of Room at the Bottom" talk in the 1950's (http://www.zyvex.com/nanotech/feyman.html).

The end of last century witnessed one of the greatest achievements in Human history, the decoding of the Human Genome. Like the transistor was to the information

technology, the Human Genome Project (http://www.ornl.gov/sci/techresources/ Human_Genome) will stand as the hallmark for the life sciences era that will characterize the XXI$^{st}$ century. This era will start to uncover the potential of miniaturization and information technology in biological sciences and will further integrate advances in the nanotechnology field. This is where this thesis is positioned…

One of the most extraordinary new instruments developed for biological sciences is the microarray. This device enables large-scale parallel analysis of a number of analytes of interest. It has been mainly used as DNA microarrays or DNA chips (Ramsay, 1998) but is starting to be used also for proteins (Zhu *et al*., 2001) and other analytes.

These devices are comprised of a solid surface (typically a microscope glass slide) onto which are generally immobilized known biomolecules, called probes, on a matrix or array arrangement. Later on a sample solution containing the analytes of interest, called targets, is incubated with the biomolecular array. If probe and target biomolecules are complementary, they recognize each other and bind. Target molecules are then bound to the surface. Subsequently, recognized targets are detected. The detection of biomolecular recognition can be made using different strategies. Typically, in DNA arrays target molecules are labelled with a small fluorescent molecule, called fluorophore, and detection is done using a fluorescent camera or scanner. Figure 1.1 shows a schematic of DNA array system and an output example.

Whilst, DNA microarrays and chips are mainly being used in large-scale gene expression studies for research and recently for clinical diagnostics (http://www.roche-diagnostics.com/ products_services/amplichip_cyp450.html) a number of other systems make use of biomolecular recognition, like pregnancy and blood type testing.

Biomolecular recognition can then be understood as the interaction between biomolecules that show affinity towards each other or are complementary. This affinity translates in the formation of intermolecular forces of varying intensity, Van der Waals forces, salt bridges or hydrogen bonds (Voet *et al.*, 1999). Examples of biomolecular recognition include DNA hybridization, antibody-antigen recognition and general ligand-receptor binding.

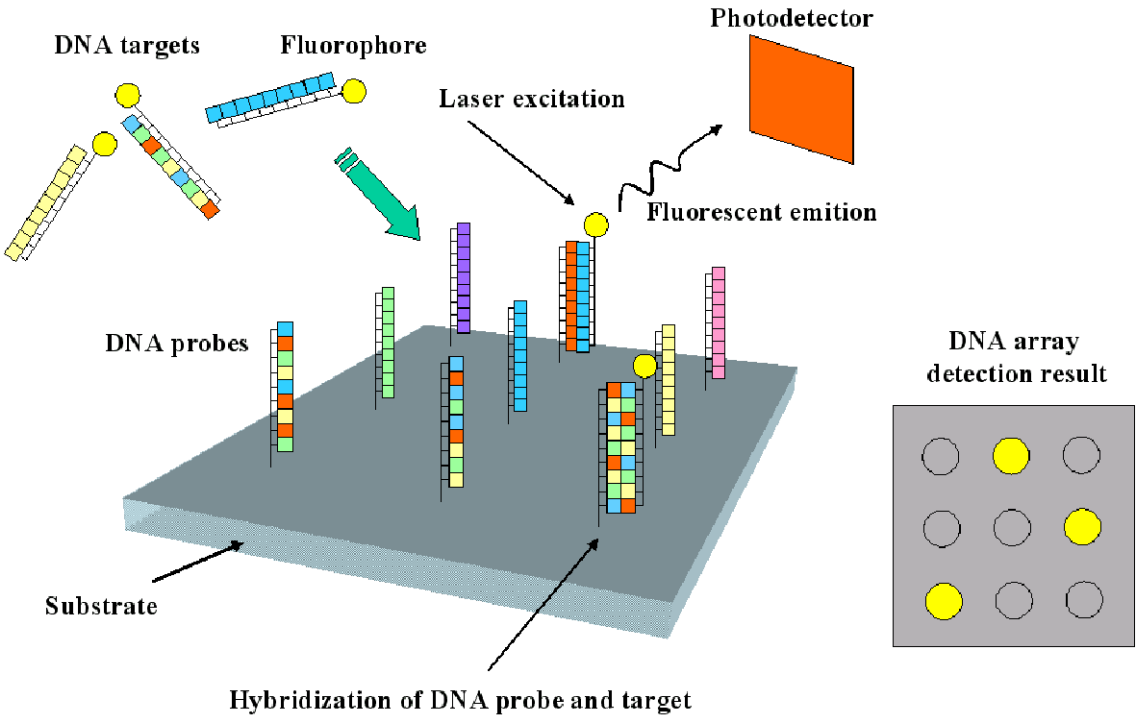


Fig. 1.1. DNA-chips or DNA microarrays are comprised of a substrate (usually glass slides) patterned with different DNA probes. These regions usually are circular spots of varying diameters (~50 to 100 μm or more) that contain millions of copies of the same DNA sequence. In these systems sample DNA targets are usually labeled with fluorophores and are incubated with the microarrays for several hours for hybridization to occur. DNA target and probe hybridization is detected by measuring the fluorescent emition of the labels with complex optical systems and photodetectors.

Consequently, assays based on biomolecular recognition are being utilized and becoming ever more important in areas such as healthcare, pharmaceuticals, environmental analysis, detection of biological warfare agents and in broad technological applications.

The detection of biomolecular recognition can be realized in a number of ways. Generally, these methods involve the labelling of biomolecules such that a distinct physical property can be measured in the event of biomolecular recognition. In the last century biomolecules were labelled with radioactive tags, but due to their hazard effects on health and requirements of relatively expensive specialized systems for readout, they started to be replaced by colorimetric and fluorescent markers.

Today, colorimetric and fluorescent markers are the standards. These can be small chemical moieties, biomolecules, enzymes, particles or a combination of these several elements.

One of the most common colorimetric methods is by use of an enzyme. These systems use enzyme-labelled biomolecules (for instance antibodies) to produce a colored compound that indicates biomolecular recognition. The widely used Enzyme-Linked Immunosorbent Assay (ELISA) systems work exactly this way.

An example is the pregnancy test: membrane functionalized antibodies against the Human Chorionic Gonadotropin (HCG) recognize the pregnancy hormone on the urine sample of a pregnant woman; later on enzyme-labeled antibodies recognize the hormone bound to the first antibodies; finally a substrate compound is catalyzed by the enzyme to produce a dye that can be seen (fig. 1.2).

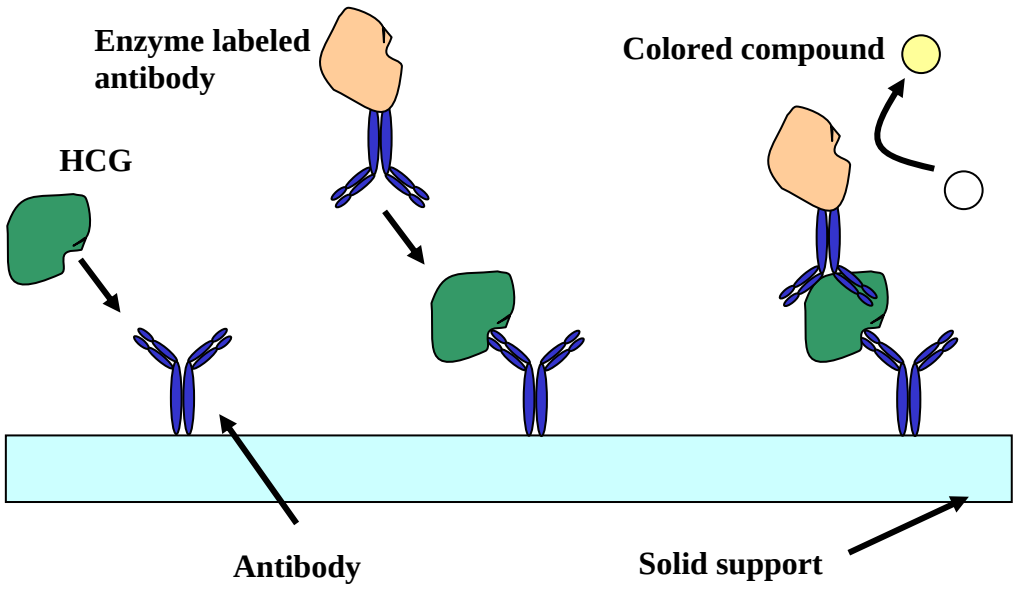


Fig. 1.2. Schematic of an ELISA-based pregnancy test. A solid support with antibodies against HCG recognizes the hormone in urine. Later on a secondary antibody labeled with an enzyme recognizes the support-bound hormone. Finally, the enzymes catalyses a substrate producing a colored compound that indicates the presence of HCG.

ELISA systems and other enzyme label based techniques offer high sensitivity and enable multiplex analysis. Nevertheless, they require additional reagents (the substrate to produce the colored compound), and the enzyme activity is sensitive to changes in

the environment, like temperature, pH, inhibitors, that limit the range of use of the method (Peruski, and Peruski, 2003).

Fluorescent label methods have been gaining importance, namely when used in Real-Time Polymerase Chain Reaction (RT-PCR) systems (Cirino *et al*., 2004) and with DNA chips and microarrays (Ramsay, 1998; Blohm and Guiseppi-Elie, 2001). Fluorescent labels are also very sensitive and enable multiplexing but often require quite expensive instrumentation. Furthermore, fluorescent labels photo-bleach when exposed to light. These factors limit the further generalized use of these systems and the retesting of the assays.

New approaches are underway though that show great potential. Some of these involve an effort to integrate standard biomolecular labelling methods with on-chip detection, like the use of microfabricated optoelectronic sensors to detect fluorescent labels (Fixe, 2005) or the use of optical waveguides for detection of dye or fluorescent molecules.

Other methods are being developed that do not require labelling. These labeless systems measure direct physical properties of the biomolecules, like charge and mass. In the first case electrochemical and potentiometric sensors are used to measure the changes in the oxidation state of biomolecules. More recently, capacitors, diodes and transistors (Gonçalves *et al*., in press), and nanowires (Patolsky and Lieber, 2005) are being used to measure directly the charge of the molecule. Here, biomolecular recognition is usually translated in a change of electrical potential or in current output of the device. The systems based on measuring charge are thus limited to charged molecules, and often in electrochemical assays additional chemical moieties are used to amplify biomolecular recognition signals.

The systems based on mass change detection are generally mechanical systems, like quartz crystal microbalances (QCM), and MicroElectroMechanical Systems (MEMS), such as cantilevers (Fritz *et al.,* 2000) and microbridges (Adrega *et al*., in press) or even Atomic Force Microscopy (AFM) tips. The effect of an additional mass upon biomolecular recognition is usually translated into a change in resonance frequency or a structural deflection of the device. These devices are more suited for gas/aerosol applications, as in liquid the higher damping results in a much limited sensitivity.

Nevertheless, AFM tips have been used for measuring biomolecular interaction forces in liquid (Florin *et al*., 1994; Moy *et al*., 1994).

Surface Acoustic Waves (SAWs) are also being used in biosensing applications. In these systems, a change of mass loading of the sensor results in a change of the propagation velocity of acoustic shear waves generated at the device. These systems are sensitive and enable real-time kinetic analysis (http://www.caesar.de).

Another interesting labeless technique is the Surface Plasmon Resonance (SPR). This is an optical method, where changes of the refractive index of a surface upon binding of complementary biomolecules to the probe biomolecules on the surface. It is also claimed as a sensitive technique enabling real-time detection (http://www.xantec.com).

Labeless systems show a great potential, as they are simpler and can, in principle, provide faster responses. Nevertheless, a great effort is being made worldwide into developing particle-based systems for the detection of biomolecular recognition. Although, requiring the extra-labelling step, these labels are showing improved sensitivities and stability in comparison with other methods. Furthermore, they are showing additional functionalities, such as biomolecular coding or transport and manipulation, as will be seen later on (Katz, and Willner, 2004).

Particles of micro and nanometer dimensions are being synthesized in a variety of materials, including metal, semiconducting and insulating particles. These are further functionalized with a variety of biomolecules for use in biomolecular recognition assays (Tansil, and Gao, 2006).

The use of gold nanoparticles enables a variety of detection methods to be used, such as optical, electrical, or electrochemical, or as amplifying systems for mass-change based methods such as QCM.

Quantum Dots (QDs), which are nanometer sized semiconducting particles, can be tuned to emit in a variety of wavelengths, and are starting to replace conventional fluorescent labels due to the higher stability and versatility. Furthermore they can be used in combination with electrochemical methods.

Silica nanoparticles, on its turn, are being used to encapsulate dyes or redox active compounds; this confers stability and a suitable surface for biomolecular functionalization. Detection of these labels relies essentially on optical and electrochemical methods.

Among the metal particles, there is a class of materials that is finding novel and interesting applications. These particles are magnetic in nature, which provides a means of control and manipulation of biomolecules at a distance by use of magnetic field gradients (Gould, 2004).

Magnetic particle have been traditionally used in biological applications for biomolecular and cell separation, has contrast agents in Nuclear Magnetic Resonance (NMR) imaging and in hyperthermia studies for cancer treatment (Hafeli, 1997). More recently, they are being studied for use in drug and radionucleotide delivery; magnetofection (gene delivery); blood detoxification (Gould, 2004) and also in the detection of biomolecular recognition.

Magnetic labels offer a number of advantages over colorimetric and fluorescent labels: they are more stable over a broad range of experimental conditions (in temperature and pH) and more stable over time (do not photo-bleach); they enable more sensitive measurements as biological samples usually do not contain magnetic material, but often show color or a fluorescent background; they can be used to discriminate between specifically and unspecifically bound biomolecules through the application of a magnetic field (Lee *et al.*, 2000); they can be transported and manipulated on-chip (Gijs, 2004; Yellen *et al*., 2005); and, finally, they can be readily detected using magnetic field sensors.

The idea behind magnetic biosensors and biochips is then to use magnetic labels instead of conventional colorimetric and fluorescent ones: biomolecular recognition between target and probe biomolecules is detected by a magnetic field transducer that senses the magnetic labels bound to the target-probe complexes.

Since magnetic biosensors were first proposed as a simple and sensitive biomolecular recognition detection technique, by making use of coils and ferrofluids (Kriz *et al.*, 1996, 1998), different assay types with different magnetic sensors and labels have been proposed and developed. Basically, two types of assays can be considered with respect to where biomolecular recognition is detected: the volume detection and the surface detection assays (fig. 1.3).

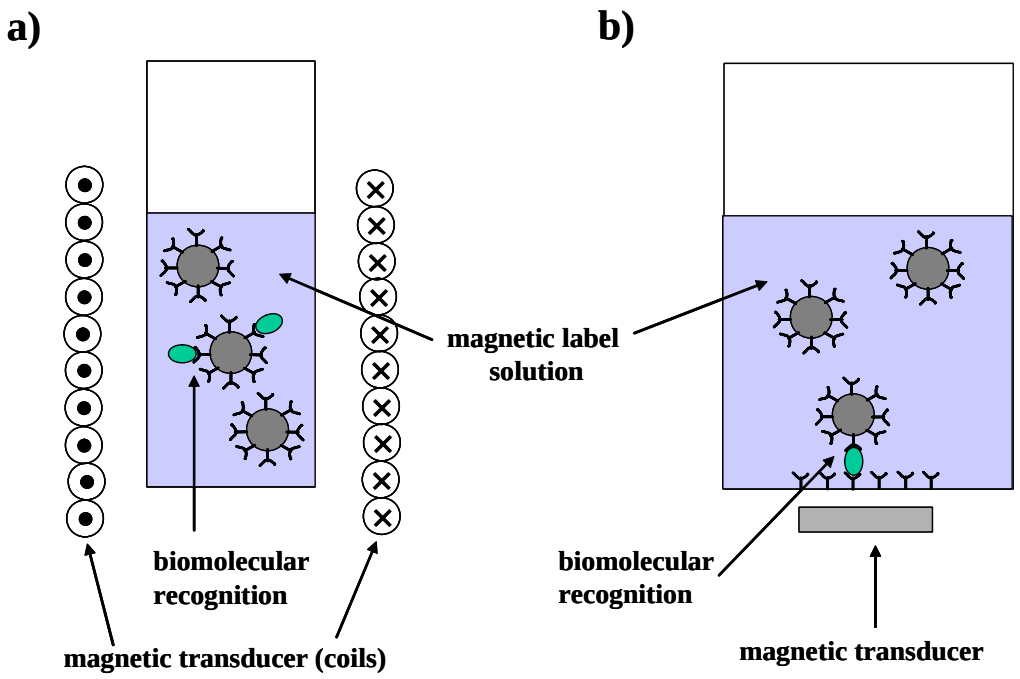


Fig. 1.3. Two types of assays for biomolecular recognition using magnetic labels. a) In volume detection assays biomolecular recognition is detect by measuring the magnetic properties of a bulk solution comprised of magnetic labels functionalized with probe molecules that recognize particular targets. b) In surface detection assays magnetic labels bound to a surface through biomolecular recognition of probe and target molecules are detected by a nearby magnetic transducer.

In volume detection assays (Fig. 1.3a) biomolecular recognition is detected in the bulk of a solution comprised of a suspension of magnetic particles functionalized with the probe molecules of interest. Upon binding of the target analytes to the probes, the hydrodynamic radius of the magnetic particles increases causing a change in their magnetic relaxation times. As a consequence, a shift in the frequency-dependent magnetic susceptibility is observed (Connolly, and St. Pierre, 2001; Astalan *et al.*, 2004; Chung *et al.*, 2004). In these assays, measurement devices such as AC magnetic

susceptometers, that measure changes in both the inductance and resistance of an induction coil, are used.

In surface detection assays (Fig. 1.3b), on the other hand, probe biomolecules are immobilized on a solid phase. In these assays target biomolecules move from the bulk solution to the solid phase surface where they are recognized by the probes. Magnetic carriers bound to the target-probe complexes are then immobilized to the surface. In this case, the magnetic relaxation processes are distinct from when the carriers are free in solution (this will be discussed later on). This difference in relaxation times is used on surface detection assays based on Super Quantum Interfering Devices (SQUIDs) (Kötitz *et al*., 1997; Chemla *et al*., 2000).

Nevertheless, the generality of surface detection assays, which correspond to the majority of bio-systems being developed, do not rely on measuring changes in the magnetic relaxation of carriers but simply uses the fact that the magnetic carriers create a magnetic stray field that can be sensed by a transducer.

Several transducers have been used so far, which vary both on physical mechanisms, geometries, properties and applications: coils (Richardson *et al*., 2001a,b); giant magnetoimpedance (GMI) sensors (Kurlyandskaya *et al*., 2003; Kurlyandskaya, and Levit, 2005; Chiriac *et al*., 2005); SQUID magnetometers (Enpuku *et al*., 1999; Katsura *et al*., 2001); complementary metal-oxide semiconductor (CMOS) Hall effect sensors (Besse *et al*., 2002); quantum-well Hall effect devices (Landry *et al*., 2004; Sandhu *et al*., 2004; Sandhu, and Handa, 2005); and finally, magnetoresistive sensors (Graham *et al*., 2004; Freitas *et al*., 2004), which are the focus of this thesis.

Further recently, it was observed that simple magnetic multilayer structures can convert energy from direct current into high-frequency magnetic rotations (Kiselev *et al*., 2003). This effect may result in new devices including microwave sources and resonators, and has been already suggested the study of device interaction with magnetic labels (Kurlyandskaya, and Levit, 2005).

Coils and giant magnetoimpedance devices assess the presence of magnetic markers by changes in the resonance frequency and in the impedance of the sensing elements,

respectively. These devices are the simplest to fabricate but their sensitivity is considerably smaller than other magnetic field sensor technologies.

SQUIDs quantify the magnetic flux created by the labels and are the most sensitive of the magnetic field sensors developed to date; they are able to sense fields in the order of 100 fT ($10^{-13}$ T). Nevertheless, for high-transition temperature SQUID devices, they require liquid nitrogen (77K) and vacuum to operate. As a consequence of the necessary apparatus, the separation between the sensor and the sample is usually of tens of micrometers, which results in a smaller effective sensitivity of the device.

Hall effect devices do not show these constraints; they measure a voltage drop built in a transversal direction to the sense current due to the Lorentz force induced by the magnetic stray fields originated from the markers. CMOS-based sensor fabrication is relatively straightforward and CMOS amplification circuitry can be easily integrated with the sensing component. Quantum-well based Hall devices although show a higher sensitivity than CMOS based ones, their fabrication is also more complex, and is comparable to more advanced spintronic devices.

Briefly, magnetoresistive sensors are electrical resistors whose resistance value varies with an applied magnetic field (Prinz, 1998), and as so they can be measured using a simple 2-point probe measurement scheme. In addition, they operate at room temperature and can be made to have sensitivities down to the pT ($10^{-12}$ T). Furthermore, there is a firmly established technology, as magnetoresistive sensors are used in magnetic reading heads, in several sensing applications (Freitas *et al*., 2000) and most recently on magnetic random access memories (MRAM) and novel magnetoelectronic devices, including biosensors (Freitas *et al*., 2006).

Magnetoelectronic sensors enable a direct transduction of biomolecular recognition events into electrical signals, which is a considerable advantage over the systems that use colorimetric or fluorescent labels. These optical systems, in their simplest form, provide a qualitative result (yes or no), or a semi-quantitative answer based on pre-defined scales, where interpretation most often depends on the person analyzing the test. On the other hand, more complex systems that often include multiplex testing require bench-top, complex and expensive optical instrumentation coupled with electrical

transduction mechanisms and specialized data-analysis software. Furthermore, these latter systems are usually not portable and cannot be used at the point-of-care.

This thesis will then focus on the efforts made in the development of a spintronic platform for the detection of biomolecular recognition over the past years. These are the result of a PhD work done at INESC-Microsystems and Nanotechnologies and at the Bioengineering Research Group of Instituto Superior Técnico.

Furthermore, throughout the text and as opportune, the latest developments on spintronic biosensors and biochips realized worldwide will be reviewed (see also Freitas, and Ferreira, *in press*).

The collective efforts of a number of scientists, women and men, are showing that these devices have the potential to become highly specific and sensitive platforms for low-cost, high-throughput and portable bioassays.

The thesis is organized in chapters. After the introduction the second chapter is devoted to the physical background of the system and issues such as magnetoresistive sensors, magnetic labels, microfluidics and magnetic transport systems will be discussed. Chapter 3, on the other hand, focuses on the biochemical background which comprises surface biochemistry, magnetic labeling and the several biomolecular recognition models studied. Chapter 4 discusses the design, fabrication and characterization of magnetoresistive chips and the detection schemes used are referred to in chapter 5. Chapter 6 focuses the experimental setups and finally, on chapter 7 results on the detection of biomolecular recognition will be presented. Chapter 8, will draw out some conclusions and point some future perspectives.

# 2. Physical Background

In this chapter the physical components of spintronic biochip platforms are discussed. These comprise magnetoresistive sensors, magnetic labels, and transport systems that use microfluidic devices and magnetic field generating microfabricated elements.

## 2.1 Magnetoresistive Sensors

### 2.1.1 Overview

Magnetoresistance is the phenomenon in which the electrical resistance of a metal or semiconductor increases or decreases in response to a magnetic field. This effect can have several flavors: normal or ordinary magnetoresistance, anisotropic magnetoresistance (AMR); giant magnetoresistance (GMR), tunneling magnetoresistance (TMR); colossal magnetoresistance (CMR); ballistic magnetoresistance (BMR) and extraordinary magnetoresistance (EMR) (Solin, 2004).

The said “normal” magnetoresistance is the result of Lorentz forces and is negligible in metals but is small to moderate in semiconductors. This is the origin of the Hall effect: under a magnetic field applied perpendicularly to the current, a voltage drop results across a device. This is due to the accumulation of charge carriers at one side and the lack of carriers on the opposite side of the device. This voltage drop is associated with a resistance that is named Hall resistance.

The anisotropic magnetoresistance (AMR), also called spontaneous resistance anisotropy, is a property of ferromagnetic materials. This effect results from spin-orbit interactions, as electron spins interact differently with d-band electrons of the ferromagnet. Thus, the resistance of the device is highest when the current is parallel to the magnetization of the material and is lowest when they are perpendicular.

The giant magnetoresistance (GMR), on the other hand, results from the spin-dependent transmission of conduction electrons between coupled magnetic layers through a non-

magnetic spacer layer. This effect depends on the relative orientation between the magnetic layers and the resistance of the device is maximum when the magnetic layers are anti-parallel and is minimum when the magnetizations are parallel.

Tunneling magnetoresistance (TMR) is in a sense similar structurally to the GMR, but instead of having a nonmagnetic layer it has an insulator separating the ferromagnetic layers. The insulator layer is quite thin (a couple of atomic layers) such that electrons tunnel through the barrier. In this case, the effect results from the spin-dependent tunneling of the electrons between the magnetic layers. In the same way, as in GMR, the resistance of the device is maximum when the magnetizations of the ferromagnetic layers are antiparallel and is minimum when in the parallel state.

On the other hand, colossal magnetoresistance (CMR) involves different materials. When a magnetic field is applied to insulating manganese oxide crystals, called manganites, they change from non-magnetic and insulating to ferromagnetic and metallic. In this case, the magnetic field then reduces the resistance of the device. This effect generally occurs only at temperatures below 150 K, and for magnetic fields of several Tesla.

Ballistic magnetoresistance (BMR) is observed when two metallic and magnetic materials are joined by a nanocontact. Here, electrons travel across the contact in the ballistic regime, and the resistance of the device is highest when the magnetizations are antiparallel and is lowest when are parallel, just like GMR and TMR effects. Nevertheless, there is some controversy of the validity of the presented experimental results.

Finally, the extraordinary magnetoresistance, like the ordinary magnetoresistance is produced in a structure that does not include magnetic materials. This effect depends on the detailed geometry of the device made out of conductive metal and semiconductor. In the absence of a magnetic field current flows through the semiconductor and through a metal shunt within the semiconductor; in this case the resistance of the device is minimum. When a magnetic field is applied perpendicular to the device, then charge builds up across the device, just like in the Hall effect. These charges create an electric field that results in the flow of current arrow the metal shunt embedded in the

semiconductor. In fact, due to the geometry of the device, the current can be confined between the metal shunt and the surface of the semiconducting material, resulting in high resistances.

The different magnetoresistance effects were presented in order of increasing resistance change with an applied magnetic field. In spite of this only some effects are being used in sensitive and biological applications so far.

Hall sensors, CMR, BMR, and EMR devices usually require high magnetic fields. In addition, CMR transducers operate only at 150 K. BMR and EMR sensors further require quite challenging methods of fabrication, as they require nanoscale processing; furthermore, their technological development is still in its infancy.

On the other hand AMR, GMR and TMR sensors, operate at room temperature, detect small magnetic fields and have good overall performances. In fact, AMR devices (the first to be discovered) were the first to be used in read-heads for magnetic storage media, replacing the less sensitive inductive coils. Later on, the discovery of GMR effect and the fabrication of sensors, lead to the replacement of AMR devices in tape and hard-disk applications. More recently, with advances in processing TMR devices have been made available and these are already replacing the GMR transducers.

So far, only AMR, GMR and TMR devices were applied in the detection of biomolecular recognition. The corresponding effects will be discussed in more detail below.

### 2.1.2 Anisotropic Magnetoresistance

As mentioned above, the anisotropic or spontaneous magnetoresistance, discovered in 1857 by Lord Kelvin, results from spin-orbit interaction in ferromagnetic materials such as Ni, Fe, Co, and their alloys. In these transition metals, the conduction electrons are 4s and due to the high density of states of 3d orbitals, there is significant sd scattering. Since individual d orbitals are not spherical as s orbitals, then the scattering and thus the

resistance of the device is dependent upon the angle between the current direction and the magnetization of the material (fig. 2.1).

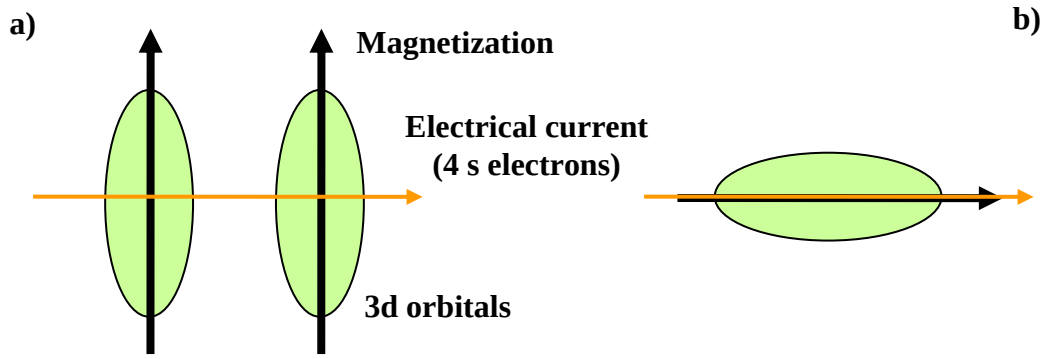


Fig. 2.1. Schematic of spin-orbit interaction, responsible for the anisotropic magnetoresistive effect in ferromagnetic materials and their alloys. a) current perpendicular to the magnetization (minimum resistance state); b) current parallel to the magnetization (maximum resistance state).

Two types of devices can be realized using the AMR effect: one where the voltage drop is measured in a parallel arrangement with respect to the current direction and the other where the voltage drop is measured perpendicularly to the direction of the current (fig. 2.2).

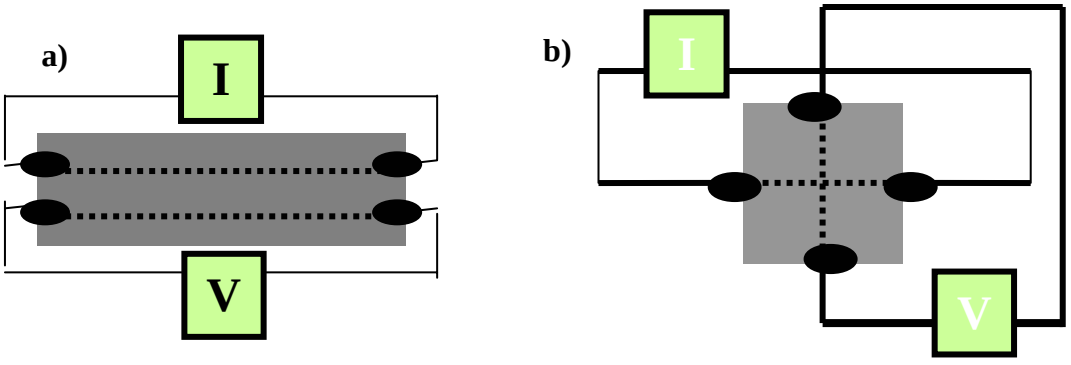


Fig. 2.2. Schematic of the two types of devices based on the AMR effect: the voltage drop is measured in an arrangement that is (a) parallel or (b) perpendicular to the current direction.

Considering the Ohm's law and not taking into account the Hall effect, which is negligible in metals and for small fields, comes (see Carias, 2005):

$$\rho(\theta) = \rho_{\perp} + (\rho_{\parallel} - \rho_{\perp})\cos^2\theta \qquad (1)$$

$$\rho(\theta) = \frac{1}{2}\left(\rho_{\parallel} - \rho_{\perp}\right)\sin 2\theta \qquad (2)$$

Where ρ is the resistivity of the device, θ is the angle between the direction of the current and the magnetization of the material, and the subscripts ⊥ and || represent the directions perpendicular and parallel to the magnetization, respectively.

Equation (1) refers to the situation, where the voltage drop is measured in the direction of the current and is named ordinary AMR. On the other hand, equation (2) refers to the situation where the voltage drop is measured perpendicularly to the direction of current and is named as the planar Hall effect, as the measurement setup is similar to the one used to measure the Hall effect above mentioned. These two measurement possibilities result in different sensor transfer curves, and whilst in the ordinary AMR the device response to field is quadratic in the planar Hall effect the response is linear around zero applied field (see fig. 2.3).

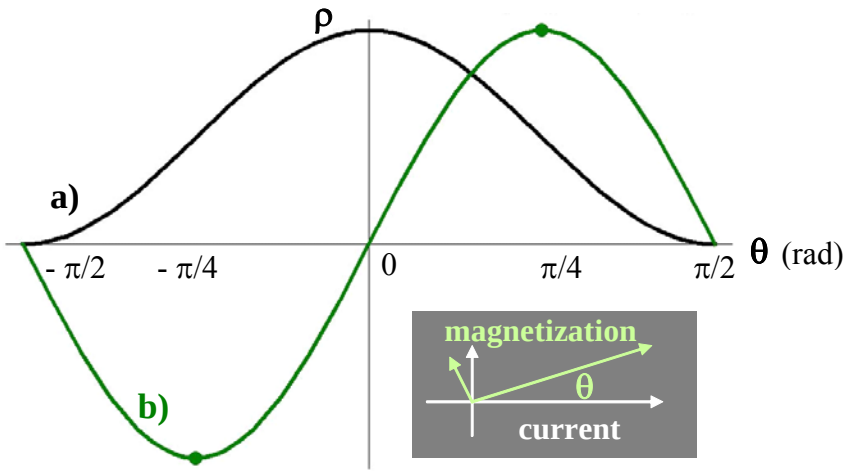


Fig. 2.3. Drawings of transfer curves for the a) ordinary AMR device and for the b) planar Hall effect transducer.

Finally, the change in resistance of the device can be translated by the AMR ratio which is defined as:

$$AMR\ ratio = 3\frac{\rho_{\parallel} - \rho_{\perp}}{\rho_{\parallel} + 2\rho_{\perp}} \qquad (3)$$

Typically the AMR ratio is between 1 to 2% for ferromagnetic alloys.

### 2.1.3 Giant Magnetoresistance

In 1986 it was observed that two magnetic layers separated by a nonmagnetic spacer layer could display a spontaneous antiparallel alignment of the magnetizations at zero field, the so called antiferromagnetic interlayer exchange coupling (Grünberg *et al.*, 1986).

Directly after this discovery it was shown that a large change in resistance could occur when the antiparallel alignment is changed to parallel (and vice-versa) with an externally applied field. The first experiments used Fe/Cr multilayers (Baibich *et al.*, 1988) and Fe/Cr/Fe trilayers (Binasch *et al.*, 1989), and unipolar transfer curves were obtained (fig. 2.4a). This change in resistance was much larger than can be expected for "normal" magnetoresistance, caused by Lorentz forces, or for the anisotropic magnetoresistance effect, caused by spin-orbit interactions. Therefore, this effect became known as Giant Magnetoresistance (GMR).

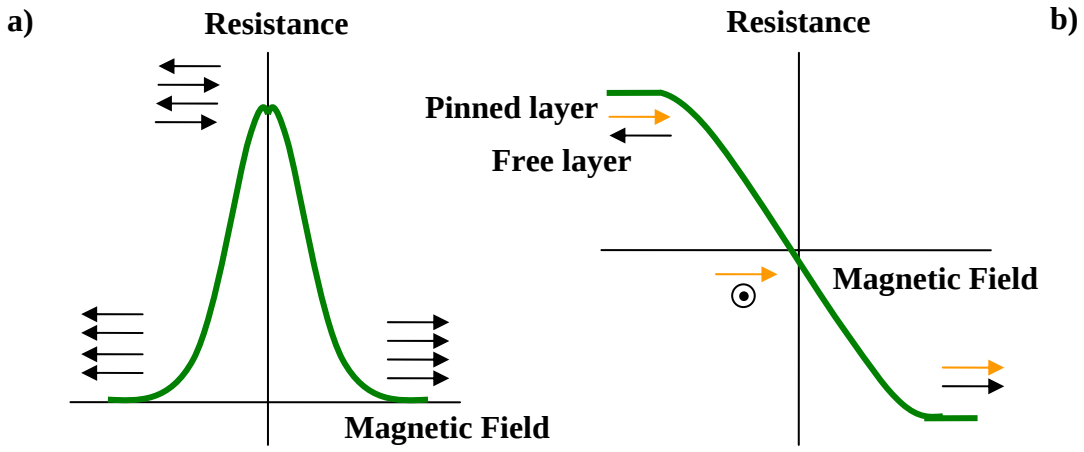


Fig. 2.4. Schematic of GMR transfer curves. a) Ordinary GMR sensor comprised of multilayers of ferromagnetic and non-magnetic materials and b) Spin valve sensor comprised of a pinned ferromagnetic, a free ferromagnetic and a non-magnetic layers. Magnetization directions of neighboring ferromagnetic layers are shown for each sensor type. At zero applied magnetic field the magnetization of the free layer is perpendicular to the pinned layer in the case of the spin valve transducer.

Apart from the antiferromagnetic interlayer exchange coupling the antiparallel alignment of the magnetizations of the ferromagnetic layers can also be achieved by use of hysteresis effects. In this case, a magnetic layer magnetization is pinned in one direction due to exchange bias effects due to an antiferromagnet, whereas other magnetic layers' magnetization is free to rotate when an external field is applied (Bürgler, and Grünberg, 2003). This is the principle of the spin valve sensor, first discovered in 1991 (Dieny *et al*., 1991) and developed and tested in 1994 (Heim *et al*., 1994). The core of these sensors is a trilayer of ferromagnetic/ non-magnetic/ ferromagnetic metal layers and shows a bipolar response, contrary to typical GMR multilayers (Fig. 2.4b).

The GMR effect, both in spin valves and multilayers, has its origins in the spin-dependent transmission of conduction electrons between the coupled magnetic layers through the nonmagnetic spacer, which then depends on the relative orientation of the moments of the magnetic layers as mentioned above.

The electrical transport in the layers can be divided in two spin-channels, currents resulting from spin-up and spin-down electrons. Electrons of distinct spins have different scattering probabilities at the interfaces and in the bulk of the layers, due to a spin-dependent potential landscape and differences in the density of states at the Fermi-level.

In general, an electron will have a higher scattering probability when its spin direction is opposite to the local magnetization direction (Fig. 2.5). When both magnetic layers have parallel moments, the spin-down electrons will have a higher scattering probability then the spin-up electrons. This spin-up channel acts as a shunting current, which lowers the resistivity of the complete stack of layers considerably as compared to the situation when the moments are antiparallel (Fig. 2.5a). In this latter case both spin-up and spin-down electrons will have a high scattering probability in one magnetic layer and a low scattering probability in the other (Fig. 2.5b).

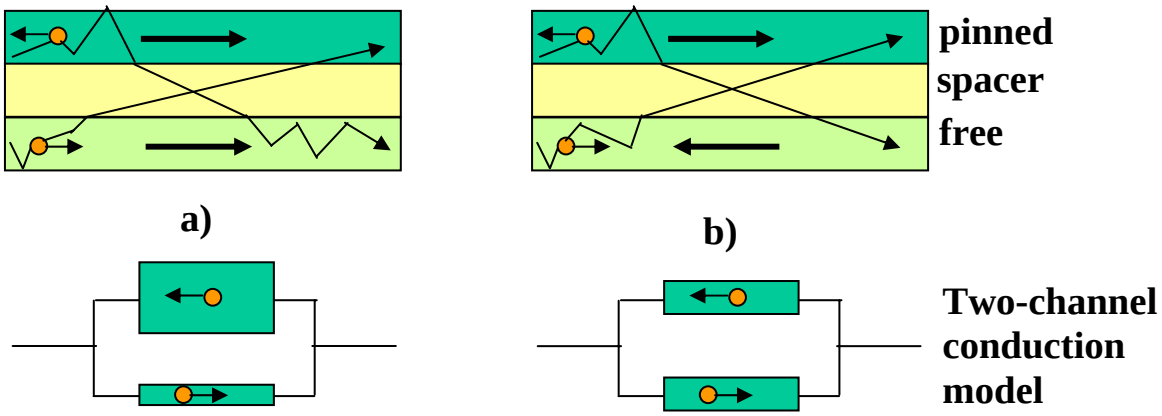


Fig. 2.5. Schematic drawing of the current-in-plane GMR effect in two magnetic layers separated by a nonmagnetic spacer layer with a) parallel and b) antiparallel magnetizations. The electrical transport in the layers can be divided in two spin-channels, illustrated as two electrons with different spin direction moving from the left to the right in the layers. Electrons with their spin opposite to the local magnetization direction experience more resistance than electrons with their spin parallel to the magnetization. In case of parallel magnetizations one current channel acts a shunting current. Also shown parallel resistor equivalent.

The relative change in resistance, the GMR ratio, or simply MR ratio, is usually defined as:

$$GMR\ ratio = \frac{R_{AP} - R_P}{R_P} \tag{4}$$

Where $R_{AP}$ and $R_P$, respectively are, the electrical resistances of the stack of layers with antiparallel and parallel magnetization states.

GMR ratio values depend on temperature and on the number of multilayers. As such, multilayers have show GMR ratios of up to 50% at room temperature, whilst spin valves typically show resistance changes of 6 to 8%, but can fabricated to hold 15 to 20% by introducing nano-oxide layers at the ferromagnet interfaces, which improve electron scattering (Bürgler, and Grünberg, 2003; Freitas *et al.*, 2006).

Furthermore, the GMR effect depends on whether the current is in plane of the device (current in plane, CIP, geometry), like the described AMR sensors (fig. 2.3) and spin valve (fig. 2.5), or the current is perpendicular to the device (CPP geometry, current perpendicular to plane).

### 2.1.4 Tunneling Magnetoresistance

The tunneling magnetoresistance (TMR) effect depends not on spin-depend scattering like GMR sensors but on spin-dependent tunneling of electrons across a barrier. Further, the CPP geometry is always used. The typical structure of a TMR based device consists of two ferromagnetic layers separated by an insulating or semiconducting barrier, although so far greater developments have been achieved with insulating oxide materials (fig. 2.6).

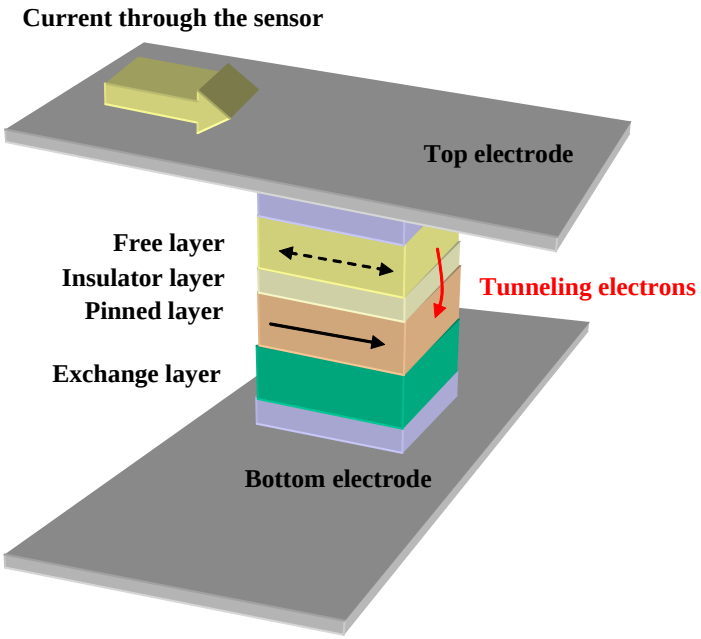


Fig. 2.6. Schematic of a magnetic tunnel junction sensor.

When a voltage is applied across the magnetic tunnel junction (MTJ) stack a quantum mechanical tunneling current flows across the barrier. This current is related to the overlap of the exponentially decaying wave functions inside the barrier, which implies that barrier thickness can not be larger than 1 to 2 nm, for the effect to be relevant.

Further the magnitude of the effect is dependent upon the magnetic polarization of the ferromagnetic layers. Ferromagnetic transition metals like Ni, Fe, Co and their alloys have distinct density of states for spin-up and spin-down 3d orbitals at the Fermi level, due to unpaired electrons. Magnetic polarization P is then defined as:

$$P = \frac{N^{\uparrow} - N^{\downarrow}}{N^{\uparrow} + N^{\downarrow}} \tag{5}$$

Where $N^{\uparrow}$ and $N^{\downarrow}$ are the number of states in the spin-up and spin-down 3d bands of the metal, respectively. Typical polarization values for transition metal based devices are around 50%. Half-metals on the other hand can show polarizations close to 100%, but usually require lower temperature operation and still require non-standard fabrication techniques.

The tunneling is then also dependent on the relative orientations of the magnetizations on both sides of the barrier, and like the GMR case, MTJ devices show a higher resistance in the antiparallel alignment than in the parallel (fig. 2.7).

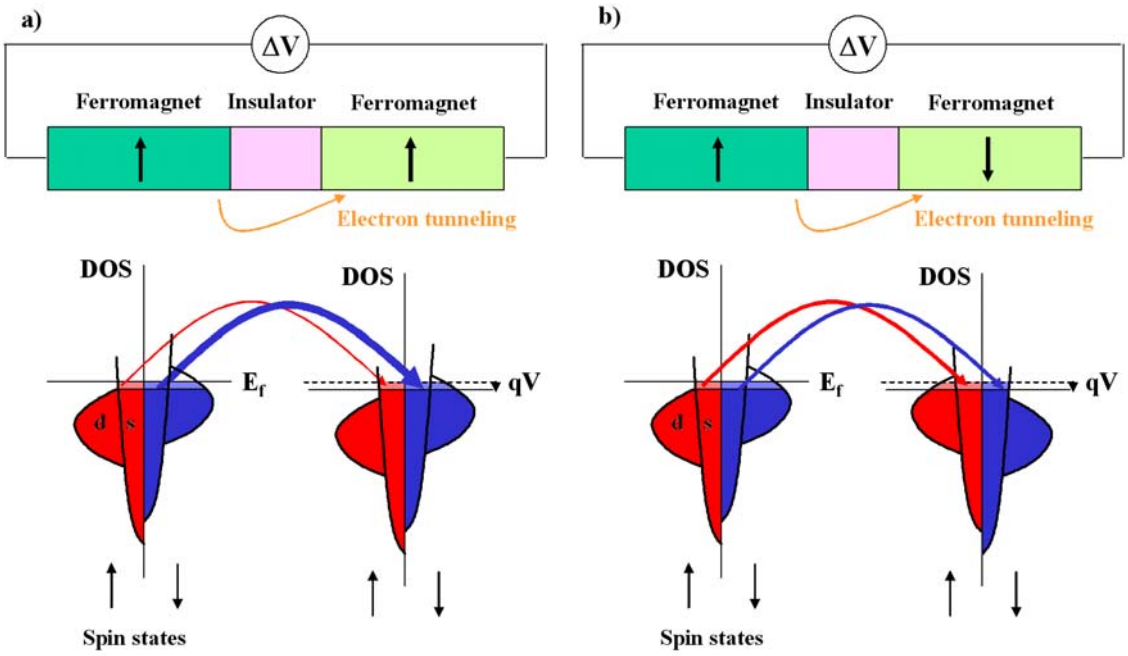


Fig. 2.7. Schematic of spin dependent tunneling effect, representing ferromagnetic layers with the magnetization directions and the corresponding density of states (DOS) diagram for parallel a) and antiparallel magnetizations b). $E_f$ is the Fermi Energy, q the electron charge and V the voltage applied across the insulator layer (adapted from Bürgler and Grünberg, 2003).

The TMR ratio is then defined as in equation (6) for GMR devices, but a relation is also found relating to the polarization of the top ($P_T$) and bottom ($P_B$) magnetic metal electrodes:

$$TMR\ ratio = \frac{R_{AP} - R_P}{R_P} = \frac{2P_T P_B}{1 - P_T P_B} \qquad (6)$$

Using AlOx barriers maximum TMR ratios between 50 and 70% were obtained, while, recently using MgO barriers record TMR ratios of above 200% were achieved at room temperature.

Tunneling magnetoresistance was first measured by in 1975 (Jullière, 1975) but interest only renewed in 1995 by the discovery of TMR at room temperature (Moodera *et al.*, 1995). MTJ based devices are now being used and in development for both magnetic recording media read-heads and Magnetic Random Access Memories (MRAMs) using the squared loop response (Freitas *et al.*, 2006), and for sensing applications, including biochips (Cardoso, 2005) using the linear transfer curve regime (see fig. 2.8).

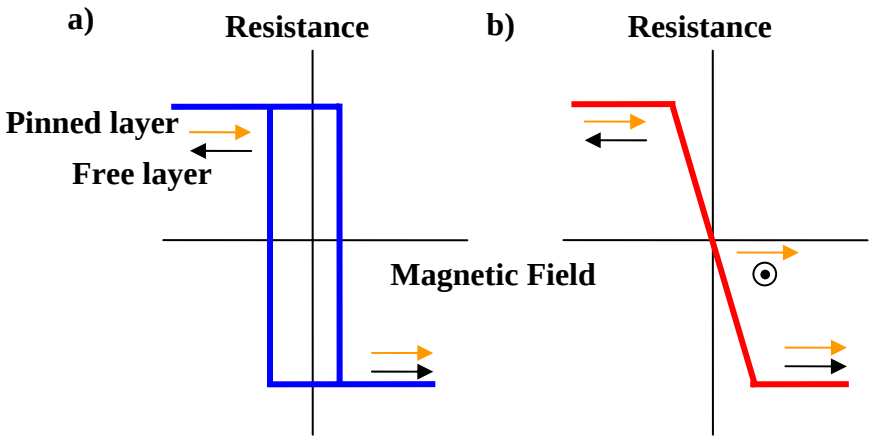


Fig. 2.8. Schematic of MTJ transfer curves for a) application to read-heads and MRAM's and for b) other sensing applications such as biochips. Relative orientation of the magnetizations of the ferromagnetic layers is also shown.

### 2.1.5 Magnetoresistive Biochips

The first magnetoresistive biochip platform was developed at the Naval Research Laboratory (NRL) and was called Bead Array Counter (BARC) (Baselt *et al.*, 1998). The BARC chip was comprised of 66 giant magnetoresistance (GMR) sensor traces of dimensions of 5 µm × 80 µm. Sensors where grouped in eight sensing zones each comprised of 8 GMR sensors. These account for 64 sensors while the remaining 2

where used as reference sensors in a half-Wheatstone bridge arrangement. The different sensing zones where later used to detect different biological warfare agents (Edelstein *et al*., 2000).

Since then, a number of research groups worldwide have been developing spintronic biochip platforms based on different magnetoresistive sensors and on distinct sensor geometries, performances and applications: anisotropic magnetoresistance (AMR) rings (Miller *et al*., 2002); planar Hall effect sensors (Ejsing *et al*., 2003; Ejsing *et al*, 2004); GMR multilayer traces (Miller *et al*., 2001), serpentines (Rife *et al*., 2003) and spirals (Schotter *et al*., 2002); spin valve traces (Graham *et al*., 2002; Lagae *et al*., 2002; Li *et al*., 2003; Wood *et al*., 2005), u-shaped (Ferreira *et al*., 2005c) or serpentine (Anguelouch *et al.*, 2004); and magnetic tunnel junctions (Shen *et al*., 2005; Cardoso *et al*., in press).

Here, a brief description of the existing spintronic biochip platforms will be given, concerning not only transducers, but also detection apparatus and magnetic labels used. These issues will be further discussed in the following sections and chapters for the work developed at INESC-MN during this thesis.

*2.1.5.1 AMR Ring Sensors*

Anisotropic magnetoresistance-based ring sensors were designed and fabricated by NRL for single micron-sized magnetic label detection (Miller *et al*., 2002). The ring sensor was fabricated in NiFe with inner and outer diameters of 3.2 μm and 5 μm, respectively. The ring was designed to detect the radial component of fringe field created by a single 4.3 μm diameter $Ni_{70}Fe_{30}$ microsphere, when excited by an out-of-plane alternate current (ac) magnetic field (see fig. 2.9a).

In the setup from NRL, two AMR ring structures (separated by 50 μm) comprised half of a Wheatstone bridge, with the other half being completed off-chip using resistors of approximately the same value of the resistances of the rings. An AC driven homopolar electromagnet was used to create a perpendicular-to-plane magnetizing field with typical field amplitudes $H_0$ between 0 and 4 kA/m (or 50 Oe), and frequencies $f$ of 200 Hz. In most magnetic field sensor platforms, paramagnetic or non-remanent magnetic

labels are used, such that only in the presence of a magnetizing field they posses a magnetic moment and thus create a field that is sense by a particular transducer (see further discussion on section 2.2 on magnetic labels).

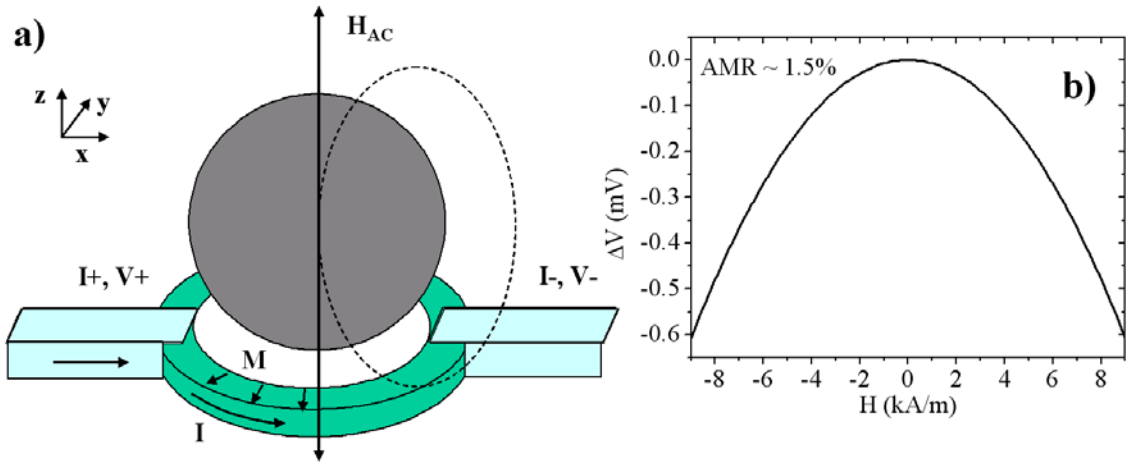


Fig. 2.9. a) Schematic showing an AMR ring sensor geometry, current flow, voltage measure points and external magnetic excitation field directions. b) Typical sensor response to a radial magnetic field as calculated from equation (7) and data from (Miller *et al*., 2002).

A direct current (dc) bias of ~1V was applied to the bridge and a single microsphere was measured by scanning the label over one of the rings using an Atomic Force Microscope (AFM) tip (to where the particle was previously glued).

The magnetoresistance of the AMR rings have roughly quadratic magnetic field dependence around zero applied field, as can be seen from the equation for the electrical response (ΔV) of a single ring structure (see fig. 2.9b).

$$\Delta V = -\left(\Delta R / R\right)_S \, I \, R_{sq} \left(2\pi r_{av} / h\right)\left(\left\langle H_{label} \right\rangle / H_k\right)^2 \qquad (7)$$

In equation (7) $(\Delta R/R)_S$ is the magnetoresistance ratio of the ring structure, which is defined by the difference in resistance between the maximum resistance state (in which the current is parallel or antiparallel to the circumferential magnetization) and the minimum resistance state (in which the current is normal to the magnetization), all divided by the minimum resistance. In this case the AMR of the NiFe ring structures was ~1.5% (for a film thickness of 20 nm), but as a two-terminal device, the lead/contact resistances reduce the effective AMR to ~1%.

Also in equation (7), I is the sense current and $R_{sq}$ is the sheet resistance defined as $R_{sq} = \rho/t$, with $\rho$ the resistivity and t the thichness of the sensing layer. $r_{av}$ is the average radius of the ring, $(r_{max} + r_{min})/2$, and h is the height of the sensor, $r_{max} - r_{min}$, , with $r_{max}$ and $r_{min}$ being the outer and inner radius of the ring structures, respectively. $<H_{label}>$ is the radial component of the field created by a magnetic particle averaged at the sensing layer (this issue will be discussed later on). Finally, $H_k$ is the effective anisotropy field that include the crystalline anisotropy and shape demagnetizing fields.

Given the quadratic response of the sensor to the field created by the label, the detection was done at 2*f*, as the expansion of the magnetoresistance yields the dominant term.

Finally, this sensor was designed for single label detection and was proposed as a sensing unit of a MRAM-like biosensor.

*2.1.5.2 Planar Hall Effect Sensors*

The use of planar Hall effect sensors for magnetic label detection was first proposed by the Mikroelectronik Centret (MIC) of the Technical University of Denmark (DTU) (Ejsing *et al*., 2003). These devices are based on the spontaneous resistance anisotropy occurring in ferromagnets, just like the AMR rings.

The fabricated sensors were simple Ni crosses (20 µm × 20 µm sensing area) and were used to detect 2.8 µm diameter superparamagnetic polystyrene microspheres (Dynabeads M-280, DynalBiotech, http://www.dynalbiotech.com).

Using this cross geometry, two leads were used for driving current through a sensor, while measuring the voltage drop developed transversally to the current direction, with the other two leads (see fig. 2.10). This voltage drop changed as a result of field created by the labels changed the direction of the magnetization of the ferromagnetic sensing layer with respect to the direction of the current, as shown in equation (8).

$$\Delta V = -1/2\,\Delta R\, I \left\langle H_{label} \right\rangle / H_k \qquad (8)$$

Here, $\Delta R = (\rho_{\parallel} - \rho_{\perp})/t$, with $\rho_{\parallel}$ and $\rho_{\perp}$ being the resistivity of the magnetic material with the sense current parallel or perpendicular to the material magnetization, respectively (see discussion above about AMR effect). For Ni, the resistivity variation is ~2% (200 Å thick film). Again t is the thickness of the sensing layer, $<H_{labels}>$ is the field created by the magnetic label averaged over the sensing area and $H_k$ is the crystalline anisotropy field.

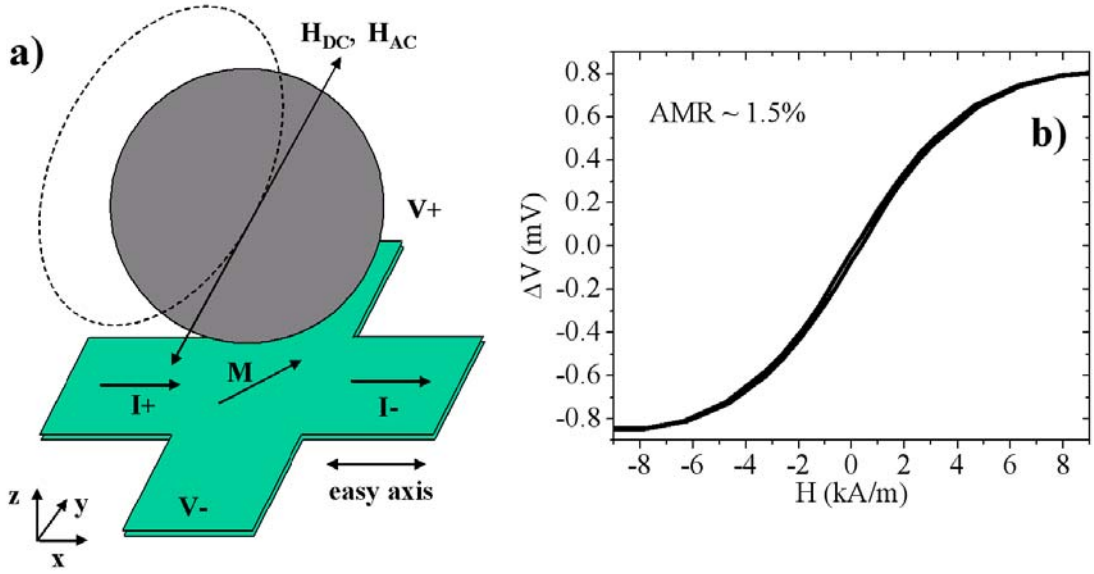


Fig. 2.10. a) Schematic showing a planar Hall cross sensor geometry, current flow, voltage measure points and external magnetic excitation field directions. b) Typical sensor response to the label's magnetic stray field as calculated from equation (8) and data from INESC-MN for a 10 μm × 10 μm sensor with the structure Ta70Å/NiFe300Å/MnPt300Å/Ta70Å.

In the MIC platform a DC sense current of 0.25 mA was used together with an in-plane magnetizing field up to 4.8 kA/m (60 Oe) perpendicular to the sense current direction (see fig. 2.10b). Particle detection was realized by measuring the sensor transfer before and after adding a magnetic label solution.

A further improvement, in collaboration with INESC-MN, consisted on the design and fabrication of exchange-biased permalloy planar Hall sensors (Ejsing *et al.*, 2004, 2005). Here a MnIr antiferromagnetic layer was used to control the anisotropy and to achieve a well-defined single domain initial magnetization state. As a consequence, $H_k$

in equation (8) represents the sum of the crystalline anisotropy field with the exchange field created by the antiferromagnetic layer.

In this case planar Hall effect crosses of dimensions of 10 μm × 10 μm were used to detect in real-time 2 μm diameter microspheres and 250 nm diameter particles (Micromer-M and Nanomag-D labels, Micromod, http://www.micromod.de). Direct sense currents ranging form 1 to 10 mA were used together with an in-plane magnetizing field of 1.2 kA/m (Ejsing *et al*., 2004). In addition, it was shown that using the sense current alone, without any external field, was sufficient to magnetize the non-remanent magnetic particles tested (Ejsing *et al*., 2005). Later on, further improvements were then on sensor design and operation at INESC-MN (see following chapters).

*2.1.5.3 GMR sensors*

GMR multilayer sensors, together with spin valves, are the sensing components used in the more developed biochip and biosensing platforms. These devices are based on the spin-dependent transmission of conduction electrons between magnetic layers coupled through a non-magnetic spacer. As was discussed, this transmission depends on the relative orientation of the magnetic moments of the magnetic layers.

GMR sensors are comprised of a multilayer of magnetic layers separated by non-magnetic spacer layers and show typical magnetoresistance ratios $(\Delta R/R)_S$ from 5 to ~15%. These are the GMR ratios commonly used in biosensing applications, although values as high as 50% have been observed at room temperature. Increased values of magnetoresistance depend not only on materials but also on the number of multilayers. The output for these sensors is given by equation (9) and is shown in fig. 2.11.

$$\Delta V = -\left(\Delta R / R\right)_S \, I \, R_{sq} \left(W / h\right) \left\langle \left| H_{label} \right| \right\rangle / H_k \qquad (9)$$

Here $(\Delta R/R)_S$ is the magnetoresistance ratio, defined as the difference between the maximum resistance of the sensor (when the magnetic layers are antiparallel) and the minimum resistance of the sensor (when the magnetic layers are parallel), divided by the minimum resistance (see equation 4). W is the width of the sensor and h is its

height. $|H_{labels}|$ is the absolute value of the component of the field created by the labels in the sensing direction, as the sensor response is unipolar (symmetrical with respect to the applied field, see fig.2.4a and fig. 2.11b). Again the field created by the labels is averaged on the sensing layer and $H_k$ is the effective anisotropy field that include the crystalline anisotropy and shape demagnetizing fields.

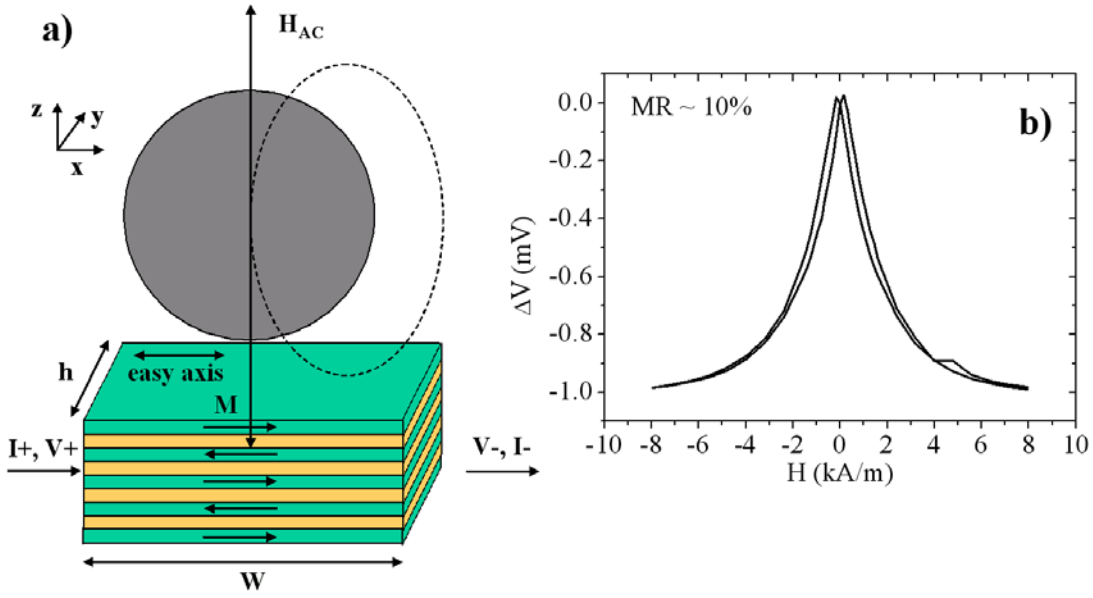


Fig. 2.11. a) Schematic showing a GMR sensor trace geometry, current flow, voltage measure points and external magnetic excitation field directions. b) Typical sensor response to the label's magnetic stray field as calculated from equation (3) and data from INESC-MN for a 2 μm× 6 μm GMR sensor with the structure NiFe60Å/[Cu19Å/NiFe13Å/CoFe4Å]$_{20}$.

The above mentioned BARC platform was the first system to be developed. In an earlier version it was comprised of 5 μm × 80 μm GMR sensor traces. These were arranged in a half-Wheatstone bridge, with a sensor for magnetic label detection in one arm of the bridge and one reference sensor at the other arm. The full bridge was completed with external resistors. Direct sense currents of 5 to 10 mA were used together with a perpendicular-to-plane external magnetizing field of 4 kA/m rms at a frequency of 200 Hz was to enable lock-in detection at 400 Hz, just as in the AMR rings setup (Baselt *et al.*, 1998). The system was then used to detect biological warfare agents through the fringe field created by 2.8 μm diameter Dynabeads that recognized the specific analytes (Edelstein *et al.*, 2000; Miller *et al.*, 2001).

In a later version, in collaboration with Non-Volatile Electronics (NVE), the BARC system encompassed serpentine GMR sensors, 1.6 μm wide on a 4 μm pitch, with a total length of 8 mm within a 200 μm diameter circular zone. This was used to better fit the surface functionalized are to the sensor area (this issue will be discussed later on chapter 4). A bias voltage across the bridge of 4 V was used together with magnetizing fields of 9.6 an 6.8 kA/m rms at the same frequencies and in the same configuration as previously. Dynal M-280 microsphere and $Ni_{30}Fe_{70}$ were detected (Rife *et al*., 2003).

The GMR approach was followed by group at Universität Bielefeld, which used 1 μm wide spiral-shaped GMR sensors of a total of 70 μm in diameter (Schotter *et al*., 2002, 2004). In this platform smaller 0.35 and 0.86 μm magnetic microspheres Bangs Laboratories (http://www.bangslabs.com) were detected. As in the NRL bio-system, an out-of-plane magnetizing field was used and the sensor response was due to the in-plane components of the fringe field created by the magnetic labels. Particle detection was achieved by recording the dc sensor response from -12 to 12 kA/m (or from -40 to 40 kA/m) with respect to a neighbouring reference element in a half Wheatstone bridge arrangement.

*2.1.5.4 Spin Valve Sensors*

Spin valve based biochips were first introduced by INESC-MN (Graham *et al*., 2002) and were followed, in collaboration, by a group at Interuniversitair Micro-Elektronica Centrum (IMEC) (Lagae *et al*., 2002). Later on research laboratories at Standford University (Li *et al*., 2003) and at John Hopkins University (Anguelouch *et al*., 2004) started independent projects on spin valve based biosensors.

As mentioned above, spin valve sensors, in its simplest form, are comprised of only a single trilayer: two ferromagnetic layers (typically $Ni_{80}Fe_{20}$, $Co_{90}Fe_{10}$ or other alloys) separated by a non-ferromagnetic spacer (typically Cu or Au), and they are also based on the GMR effect. One of these ferromagnetic layers is called the reference layer as it is pinned by exchange coupling to an antiferromagnetic layer (for example, MnIr, MnPt or MnNi), and consequently is not sensitive to low applied magnetic fields. The other ferromagnetic layer is called the free layer as it senses even very small magnetic fields. As in GMR multilayer sensors, the spin valve sensor resistance depends on the relative

orientation of the magnetic moments of the magnetic layers. If carefully engineered, spin valves can show a linear response to near zero applied fields. Shape demagnetizing effects or perpendicular easy-axis definition for the free and pinned layers during spin valve deposition are some means to accomplish that, for instance. The sensor response in this case is said to be bipolar and is given by equation (10) (see fig. 2.4b and fig. 2.12b).

$$\Delta V = -1/2\left(\Delta R/R\right)_S \, I \, R_{sq} \left(W/h\right)\left\langle H_{label}\right\rangle / H_k \tag{10}$$

Here, symbols are the same as for the GMR sensors. As mentioned above, typical values for the magnetoresistance ratio for spin valve sensors are 6 to 8%. Specular spin valves on the other hand show higher $(\Delta R/R)_S$ values from 15 to 20%.

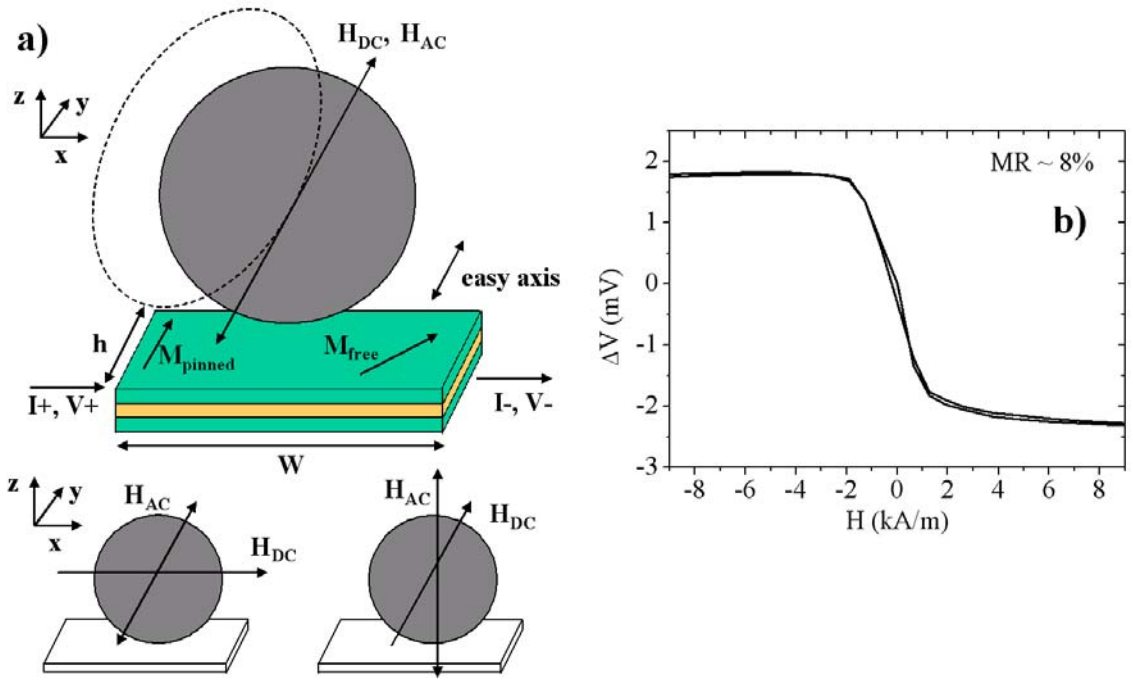


Fig. 2.12. a) Schematic showing a spin valve sensor geometry, current flow, voltage measure points and used external magnetic excitation field directions (larger scheme, INESC; smaller schemes, Stanford). b) Typical sensor response to the label's magnetic field as calculated from equation (10) and for a multilayer Ta20Å/NiFe30Å/CoFe25Å/Cu26Å/CoFe25Å/MnIr60Å/Ta30Å structure (Graham *et al.*, 2005).

At INESC-MN 2 μm × 6 μm spin valve sensors (with a full sensor length of 14 μm) were fabricated to detect single 2 μm microspheres (Micromer-M) (Graham, *et al.*, 2002) and several magnetic labels of different iron oxide compositions and different

sizes ranging from 50 nm up to 2.0 μm were tested (see next section and Ferreira *et al*., 2003). Shape demagnetization effects were used to obtain a sensor linear response (Fig. 2.12b). Typical dc sense currents of 5 to 8 mA were used together with small 1.2 kA/m dc magnetizing fields applied in the spin valve sensing direction (see Fig. 2.12a). Measurements were done in real-time in a liquid medium using a simple multimeter (see chapter 6).

A differential dc measurement setup comprised of 2 μm × 6 μm sensors in a half Wheatstone bridge (with external resistors completing the other half) was used for detection of biomolecular recognition in the model system biotin-streptavidin (Graham *et al*., 2003). In this case a spin-valve sensor was functionalized with biotin and was then able to detect bound streptavidin-coated magnetic labels. Another sensor (75 μm away) was covered with a photoresist mask and as used as a reference sensor, as biomolecular recognition was not observed over the photoresist layer (see details in chapters 5, 6 and 7)

More recently, larger 2.5 μm × 80 μm u-shaped spin valves were used for an increased dynamic range (higher number of particles to be detected), in applications for genetic disease diagnostics (Ferreira *et al*., 2005c, in press) and for detection of pathogenic microorganisms (Martins *et al*., 2005, submitted) (see chapter 3 and 7). Magnetic label detection in this case was done using a lock-in amplifier for lower noise and decreased thermal drift dependence. Direct sense currents of 1 mA were used together with a combination of external ac magnetizing fields (~1 kA/m rms at 30 Hz) and dc bias fields (0.8 to 1.2 kA/m) applied in the sensing direction of the spin valves.

Additionally, some INESC-MN sensing platforms made use of on-chip biomolecule transport using magnetic particles as carriers (see following sections).

IMEC used 2 μm × 16 μm spin valve sensors to detect ensembles of nanometer sized particles. Sensors were linearized by shape anisotropy as in the INESC-MN approach. A sense current of 10 mA was used, and the magnetization of the superparamagnetic labels was achieved by the field created by two metal conductors adjacent to sensor. Current passes alternatively to one or the other conductor, resulting in particle movement over the sensor and, consequently, on label detection (Lagae *et al*., 2002).

In that respect, both approaches from INESC-MN and IMEC are unique with respect to other magnetoresistive biochip platforms and even to more general magnetic field biosensors. Both research groups make use of on-chip conductors combined with a magnetic transducer to be able to manipulate and move magnetic labelled biomolecules on-chip and to detect biomolecular recognition in almost real-time (see also chapter 4).

In the case of INESC-MN, the use of tapered metal conductors (Graham *et al*., 2002) or u-shaped lines (Ferreira *et al*., 2005b) enabled the acceleration of biomolecular recognition between complementary DNA strands (Graham *et al*., 2005; Ferreira *et al*., 2005c). IMEC proposes to use on-chip tapered conductors (Lagae *et al*., 2002) for the detection of biomolecular recognition using a magnetic label cleaving process (Lagae *et al*., 2005). These issues will be further discussed in chapter 4.

Stanford University research group first used spin valve sensors of 2.5 to 3 μm height and ~4 μm width (active areas) to detect a single 2.8 μm diameter Dynabead (Li *et al.*, 2003a). Herein, shape demagnetization was also used to achieve a linear response from the spin valve. Furthermore, a half Wheatstone bridge arrangement was used, with one active sensor and one reference sensor covered with hard-baked photoresist, just like the INESC-MN approach (Graham *et al*., 2003). Magnetizing fields were applied in-plane. A dc longitudinal bias field (in the hard axis direction) was used to polarize the magnetic beads and an orthogonal ac field (in the sensing direction) was used to modulate their magnetizations. DC bias fields between 7.5 and 9.5 kA/m were used, together with ac orthogonal fields of ~3 kA/m rms at 40 Hz. Bridge bias voltages as high as of 30 or 100 V were used and the bridge ac response was measured with a lock-in amplifier.

The laboratory at Standford University detects particles after a label solution as dried out and particles remained settled over the sensor. A later stage, particles are dissolved back in water and are washed away. This contrasts with the approach followed at INESC-MN, where particle and biomolecular recognition measurements are all performed in liquid.

In a further conception of the system (Li *et al*., 2004), the Stanford group used smaller 0.3 μm × 1.5 μm (active area) sensors for the detection of 16 nm $Fe_3O_4$ magnetic nanoparticles (Sun and Zeng, 2002). The experimental setup was similar to the previous one, but in this one a dc bias field of 6.4 kA/m was applied transversely to the sensor (in the sensing direction) to polarize the nanoparticles and ac field of ~8 kA/m at a frequency *f* of 208 Hz was applied perpendicular to plane, similarly to GMR sensors. Measurements were performed at 2*f*. In this study, a nanoparticle monolayer was patterned over the sensor surface using a polyethilenimine mediated self-assembly method (Sun *et al*., 2002).

More recently, a collaborative work between the John Hopkins University and NVE resulted in a platform that uses serpentine or meander spin valve sensors in a full Wheatstone bridge arrangement on chip (Anguelouch *et al*., 2004). These meander lines were 4 μm wide on a 6 μm pitch, comprising active sensing areas of 100 μm × 100 μm or 200 μm × 200 μm. Two of the bridge resistors were laid out as interlaced meander lines and served as the sensing elements, while the remaining sensors were covered by a protective layer 6 μm and served as compensating elements. DC currents of 1 mA were used for detection of 5 μm and 30 μm length ferromagnetic nanowires. These nanowires have the potential to be used as biomolecular labels and for cell manipulation (Reich *et al*., 2003).

*2.1.5.5 MTJ Sensor*

As mentioned above, these devices are based on the spin dependent tunneling of electrodes across an insulator that separates two ferromagnetic layers. As with GMR sensors, the electron tunneling through an insulating barrier depends on the relative orientation of the magnetizations of the magnetic layers.

Just, the same way as spin valves, MTJs can be fabricated to have a linear response. In this case, which is the most suitable for biosensing applications, the transducer output is given by:

$$\Delta V = -1/2\left(\Delta R / R\right)_S \, I\left(RA/Wh\right)\left\langle H_{label}\right\rangle / H_k \qquad (11)$$

In equation (11) symbols hold the same meaning as for GMR and SV sensors, while RA represents the magnetic tunnel junction resistance area product. A transfer curve for the MTJ sensor is shown in fig. 2.13.

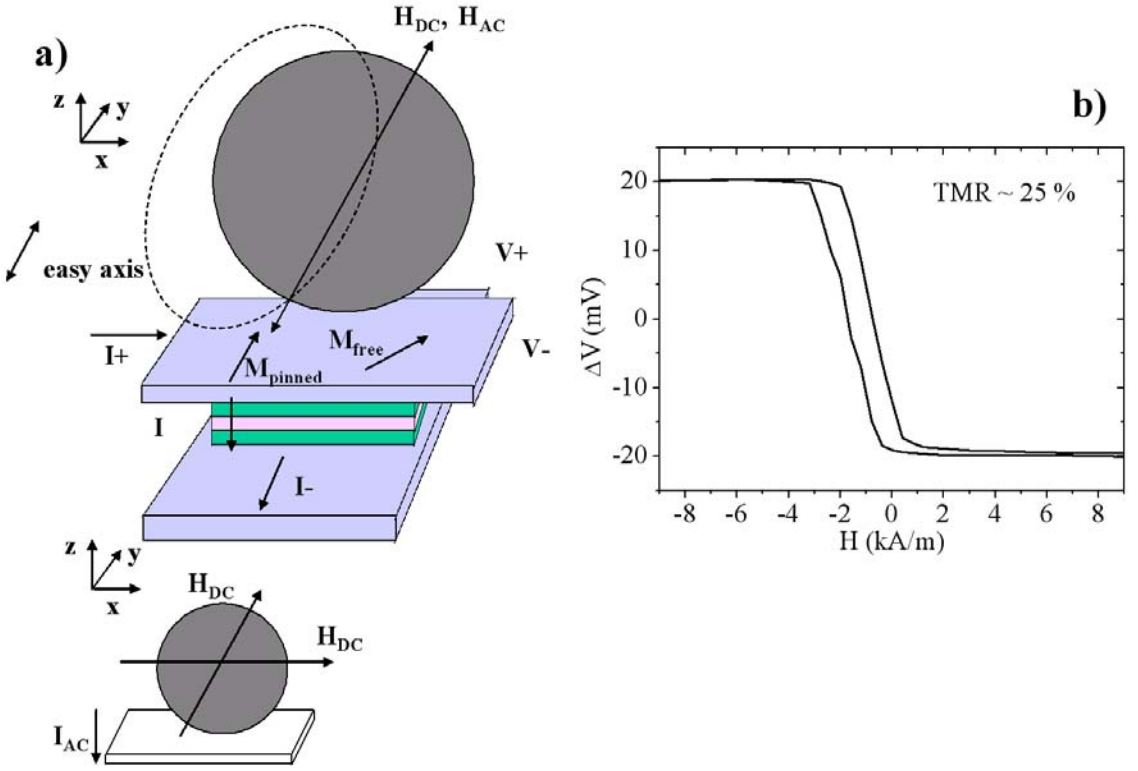


Fig. 2.13. a) Schematic showing a spin valve sensor geometry, current flow, voltage measure points and used external magnetic excitation field directions (larger scheme, INESC; smaller schemes, Brown). b) Typical sensor response to the label's magnetic stray field as calculated from equation (11) and data adapted from (Cardoso *et al*., in press) for a lower resistance magnetic tunnel junction.

Of the magnetoresistive sensor family, MTJ sensors show the highest values of the magnetoresistance ratio, ~50 to 70% for AlOx barrier junctions and, recently, >200% for MgO tunnel barriers (Parkin *et al*., 2004; Yuasa *et al*., 2004).

Magnetic tunnel junction based biosensors have been recently proposed (Shotter *et al*., 2002; Freitas *et al*., 2004; Wang *et al*., 2005) and magnetic label detection has been demonstrated (Shen *et al*., 2005; Cardoso *et al*., in press).

A group from Brown University (Shen *et al*., 2005), fabricated 2 μm × 6 μm MTJ sensors to detect single superparamagnetic M-280 Dynabeads. The sensor was operated

in an ac bridge configuration (1 V rms at 8 kHz bias voltage), and the sensor response was read using a lock-in amplifier. Two external dc applied fields in the sensing direction (1.2 kA/m) and perpendicular to the sensing direction (1.6 kA/m) were applied such that the MTJ sensor operated in the most sensitive and linear region of the transfer curve.

Recently, INESC-MN demonstrated the detection of 250 nm diameter magnetic labels (Nanomag-D) using a sensing unit comprised of a AlOx barrier MTJ in series with a hydrogenated amorphous silicon (a-Si:H) thin film diode (Cardoso *et al*., in press). This sensing unit is the basis for an MRAM-like biosensor as was previously proposed (Baselt *et al*., 1998), and a 16 × 16 MTJ-diode matrix was already fabricated (this will be further discussed in chapter 4).

### 2.1.6 Detection of Magnetic Labels

In magnetic biosensing applications is important to quantify the number of labels that are being detected in order to determine the number of biomolecular recognition events.

To calculate the response of a magnetoresistive sensor to the presence of magnetic labels it is usually assumed that the sensing layers respond to an average field $\langle H_{label} \rangle$, rather than to the inhomogenous local field they create (Tondra *et al*., 2000). In fact, a good agreement was obtained between analytical calculations, assuming this average field, and micromagnetics simulations (Li and Wang, 2003). Furthermore, it is assumed that the sensing layers rotate coherently with $\langle H_{label} \rangle$, as described by the Stoner-Wohlfarth model (Stoner and Wohlfarth, 1948). Here, the sensing layers correspond to the exchanged-bias NiFe layer in planar Hall sensors; the GMR multilayers; or the free layer of spin valves and magnetic tunnel junctions.

Although, several analytical models and numerical simulations (Tondra *et al*., 2000; Ferreira *et al*., 2003; Li and Wang, 2003; Schepper *et al*., 2004) have been developed according to the type of sensor and to the particular detection methods, they all consider the assumptions made above together with the dipole field approximation (in SI units):

$$\mathbf{H}_{\mathbf{label}}(\mathbf{r}) = \frac{1}{4\pi}\left(\frac{3(\mathbf{m}\cdot\mathbf{r})\mathbf{r}}{r^5} - \frac{\mathbf{m}}{r^3}\right) \tag{12}$$

Here, it is assumed that the magnetic moment **m** of the label is located at its centre, and that **r** is the distance between the center of the label and the point of the sensor where the field is calculated.

The dipole field in equation (12) is inhomogeneous at the sensing layer, and consequently, the sensor response depends on the position of the magnetic label with respect to the sensor (see fig. 2.14a). In unipolar response transducers, such as AMR rings and GMR sensors, labels adjacent to the transducer also contribute to a change in resistance, though this effect is relevant only for labels few micrometers apart (see fig. 2.14a right). On the other hand, for the case of transducers with a bipolar response such planar Hall sensors, spin valves, and magnetic tunnel junctions, adjacent labels can even have an opposite contribution to the field created by the labels on top of the sensing structures (fig. 2.14b). Consequently, in these devices, particular care must be taken in the definition of the functionalized area and in the estimation of the number of detected labels.

In addition, as will be discussed in subsection 2.2, labels usually show a paramagnetic behavior, meaning that they only possess a magnetic moment in presence of an externally applied magnetic field. As such, the magnetic moment of the label can be given in SI by $\mathbf{m} = \chi\,\mathbf{H} / V$, where $\chi$ is the susceptibility per label, **H** is the total applied field and V is the volume of the label.

Models have utilized several magnetizing field conditions, where the only requirement is that the induced moment on the labels gives rise to magnetic field components in the sensing directions of the transducer (see previous discussion on sensors). Nevertheless, these models only take into account the externally applied field as the magnetizing field.

At INESC-MN a program written in IDL language (RSI) was used to calculate the field created by a single magnetic label at the free layer of a spin-valve sensor (as shown in fig. 2.14) and the expected sensor output. Theoretical values for a single 2 μm

microsphere were shown to agree well with experimental results using the direct current measurement conditions (see chapter 6 and Ferreira *et al*., 2003).

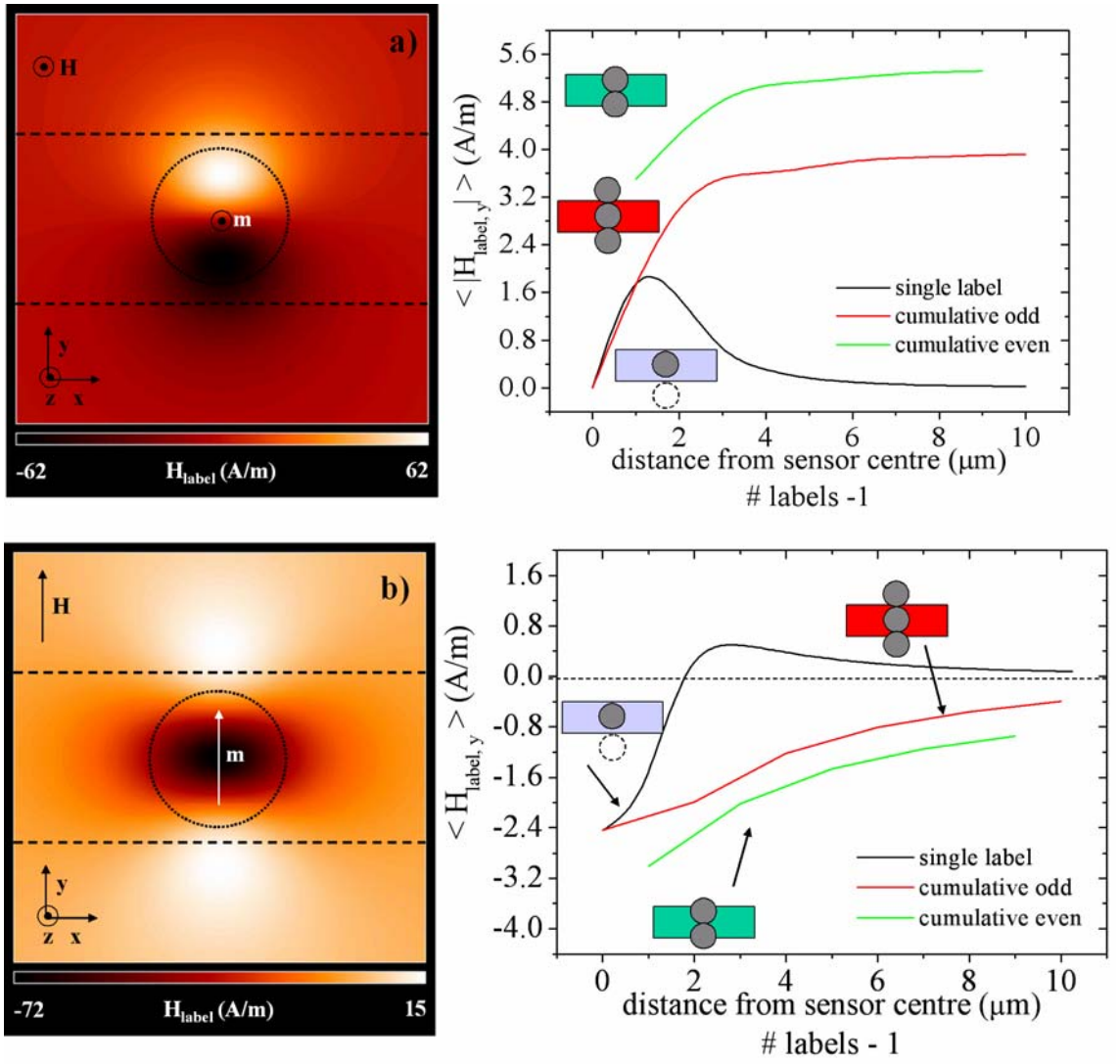


Fig. 2.14. a) Left: inhomogeneous magnetic field created by a 2 μm microsphere, which shows a magnetization of 0.48 kA/m under a 1.2 kA/m external magnetizing field applied perpendicular to the plane of the sensor; 2.5 μm high sensor and particle outlines are shown in dashed lines. Right: magnetic field created by a single label at varying distances from the centre of the sensor (in black); also shown are the fields created by multiple labels placed on a row in two distinct arrangements (in red and green) over a spin valve sensor (the number of labels in the arrangements is indicated in the horizontal axis); fields are averaged over a 2.5 μm × 40 μm spin valve trace b) Left: inhomogeneous magnetic field created by a 2 μm microsphere under a 1.2 kA/m external magnetizing field applied in-plane in the spin valve sensing direction; Right: magnetic field created by a single label at varying distances from the centre of the sensor and the fields created by multiple labels placed on a row in two distinct arrangements: a label at the center of the sensor and additional adjacent labels (cumulative odd); two labels over the sensor and additional labels on both sides (cumulative even).

Later on, it was experimentally observed that even in the absence of an externally applied field $\mathbf{H_{ext}}$ magnetic label detection was possible. This was attributed to the sense current that creates a magnetizing field $\mathbf{H_j}$ (Ejsing *et al*., 2005). The magnetic field created by a structure of volume V transversed by a current density **J** was calculated from the Biot-Savart law (Jackson, 1975):

$$\mathbf{H_j}(\mathbf{r}) = \frac{1}{4\pi}\int_V \frac{J(\mathbf{r}')\times(\mathbf{r}-\mathbf{r}')}{|\mathbf{r}-\mathbf{r}'|^3} d\mathbf{r}' \qquad (13)$$

Again **r** is the position where the field is calculated. Furthermore, this same expression is also used to calculate the magnetic field created by the magnetic transport structures (see next section).

Nevertheless, experiments showed that the combination of external $\mathbf{H_{ext}}$ and sense current fields $\mathbf{H_j}$ did not explain all of the results. Additional magnetostatic fields created by the magnetic layers of the sensors $\mathbf{H_m}$ were then considered for the first time in modeling sensor response to the presence of magnetic labels (Ferreira *et al*., 2005a). The magnetostatic fields were calculated using the equation (Bertram, 1994):

$$\mathbf{H_m}(\mathbf{r}) = -\int_V \frac{\nabla\cdot\mathbf{M}(\mathbf{r}')(\mathbf{r}-\mathbf{r}')}{|\mathbf{r}-\mathbf{r}'|^3} d^3r' + \int_S \frac{\hat{\mathbf{n}}\cdot\mathbf{M}(\mathbf{r}')(\mathbf{r}-\mathbf{r}')}{|\mathbf{r}-\mathbf{r}'|^3} d^2r' \qquad (14)$$

Here, **M** is the magnetization or magnetic moment per volume (**M** = **m**/V), V is the volume of magnetic material and **n** is the normalized vector perpendicular to the surface S that delimits the volume V.

The field that magnetizes the labels is then the combination of the different fields considered above $\mathbf{H = H_{ext} + H_j + H_m}$. The sensor response then directly depends on the directions and magnitudes of these fields, which on the other hand depend on the magnetic layer structure and dimensions of the sensors and also on the operation conditions.

At INESC-MN a study was made on the detection of 250 nm diameter magnetic labels (see next section) using 2 μm × 6 μm top pinned spin valve sensors. These sensors were fabricated with the structure Ta 30 Å/ NiFe 30 Å/ CoFe 25 Å/ Cu 26 Å/ CoFe 25 Å/ MnIr 60 Å/ Ta 30 Å/ TiW (N) 150 Å and showed a linear range roughly between -2.5 and 1.5 kA/m (or -32 to 18 Oe) at 8 mA sensor bias current.

Values for $\mathbf{H_j}$ and $\mathbf{H_m}$, averaged along the sensitive direction of the spin valve (smaller dimension) and at a distance of ~300 nm from the sensing layer, were $\langle H_y^j \rangle \sim -0.18$ kA/m per mA sense current and $\langle H_y^m \rangle \sim -1.0 - 1.7 \sin\theta$ (field in kA/m), with θ the angle between the magnetization of the free layer and the sense current direction (for $\theta = 90^o$ the sensor is in the minimum resistance state as the pinned are free layers are parallel) (Bertram, 1994). As a consequence, the intensities of the several fields were comparable (Ferreira *et al*., 2005a). Table I shows the intensities for these fields for 3 conditions:

Table I. Magnetic fields acting on a 250 nm particle located on top of a spin valve sensor (2 μm × 6 μm). The distance between the centre of the label and the sensing layer is ~ 300 nm. External uniform magnetic fields $\mathbf{H_{ext}}$ were applied in the sensing direction (*y* axis in fig. 2.14) and magnetostatic fields $\mathbf{H_m}$ and the field created by an 8 mA sense current $\mathbf{H_j}$ were averaged along the smaller dimension of the sensor. The total magnetic field **H** was also calculated for the three conditions presented.

| | Magnetic fields (kA/m) | | |
|---|---|---|---|
| $H_{ext}$ | -1.20 | 0 | 1.20 |
| $\langle H_y^m \rangle$ | -0.56 | -1.43 | -2.31 |
| $\langle H_y^j \rangle$ | -1.44 | -1.44 | -1.44 |
| $\langle H_y \rangle$ | -3.20 | -2.87 | -2.55 |

In fact, for the external applied fields considered in table I, the resulting total magnetic fields acting on the labels are always negative with respect to the *y* axis of figure 2.14 (opposite to the pinned layer magnetization direction). This means that in all of these cases the stray magnetic fields created by the labels are parallel to the direction of the pinned layer and thus contribute to a decrease in the resistance of the transducer (see further down).

The existence of magnetostatic fields had further consequences on sensor operation when using an ac external excitation field: a dc external bias field was required for optimum sensor operation (see chapter 6 and Ferreira *et al*., 2005c, in press).

Without considering the effect of magnetostatic fields, an ac excitation field results in the induction of a magnetic moment in the same direction as the applied field and consequently, the stray fields of the labels at the sensing layer oppose the applied field. The labels then shield the sensor from the external field, resulting in a decrease of the peak-to-peak signal or the root-mean square (rms) output (see sensor transfer curve in fig. 2.15a top). Figure 2.15a in the bottom shows the rms signals obtained for a 2.5 µm × 80 µm spin valve sensor with a 25% sensor coverage of 250 nm particles, by applying a dc bias and different ac excitation fields. It is observed that the sensor output increases with the magnitude of the ac field up to a maximum, where the ac field is large enough to surpass the linear regime of the sensor and move into the saturation regions.

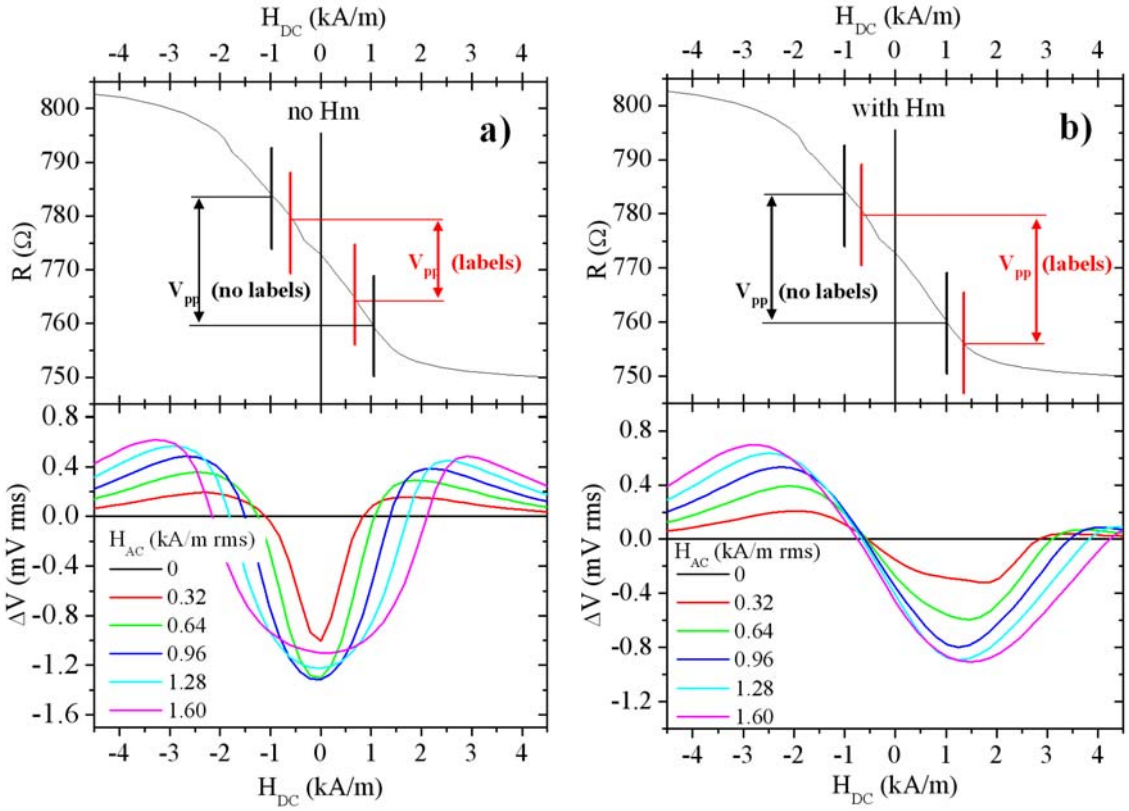


**Fig. 2.15.** a) Without magnetostatic fields. Top: the spin valve sensor response to the presence of labels results in a decrease of the peak-to-peak signal due to the shielding of the external applied field provided by the magnetic labels. Bottom: corresponding ac signals for varying dc bias and ac applied fields. b) Considering magnetostatic field effects. Top: the spin valve sensor response to the presence of labels results in a shift of the peak-to-peak signals in the sensor transfer curve, as the sensor resistance diminishes both for negative and positive applied fields. Bottom: corresponding ac signals for varying dc bias and ac applied fields.

On the other hand, when considering magnetostatic fields the induced magnetic moment of the labels is always negative, resulting in a decrease of the resistance of the sensor for all applied fields. As a consequence, the peak-to-peak signal window is shifted to lower resistances, while maintaining the magnitude of the signal in the linear region of the transfer curve. This results in a small or near zero variation of the rms signals in this regime (fig. 2.15b top). Applying a dc bias signal results in an increase of the sensor output to labels (25% sensor coverage) up to a maximum field where the ac excitation field goes deep into the saturation regions (see fig. 2.15b bottom).

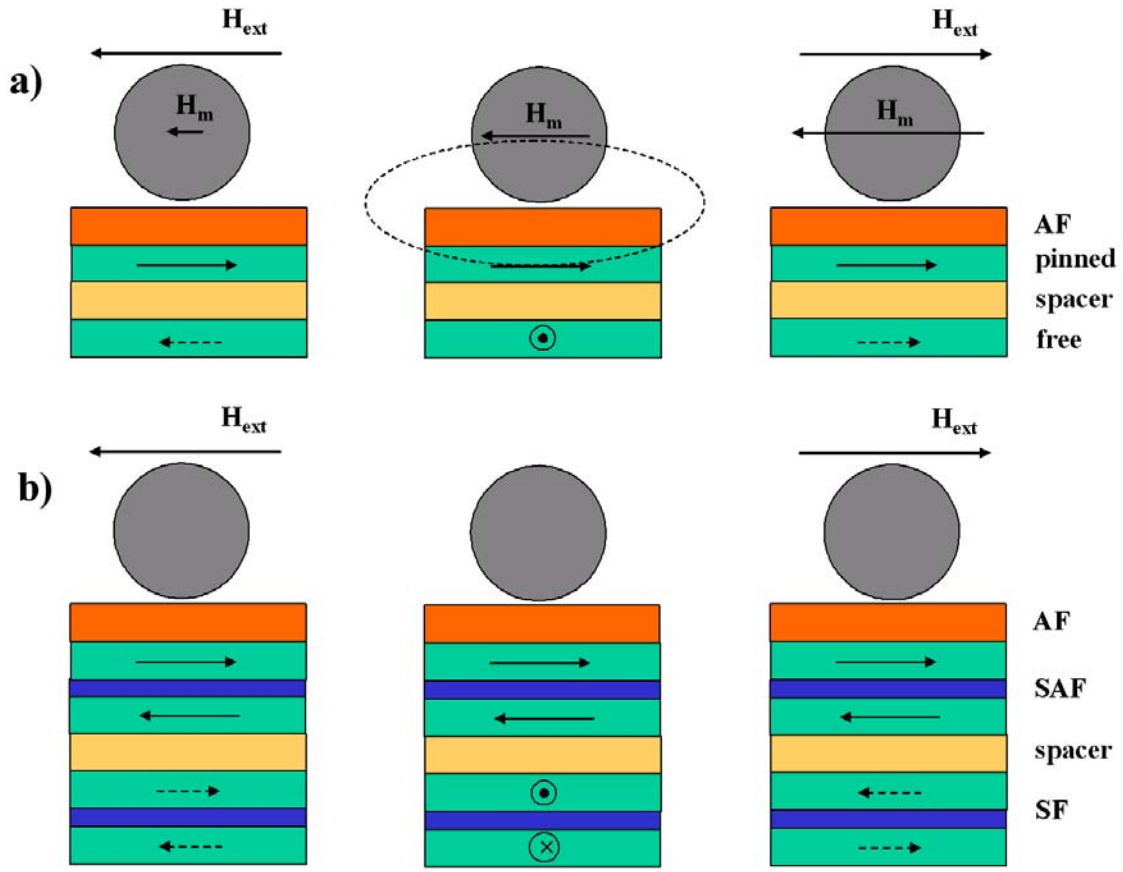


**Fig. 2.16.** a) Cross-section schematic of a top pinned spin valve sensor showing the effects of the magnetostatic fields created by the ferromagnetic layers of the sensor. Three conditions are considered: with the external magnetic field applied in the negative direction (opposite to the magnetization of the pinned layer), without external magnetic field and with the external field applied in the positive direction (direction of the magnetization of the pinned layer). b) Cross-section schematic of a spin valve sensor with synthetic free (SF) and synthetic antiferromagnetic (SAF) layers. When these layers are compensated the resulting magnetostatic fields are null and labels respond only to the external magnetizing fields.

Finally, in order to be sensitive only to the external magnetizing field (or at least be the dominant magnetizing field) low sense currents may be used and sensors may be designed and fabricated with synthetic free (SF) and synthetic antiferromagnetic (SAF) pinned layers, such that magnetostatic fields are minimized (Guedes *et al*., in press). In these conditions the dc bias external field is no longer necessary for ac detection (see fig. 2.16).

Both sense current and magnetostatic field enable the detection of magnetic labels without the need for external field. This is advantageous, as it simplifies the experimental setup and measurement protocols. Nevertheless, care must be taken when designing sensors and implementing the optimum detection methods.

Further on chapter 7, results concerning the detection of magnetic labels in function of label solution concentration will be discussed. The estimation of the number of particles detected will also be given based on the model just described (Ferreira *et al*., in press).

### 2.1.7. Quantification of Biomolecular Interactions

Beyond the detection of magnetic labels lies the possibility of quantifying the number of biomolecular recognition events.

The magnetic particles used so far usually were much larger than the biomolecules they label. The smallest labels were 50 nm and the largest 2.8 μm in diameter (see next section), whilst tested biomolecules typically had dimensions of a few to 10's of nanometers (see chapter 3). As a consequence each magnetic particle may label a large number of biomolecules, depending on the surface chemistry and on magnetic labeling protocol (see chapter 3).

In order to determine the number of biomolecular interactions detected per label a model was developed for a DNA chip, although the methodology is transposable to other biomolecular interactions such as antibody-antigen (Graham *et al*., 2004).

As will be discussed later on chapter 3, the labeling of target oligonucleotides was achieved through the biotin-streptavidin interaction. The oligonucleotides were labeled

with biotin and later on were incubated with streptavidin coated magnetic particles. The incubation protocol was 1 target per streptavidin molecule. The number of targets per magnetic label is then set equal to the number of streptavidin molecules originally coated on the particles' surface (see table II). Nevertheless, the labeling protocol can be adjusted such that targets are incubated with particles in a 1:1 relationship.

Although, particles can label a relatively large number of biomolecules, only a fraction of those can interact with biomolecules at the surface of the sensors. An estimation of the maximum number of biomolecular interactions was done based on the calotte of the spherical particle (or assumed to be spherical, see following section) that is in contact with the sensor. This area was determined based on the length of the biomolecule, herein considered a 50 nucleotide long single stranded DNA molecule (or 50-mer), that interacts with the sensor-bound probe DNAs (see fig. 2.17).

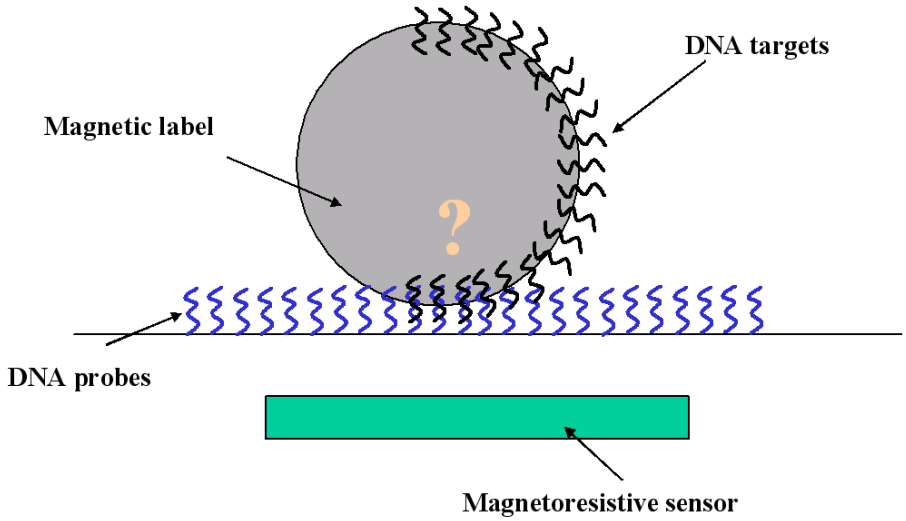


Fig. 2.17. Schematic of the interaction between magnetically labeled DNA targets with complementary DNA probes bound to the surface of the magnetoresistive chip.

The basis for the calculation of the number of DNA-DNA interactions is based on the given assumptions: the label is spherical and has uniform size; the surface of the particle in contact with the sensor depends on the length of the biomolecule and any eventual spacer molecules (~18 nm for the 50-mer oligo + 12 nm target overlap with probe + 4 nm cross-linkers = 34 nm); target DNA is on a 1:1 relationship with streptavidin biomolecules; and biomolecules are uniformly distributed on the label's surface (see details on calculation in Graham *et al.*, 2004).

The theoretical calculation for several of the magnetic particles studied (see also next section) is shown in table II below:

Table II. Theoretical calculation data for DNA-DNA molecular interactions detected per magnetic label. a) these labels are only available with biotin coating, so an estimation based on similar 100 nm labels was done.

| **Magnetic Label** | **Diameter (nm)** | **# DNAs/ label** | **# DNA-DNA detected interactions** |
|---|---|---|---|
| Micromer-M | 2,000 | 77,000 | 1300 |
| Nanomag-D | 250 | 500 | 70 |
| Nanomag-D | 130 | 70 | 20 |
| Nanomag-D-spio | 100 | 20 | 3 |
| Nanomag-D-spio | 50 | 2[a)] | 1 |

It can be seen from table II that each 2 μm microsphere detected correspond to a maximum of a thousand DNA-DNA interactions, whilst smaller labels correspond only to a few tens or less of biomolecular recognition events. As will be discussed in the following subsection and later on chapter 7, sensors are able to detect a single microsphere and potentially can detect single 50 nm labels, provided that experimental noise can be reduced.

Consequently, magnetoresistive biosensing offers a relatively straightforward means to detect single biomolecular recognition events, something that is not within reach of conventional techniques (Graham *et al.*, 2004). Also magnetic labeling protocols were not optimized and the goal would be to have a single target per label.

Finally, efforts are on-going to quantify the number of biomolecular interactions occurring between magnetic label and sensor surface by using an atomic force microscopy technique and comparing with magnetoresistive sensing.

### 2.1.8 Sensor Performance

In sensing applications the figure of merit to be considered is the signal-to-noise ratio (SNR), although the absolute signal is also important as the highest the signal is the lesser is the requirement for amplification steps and simpler is the detection apparatus. For instance, in earlier INESC-MN studies single magnetic microspheres were detected by simply measuring the dc voltage drop across a spin valve resistor using a common multimeter (see chapter 6 and Graham *et al*., 2002).

In order to define sensor performance is also necessary to consider the application for which the sensor is designed: the detection of a great number of labels with a considerable dynamic range (number of particles to be detected); or detection of single labels and single biomolecular recognition events (Graham *et al*., 2004). As such, sensor geometry is something to take into account, not only for dynamic range but also in terms of sensitivity (as will be discussed further in chapter 4).

As sensors respond to the average field created by the labels on the sensing layer it is natural to expect that sensor sensitivity to a single label improves as the dimensions of the sensor are made comparable to those of the label (Tondra *et al*., 2000).

On the other hand, sensor sensitivity in the broader sense depends on the magnetoresistance ratio of the bulk magnetoresistive material, on the sensor geometry (which can be used to obtain a linear response through shape demagnetizing fields) and on externally applied bias fields (which can also be used to linearize the sensors).

Here, the SNRs of the several magnetoresistive sensors was determined taking into account the detection of a single 2 μm microsphere (Freitas *et al*., 2004) and the noise levels obtained in the linear regime of the sensor.

Table III shows a comparison of the performance of the different types of magnetoresistive sensors mentioned above, with respect to the signal-to-noise ratio. The magnetic properties shown are typical for these sensors and the sensor size was chosen for optimal single 2 μm microsphere under a magnetizing field of 1.2 kA/m (particle

magnetic moment of $2 \times 10^{-15}$ J/T). Thermal or Johnson or white noise was calculated from:

$$V_{rms}^{N} = \sqrt{4k_B TR} \tag{15}$$

Here $k_b$ is the Boltzmann constant ($1.38 \times 10^{-23}$ J/K), T is the absolute temperature (taken as 300 K) and R is the resistance of the transducer.

In addition, the noise for the MTJ sensors with AlOx or MgO barriers was calculated from the summation of the thermal and shot noise:

$$V_{rms}^{N} = \sqrt{4k_B TR + 2IeR^2} \tag{16}$$

Here I is the sense current and e is the charge of the electron ($1.6 \times 10^{-19}$ C) (Raquet, 2001; Almeida *et al*., in press). Finally, the minimum detectable field and the SNR was calculated for the minimum noise of these magnetoelectronic devices.

Table III shows that due to its highest magnetoresistance ratio, the MgO barrier magnetic tunnel junction transducers show the highest sensitivity and consequently, the highest signal per label, followed by AlOx MTJs, spin valves, GMR sensors, AMR rings and planar Hall crosses. On the other hand, for low resistance tunnel junctions (as shown), the minimum noise level is comparable to the noise levels of the other transducers, this then results in a smaller minimum detectable field and a higher SNR.

Note that the sense current was kept constant at 1 mA. Some of the sensor performances relations may differ if different currents are applied through the sensors, as the different sensors show distinct limits of operation. As an example, MTJ sensors show a decrease in TMR with increasing sensing currents (voltage bias) and there is an increase in shot noise; while for spin valves, 10 mA currents can be applied, increasing the sensor response to a single label by a factor of 10, while maintaining mostly the same thermal noise level.

Table III. Comparison of the performance of different magnetoresistive sensors used for the detection of magnetic labels, including magnetic tunnel junctions with AlOx and MgO barriers. Typical magnetic properties for these sensors were used, and sensor geometries were chosen for the detection of a single 2 μm magnetic label of magnetization of 0.48 kA/m. $t^*$ represents the magnetic sensing layer thickness. Remaining symbols are as detailed in previous sections for each of the sensor types. The field created by the label in the AMR sensor case was averaged in an annulus of radius and height of 1 μm. For the remaining sensors the label field was averaged in a squared area. The thermal noise is shown for the different sensors, whilst for MTJ sensors the presented noise is the summation of the thermal and shot noise (see text for details). The signal-to-noise ratio was obtained dividing the signal per 2 μm microsphere, ΔV, by the noise.

| Sensor type | width (μm) | height (μm) | $t^*$ (nm) | $R_{sq}$ (Ω cm) RA (Ω μm$^2$) | ΔR/R (%) | $H_k$ (kA/m) | S (V/T A) |
|---|---|---|---|---|---|---|---|
| AMR ring | $r_{ext}$ = 1.5 $r_{int}$ = 0.5 | 1 | 20 | 10.5 | 1.5 | 14.5 | 27 |
| Planar Hall | 2.5 | 2.5 | 30 | 7 | 1.5 | 2.4 | 17 |
| GMR | 2.5 | 2.5 | 72 | 2.8 | 10 | 2.4 | 93 |
| Spin valve | 2.5 | 2.5 | 5 | 20 | 8 | 2.4 | 265 |
| MTJ AlOx | 2.5 | 2.5 | 5 | 80 | 25 | 2.4 | 531 |
| MTJ MgO | 2.5 | 2.5 | 5 | 150 | 150 | 2.4 | 5,968 |

| Sensor type | I (mA) | $<\mu_0 H_{label}>$ (μT) | ΔV (μV) | Thermal noise/ shot noise (nV/Hz$^{0.5}$) | $<\mu_0 H_{label}>_{min}$ (nT) | SNR |
|---|---|---|---|---|---|---|
| AMR ring | 1 | 60 | 1.6 | 0.7 | 27 | 2,200 |
| Planar Hall | 1 | 28 | 0.5 | 0.3 | 20 | 1,400 |
| GMR | 1 | 28 | 2.6 | 0.2 | 2.3 | 12,000 |
| Spin valve | 1 | 28 | 7.4 | 0.6 | 2.2 | 13,000 |
| MTJ AlOx | 1 | 28 | 15 | 0.5 | 1.0 | 29,000 |
| MTJ MgO | 1 | 28 | 170 | 0.8 | 0.1 | 220,000 |

Also, the results in table III are shown for the minimum noise level, that is, beyond the 1/f noise regime (see also chapter 5). For low frequencies applications, for instance, planar Hall sensors seem to be the most sensitive for magnetic label detection (Freitas *et al*., 2004).

Nevertheless, MgO barrier based MTJ transducers show the promise of being the most sensitive of spintronic transducers ever, being capable of detecting magnetic fields in the pT range. This may enable the detection of single 10 nm magnetic particles and, consequently, of single biomolecular interactions. This further shows that magnetoresistive biochips have the potential to become useful tools for molecular biology.

## 2.2 Magnetic Labels

### 2.2.1. Overview

Different kinds of magnetic labels have been used in magnetic biosensing applications, ranging from nanometer to micrometer sized particles (Pankhurst *et al.*, 2003; Berry, and Curtis, 2003) and nanowires (Reich *et al.*, 2003). In addition, ferromagnetic, paramagnetic or superparamagnetic labels have been chosen according to the application, transduction mechanism and assay type.

Several ferromagnetic materials, such as Ni, Fe, Co, and their alloys, and ferrimagnetic materials, such as $\gamma$-$Fe_2O_3$ (maghemite) and $Fe_3O_4$ (magnetite), have been used in magnetic particle preparation. Nevertheless, their magnetic properties depend, not only on the material used but also on the label size.

For instance, large labels, of dimensions of hundredths of nanometers or more, usually show a multi-domain structure, as this represents a minimum magnetic energy of the system. Nevertheless for smaller labels (roughly below the 100 nm range), the energy is minimum in a single-domain state rather than including domain walls (fig. 2.18).

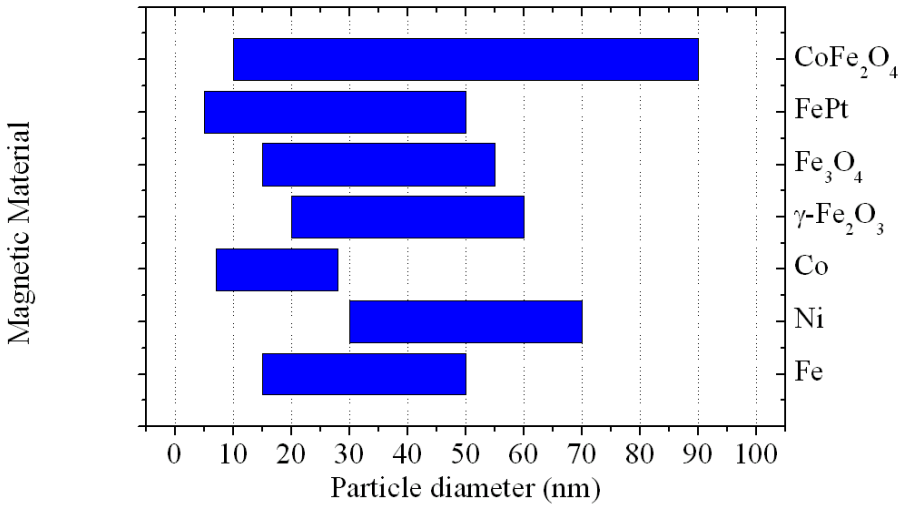


Fig. 2.18. Particle diameters for stable single domain magnetic nanoparticles (adapted from Chung *et al*., 2004).

As such, the response of these particles to an applied magnetic field is a large hysteresis loop (see fig. 2.19). Multi-domain magnetic particles, on the other hand, show a narrow hysteresis loop, as domain walls require a smaller energy to move. Both multi and single domain particles show a non-zero magnetization under no applied field, and as such they are called remanent magnetic particles.

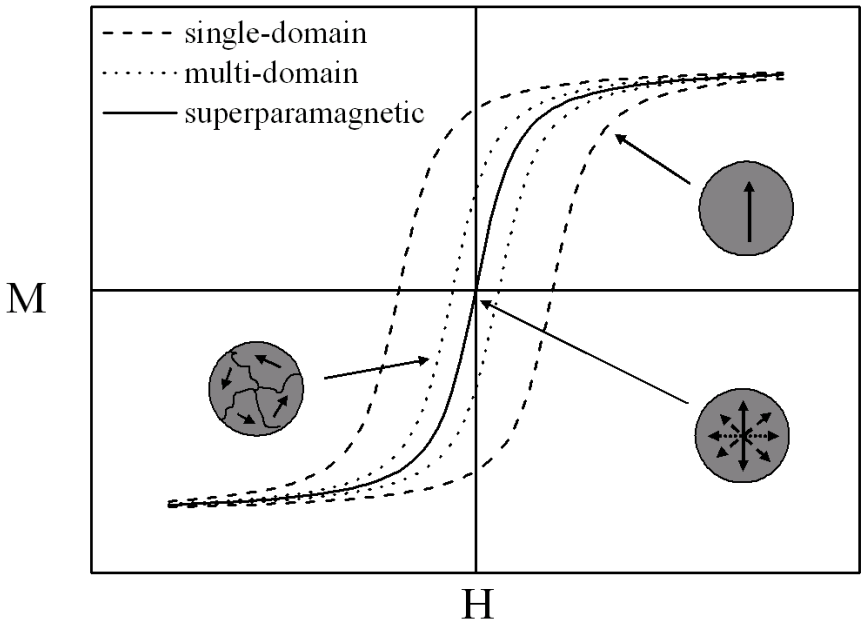


**Fig. 2.19.** Magnetization vs applied field curves for single-domain, multi-domain and superparamagnetic labels.

Smaller particles or labels, with dimensions on the order of tens of nanometers or less, have a magnetocrystalline and shape anisotropy energy that are in the order of or smaller then the thermal energy (Kittel, 1996). As a consequence, the labels magnetic moment fluctuates with the temperature, and have a zero net magnetization under a zero applied magnetic field (non-remanent particles). These labels show a non-hysteretic behavior with an applied magnetic field, which is a signature of superparamagnetism (fig. 2.19).

Under an externally applied field, magnetic labels align with the field but, after the field is removed the magnetization of the particles relaxes. Relaxation occurs through two mechanisms, Néel (Néel, 1955) and Brownian (Debye, 1929), and the predominance of one of the mechanism over the other depends on label size.

Néel relaxation is related to superparamagnetism, as the magnetic moment of a label fluctuates thermally inside the particle (fig. 2.20a), and it is characterized by the relaxation time $\tau_N$:

$$\tau_{\mathbf{N}} = \tau_0 \exp\left(\frac{\Delta E}{k_B T}\right) \tag{17}$$

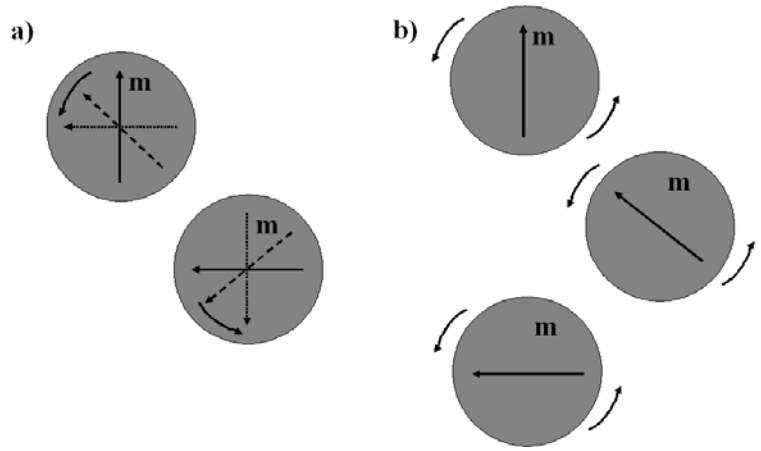


Fig. 2.20. a) Néel relaxation mechanism (dominant for superparamagnetic particles): labels magnetic moment rotates with thermal energy without being accompanied by label rotation. b) Brownian relaxation mechanism (more relevant in single and multi-domain particles): labels magnetic moment relaxes together with the rotation of the whole label in the carrier liquid.

In equation (17) $\tau_0$ is usually taken as 1 to 100 ps (Brown, 1963), $\Delta E$ is the energy barrier to the moment reversal and includes the magnetocrystalline and shape anisotropies. $k_B$ is the Boltzmann constant and T is the absolute temperature (in Kelvin). Néel relaxation is dominant for particles with sizes smaller than 10 – 20 nm.

Larger magnetic particles have a relaxation time $\tau_N$ in the order of tens or hundredths of seconds and thus exhibit remanance. Nevertheless, their magnetization relaxes through the Brownian rotation of the whole label in the carrier liquid (fig. 2.20b). The moment is fixed within the particle. It is characterized by the time constant $\tau_B$ :

$$\tau_{\mathbf{B}} = 4\pi\eta \frac{r^3}{k_B T} \qquad (18)$$

Here $\eta$ is the viscosity of the carrier liquid (e.g. for water, 0.001 N s/m$^2$) and r is the hydrodynamic radius of the label.

It is these distinct magnetic properties that are used in the different biosensing approaches. Volume assays are based on Brownian relaxation of nanoparticles in solution. When labels recognize a particular analyte in solution, through probe biomolecules immobilized on the particles surfaces, their hydrodynamic radius increases. As a consequence, the ac susceptibility peak of the solution shifts to lower frequencies (Connolly, and St. Pierre, 2001; Astalan et al., 2004; Chung et al., 2004).

SQUIDs, on the other hand, have been use to distinguish between surface immobilized magnetically labeled biomolecules and particles free in solution (Kötitz *et al*., 1997; Chemla *et al*., 2000). In these cases, after removal of an applied field, surface-bond labels only show a relatively slow Néel relaxation, while unbound free-in-solution labels relax mainly via the Brownian mechanism and are distinguished by the transducers.

The remaining surface-based assays are based on the detection of magnetic stray fields created by the labels bound to the surface through the biomolecular recognition between target and probe biomolecules. Here, ~10 nm superparamagnetic labels are used, or

more frequently larger >50 nm to micrometer sized labels. The larger labels are comprised of smaller superparamagnetic labels dispersed in or coated with a polymer, metallic or oxide layer, and show a paramagnetic or a non-remanent behaviour.

In magnetoresistive bioassays, magnetic labels should comply with certain requisites: have a high saturation magnetization (made of materials like Ni, Fe, Co, and their alloys) so that the signal per particle is the maximum possible; show material stability over time (like iron oxides); be biocompatible and non-toxic (like iron oxides); be monodispersed and do not cluster, i.e., be superparamagnetic; have low size dispersion and magnetic content variability; show low unspecific adsorption to undesired biomolecules and surfaces; and ideally, each particle should label or tag a single biomolecule. In addition, material stability and biocompatibility requisites should apply as well as to the encompassing matrix or the coating.

The technology of magnetic particles for biosensing applications involves several fields of knowledge, namely, inorganic and organic chemistry, materials science, and molecular biology. In fact, magnetic properties are as important as suitable coating and biomolecule functionalization chemistries.

Recently, bio-inspired approaches are being undertaken on the synthesis and preparation of magnetic labels with the advantages of being naturally biocompatible, and providing a suitable surface for functionalization and also of having narrow size distribution.

One of the ideas being pursued at Montana State University and at the Massachusetts Institute of Technology is to use protein cages, like the Fe-storage protein ferritin (Resnick *et al*., 2005). These protein cages can be further engineered to hold different magnetic materials (Klem *et al*., 2005). Curiously, the need and interdisciplinary knowledge drove be in the beginning of this PhD to look at ferritin as a potential label for magnetic biochips. Inevitably, and actually not for the first time, other people facing similar problems or driven by other motives ended up looking for the same solutions.

Another approach, taken by the Argonne National Laboratory, is to use virus as shells for nanoparticle synthesis. These produce uniform particles and their shape can be engineered by directed mutation of virus genetic information (Liu *et al*., unpublished).

Finally, a further solution I was considering since I learn of these organisms is the use of magnetosomes. These magnetic particles are naturally produced by magnetostatic bacteria, forming a chain. This enables the orientation of this unicellular organism in the earth's magnetic field. I found out recently, that this approach is being thought for biotechnological applications by a research group in Bremen, Germany (http://magnum.mpi-bremen.de/magneto).

### 2.2.2. Study and Use of Magnetic Labels in Magnetoresistive Chips

At INESC-MN, several particles of diameters ranging from 50 nm up to 2.8 µm were studied. Their magnetic properties were measured using vibrating sample magnetometry (VSM) of dried (Ferreira *et al.*, 2003) or liquid particle samples (Freitas *et al.*, 2004) (see fig. 2.21).

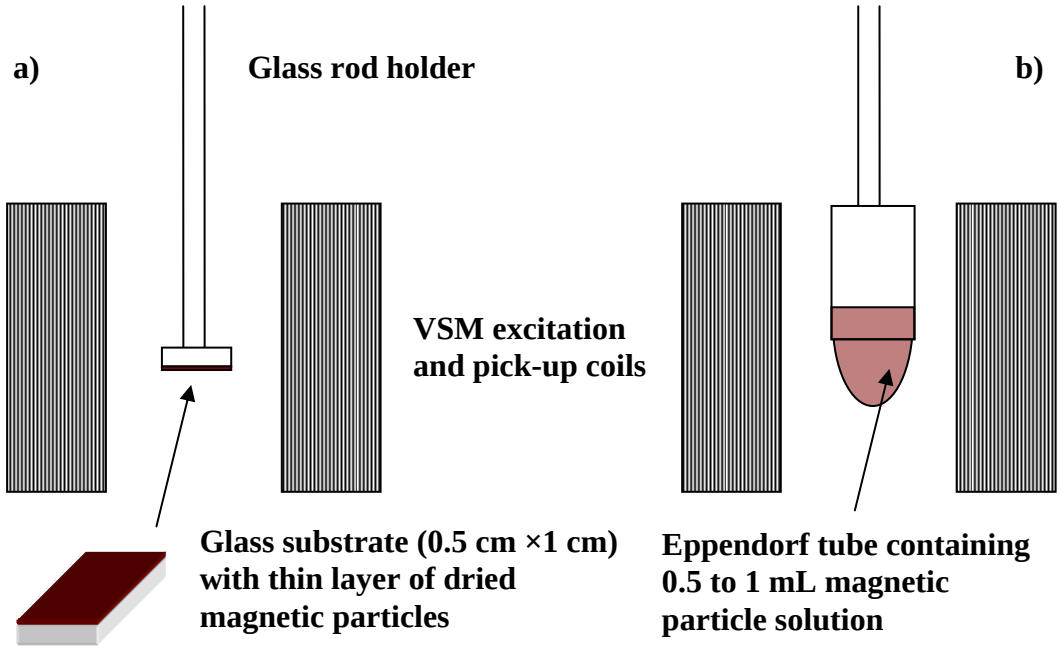


Fig. 2.21. Schematic for magnetic particle characterization of a) dried and b) liquid samples, using vibrating sample magnetometry.

Table IV shows some of the magnetic properties of the labels tested by INESC-MN and other research laboratories.

Table IV. Properties of several magnetic labels used in magnetoresistive biosensing platforms. Data was obtained by vibrating sample magnetometry at INESC-MN, unless indicated otherwise.

| Label | Manufacturer | Diameter (nm) | Magnetization (kA/m)[a] | Susceptibility[b] | Material[c] |
|---|---|---|---|---|---|
| 4SP NiFe powder[d] | Novamet | 3300 | 5.00 | 4.2 | $Ni_{70}Fe_{30}$ (~100%) |
| Dynal M-280[d] | Dynal Biotech | 2800 | 0.40 | 0.35 | FeOx (17%) |
| Micromer-M | Micromod | 2000 | 0.48 | 0.22 | FeOx (15%) |
| CM01N/7228[e] | Bangs Laboratories | 860 | 1.88 | 1.57 | FeOx (27.5%) |
| CM01N/7024[e] | Bangs Laboratories | 350 | 0.99 | 0.825 | FeOx (45.8%) |
| Nanomag-D | Micromod | 250 | 20.10 | 4.81 | FeOx (75%) |
| Nanomag-D | Micromod | 130 | 17.80 | 4.44 | FeOx (75%) |
| Nanomag-D-spio | Micromod | 100 | 0.34 | 0.28 | FeOx (35%) |
| Nanomag-D-spio | Micromod | 50 | 0.85 | 0.71 | FeOx (35%) |

[a] Magnetization per particle at an excitation field **H** of 1.2 kA/m.

[b] Average susceptibility for $1 < |\mathbf{H}| < 4$ kA/m.

[c] FeOx represents $\gamma$-$Fe_2O_3$ and $Fe_3O_4$. % values represent the magnetic content of the particles (data from supplier).

[d] Magnetization and susceptibility values were taken from magnetization curves shown on (Rife *et al.*, 2003).

[e] Magnetization values were estimated from data shown in (Schotter *et al.*, 2004) admitting a constant susceptibility from 0 to 40 kA/m.

Note that 130 and 250 nm (Nanomag-D) particles and 2 µm microspheres (Micromer-M) do not show a pure paramagnetic behavior at low applied fields as they do not fit the Langevin equation in this regime (Freitas *et al.*, 2004).

$$M = M_S\left[\coth(qH) - \frac{1}{qH}\right] \tag{19}$$

In equation (19), M is the magnetization of the label, $M_S$ is its saturation magnetization, H is the applied field and $q = \mu_0 m_p / k_B T$, where $\mu_0$ is the magnetic permeability in vacuum ($4\pi \times 10^{-7}$ T m/A or H/m) and $m_p$ is the average moment of each nanoparticle that comprises the label.

These labels show an increased magnetic susceptibility near zero, which may be the consequence of interacting smaller nanoparticles that comprise the larger ones (fig. 2.22 and 2.23).

In figure 2.23 it is further shown the susceptibility for highly permeable homogeneous paramagnetic or soft ferromagnetic multidomain particles. In these cases, the magnetization of the particle scales with the applied field, like (Jackson, 1975):

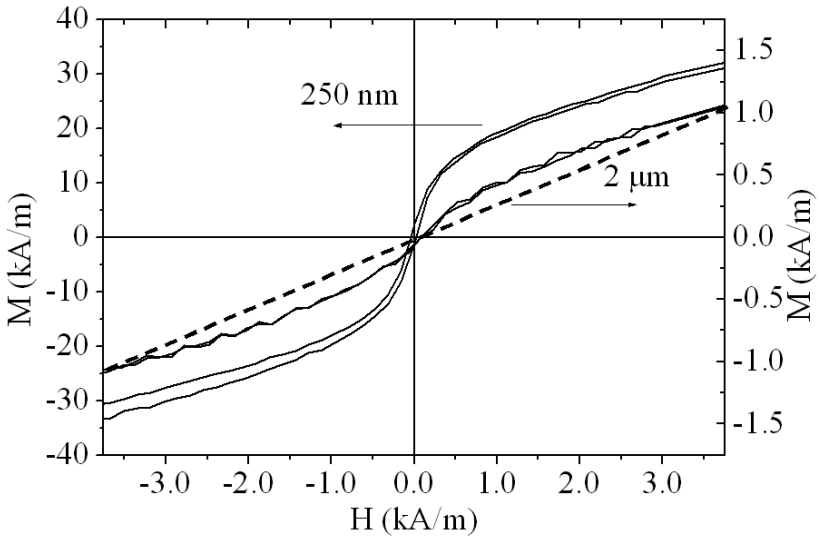


Fig. 2.22. Magnetization curves for 2 μm microspheres and 250 nm diameter nanoparticles in the low field regime. It is observed an increased magnetic susceptibility near zero applied field and in, particular, for smaller particles. Pure paramagnetic behavior is represented by a dashed line.

$$M = 3\frac{\mu - 1}{\mu + 2} H \qquad (20)$$

Here μ is the magnetic permeability of the medium. Resulting for high permeability materials, M = 3 H. This is the paramagnetic limit and shows that the magnetic particles

used have indeed a non-paramagnetic behavior, either they show an increased susceptibility at low fields (130 and 250 nm diameter labels) or show reduced susceptibilities as a result of large demagnetizing fields within the magnetic grains (remaining particles) (see also table IV and fig. 2.22).

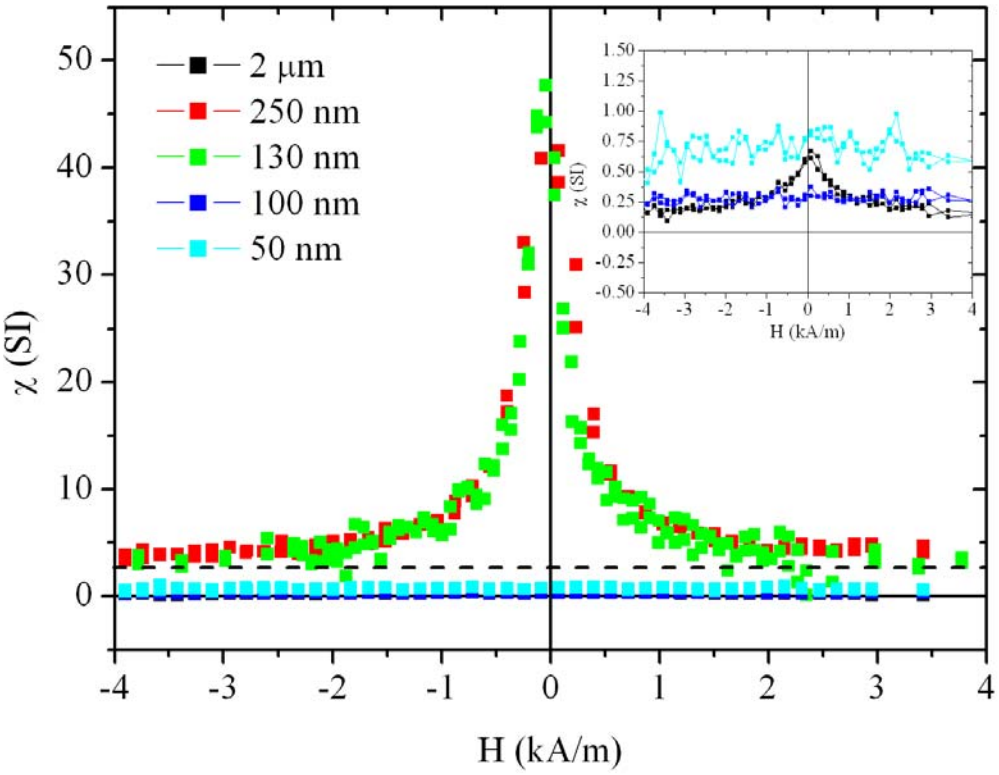


Fig. 2.23. Experimental magnetic susceptibility of studied FeOx based magnetic particles and beads. The dashed line is the susceptibility of a homogeneous, highly permeable magnetic sphere in a magnetic field ( $\chi = 3$). Inlet shows curve for 2 μm microspheres and 50 and 100 nm particles.

These labels possess a small magnetic moment (or magnetization per particle volume, see previous section) for relatively low excitation fields. Consequently, very small magnetic stray fields are created that must be detected by the magnetoresistive transducers. Nevertheless, these sensors are quite sensitive and the detection of single magnetic microspheres has already been demonstrated (Graham *et al*., 2002).

The size and moment of the magnetic labels limit the dynamic range (maximum and minimum number of particles that can be detected) together with the sensor characteristics and the experimental setup (see further discussion on chapter 6).

Figure 2.24 shows the magnetic moment per label in function of the mass of iron oxide calculated from supplier's data. The studied particle show a linear relationship between these two quantities, as expected for labels made up of the same FeOx material. In addition, the detection limits for different experimental setups and operation conditions.

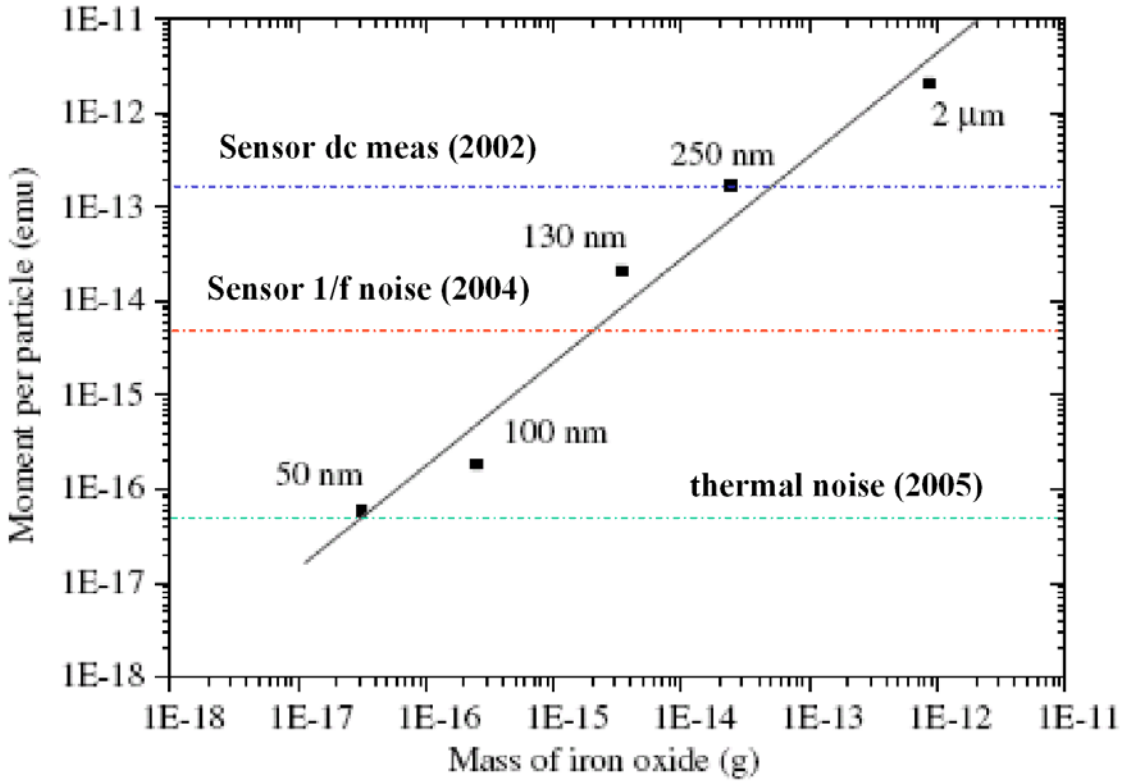


Fig. 2.24. Magnetic label moment at 1.2 kA/m magnetizing field in function of the mass of iron oxide for Micromod particles of sizes ranging from 50 nm up to 2 µm. Also included detection limits for: direct current measurement setup (see chapter 6); estimated sensor 1/f noise at 30 Hz, using an ac measurement setup; and thermal noise estimation based on noise spectra measurements of spin valve transducers (see section 2.1 and chapter 5).

Using the simplest direct current (dc) measurement setup, the noise of the apparatus corresponded to the detection of a single 250 nm diameter label (Ferreira *et al*., 2003), which at the time was difficult to confirm experimentally and optically due to the very small size of these labels. Nevertheless, single 2 µm spheres were clearly detected with the 2 µm × 6 µm spin valve sensors (see chapter 7 and Graham *et al*., 2002).

Later on, using an ac measurement setup, the intrinsic 1/f noise of the same sized spin valve transducer was calculated for an operating frequency of 30 Hz and a lock-in integration time of 300 ms, and a sense current of 1 mA (see chapter 6 and Freitas *et al*.,

2004). Although, the intrinsic noise shows that the detection of single 130 nm labels would be possible, the noise of the apparatus was considerably higher but enabled the detection of single 250 nm labels (see chapter 7).

Finally, based on measured sensor spectra for larger 2.5 μm × 80 μm spin valve sensors (Ferreira *et al*., in press) the thermal noise for a 2 μm × 6 μm spin valve sensor operating at 1 mA sense current. This represents the lowest possible noise for the sensor, but measuring frequencies above the 1/f knee (1 kHz) are required. If this is accomplished then the detection of 50 nm diameter labels is possible.

Furthermore, if 10 mA sense currents are used instead then magnetic fields 10 times smaller can be sensed, and consequently the detection of smaller iron oxide labels is within reach. The increase in current though, translates into the increase of the 1/f knee (100 kHz) (see further on chapter 5 and Ferreira *et al*., in press).

From the results of the spin valve sensors alone, it can be seen that the spintronic biochip system has the potential for detecting single biomolecular interactions, something that is not within reach of traditional sensing techniques (see also discussion on sections 2.1.7 and 2.1.8).

## 2.3 Microfluidics

Microfluidic devices were first developed at INESC-MN in 2002, as a need to control fluid flow on magnetoresistive biochips.

### 2.3.1 Overview

Micro and nanofluidics is the scientific area that studies fluid flow and fluid properties at the small scale. Unlike at the macroscale, fluid behavior is determined by surface forces and interfaces rather than by volume forces such as gravity and other inertial forces. Capillary forces and surface tension; ionic strengths; the hydrophilic or

hydrophobic nature of the different molecules; and other intermolecular forces such as Van der Waals forces, hydrogen bonds, and salt bridges are now the dominant effects.

This “new” field of knowledge is giving rise to novel and interesting applications and is also providing new insights into biological systems, as they “work” at these same scales.

Microfluidics is naturally important in chemical and biotechnological applications (Berthier and Silberzan, 2006), as most samples are liquid and/or the biochemical species or reagents are diluted in a buffer fluid or carrier liquid. Microfluidics is then a key component in micro-Total Analysis Systems (μTAS) or Lab-on-a-Chip devices, where unitary chemical and biochemical operations, such as sample preparation, purification, mixing, reactions, separation and fraction collection are integrated into a single device (Geschke *et al*., 2004; Chován and Guttman, 2002; Ahn *et al*., 2004).

Lab-on-a-Chip devices usually include not only microfluidics but also electronic, optical and mechanical components, such as sensors, heaters, valves, pumps, mixers, and others. In fact, this is a highly interdisciplinary technology that promises to revolutionize the way that chemistry and biology are done (Erickson and Li, 2004).

The most immediate advantages of these miniaturized systems are reduced sample and reagent consumption, minimization of waste production, high portability, efficient heat dissipation due to large surface-to-volume ratios, high control on reaction parameters such as temperature, pH and kinetics, fast responses and finally low-cost.

Many different materials have been used and different approaches have been taken for the fabrication and operation of these microfluidic devices.

Typical materials include: glass and quartz; polymers, such as polydimethylsiloxane (PDMS), polymethylmetacrylate (PMMA), polycarbonate (PC), polyimide (PI) and others; silicon and ceramic composites. Glass and quartz are chemically inert and biocompatible but are also expensive. On the other hand, polymers can be made also inert and biocompatible but can be fabricates at a much lower cost, making them suitable for large-scale production and fabrication of disposable devices. Finally, silicon

has the advantage that can add extra functionality to these devices, such as integrated sensing and control of analytes, pH, temperature, etc.

The fabrication techniques and functionalities depend clearly on the material chosen and frequently hybrid-devices showing combined properties are devised and fabricated.

These devices can be designed for different application and with different sample and fluid handling techniques in mind. These include mainly pressure-driven and electroosmotic flow-based systems, and also electrophoresis, dielectrophoresis, immunochromatography, magnetic (Gijs, 2004; Pamme, 2006) and diffusion based schemes (see for details Ferreira, 2006).

When fluid flow is controlled by exerting a force on the fluid it said that the transport of biomolecules is direct, of which pressure-driven (mechanical actuation) and electroosmotic flow (electric actuation) are the best known examples. On the other hand, when no force is applied, biomolecules diffuse in solution. This type of transport is thus known statistical transport as it is entropy-driven. In reality, even in a direct transport based device diffusion will be observed. Nevertheless this latter transport can be controlled by the design and operation of the microfluidic system (Geschke *et al*., 2004).

In addition, each of the referred fluid control schemes may require a particular design and/or actuators such as pumps and valves to properly handle fluid and mixers to promote biochemical reactions.

Fluid flow is characterized by the Reynolds number:

$$Re = \frac{\rho D_h v}{\eta} \qquad (21)$$

Here, $\rho$ is the density (1 g $cm^{-3}$ for water at 20 ºC) and $\eta$ is the viscosity ($10^{-2}$ g $cm^{-1}$ $s^{-1}$ for water at 20ºC) of the fluid. v is the average fluid velocity and $D_h$ is the characteristic or hydraulic diameter of the microstructure, which is given by:

$$D_h = \frac{4A}{P_{wet}} \tag{22}$$

Where A is the cross-sectional area of the structure and $P_{wet}$ is the wetted perimeter (the entire perimeter that is in contact with the fluid). For a cylindrical tube then, $D_h$ is equal to the geometrical diameter.

Empirical studies have shown that for Re < 2000 the flow is laminar (which happens in most of the cases at the microscale), whilst for values between 2000 and 3000 the flow regime is called transitional and above 3000, the flow is turbulent.

As mentioned above transport of biomolecules in microfluidic system is usually of two types: statistical, if there is diffusion of the biochemical species in the liquid phase; and direct, if the fluid movement is controlled by an externally applied force. In this latter case biomolecules move with the carrying fluid.

For the statistical transport the Einstein-Smoluschowski relation for the random Brownian motion is taken into account:

$$\Delta x = \sqrt{2D_{diff}t} \tag{23}$$

Where $\Delta x$ is the average distance moved after an elapsed time $t$ between molecule or particle collisions and $D_{diff}$ is the coefficient of diffusion of the particular entity, which can be estimated from the Stokes-Einstein equation:

$$D_{diff} = \frac{k_B T}{6\pi\eta r} \tag{24}$$

Where $k_B$ is the Boltzmann constant ($1.38\times10^{-16}$ erg $K^{-1}$ or $1.38\times10^{-23}$ J $K^{-1}$), $T$ is the temperature, $\eta$ is again the viscosity of the carrying fluid and $r$ is the hydrodynamic radius of the molecule or particle.

Typical diffusion coefficients for small biochemical species are in the order of $10^{-5}$ and $10^{-6}$ $cm^2$ $s^{-1}$ (Freitas Jr., 1999).

The overall effect of random motion of particles results in temporal and spatial changes in the concentration of a particular analyte. This is translated by the Fick's law of diffusion:

$$J = D_{diff} \frac{\partial C}{\partial x} \tag{25}$$

Where $J$ is the flux of the analyte, that is, the number of molecules crossing a certain cross-sectional area $A$ during a time span $t$, and $C$ is the concentration of the analyte.

The time that a molecule or biochemical species would take to travel within a microfluidic device can be calculated from equations (23) and (24). Times can range from a couple of seconds to hours or days, depending on the size of the fluidic structures (see next subsection). As such, diffusion is not suitable as a driving mechanism for most of the envisioned applications.

Other more efficient transport mechanisms comprise hydrodynamic or pressure-driven and electric field based transport. Here only, hydrodynamic flow is discussed, since it was the transport mechanism used experimentally, the other transport mechanisms are discussed in detail elsewhere (Geschke *et al*., 2004; Ferreira, 2006).

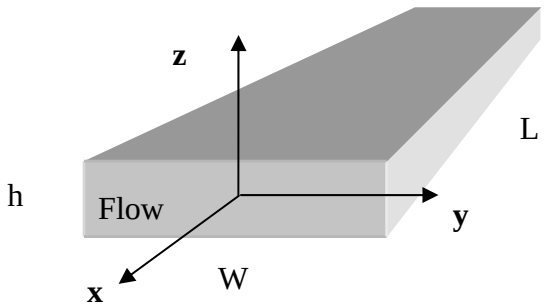


Fig. 2.25. Schematic of a microchannel structure of rectangular cross-section and with length L, width W and height h. Here a low-aspect ratio is considered (W >> h). The axis origin in the geometrical centre of the cross section and the fluid flow is along the x direction.

Hydrodynamic transport results from pressure gradients between the ends (inlet and outlet) of a microfluidic structure. Fluid flows from the high-pressure to the low-pressure ends carrying biomolecules and other analytes with it.

Considering a microchannel structure with a rectangular cross-section, as shown in fig. 2.25, and assuming a laminar flow, then the velocity distribution in the cross-section is given by (White, 1974):

$$v(y,z)=\frac{4W^2}{\eta\pi^3}\left(-\frac{dp}{dx}\right)\sum_{i=1,3,5,\ldots}^{\infty}(-1)^{(i-1)/2}\left[1-\frac{\cosh(i\pi z/W)}{\cosh(i\pi h/2W)}\right]\frac{\cosh(i\pi y/W)}{i^3} \qquad (25)$$

Here dp/dx is the pressure gradient between the inlet and the outlet of the microchannel. It was further assumed that steady flow was developed at the some region away from the channel's ends, that an incompressible and Newtonian fluid (such as water) was used, and that the fluid velocity at the channels' walls is null (non-slip condition) (see for details White, 1974; Parracho, 2002).

Equation 25 is quite complex as it results from the application of Navier-Stokes equation to a rectangular cross-sectional channel, under the above assumptions. Nevertheless, for simple geometries such as cylindrical structures the expression is quite simpler (see Geschke *et al*., 2004; Ferreira, 2006). Further, the above equation results in a parabolic flow profile typical of hydrodynamic transport (see next subsection).

From the flow velocity distribution the mean velocity v at equation 21 can be calculated. In addition, the flow rate Q can be determined:

$$Q = vWh \qquad (26)$$

Typical flow rates are of the order of 0.01 to 10 μL $min^{-1}$, which correspond to average flow velocities of the order of 10 μm $s^{-1}$ to 1 cm $s^{-1}$ for low cross-sectional area structures such as the one discussed in front (Ferreira, 2006). These flow rates depend of course on the pumping system.

Mechanical pumping usually relies on variety of pumps, either external or integrated on chip, based on a variety of physical mechanisms: piezoelectric, electrostatic, magnetic, thermal and peristaltic (see for details Geschke *et al*., 2004). These systems offer a pulsating flow, which may result in some back flow that could be disadvantageous for the control and the progress of some biochemical reactions. Other systems based on syringe pumps, constant-pressure gas reservoirs, centrifugal forces, and the already mentioned electrically-driven transports can provide a steady non-pulsating flow.

In addition, other components are often present to control the direction of the fluid flow, the valves. These are discussed in detail elsewhere (Geschke *et al*., 2004; Ferreira, 2006).

### 2.3.2 Study and Use of Microfluidic Structures

In the work done during this thesis, microfluidic structures were used for sample transport and for paving the way for the integration of the magnetoresistive biosystem (see further on chapter 8 and Tamanaha *et al*., 2002).

Microchannels, 25 μm high, 100 μm wide and about 3 mm long, were fabricated in PDMS by a molding technique (Duffy *et al*., 1998) and assembled on top a magnetoresistive chip design for the effect (see chapter 5; Parracho, 2002 and Ferreira *et al*., 2004). Inlet and outlet reservoirs were 2 mm in diameter (see fig. 5.7).

Given these dimensions the transport by diffusion can be quite slow and thus unsuitable for the applications in mind (see table V).

The flow velocity profile was calculated for a cross-section of a microchannel of the above mentioned dimensions and for water at 20 ºC using a program made in IDL 5.4 (RSI).

Table V. Calculated diffusion times for small biochemical species along the dimensions of a microchannel. Diffusion constants in the order of $10^{-5}$ to $10^{-6}$ $cm^2$ $s^{-1}$ were considered (Freitas Jr., 1999).

| Channel dimension | Diffusion time |
|---|---|
| Height = 25 µm | 30 s to 5 min |
| Width = 100 µm | 8 min to 1h30 |
| Length = 3 cm | > 1week |

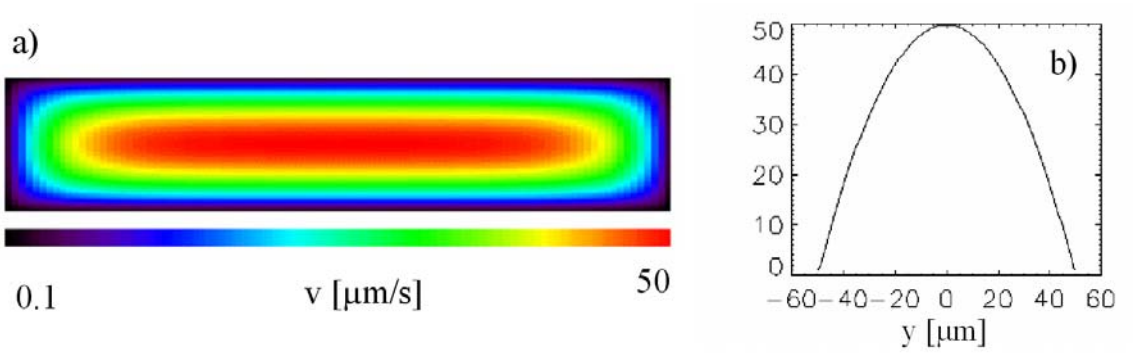


Fig. 2.26. a) Calculation of the velocity profile (equation 26) at the cross-section of a microchannel of dimensions of 25 µm height and 100 µm width. b) Parabolic velocity profile through a cut at half-height.

The hybrid microchannel-magnetoresistive device was used to experimentally measure the flow velocity of the fluid by measuring the passage of an ensemble of 250 nm magnetic particles (Nanomag-D, see previous section) over two 2 µm × 6µm spin valve sensors separated from each other by ~1.65 mm. The particle solution was pumped through the microchannel using two syringes and applying manually a differential pressure to the reservoirs (see chapter 6).

Flow velocities of 50 to 250 µm $s^{-1}$ were measured, corresponding to a Reynolds number ~$10^{-3}$ (see chapter 7) and applications, other than integration in magnetoresistive biosensing system, were envisioned. These include a system for imaging fluid flow using an array of spin valve sensors; the development of a feedback system for controlling fluid flow; and the measurement of fluid properties (like viscosity) of liquid samples such as blood, plant sap or other (Ferreira *et al*., 2004).

This system was quite innovative, as it provided a means to measure flow velocity using a direct electrical measurement, instead of relying on the traditional complex and

expensive optical systems (Ferreira *et al*., 2004). This approach was already followed and cited by others (Pekas *et al*., 2004; Pamme, 2006; Salgado *et al*., 2006).

Further tests and approaches on microfluidic device fabrication done at INESC-MN can be seen elsewhere (Parracho *et al*, 2002).

Finally, during microfluidics studies in 2002 I envisioned a micro-scale analog to a magnetic stirred device used typically in bioreactors. A magnetic micro-mixer was then designed and fabricated. Tests showed that some improvements were required with respect to design and operation, namely the need to create higher on-chip magnetic fields and probably the use of larger particles or long magnetic nanowires could be advantageous (Parracho, 2002).

## 2.4 Magnetic Transport Systems

### 2.4.1. Overview

One of the greatest advantages of using magnetic particles as biomolecular labels is the ability to control and to manipulate them on-chip.

Several devices were fabricated to move and place magnetic particles on specific regions on chip.

Harvard University used serpentine wires in combination with an external permanent magnet to move magnetic particles in 1 dimension (Deng *et al*., 2001). Another group at the same university used metal rings to focus magnetic particles and magnetotatic bacteria inside the microfabricated structure, and a microelectromagnet matrix to control labels with micrometer precision (Lee *et al*., 2001).

Later on, work at INESC-MN resulted in the development of tapered metal line designs that enabled the control and detection of single magnetic microspheres (Graham *et al*., 2002) and ensembles of nanoparticles (Lagae *et al*., 2002). The tapered design further

evolved at IMEC to a unidirectional magnetic transport system, using saw tooth shaped metal lines (Wirix-Speetjens, and de Boeck, 2004; Wirix-Speetjens *et al*., 2005).

Inspired also by the tapered design, the University of Bielefeld developed a magnetic particle-based mixer that very closely resembles what I proposed in 2002 (Parracho, 2002), when I thought of an analog of a magnetic stiring device used in bioreactors, but now at the microscale (see previous subsection). The group at the Universisty of Bielefeld further developed a kind of ring structure with kinks in the inner diameter, which were used to capture single microparticles (Brzeska *et al*., 2004)

At the same time at INESC-MN, a u-shaped metal line structure was developed, which in combination with external applied magnetic fields enabled the focusing of magnetic labels in on-chip areas of about 1000 $\mu m^2$.

Nevertheless, the importance of these structures is beyond manipulation of simple magnetic particles. When beads are functionalized with biomolecules, magnetic fields can be used as a means to manipulate biomolecular interactions. As shown by the NRL, magnetic fields can be used as a stringency method in bioassays. Magnetic fields acting upon magnetically-labeled biomolecules create a force that can distinguish between target molecules that are specifically or unspecifically bound to the probe molecules at the surface (Baselt *et al*., 1998; Lee *et al*., 2000).

Using again the same principle, the Univesity of Bielefeld studied and quantified the intermolecular forces between biotin and streptavidin, by creating on-chip forces created by a metal conductor to pull streptavidin-coated magnetic labels bound to a biotinylated surface (Panhorst *et al*., 2005).

In addition, at INESC-MN, using on-chip tapered conductors that created higher magnetic field intensities and gradients at the sensor site, enabled the interaction between complementary DNA strands to occur in only a few minutes, in comparison, with normal time scales of 3 to 12 hours (Graham *et al*., 2005). Later on, using the u-shaped metal current lines frequency dependent biomolecular interactions was shown in time scales of minutes also (Ferreira *et al*., 2005b, 2005c).

On-chip magnets and electromagnets have also been used for magnetic particle patterning (Yellen *et al*., 2005) and in combination with microfluidic structures for separation (Tondra *et al*., 2001; Smistrup *et al*., 2005) and analysis (Choi *et al*., 2000, 2002), and also for a number of novel applications (Gijs, 2004; Pamme, 2006).

All these approaches are based on the creation of on-chip magnetic field gradients that attract magnetic labels to the minimum energy state of the magnetic energy of the system $E_m$:

$$E_m = -(\mathbf{m} \cdot \mathbf{B}) \tag{27}$$

Where m is the magnetic moment of the label and B is the magnetic field induction, with $B = \mu_0 H$, where H is again the magnetic field intensity.

The magnetic force $F_m$ acting on the particles is then:

$$\mathbf{F_m} = \nabla(\mathbf{m} \cdot \mathbf{B}) \tag{28}$$

The magnetic moment on the other hand is given by $\mathbf{m} = V \chi_m \mathbf{H}$, with V the volume of the label, and $\chi_m$, the magnetic susceptibility of the particles. In the simplest case where $\chi_m$ is constant within a certain field range, the magnetic force is given by:

$$\mathbf{F_m} = V\chi_m \nabla(\mathbf{H} \cdot \mathbf{B}) \tag{29}$$

However, this is not the case for some of the labels studied under low applied magnetic fields (see section 2.2 on magnetic labels).

Although for these small micrometer and nanometer particles the gravitational force and impulsion are negligible, the forces due to drag from the fluid and from the interaction with the chip surface are of utmost importance for on-chip particle movement.

Label-surface interactions encompass Van der Waals, hydrogen bonds, and mainly electrostatic forces. These depend on temperature and pH, and on the

hydrophobic/hydrophilic nature of both particle and chip or channel surfaces. A study on some of these effects was done recently (Wirix-Speetjens *et al.*, 2005).

A simpler analysis can be made by considering only magnetic, $F_m$, and drag, $F_d$, forces. Considering a spherical particle, the drag force is given by:

$$\mathbf{F_d} = 6\pi\eta r\mathbf{v} \tag{30}$$

Again, $\eta$ is the viscosity of the carrier fluid ($\sim 10^{-3}$ Kg $m^{-1}$ $s^{-1}$ for aqueous solutions), and r is the (hydrodynamic) radius of the particle.

The equations above will be used in the following section.

### 2.4.2. Study and Use of On-Chip Magnetic Transport Systems

The work on on-chip biomolecular transport using magnetic particles as carriers started at INESC-MN in 2000 (Ferreira, 2000). The approach followed from the start was to combine the transport and the detection of magnetic labelled biomolecules. This strategy was unique and has characterized the work developed at INESC-MN. It further inspired another research group from IMEC, which collaborated with us in the scope of a summer internship, and within an European project.

The main advantage of direct transport of biomolecules onto sensing sites is to overcome mass-transport limitations. In typical bioassays, target biomolecules usually diffuse in solution until finding, and interacting with, the surface-immobilized probes.

Diffusion limits the analyte detection limit for reasonable assay times (Sheehan, and Whitman, 2005). For instance, conventional DNA microarrays require overnight time-scales for incubation of target solutions with the probe arrays (Pappaert *et al.*, 2003). This will be further discussed later on chapter 4.

The first structure to be designed and fabricated was a simple metal line structure (see fig. 4.5). The field created by this line can be calculated from the Biot-Savart law (see equation 13), and is shown in figure 2.27 (calculation made in Mathematica software).

It was observed that this line structure created an on-chip magnetic field gradient, enough to attract a prototype sample of 400 nm magnetic labels (Micromod). In fact, it was observed that particles were attracted preferably to the edges of the line, where the generated magnetic field is also highest (see fig. 2.27).

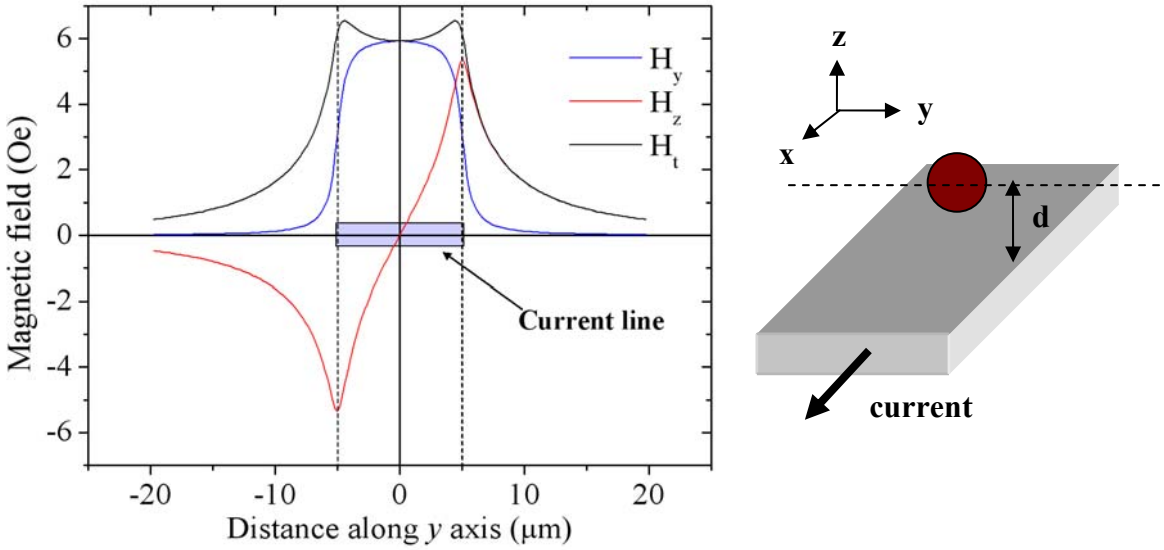


Fig. 2.27. Magnetic field created by a current line 300 nm thick, 10 µm wide and 100 µm long transversed by a direct current of amplitude 10 mA. Both $H_y$ and $H_z$ components of the field were calculated, as well as the total field intensity $H_t$, along the *y* axis at half structure length (dashed line) and at a distance *d* from the line surface of 300 nm + 125 nm, which corresponds to the sum of the thickness of a passivating oxide layer with half the diameter of a 250 nm magnetic particle (see right-hand-side scheme).

Later on, this design evolved into a structure that was tapered from 150 µm at the contact leads down to 5 µm at a central region, adjacent to a sensing element (see fig. 2.28 and fig. 4.9). The narrower part of the line is transversed by a higher current density, and consequently (equation 13) generates a higher magnetic field and a higher magnetic field gradient.

This tapered structure was then used to focus magnetic particles and labels at a small on-chip region. The use of two adjacent tapered current lines, by turning on and off alternatively each one of them, enabled the controlled movement of the labels between

the lines (see fig. 2.29). Furthermore, it enabled the manipulation of individual microspheres over a spin valve sensor (see chapter 7; Graham *et al*., 2002).

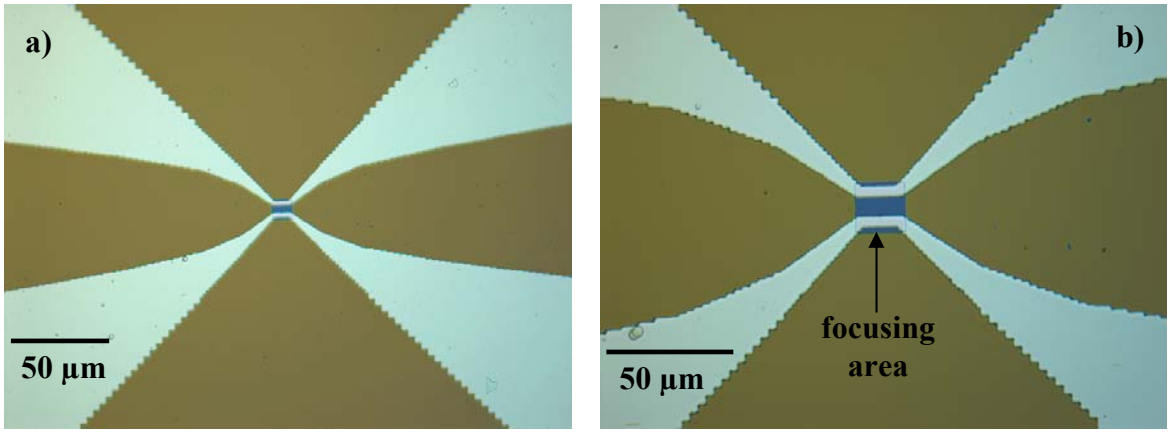


Fig. 2.28. a) Tapered current line design: metallic lines are tapered in width from 150 µm at the pads to 5 µm at a central region. b) Close-up, showing central region where magnetic labels are focused (20 µm × 20 µm area) and where magnetic sensors are fabricated (see fig. 4.9); adjacent 5 µm wide lines are 10 µm away from each other.

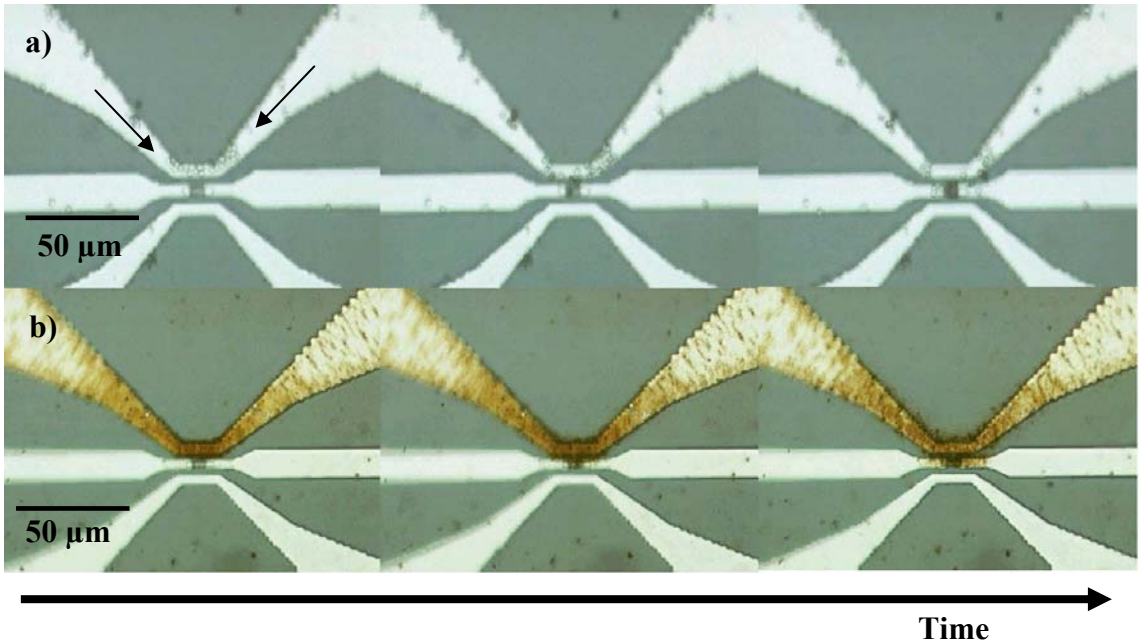


Fig. 2.29. Time-sequences for the movement of a) 2 µm microspheres and b) 250 nm particles between a tapered current line and a spin-valve sensor and sensor leads.

Figure 2.29 shows two time-sequences taken from a video of 2 µm (top) and 250 nm (down) particle movement. In the first frame, the top tapered current line is on and attracts particles from the wider regions to the narrowest region of the line. In the second frame the current line is turned off and magnetic particles start to jump to the

sensor and sensor leads that are also transversed by current. In the third frame particles completely cover the sensor. In subsequent frames (not shown) the top current line was turned on again and particles jumped back to its narrowest region, adjacent to the sensor.

In the experiments shown, a direct current of 40 mA was applied to the top current line, while the bottom current line was turned off. Meanwhile, the sensor was also transversed by current (8 mA), which in itself created a local magnetic field and magnetic field gradient (see equation 13 and discussion on section 2.1.6). Consequently, the transducer is a magnetic transport system in its own right, as labels are attracted to it.

Nevertheless, it was observed that in particular experimental setup conditions the use of external magnetizing fields opposite to the sense current field results in the repulsion of labels from the sensor (Ferreira *et al*., 2005a).

In addition, by turning on the bottom current line and turning off the top line and vice-versa, the movement of particles back and forth between the lines was observed. This mechanism further inspired a new design (see below).

This magnetic focusing system was, in addition, compared to the electrical transport of a DNA using the same structure. For this simple comparison a single DNA strand, 100 nucleotide-long, was considered either free in solution for electrical transport, or magnetically labeled with 2 μm microspheres and 250 nm nanoparticles from Micromod (see chapter 2). The comparision was made using finite-element commercial software (QuickField 4.3, Tera Analysis).

DNA has a phosphate-sugar backbone that is charged negatively due to the presence of a single unpaired electron on the phosphate group (see Voet *et al*., 1999; Cooper, 2000 and also chapter 3). Consequently, a 100-mer has a charge Q of 100 e, where e is the electron charge ($1.6\times10^{-19}$ C). On the other hand each nucleotide has an average mass of 300 Da, so the total mass of the DNA strand is about 30 kDa (see fig. 2.30).

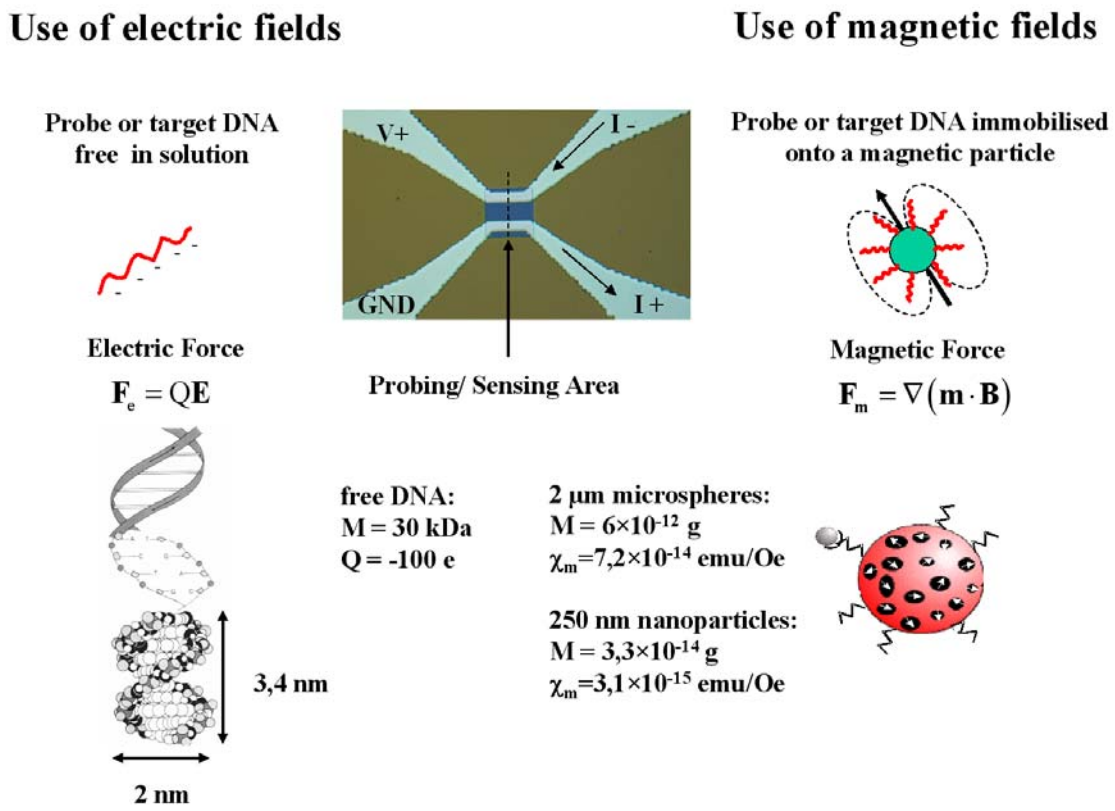


Fig. 2.30. Parameters and conditions for the calculation of electric field (left-hand-side) and magnetic field (right-hand-side) based on-chip transport of biomolecules using the tapered line structure of fig. 2.28.

Figure 2.30 shows the conditions, the properties of biomolecules and carriers (taken from Freitas *et al.*, 2004), and the intervening forces used on the electrical (left-hand side) and magnetic (right-hand-side) based transport systems.

In electric field based transport, each of the tapered lines was considered to work as an electrode, one is set at a positive voltage and the other is grounded (or applied a negative voltage). The free negatively charged oligos are attracted by an electric force $\mathbf{F_e} = Q\,\mathbf{E}$, where **E** is the electric field created between the two electrodes. In the calculation using the finite-element software a 1V difference between the electrodes was considered.

On the other hand, on the magnetic field based transport currents are applied in the tapered lines. In the calculation currents of 45 mA through each line were considered and the direction of the current was set to be opposite such that the created magnetic fields would sum up at the middle region between the lines. Furthermore, a constant

magnetic susceptibility per label was assumed and corresponds to the average susceptibility determined for the used particles (see table IV and Freitas *et al*., 2004).

Table VI. Results from finite-element calculations of tapered line system used for electric field or magnetic-field based transport of biomolecules. Magnetic labels of 2 μm and 250 nm diameter were used in the calculations.

| | **Electric Field** | | **Magnetic Field** | |
|---|---|---|---|---|
| Distance to chip surface | 1 μm | 10 μm | 1 μm | 10 μm |
| **E** (kV/m), **B** (mT) | 70.4 | 26.2 | 4.5 | 1.5 |
| $\mathbf{F_e}$, $\mathbf{F_m}$ (pN) | 1.13 | 0.42 | 0.91 (2 μm)<br>0.03 (250 nm) | 0.41 (2 μm)<br>0.02 (250 nm) |

Electric and magnetic forces acting upon the DNA strand and on the magnetic labels were calculated at a two distances from the chip surface, 1 and 10 μm over the sensing region and along a transversal cut, as shown in fig. 2.30 in a dashed line. The overall results are shown in table VI above.

Results show that, the forces created on-chip at the middle of the line structures are similar in both electric and magnetic cases. This shows that magnetic field attraction scheme should be as good as more conventional electric transport schemes. Note, that here, just for the sake of comparison, drag forces (see equation 30) were not included in the calculations.

In comparison with the electric field based transport, the magnetic transport has the inconvenience of requiring an extra magnetic labeling step, but has additional advantages such that it can be used to carry non-charged or low polarizability biomolecules, to be used in purification of biomolecules from a complex solution (Häfeli *et al*., 1997) and can be straightforwardly detected using integrated magnetoresistive sensors, as shown in this thesis.

Nevertheless, a combination of both electric (Fixe *et al*., 2004c, 2005b) and magnetic (Graham *et al*., 2002; Ferreira *et al*., 2005b) systems developed at INESC-MN for the transport of biomolecules was envisioned. This approach could result in combined advantages of both systems such as: probe immobilization (Fixe *et al*., 2003) in the

submicrosecond time-scales; biomolecular recognition in reduced times associated with magnetic-based purification; target mismatch discrimination (Fixe *et al.*, 2005a; Lee *et al*., 2000), and finally on-chip detection (Fixe *et al*., 2004d; Graham *et al*., 2004). Unfortunately this was never tested during this thesis. It would be worthwhile to test it in the near future.

Also, regarding the results on table VI, it is seen that forces acting upon the 250 nm particles are quite small. This is due to the fact that they possess a smaller magnetic moment per particle, but also because at the central region between the lines the magnetic field is almost constant. Nevertheless, increasing forces are generated closer to each line, especially near the edges, as mentioned above.

In fact, this effect can be used for the measurement of bond-forces of ligand-receptor pairs, as envisioned in the beginning of the magnetoresistive biochip project at INESC-MN. This has been shown recently by the Bielefeld group using line structures in adjacent configuration, in a similar manner as the one discussed above (Panhorst *et al*., 2005).

Biomolecular recognition forces were measured for biotin-streptavidin (55 and 245 fN) and biotin-avidin (16 and 58 fN) coupling. The measurements were in agreement with what was published with respect to the two-conformation binding systems, but the bond-forces were orders of magnitude lower than previous data. For instance, for the biotin-streptaviding coupling forces of about 260 pN were measured using atomic force microscopy (AFM) (Florin *et al*., 1994; Moy *et al*., 1994). Nevertheless, a dependence of the binding force on the loading rates has also been observed, and whereas AFM measurements have a loading rate up to 1 pN/s and higher, the use of current lines results in very low loading rate of 1 fN/s, which justifies the low values of the binding forces (Panhorst *et al*., 2005). Consequently, the magnetic transport system can be an interesting and powerful tool for biomolecular studies, and in particular for single biomolecular interactions (see chapter 8 and Graham *et al*., 2004).

Magnetic transport devices further evolved at INESC-MN as a need to suit a targeted application for the diagnostics of cystic fibrosis (see chapter 3). Since the diagnostics was based on the quantification of the expression of cystic fibrosis related genes, then a

higher dynamic range was required for the sensors, and consequently 2.5 µm × 80 µm spin valve sensors were developed (see chapter 4).

In order to focus magnetic labels at larger on-chip areas (1000 to 2000 $\mu m^2$) and to achieve higher biological sensitivities a new magnetic transport structure was designed and fabricated (see fig. 2.31), based on an initially studied ring structure (Feliciano, 2003).

These u-shaped current lines were used to focus and manipulate particles in the inside region of the line (see Feliciano, 2003; Ferreira *et al*., 2005b). It is in this region where a u-shaped spin valve sensor is fabricated for sensing applications (see fig. 4.14 and Ferreira *et al*., 2005c).

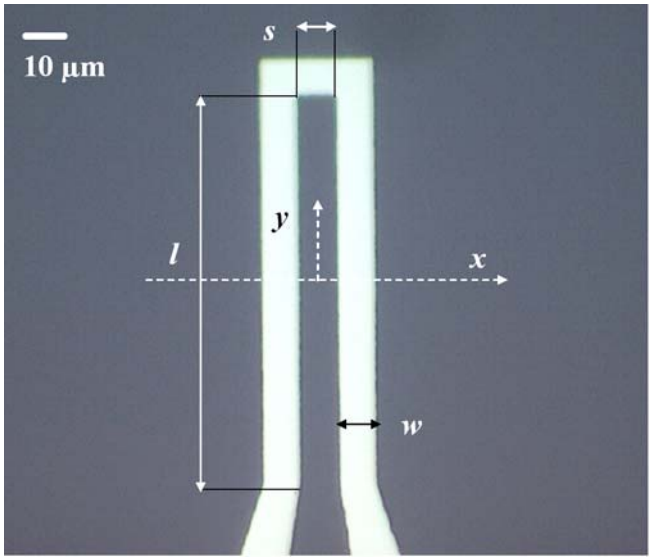


Fig. 2.31. U-shaped aluminum current line structure of width w = 10 µm, length l = 100 µm, thickness t = 0.3 µm and intra-line spacing s = 10 µm.

Magnetic label focusing method worked as schematized on fig. 2.32. First a dc current line was applied to the u-shaped metallic (aluminum) structure. This resulted in the attraction of particle to both arms of the line. Using a u-shaped design a single structure is able to attract particles to two parallel lines, whereas in the previous tapered line design two independent current lines were used. This is an advantage as it is a simpler system and saves outside contact pads (see design considerations on chapter 4).

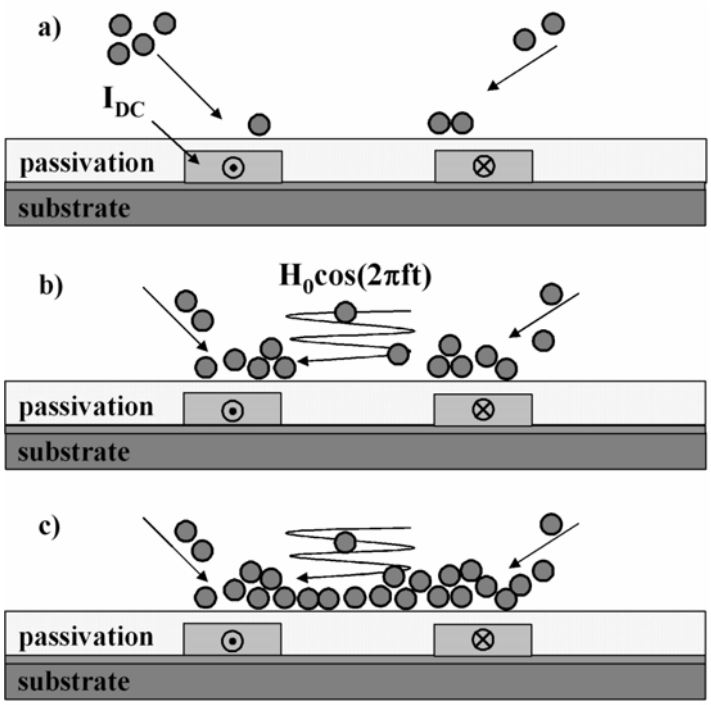


Fig. 2.32. Schematic of the focusing mechanism of the u-shaped current line structures. a) A dc current is applied to the u-shaped structure resulting in the attraction of magnetic labels towards both arms of the line. b) An external ac magnetic field is then applied, resulting in the movement of the particles between the arms of the line. c) Over time labels accumulate in the inside region.

Second, an external alternate current (ac) magnetic field at a particular frequency f and a magnitude $H_0$ was applied, which resulted in the back and forth movement of the particles between the lines. Finally, over time particles accumulate in the intra-line region, which corresponds to the sensing region of the magnetoresistive biochips (Ferreira *et al*., 2005c; Martins *et al*., submitted).

Figure 2.33 shows a time-sequence of the focusing of magnetic labels to the current line.

The back-and-forth movement can be explained by the motion of the particles to local energy minima (equation 27) that change in time from one arm of the line to the other. The combination of both the dc magnetic field created by the lines with the external ac magnetic field results in an alternating magnetic energy profile, as shown in fig. 2.34.

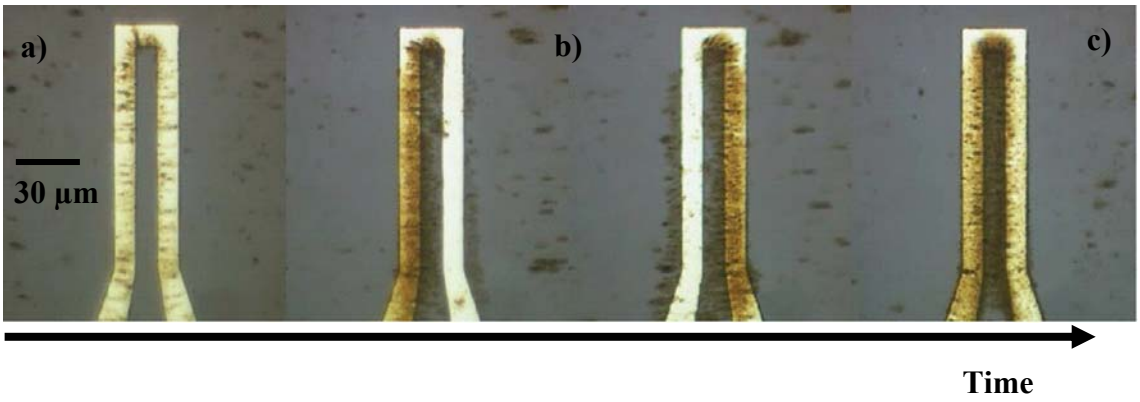


Fig. 2.33. Time-sequence of magnetic label focusing using the u-shaped current line structure. Frames a) at the left, middle frames b) and frame c) at the right correspond to a), b) and c) situations of the schematic on fig. 2.32.

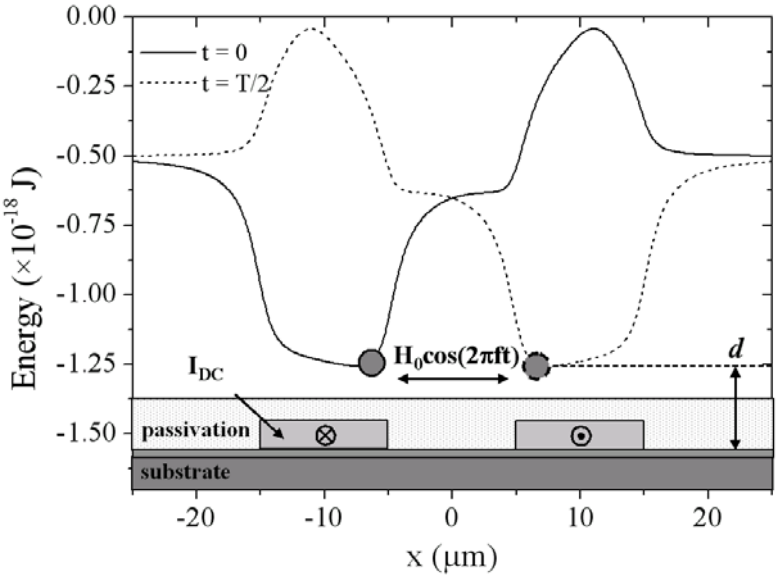


Fig. 2.34. Energy profile calculated along the *x* axis of fig. 2.31 for a nanoparticle at a distance *d* from the chip surface. The profile is shown for time t =0 and t=T/2, where and external 1.4kA/m rms field of frequency f =1/T is applied together with a 40 mA dc current through the u-shaped line. Line dimensions are the same as in fig. 2.31. The u-shaped line and the movement of a magnetic nanoparticle between energy minima are shown at the bottom of the figure.

In the energy calculation for figure 2.34, a sinusoidal external magnetic field $H_0$ cos ($2\pi ft$) of amplitude $H_0$ = 1.4 kA/m rms (17.5 Oe rms) was used together with a 40 mA dc current through the u-shaped line. Furthermore, the moment **m** was taken from the VSM measurement of the 250 nm particles by fitting the curve with a Boltzmann-like equation in Origin software (see fig. 2.22). Finally, the distance d (1.125 µm) was taken as the sum of thickness of the aluminium line, the thickness of the passivating oxide layer, the thickness of the layer of fluid and a half the radius of the nanoparticle. The

layer of fluid between the chip surface and the particle was considered because it was observed that when particles are settled down the movement is harder due to particle interaction with the oxide surface (see a study on surface-particle interactions in Wirix-Speetjens *et al*., 2005).

The alternating magnetic energy profile can result as well as from an ac current applied to the u-shaped line and an external dc field. This was observed experimentally using the same line structures and was further used later on with an integrated sensor for biomolecular recognition experiments (Ferreira *et al*., 2005c). In fact, the referred profile can result from different combinations of ac + dc currents and dc + ac external magnetic fields, such that other and more complex label manipulation can be achieved.

It was further observed that label movement was not only time dependent but also showed a dependency on the frequency of the external applied field. This effect could not be explained by the magnetic energy model alone. Consequently, particle dynamics was further studied taking into account both magnetic and drag forces (equations 28 and 30):

$$\mathbf{F} = \mathbf{F_m} + \mathbf{F_d} \Leftrightarrow m_p \mathbf{a} = \mu_0 \nabla \left( \mathbf{m} \cdot \mathbf{H} \right) + 6\pi\eta r \mathbf{v} \qquad (31)$$

Here, symbols are the same as defined above with $\mathbf{B} = \mu_0 \mathbf{H}$, and $m_p$ is the mass of the particle (with density 4 g $cm^{-3}$) and **a** is its acceleration. Finally, since **H** is the result of the sum of the dc and ac magnetic fields then **m** and **H** are both position and time dependent.

Figure 2.35 shows a numerical calculation of the average position and the motion amplitude of a nanoparticle along the *x* axis direction (see fig. 2.31) in function of the frequency of the external magnetic field. Calculations were made for different initial positions for the nanoparticle, either to the left (x < 0 μm) or to the right (x > 0 μm) of the centre of the u-shaped structure.

In the case that only the dc current is applied to the current line, then both arms attract the label the same way, but when an external dc (f = 0 Hz) field is applied the energy

minimum is located over one arm only (as in fig. 2.34) and the particle converges to this minimum (dc point in fig. 2.35).

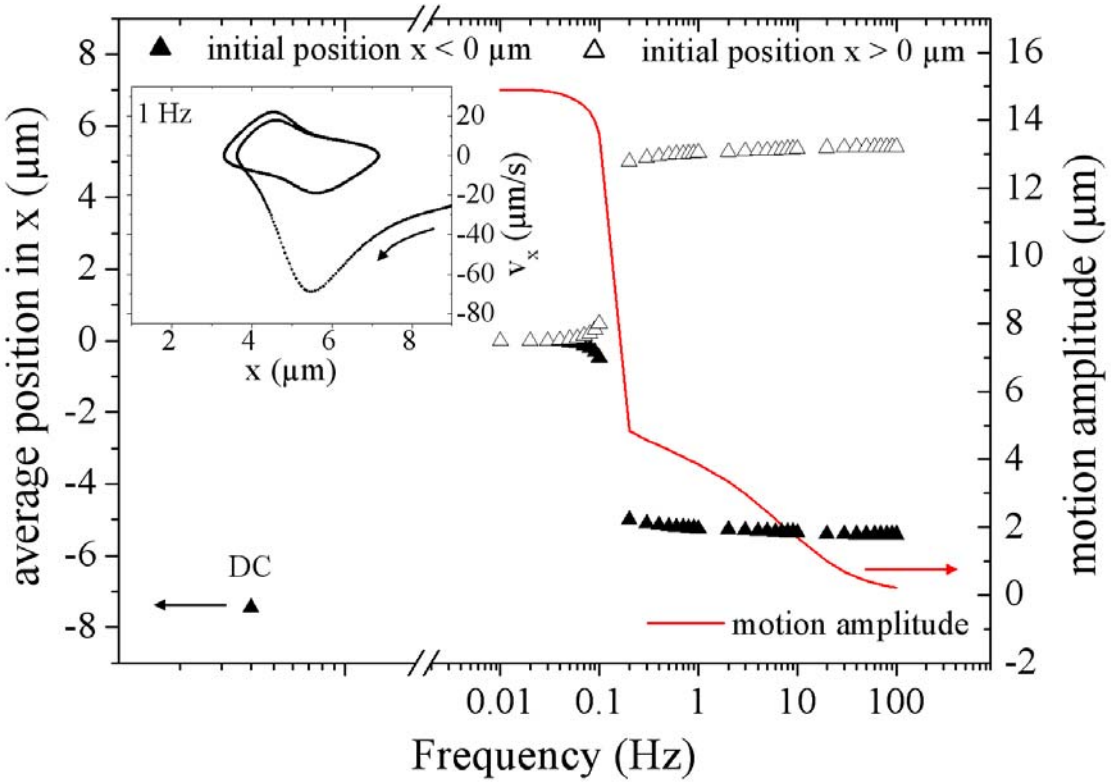


Fig. 2.35. Numerical calculation of the average position and motion amplitude of a 250 nm magnetic label along the *x* axis direction and in function of the frequency of the external magnetic field. Calculations were made in the conditions described in fig. 2.34 and for different initial positions for the nanoparticle, either to the left (x < 0 µm) or to the right (x > 0 µm) of the centre of the u-shaped structure of fig. 2.31. Inset: phase diagram for a magnetic field of frequency 1 Hz and an initial position for the nanoparticle to the right of the u-shaped line.

For ac fields of very low frequencies, up to ~0.1 Hz, the nanoparticle moves between the arms of the line with the frequency of the applied field: it moves between the energy minima which are distanced by ~ 15 µm, and accumulate inside it.

When higher frequencies are considered, then the external field changes sufficiently rapid such that the magnetic label is no longer able to move between the arms of the line. The particle oscillates closer to one of the arms, depending if its initial position was closer to one of the arms or the other.

Up to 1 Hz, the amplitude of the motion is still 4 to 5 μm but rapidly decreases to ~1 μm for a frequency of 20 Hz. Experimentally though, it observed that carrier accumulation in the intra-line spacing was still efficient within 5 min of ac field application.

In the inset of fig. 2.35, a phase diagram for 1 Hz applied field shows that the particle is attracted to the intra-line spacing region and remains oscillating around an equilibrium point at 5 μm with amplitude of ~4 μm.

In addition it is seen in the figure above that for even higher frequencies (> 30 Hz) the amplitude of vibration is progressively smaller. In fact, experimentally the vibration was no longer visible under the optical microscope. Finally, it was confirmed that the equilibrium points at high frequencies correspond to the minima of the magnetic energy averaged in time.

This model agreed well with experimental observations, and confirms that for the dc currents and field intensities used, the frequency range that is most efficient for magnetic label focusing and accumulation in the intra-line spacing region is ~0.1 to 20 Hz.

The focusing efficiency dependence on the frequency of the external field resulted also in frequency dependent biomolecular recognition processes. This was explained as the availability of magnetic labeled target biomolecules at probe sites (see chapter 4 on detection schemes) modulated the rate or degree at which biomolecular recognition processes can occur. The effect was demonstrated with the hybridization of magnetic labeled target DNAs to chip immobilized complementary DNA probes (see chapter 7 and Ferreira *et al*., 2005b).

It was further envisioned that during and after biomolecular recognition reactions, the interaction between the complementary biomolecules could be modulated by applying particular conditions of field and frequency to the magnetic labels. During this thesis, unfortunately, this study was not thoroughly done.

A patent on the u-shaped line system together with a device comprising the u-shaped metallic structure and a sensing element such as a magnetoresistive transducer was submitted and is presently pending.

Both focusing methods, using tapered or u-shaped conductors further enabled smaller biomolecular recognition times. Hybridization times as small as 5 to 25 min were observed and detected with both systems (see chapter 7 and Graham *et al.*, 2005; Ferreira *et al*., 2005b, 2005c). This was primarily due to the increase in the proximity of target and probe DNA molecules. In fact, these focusing systems overcome the diffusion limits present traditional hybridization methods. These assays require from 3 hours to, more often, overnight time-scales for hybridization to occur at sufficient degree such that it can be detected.

Finally, it was further shown that integrated detection schemes based solely on passive diffusion of biomolecules or even on conventional microfluidic delivery systems (see previous sub-section) are limited in sensitivity (fM range) for assays performed in minutes. Focusing systems like the ones presented above can overcome those limitations and reach higher sensitivities in small time-scales using micrometer and nanometer sized transducers (Sheehan and Whitman, 2005).

# 3. Biochemical Background

## 3.1 Surface functionalization

### 3.1.1 Overview

A magnetoresistive sensing platform can only be used for biosensing after it has been functionalized with biomolecules. This issue is as important as the magnetic transducers themselves, and implies a great control of surface and label functionalization biochemistries and assay protocols.

Currently, several protocols for the functionalization of nucleic acids and proteins (including antibodies and enzymes) have been developed. These methods depend on the biomolecule but also on the surface to be functionalized. Most common biochip surfaces include glass (Joos *et al.*, 1997), silicon dioxide (Chrisey *et al.*, 1996), gold (Bamdad, 1998) and polymers (Fixe *et al.*, 2004a).

Generally, surface derivatization protocols for glass or silicon dioxide (as done in INESC-MN) consist of the following steps: activation; silanization; cross-linking; and probe biomolecule immobilization.

The activation step, may or not be necessary, and consists in formation of reactive hydroxyl groups at the biochip surface (see fig. 3.1a); for that several cleaning and oxidizing procedures have been developed (Cras *et al.*, 1999). Nevertheless, in magnetoresistive biochip applications mild conditions are required not only for cleaning but also for all derivatization protocols. As such, low salt solutions, and weak acids or weak bases should be used; otherwise surfaces, sensors and current line structures may be corroded (Freitas *et al.*, 2004).

The silanization protocol involves the use of trialkoxy silane derivatives containing an organic functional group such as an amine (Weetall, 1976). A silane molecule, such as 3-aminopropyltriethoxysilane (APTES, $C_9H_{23}NO_3Si$) reacts with the hydroxyl (-OH) groups on the surface leaving amino groups available to react further (fig. 3.1b).

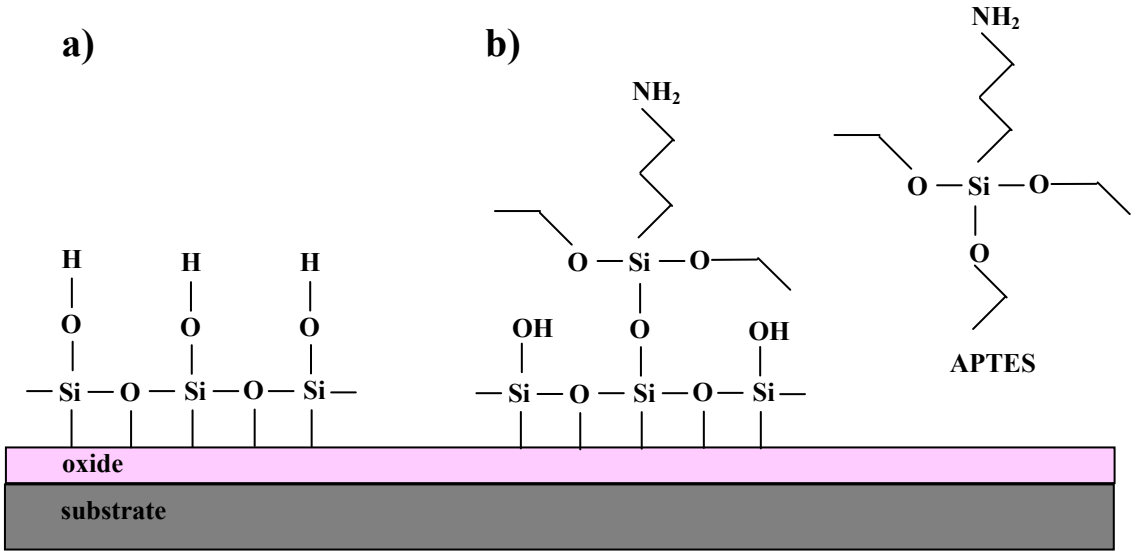


Fig. 3.1. Oxide surface biochemical functionalization protocol: a) Surface activation: formation of hydroxyl groups on the surface; b) Silanization (formation of reactive amino groups) using a 3-aminopropyltriethoxysilane (APTES) solution.

After silanization, usually a cross-linker is used to enable the covalent binding of two distinct chemical entities that are unreactive toward each other (e.g. amino $-NH_2$ and thiol –SH groups) (fig. 3.2). A cross-linker serves another important purpose: it provides a physical spacer that gives a larger mobility and freedom to the immobilized biomolecules. This greater accessibility is important to facilitate biomolecular recognition. In fact, it has been shown that hybridization efficiency depends on the cross-linker size, as larger spacers enable an easier access of target molecules to the surface-immobilized probes (Southern *et al*., 1999).

Cross-linking molecules are designated by homobifunctional, if they present identical reactive groups at the each end of the spacer (e.g. glutaraldehyde) or, on the other hand, they are called by heterobifunctional if they have distinct functional groups (like *N*-[ε-maleimidocaproyloxy]sulfosuccinimide ester or sulfo-EMCS) (fig. 3.2). In bioarray applications heterobifunctional cross-linkers are preferred as they diminish the potential for multipoint reactions.

Finally, probe biomolecule immobilization can also be done using distinct protocols, depending on the biomolecule, functional groups of the spacer and the surface type. Usually, DNA probes modified at one end with an amino, carboxylic (-COOH) or thiol

group are covalently bound to the cross-linker molecules (fig. 3.3). In case of proteins, unreacted functional groups of aminoacid residues are used for the same end.

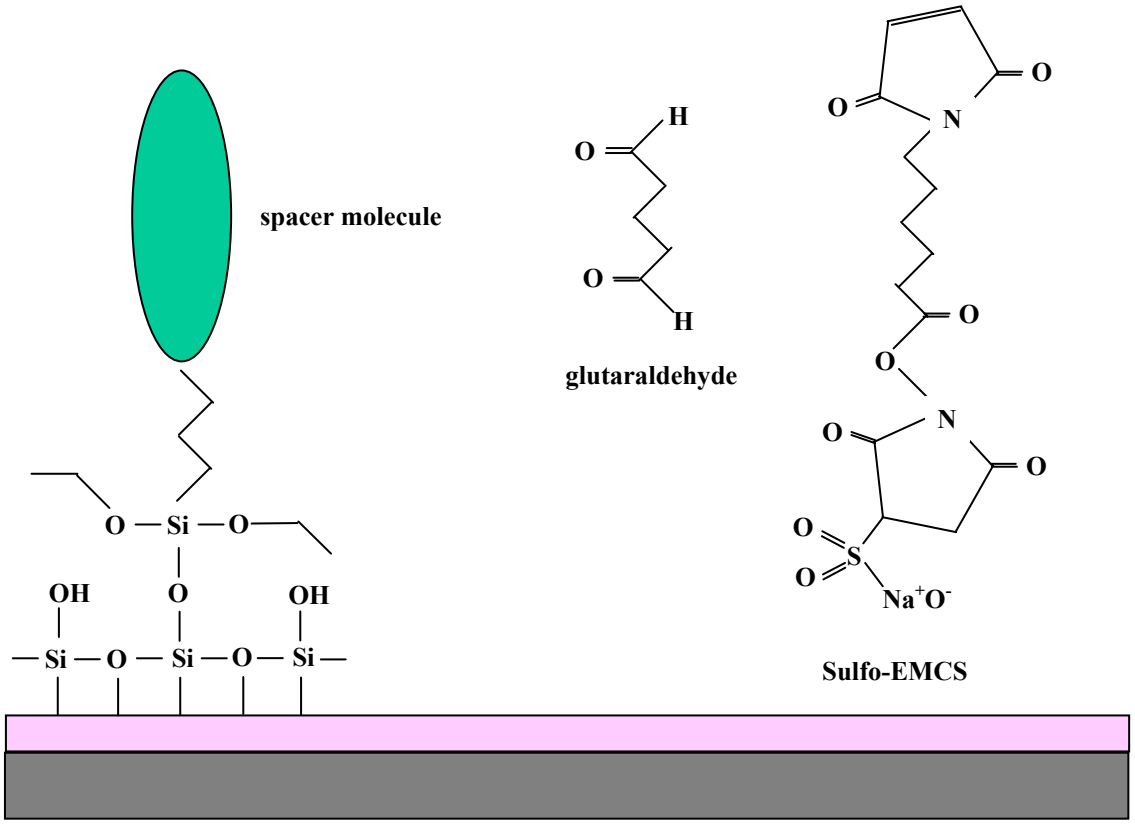


Fig. 3.2. Oxide surface biochemical functionalization protocol: cross-linking with spacer molecules such as glutaraldehyde and sulfo-EMCS.

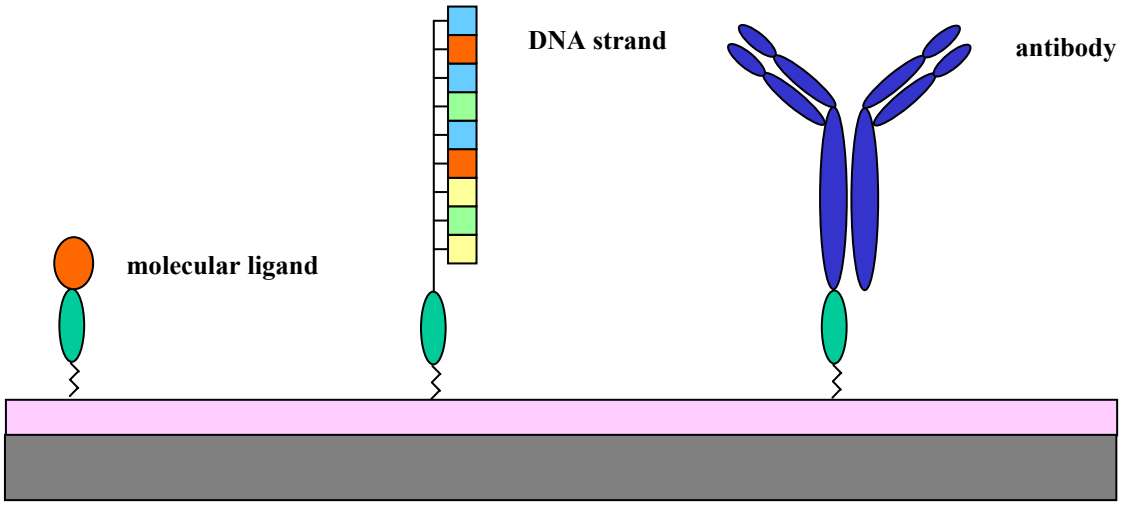


Fig. 3.3. Oxide surface biochemical functionalization protocol: Probe biomolecule (nucleic acids, proteins, etc.) immobilization to the surface through the covalent reactions between functional groups in the molecules and the cross-linkers.

Biofunctionalization of gold surfaces (Bamdad, 1998) is also one of the most common approaches as the protocols are relatively straight-forward. Thiolated biomolecules, such as DNA strands modified at one end with a thiol or a thiolated spacer, bind to the gold suface forming a self-assembled monolayer (SAM).

Polymer functionalization may be similar other surfaces such as glass or silicon oxide, involving activation, amination of the surface, cross-linking and probe immobilization (Fixe *et al*., 2004a). Nevertheless, by using native functional groups in the polymer, such as methyl esters groups in poly(methylmetacrylate) (PMMA), probe immobilization can be done in on-step (Fixe *et al*., 2004b). This has great advantages over traditional methods, as it is both labor time and reagent-cost saving.

Again, probe biomolecule immobilization chemistries must be optimized for each case, and in biochip applications mild conditions should be used. The surface density of bound probes is an important parameter, as low surface coverage will yield low biomolecular interaction rates and, consequently, low detection signals. High surface density of probes, on the other hand, may result on biomolecular steric hindrance and consequently low biomolecular interaction rates and detection signals may be observed. In addition, probe immobilization protocols should lead to a well-defined probe orientation accessible to the target for recognition, should be thermally and chemically stable, and finally, should also be reproducible.

A bioarray is a two-dimensional set of distinct biological probes. These are designed to enable an analysis of several components in the same assay in a parallel fashion. For instance, DNA microarrays may be used to investigate the expression of genes of an ill tissue and compared it with the case of a healthy one, or they may be used to screen a particular genetic mutation related to a hereditary disease. Usually, in designing a bioarray, there is redundancy of probes (i.e. each probe is represented at several places over thee chip) for statistical purposes, and both positive and negative controls are included to assess the good functioning of the assay and to determine the background noise.

Currently, there are several ways to produce a bioarray. One of the approaches is by on-chip synthesis of oligonucleotides, which uses a combination of microelectronic

photolithographic techniques and combinatorial chemistry (Pease *et al*., 1994). Although, this method allows the fabrication of highly dense arrays, representing more than 100,000 genes in an area of 1.28 cm × 1.28 cm, the procedure is costly and time consuming, and is not applicable to proteins. These aspects prevent then a widespread use of the system (Affymetrix, http://www.affymetrix.com). The present technology enables the fabrication of probe regions with feature sizes of ~10 µm.

The most common method to make DNA or protein arrays is the immobilization of pre-synthesized DNA strands and protein solutions, respectively, using devices called microspotters (Arrayit Telechem International, http://www.arrayit.com; GESIM, http://www.gesim.de), which enable the immobilization of up to 100,000 different biomolecules represented in a glass slide (Ramsay, 1998; Okamoto *et al*., 2000). A typical biomolecule spot size is ~50-100 µm, but improving technologies are rapidly reaching smaller sizes, even to the nanometer scale using techniques such as dip-pen nanolithography (Demers *et al*., 2002) and supramolecular nanostamping (Yu *et al*., 2005).

Alternative methods of probe immobilization include the use of electric fields (Nanogen, http://www.nanogen.com), which enable much shorter probe immobilization times in comparison with the previous methods (Heller, 1996; Fixe *et al*., 2003), and the potential use of magnetic fields for biomolecular patterning (Yellen *et al*., 2005).

Label functionalization protocols are similar to the ones referred above for chip surface functionalization and, consequently, should also comply with the same requirements: mild-conditions surface biochemistries; reproducibility; thermal and chemical stability; non-toxic surface properties; and suitable biomolecular surface density.

The chemistry will depend then on the surface or coating of the particles: silica, gold, polymer or other (del Campo *et al*., 2005; Bao and Krishnan, 2005; Nishibiraki *et al*., 2005; Joshi *et al*., 2004) and on the biomolecule to be functionalized. This later one is related to the bioassay to be performed and the detection scheme. As such, magnetic labels may be functionalized with target molecules (e.g. analyte DNA) or with a detector biomolecule (e.g. antibody or another protein) (see chapters 4. and 7.).

### 3.1.2. Nucleic Acid Chips

The protocol for preparing a magnetoresistive DNA-chip is shown below. In addition a more detailed run-sheet is presented at the appendix.

**STEP 1:** Substrate cleaning

Before the chemical treatment, the chip is usually washed with acetone and isopropyl alcohol (IPA) and rinsed with de-ionized (DI) water, as the surface is usually covered with photoresist after chip dicing (see chapter 5). Alternatively, a photoresist solvent (Microstrip 2001 photoresist stripper, Fujifilm) at 80ºC can be used instead of acetone. Usually, though the chip is already wirebonded to a chip carrier before surface functionalization, and in these cases the surface is just washed with acetone, IPA and water to remove any eventual grease.

**STEP 2:** Activation

This step is optional, as it was observed that cleaned silicon dioxide ($SiO_2$) chip surfaces possess enough hydroxyl groups for the silanization procedure. If necessary, in order to increase the density of these functional groups and to further clean the substrate, a 2% (w/v) cholic acid (a mild acid) is used overnight at room temperature (RT).

**STEP 3:** Silanization

The chip is then treated with a 15% (v/v) aqueous solution of 3-aminopropyltriethoxysilane (APTES, Sigma-Aldrich) for 30 min at RT, and then is rinsed with water (Graham *et al*., 2005). Alternatively, a 10% (v/v) aqueous solution of the same compound but for 2 hours at RT can be used (Martins *et al*., submitted). In another protocol, silanization can be done by treating the chip with 2% (v/v) APTES in acetone for 2h at RT, followed by rinsing with DI water, drying using compressed air gun, and curing for 10 min at 40ºC (Fixe *et al*., 2003). When using organic solvents, the curing step is necessary to promote covalent bonding between APTES molecules and the hydroxyl groups at the surface.

**STEP 4:** Cross-Linking

Afterwards, the silanized surface, with available amino reactive groups, is reacted with a solution of 0.7 mg/ml sulfo-EMCS heterobifunctional cross-linking spacer (Pierce) in 100 mM borate buffer, pH of 8.5, containing 150 mM NaCl. The reaction is left to occur for 2 hours at RT, after which the chip is washed with the same borate buffer and with phosphate buffer saline (PBS, 100 mM phosphate buffer, pH of 7.0, containing 150 mM NaCl) , to remove non reacting cross-linker molecules. The surface is then left with reactive thiol groups.

**STEP 5:** DNA probe immobilization

The probe DNAs (thiolated in the 3' end) are applied then to the chip surface as a 3 µM solution in the same phosphate buffer as before, for 3 hours at RT. The chip is then washed with 100 mM phosphate buffer, pH of 7.0, containing 1 M NaCl to remove unbound probe molecules, and is washed again with the previous phosphate buffer.

**STEP 6:** Pre-hybridization

In order to reduce unspecific binding during the assays, a blocking step before hybridization is done by incubating the probe functionalized chip with 2.0 % (w/v) bovine serum albumin (BSA) in PBS for 2 hours at RT. BSA binds unspecifically with unreacted amino or thiol groups, reducing posterior unspecific binding of DNA targets or magnetic labels.The chip is finally washed with PBS again, and is left with PBS for hybridization testing.

Alternative probe immobilization and pre-hybridization protocols can be found elsewhere (Martins *et al*., submitted), inclusively these process can be done using electric fields (Fixe *et al*., 2003, 2004c).

In addition, for multiplexing tests, where distinct DNA probes are spotted onto a single chip, the silanized surface is dried for a few minutes at 40ºC, and then small droplets (1 µL) of DNA probe solutions are dispensed over specific regions of the chip using a micropippete (pipetman, Gilson). In these cases, the droplets are continuously re-fed over a period of 3 hours, as the liquid started to dry. These procedures are done under an optical microscope or magnifier system (see chapter 7 and Ferreira *et al*., 2005c).

Finally, these chips are ready to be used with either biotin or magnetically labeled DNA targets (see chapters 4 and 7).

### 3.1.3. Protein Chips

In the preparation of protein chips the same steps 1 to 3 are used as described above. The differences in the subsequent steps rely on the nature of the biomolecules being immobilized. The protocol for antibody functionalization is briefly described below, and can be found in more detail in (Martins *et al*., submitted).

**STEP 4:** Antibody immobilization

The natural carbohydrate moieties of the Fc (constant) region of the antibody are oxidized using a solution of 10 mM sodium *m*-periodate in acetate buffer, 100 mM, pH of 5, containing 150 mM NaCl. The reaction was done in dark for 30 min at RT. The oxidizing reaction was removed by dialysis (30 kDa cut-off Centricons, Milipore) at 4 ºC.

Carbonyl (-HC = O) groups resulting from this procedure react for 4 hours at RT with the free amino groups of the silanized surface leading to site-directed antibody immobilization, with the antigenic binding sites facing away from the surface in order to capture antigens. Subsequently, a 1 mM sodium borohydride solution in 100 mM phosphate buffer, pH of 7, is used to reduce the resulting Schiff's base (-N = C-) and turn the immobilization irreversible. The reaction was carried for 10 min at 4ºC.

**STEP 5:** Blocking

After antibody immobilization the remaining free binding sites were inactivated using a blocking solution 1% (v/v) BSA and 0.05% Tween 20 in PBS for 1 hour at RT.

These chips are then ready to be incubated with a solution containing pathogenic bacteria for instance (e.g. *Salmonella* cells).

## 3.2. Magnetic Labeling

Like the chip derivatization depends on the nature of the surface and of the biomolecule to be immobilized, the functionalization of magnetic particles or the magnetic labeling of biomolecules also depends on the nature of the surface of the particles and on the biomolecule to be tagged, which can be nucleic acids, proteins, antibodies, enzymes, etc. Here two examples of biomolecular magnetic labeling are shown for enzymes and DNA.

### 3.2.1. Magnetic Labeling of Enzymes

In early studies of the biochip platform and of magnetic bead on-chip manipulation, a model enzyme called horseradish peroxidase (HRP, E.C. 1.11.1.7; Ryan *et al*., 1994) was used to assess the viability of the magnetic labeling approach (Graham *et al*., 2002).

HRP is a well known enzyme and is often used in biosensors to report a chemical reaction or a biomolecular interaction. This enzyme catalyzes the oxidation of an uncolored chemical compound like guaiacol (see Ferreira, 2000) or o-dianosidine (Ferreira, 2006) in the presence of hydrogen peroxide producing a colored substance. This dye is detected optically, and in fact the use of the enzyme results in the amplification of the signal as long as enough time and substrates are available. The properties of this enzyme are shown in the table below (see also Ferreira, 2000, 2006) and the crystallographic structure can be seen in figure 3.4.

| **Horseradish Peroxidase (HRP; POD)** |
|---|
| Hydrogen peroxide oxireductase (E.C.1.11.1.7) |
| Cheap and commercially available |
| Small (medium weight 44 kDa ; Stokes radius 27 Å ) |
| Amino acid sequence known |
| Assay methods readily available |
| Can be stabilized in aqueous or organic solvents |

Table 3.1. Properties of the model enzyme Horseradish Peroxidase (HRP).

The immobilization of HRP to superparamagnetic particles can be done using several procedures. Two approaches were followed, each based on the functional groups present at the surface of different labels. HRP was bound to Nanomag-D particles (see section 2.2) functionalized with free carboxyl groups using the negatively charged polymer polyethylenimine, the cross-linking reagent glutaraldehyde and para-benzoquinone. HRP was also immobilized to Micromer-M microspheres (see section 2.2) with free amino functionality using the common glutaraldehyde methodology (see fig. 3.5 and Ferreira, 2000).

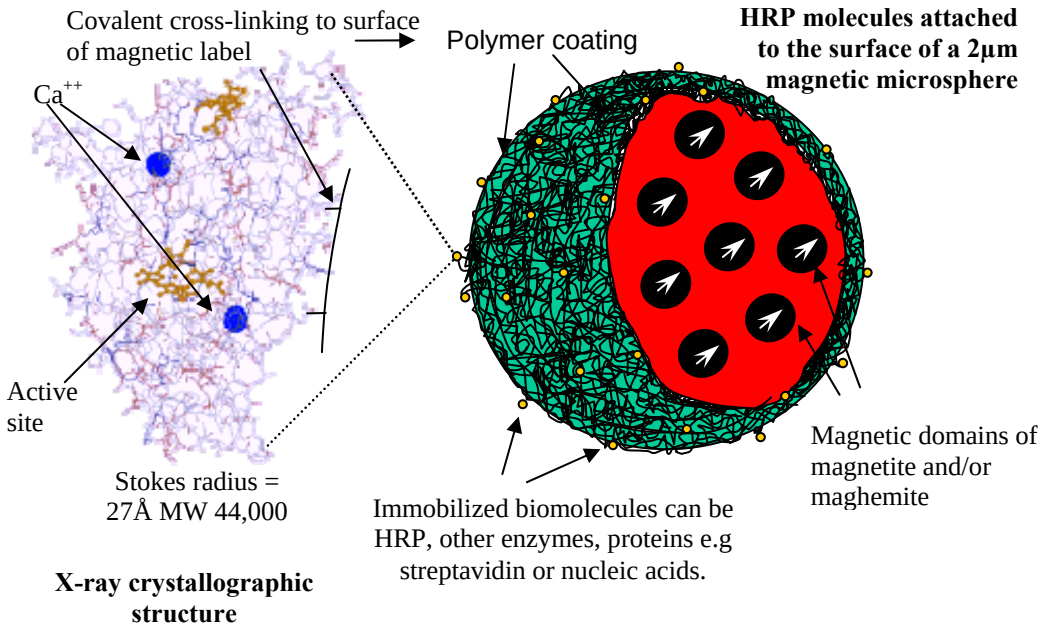


Fig. 3.4. Schematic showing HRP molecules immobilized to a 2 µm microsphere. An enlargement shows the x-ray crystallographic structure of the enzyme.

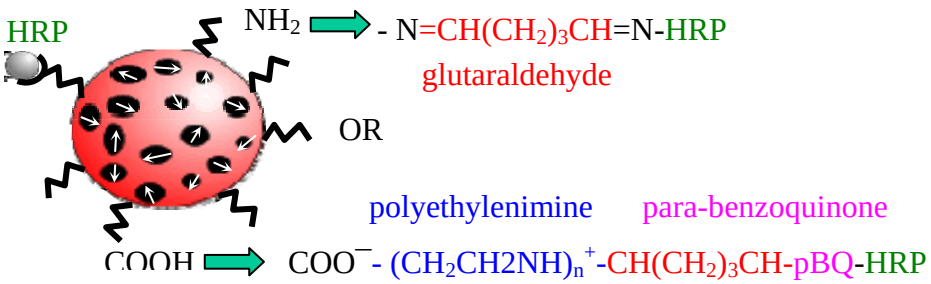


Fig. 3.5. Methodologies for magnetically labeling HRP molecules using carboxyl or amino groups of the particles' surface.

It was further observed, using spectrophotometric methods, that the enzyme remains active after immobilization onto the solid supports (see details in Ferreira, 2000). In addition, by comparison with a solution of free HRP it was estimated that each 2 μm microspheres contained ~20 fully active enzymes while smaller 400 nm magnetic particles contained each ~40 enzymes. The higher enzyme activity per 400 nm diameter label indicates that enzyme functionalization was more successful than with the larger markers (see Ferreira, 2000).

### 3.2.2 Magnetic Labeling of Nucleic Acids

Besides enzymes, target DNA strands were also labeled with magnetic particles. This was accomplished by biotin-streptavidin coupling (see following section). In the work presented here two approaches were followed depending on the nucleic acid origin.

In a sequence of experiments polymerase chain reaction (PCR) products were biotinylated at the 3' end (3'-end biotinylation kit, Pierce) (see Graham *et al*., 2005). In more recent experiments 3'-end biotinylated oligonucleotides were chemically synthesized (MWG Biotech) (see Ferreira *et al*., 2005). Some more details on these DNA sequences can be found in subsection 3.3.3. and chapter 7.

In the first case double-stranded biotinylated PCR produts were incubated with a solution of streptavidin-coated magnetic particles in a 100 mM phosphate buffer, pH of 7, for 3 hours at room temperature with gentle mixing. A proportion of 1 DNA target molecules per streptavidin on the particle was chosen. Consequently, about 500 DNA molecules were incubated per 250 nm diameter particle (see section 2.2). The solution was then centrifuged for 1 min at 10,000 rpm (Eppendorf Centrifuge 5415R). The supernatant was then removed leaving a pellet of DNA-functionalized nanolabels. The pellet was re-suspended in the same phosphate buffer and the process repeated two times to remove any unbound DNA molecules. In the final step, the pellet was re-suspended in hybridization buffer (50 mM histidine). Prior to incubation with the probe-functionalized chips the magnetically labeled double stranded target DNA samples were denaturated at 95ºC for 5 min and cooled on ice, in order to produce magnetic labels with single-stranded targets (see fig. 3.6).

In the case were chemically synthesized oligos were used the same protocol was used with the exception of not requiring the final denaturing step, as target molecules are already single stranded (see fig. 3.6).

As a note, the incubation time was not optimized, nor was the proportion of DNA targets per magnetic particle. The goal would be to achieve a faster magnetic labeling protocol with a single target per magnetic label, such that each magnetic label detected would correspond to a single biomolecular interaction (see discussion on subsection 3.3.3).

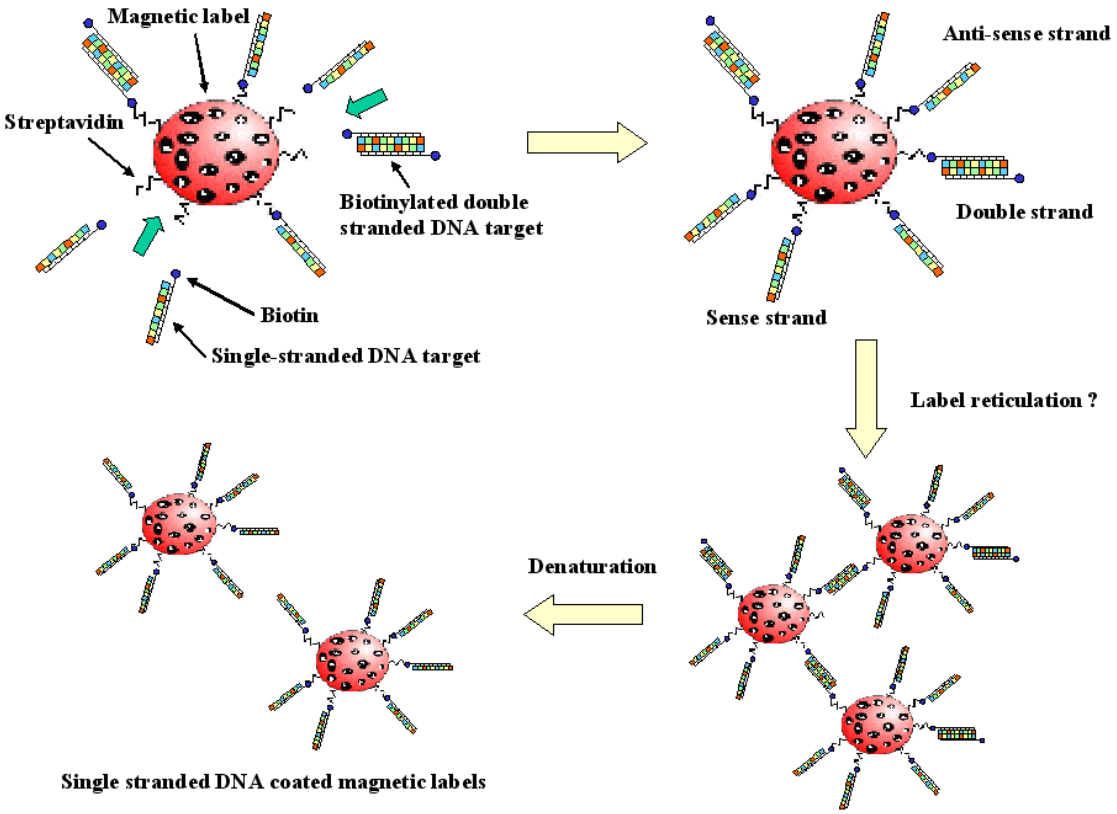


Fig. 3.6. Schematic for magnetic labeling of biotinylated PCR targets. In this case magnetic labels with single stranded sense and anti-sense sequences and double stranded targets can results. Also magnetic label reticulation may be promoted due to base pairing of complementary DNA targets. Denaturation produces single stranded free magnetic labels. In the alternative case of using synthesized oligos biotinylated at the 3' end, single stranded DNA coated magnetic labels are produced.

## 3.3. Biological Models

During this work several biomolecular interaction models were tested in order to demonstrate the versatility of the magnetoresistive biochip platform for different applications. Those models include analytes of distinct nature: proteins and small organic compounds; structural and membrane proteins and antibodies; and nucleic acids, namely DNA.

### 3.3.1. Biotin-Streptavidin Binding Model

Initial experiments on the detection of biomolecular recognition started with the biotin-streptavidin binding model. Streptavidin is a tetrameric protein with a molecular weight of 60 kDa (http://www.genevue.com/A_MModel/Strep_3.html), which binds with a high affinity to a small biomolecule called biotin (Florin *et al*., 1994; Moy *et al*., 1994). Biotin is found in many living systems where it functions as a co-factor (vitamin B12, http://www.roche.com/vitamins/what/anh/vits/biotin.html) (see fig. 3.7).

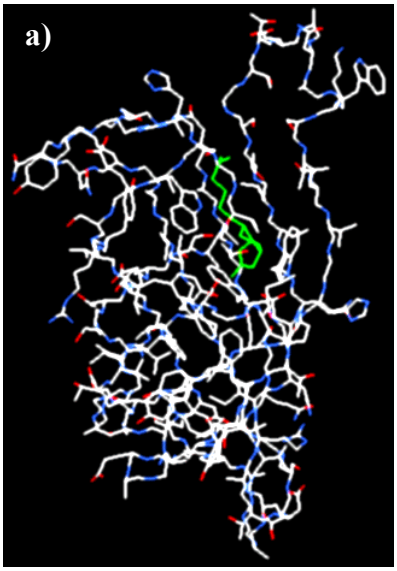


b)

**Structure of Biotin**:
Hexahydro-2-oxo-1H-
thienol[3,4]imidazole-4-pentanoic acid

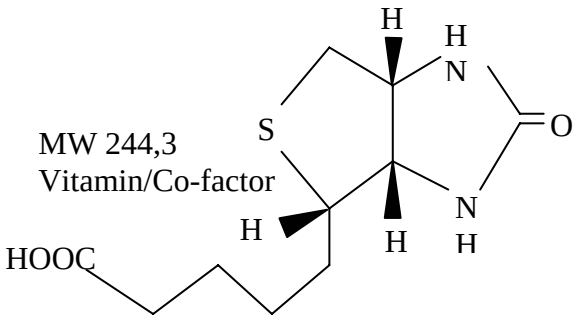


Fig. 3.7. a) Tridimensional structure of streptavidin protein with bound biotin (biotin is seen in green). b) Chemical structure of biotin.

The strategy used involved the chemical binding of biotin to the surface of a spin valve sensor surface and the subsequent biological binding of streptavidin functionalized magnetic particles (Ferreira, 2001).

The chip surface functionalization protocol was similar to the ones presented above. The main difference is that a biotinylated cross-linker (sulfosuccinimidyl-6-biotinamido-hexanoate, Sulfo-NHS-LC-Biotin, Pierce) was used instead. After silanization with APTES the surface was treated with 0.75 mg/mL of the Sulfo-NHS-LC-Biotin cross-linker in a solution of 100 mM phosphate buffer, pH of 7, containing 150 mM NaC for 40 min at room temperature. The chip was then washed with the 100 mM phosphate buffer, pH of 7, to remove unreacted cross-linker molecules. Chips were then ready to be tested with commercially available streptavidin coated magnetic particles (see section 2.2 and chapter 7).

In addition, previous to magnetic sensing experiments of biomolecular recognition, the surface chemistry and streptavidin-biotin binding was tested on different sized glass substrate surface areas. For that purpose a photoresist mask comprised of arrays of open squares of several sizes was designed. The polymer layer was deposited on a glass substrate and then was exposed and developed. Subsequently, the surface was biotinylated and incubated with streptavidin coated magnetic labels. The polymer layer was then removed using acetone or a photoresist stripper (Microstrip 2001, FujiFilm). Different sized arrays of 2 μm microspheres were then produced (see fig. 3.8 and Ferreira, 2001).

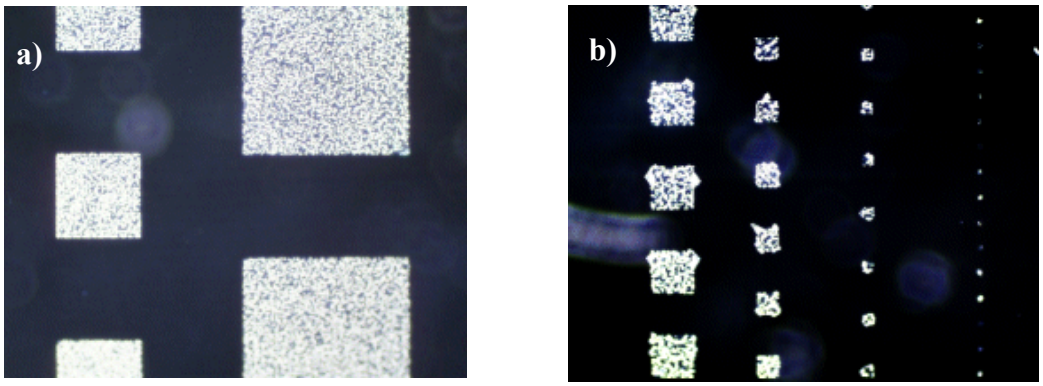


Fig. 3.8. Arrays of 2μm beads in a glass substrate: a) 400×400 and 200×200μm$^2$; and b) 100×100, 50×50, 25×25 and 10×10μm$^2$.

### 3.3.2. Protein A-IgG Recognition

The detection of binding of a class of proteins related to the immune system called immunoglobolin G (IgG) to a ligand called Protein-A was also tested, as a model for an immunoassay.

IgG is a class of antibodies, where each consists of four polypeptides, two heavy chains and two light chains joined to form a "Y" shape (see fig. 3.9, http://www.biology.arizona.edu/immunology/tutorials/antibody/structure.html). The aminoacid sequence in the tips of the "Y" varies greatly among different antibodies and includes the ends of the heavy and light chains. It is this region that confers antibodies their specificity towards an antigenic determinant or epitope, the part of the antigen that is direct contact with the antibody. Each IgG antibody has an average molecular mass of 150 kDa and a Stokes radius of ~55Å (Yang *et al*., 2003).

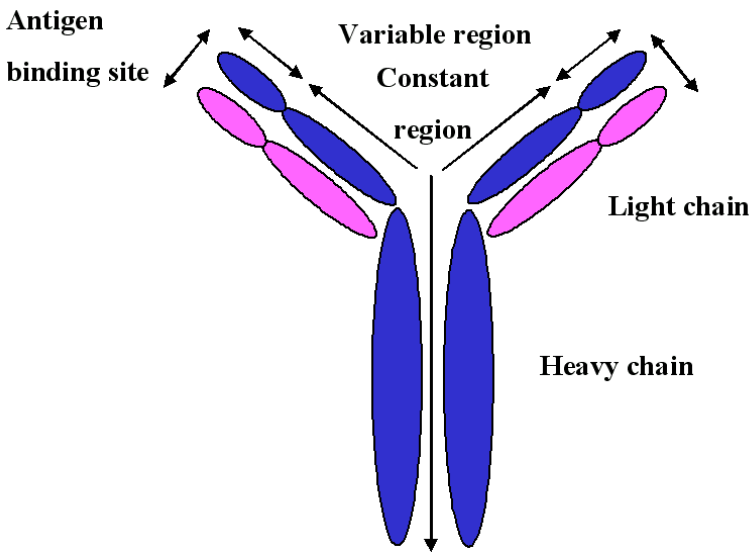


Fig. 3.9. Schematic of the structure of an antibody.

When treating the antibody with proteases (protein degrading enzymes), antibody fragments can result: Fab or fragment antigen binding that includes the variable ends of the antibody, and Fc, which is the constant fragment of the antibody.

IgG antibody is involved in pathogen neutralization in tissues, among other functions, and its Fc region binds to Protein-A. In fact, this protein is commonly used in unspecific antibody purification (http://www.sigmaaldrich.com). Protein-A is produced from

*Staphylococcus aureus* strains and has a molecular weight of 42 kDa and a radius of ~ 12.5Å (Yang *et al*., 2003). It has also shown to bind to at least two IgG molecules simultaneously.

The strategy followed here was to immobilize the IgG antibodies in the chip surface and incubate the chip with Protein A coated magnetic microspheres of 2 µm of diameter (Micromer-M, Micromod) (see fig. 3.10).

The surface chemistry used was similar to the one presented above for protein chips and antibody-ligand interaction was detected using 2 µm × 6 µm spin valve sensors (see chapter 7).

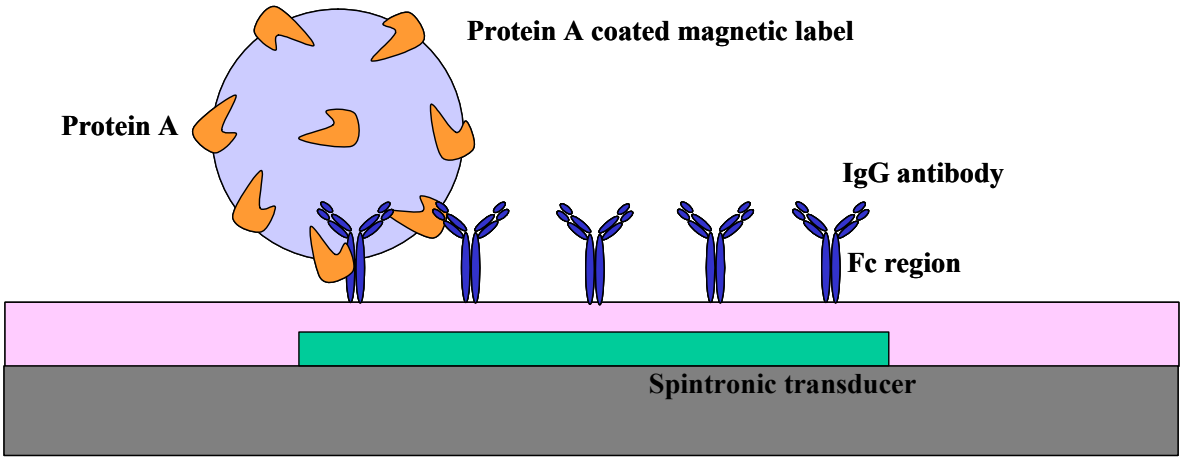


Fig. 3.10. Schematic for the detection of antibody-ligand binding (drawings not to scale).

### 3.3.3. DNA Hybridization

Another biomolecular recognition model studied was nucleotide complementary base pairing. Short DNA single strands (oligonucleotides) of a known sequence were used as probes and were immobilized on sensor surfaces using the protocol described above. The resulting DNA chips were tested with laboratory samples of target DNA, either labeled with a reporter biotin molecule or with a magnetic particle (see next chapter).

Cystic fibrosis was chosen as a model disease for DNA hybridization detection (Freitas *et al*., 2004; Lagae *et al*., 2005). This is the most common lethal recessive genetic disorder among the Caucasian population, with an incidence of ~1:3000. It is

characterized by mutations in the cystic fibrosis transmembrane regulator (CFTR) gene, which is located in chromosome 7 (Collins, 1992; Bobadilla, *et al*., 2002).

Presently, more than 1000 mutations have been described for cystic fibrosis (Cystic Fibrosis Mutation Database, http://www.genet.sickkids.on.ca/cftr), and their prevalence among populations varies according to race and geographical distribution. The majority of these mutations consist of variations in a small number of nucleotides, frequently a single nucleotide is either replaced by another base, inserted or deleted (single nucleotide polymorphisms, SNPs). Nevertheless, other mutations include the insertion and deletion of more than one nucleotide. For instance the most common mutation, F508del, refers to the deletion of 3 nucleotides that corresponds to the deletion of a phenylalanine aminoacid at the position 508 in the CFTR protein. Finally, other mutations are related to the incorrect splicing of the pre-mRNA (transcript of the genomic DNA), resulting in the inclusion of introns or the exclusion of exons in the final mRNA strand. These mutations are then called splice-site mutations.

Two approaches were underlined for the diagnostics of cystic fibrosis: one corresponded to screening the messenger RNA (mRNA); the other one corresponded to the analysis of genes, others than the CFTR gene, whose expression is consistently increased or diminished in cells and tissues with cystic fibrosis than in healthy ones (see fig. 3.11 and Galvin *et al*., 2004; Clarke *et al*., 2004).

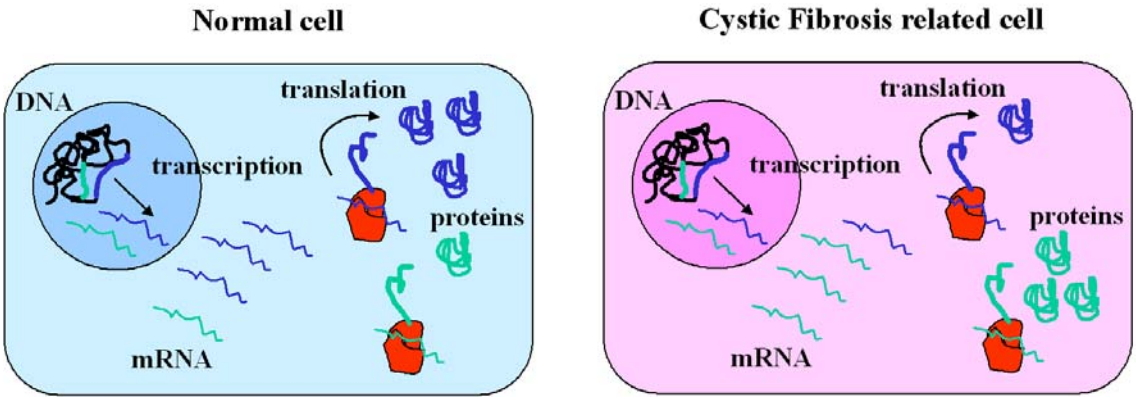


Fig. 3.11. Scheme showing the central dogma of molecular biology: the transcription of DNA into mRNA and the translation of mRNA into proteins; and the differential gene expression concept: genes can be over-expressed (in green) or sub-expressed (in blue) in cystic fibrosis related cells and tissues than in normal or healthy ones. Monitoring the expression of these genes against a control gene that does not change its expression in healthy and sick tissues can be used as a diagnostic.

With respect to the first approach, a 50-mer oligonucleotide (50 nucleotide long DNA strand) probe was used. This probe corresponded to the anti-sense or non-coding strand of the CFTR gene spanning the region of exon 10, where the most frequent mutation F508del occurs. The sequence was 5'-ATT-CAT-CAT-AGG-AAA-CAC-CAA-AGA-TGA-TAT-TTT-CTT-TAA-TGG-TGC-CAG-GC-3' and the oligos were prepared (MWG Biotech) with 3'-thiol functionality for surface immobilization (see above) and with or without 5'-fluorescein label, which was used to confirm the immobilization procedure using fluorescence microscopy (see fig. 3.12).

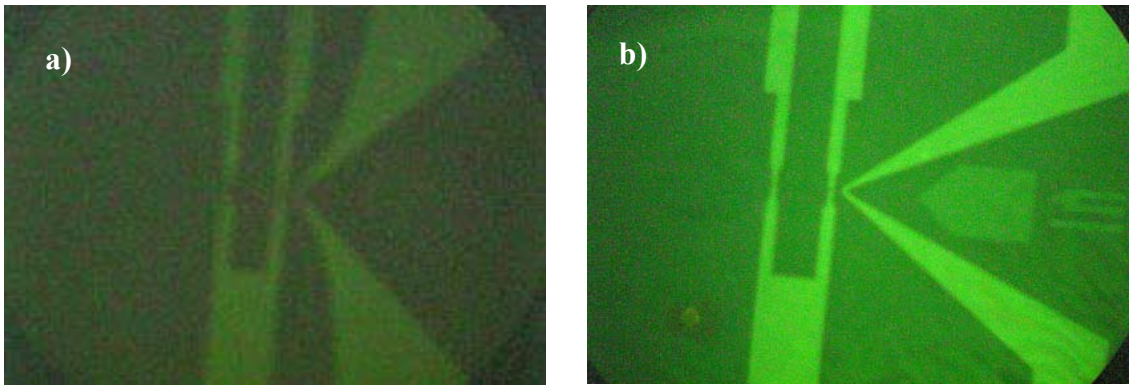


Fig. 3.12. Fluorescence microscope images from (a) an untreated chip surface and (b) a surface immobilized with fluorescently labeled oligos.

Complementary and non-complementary DNA target sequences were double stranded PCR products amplified from exon 10 of the CFTR cDNA (complementary DNA, results from reverse transcription of mRNA) (Ramalho *et al*., 2002) and exons 4 and 5 of the unrelated proto-oncogene Rac1 (Jordan *et al*., 1999). The complementary target was 96 bp long and the sequence was 5'-TTT-CCT-GGA-TTA-TGC-CTG-GCA-CCA-TTA-AAG-AAA-ATA-TCA-TCT-TTG-GTG-TTT-CCT-ATG-ATG-AAT-ATA-GAT-ACA-GAA-TCA-TCA-AAG-CAT-GCC-AAC-3' (sequence complementary to probe is underlined). On the other hand, the non-complementary target was 75 bp long with the sequence 5'-CCT-GCA-TCA-TTT-GAA-AAT-GCT-CGT-GCA-AAG-TGG-TAT-CCT-GAG-GTG-CGG-CAC-CAC-TGC-CCC-AAC-ACT-CCC-ATC-ATC-3'.

Both targets were biotinylated at the 3'-end using a 3'-end biotinylation kit (Pierce) and were used to directly interrogate a probe functionalized chip surface (Freitas *et al*., 2004; Graham *et al*., 2004) or were incubated with magnetic particles for magnetic field

assisted hybridization experiments (see discussion above and Graham *et al*., 2005; Ferreira *et al*., 2005b).

In the second approach, again 50-mer oligonucleotides probes were used. In this case though the probes were related to genes that were found to be either over (*rpl29*) or sub (*asah*) -expressed in cystic fibrosis related cell lines with respect to normal tissues (Clarke *et al.*, 2004). In addition, multiple probes were immobilized or patterned on the same chip at distinct sensing locations (Ferreira *et al*., 2005c). These chips were interrogated with magnetically labelled 50-mer targets complementary to the probes in multiplexing experiments (see following chapters). Both probe and targets were chemically synthesized (MWG Biotech) with either 3'-thiol or 3'-biotin functionalities for probes and targets, respectively.

This approach for cystic fibrosis diagnostics is related then to cystic fibrosis, while the previous one can be related more to splice-site mutation detection. Presently, though efforts are being undertaken to develop a platform for cystic fibrosis related SNPs within the scope of an European project. The detection of SNP involves additional challenges in the discrimination of closely matching DNA sequences, where only one nucleotide differs.

### 3.3.4. Cell detection

In a continuation of both protein recognition and DNA hybridization detection experiments cell detection assays were developed. The goal of these assays was to show the proof-of-concept for an application on microbial monitoring of water quality. *Escherichia coli* and *Salmonella* were chosen as model organisms to detect, and two strategies were developed (Martins *et al*., submitted).

One of the strategies involved the detection of DNA oligonucleotides sequences complementary to *E. coli* 16S ribosomal subunit. Probe DNA sequences were immobilized to the surface as mentioned above and target DNA probes were biotinylated and hybridized to the immobilized probes. Subsequently, streptavidin coated magnetic labels were incubated with the chip and the hybridization detected

using a magnetoelectronic transducer (see post-hybridization detection scheme in chapter 4).

The other strategy relayed on using antibodies specific for *Salmonella*. Primary antibodies were immobilized on the chip surface using the protocol described above and the chip was incubated with a solution containing *Salmonella* whole cells. These remained bound the chip surface through the interaction between epitopes at the cell surface and the surface bound antibodies. Subsequently, magnetic labels functionalized with the same antibody against *Salmonella* were incubated with the chip. These secondary antibodies bound to the cells were then detected with the magnetic field sensors. The resulting "sandwich" like arrangement is similar to an ELISA assay where the enzyme reporter is replaced by a magnetic label (see fig. 3.13, and discussion on chapter 1).

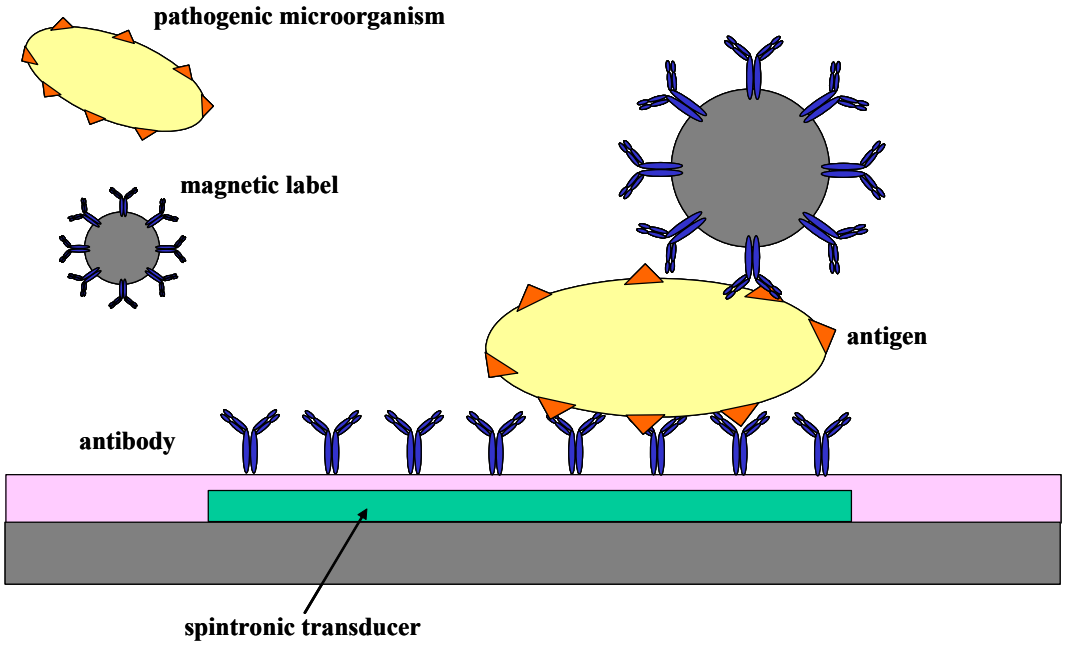


Fig. 3.13. Schematic showing detection strategy for the detection of whole cells of pathogenic microorganisms. A sensor surface, functionalized with antibodies against a particular microorganism such as *Salmonella*, is incubated with a testing solution. In the case that the pathogen is present, the antigens present at its membrane surface are recognized by the surface bound antibodies. Later, magnetic labels functionalized with antibodies for the same microorganism bind to it, indicating its presence by measurement of the stray filed of the labels.

Although the magnetoresistive biochips developed during this thesis were also used for the detection of pathogenic cells, the results obtained from the work will not be reported here as these are still preliminary. Furthermore, cell detection using magnetoresistive sensors is the specific topic of on-going doctoral studies of a collegue. Results can, nevertheless, be found elsewhere (Martins *et al*., 2005, submitted).

# 4. Bioassay Detection Schemes and Chip Architectures

## 4.1. Bioassay Detection Schemes

Magnetoresistive biochip design involves a number of considerations, ranging from materials, type of sensor and detection setup, to surface functionalization, type of bioassay and desired sensitivities and dynamic ranges.

These biochips have been so far mostly used for the detection of DNA hybridization in applications concerning screening of biological warfare agents (Edelstein *et al*., 2000; Miller *et al.*, 2001) and diagnostics of cystic fibrosis (Graham *et al*., 2004, 2005; Ferreira *et al*., 2005c; Lagae *et al*., 2005).

Two hybridization detection strategies have been followed, the post-hybridization detection method and the magnetic-field assisted detection method.

In the post-hybridization detection method (followed by both the NRL; the University of Bielefeld; and INESC-MN), target biomolecules are labeled with a small reporter biomolecule called biotin. After target hybridization with the probe DNA strands immobilized on the chip surface, a solution of magnetic labels is dispensed over the chip. These labels are coated with a detector protein called streptavidin that recognizes the reporter biotin molecules that tag the hybridized DNA targets. Subsequently, the stray field created by the magnetic labels is detected with the use of on-chip magnetoresistive sensors, indicating that hybridization occurred (fig. 4.1).

In this method, the analyte solution is dispensed over the chip and the biotinylated DNA targets diffuse, passively, in solution until finding their complementary probe molecules at the chip surface. This way, hybridization times alone take usually from 3 to 12 hours (see section 2.4 and Sheehan and Whitman, 2005; Lagae *et al*., 2005). This limits these systems to applications or assays were response times are not critical.

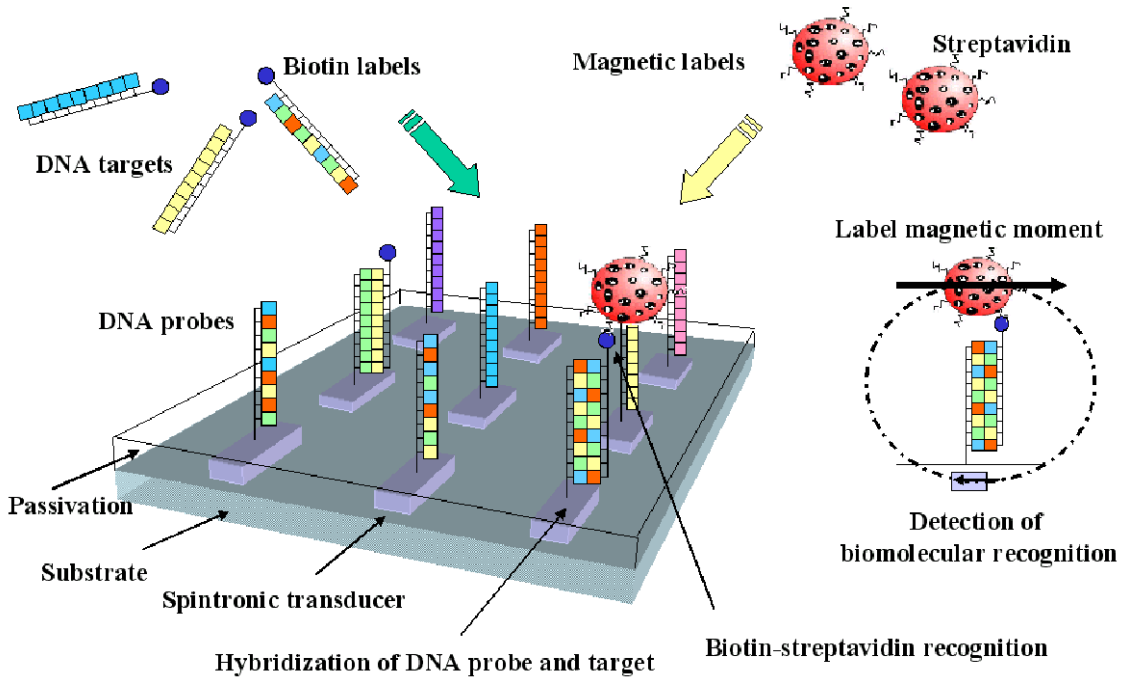


Fig. 4.1. Post-hybridization detection method. Spintronic biochips functionalized with DNA probes are incubated usually for several hours with DNA targets labeled with a biotin reporter molecule. After hybridization has occurred, streptavidin coated magnetic labels are dispensed over the chip. The streptavidin proteins recognized biotin molecules available were hybridization occurred. Finally, magnetic labels bound to hybridized sites are detected by spintronic transducers that sense the labels' stray fields.

In order to overcome this limitation, a detection method based on magnetic field assisted hybridization was developed at INESC-MN. In this method DNA targets are labeled with magnetic labels and are transported to probe immobilized sensor sites by on-chip current carrying conductors that generate local magnetic field gradients (see section 2.4). The close proximity of target and probe biomolecules accelerates then the rate at which biomolecular recognition reactions happen. This way hybridization is detected almost in real-time (Fig. 4.2).

Using different designs, comprised of tapered on-chip conductors (see fig. 2.29 and Graham *et al.*, 2002; Lagae *et al.*, 2002) or u-shaped current lines (see fig. 2.32 and Ferreira *et al.*, 2005b) enabled the detection of hybridization between complementary DNA strands in times of less than 5 min (Graham *et al.*, 2005) and 30 min (Ferreira *et al.*, 2005c). These systems show the potential to be used in the rapid detection of biological warfare agents, in pathogen identification or in clinical diagnostics in the point of care.

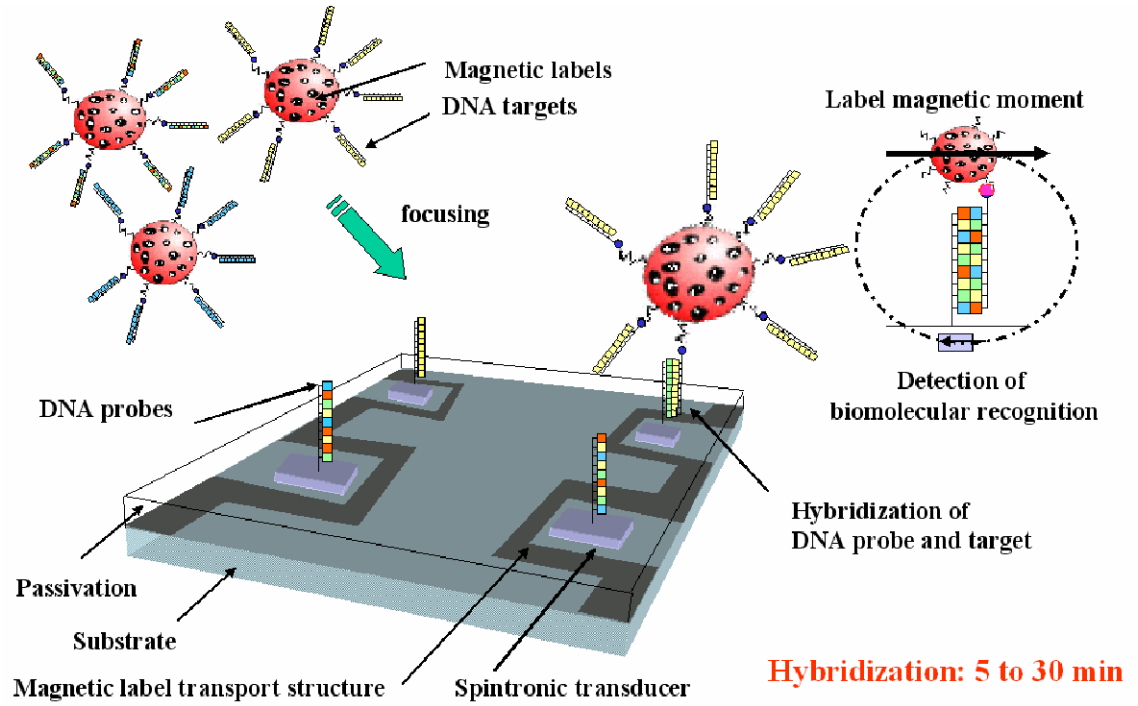


Fig. 4.2. Magnetic field assisted hybridization and detection. Spintronic biochips functionalized with probe DNA are incubated with magnetically labeled DNA targets. On-chip current carrying conductors that create local magnetic field gradients are used to attract the magnetically labeled molecules to functionalized sensing regions. The proximity of target and probe molecules accelerates the hybridization reaction rate, enabling faster hybridization times and the detection of biomolecular recognition in almost real-time.

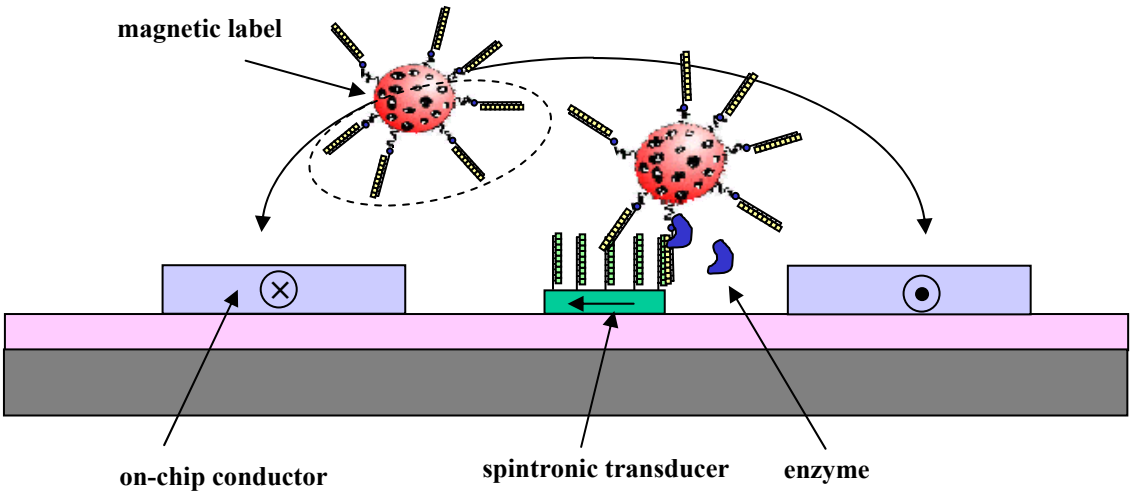


Fig. 4.3. Variant of the magnetic field assisted hybridization method. After hybridization occurred enzymes are used to cleave bound magnetic labels. Labels are then moved back and forth across the sensor using on-chip current conductors, enabling label detection.

Another variant of the magnetic field assisted hybridization method involves the use of enzymatic cleavage of the magnetic labels bound after hybridization has occurred (Lagae *et al*., 2005). After release, labels can be detected by moving them over the sensor by alternatively applying current through tapered line structures adjacent to the sensor (Lagae *et al*., 2002) (fig. 4.3).

## 4.2. Chip Architectures

Magnetoresistive biochips (Freitas *et al*., 2004) have "evolved" in order to fit with fabrication and detection apparatus constraints, but also to fit with biological requirements of the bioassays and their applications. One of such biological requirements is the probe functionalized area, which, typically, has been defined by microspotting of the chip surface above the sensing elements (see chapter 3).

The initial BARC chip from NRL (Baselt *et al*., 1998) was comprised of 8 sensing zones, each containing 8 GMR sensor traces of dimensions of 5 μm × 80 μm. Each sensing zone was ~250 μm in diameter and was functionalized with a particular DNA probe (Edelstein *et al*., 2000; Miller *et al*., 2001). Since magnetic labels were only detectable over or adjacent to the GMR sensors, the effective biomolecular recognition sensing area was relatively small (~10% or less) in comparison with the total functionalized area. In this case, for low DNA target concentration, target molecules could hybridize in ~90% of the functionalized area and not being detected.

A later version of the BARC chip (Rife *et al*., 2003) was designed to overcome this limitation, as the GMR sensors were fabricated in a serpentine shape that comprised a diameter of ~200 μm and, consequently, fitted better the functionalized area (even so the sensing area was <70% of the total area with probe DNA). At the same time the number of sensing areas in the latest chip increased from 8 to 64.

One aspect to take into account is that an increase in the probe immobilized area corresponds to an increase in the biological sensitivity of the system, as the highest is the number of probe biomolecules on the surface the highest is the possibility to capture a complimentary target biomolecule that diffuses in the analyte solution being tested.

As such, an increase of the sensing area to fit the functionalized area resulted in the overall increase of the biological sensitivity of the system. With the increase of the sensor size increases also the dynamic range of operation of the sensor, i.e., the number of magnetic labels that can be detected increases, and consequently the number of detectable biomolecular interactions also increases. Nevertheless, the sensitivity to lower number of particles or to single particles diminishes. Thus, in sensor design a compromise has to be made with respect to biological sensitivity and dynamic range with the single label sensitivity (fig. 4.4).

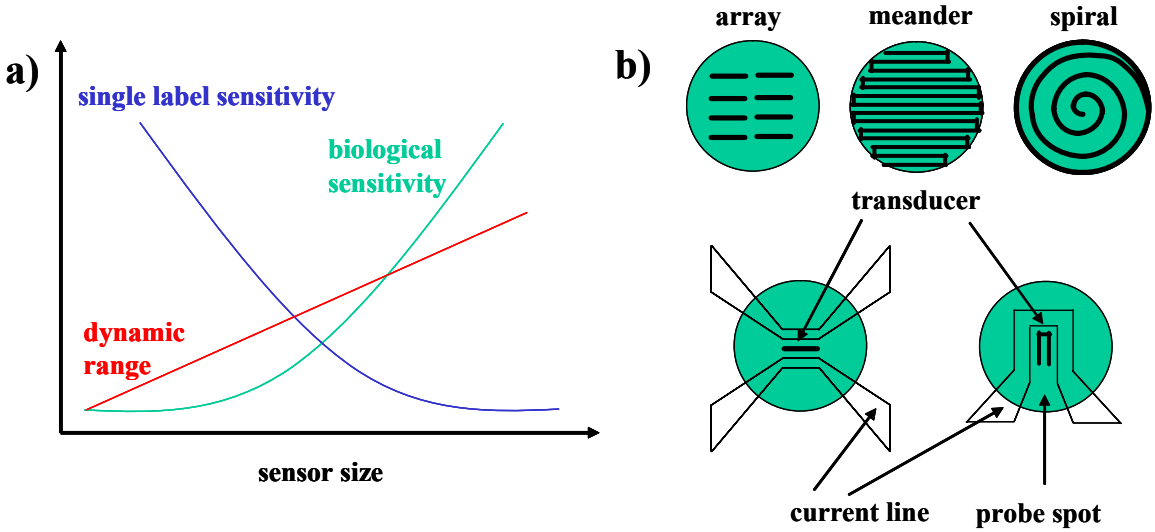


Fig. 4.4. a) Diagram showing the dependence on sensor size of biological sensitivity of the system, single label sensitivity and sensor dynamic range; a compromise must be found for these variables depending on the sensor and the application. b) Different strategies for fitting the sensor size to the probe functionalized area: array of sensors and meander (NRL); and spiral sensor (University of Bielefeld). Using on-chip current conductors overcomes the large difference between sensor size and probe area by focusing the magnetically labeled targets at the sensing sites.

The group at the University of Bielefeld has also followed the strategy of fitting the sensor size to the probe immobilized area. In their case, they fabricated spiral shaped GMR sensors with a diameter of 70 µm in order to fit DNA spots of 100 µm in diameter. A first version of the chip included 30 sensing elements, with half of them being used for reference purposes (Schotter *et al.*, 2002). In a later version, where the magnetoresistive sensing platform was compared favorably with a fluorescence-based

system, the chip included 206 spiral GMR sensors, with 6 of them being used as references (Schotter *et al*., 2004).

Since the first device was developed at INESC-MN (Ferreira, 2000) different designs were made and chips fabricated according to the technological (see chapters 5 and 6), biochemical (see chapter 3) and biological assay requirements, as discussed above. Nevertheless, a distinct and innovative approach was undertaken by combining both transport and detection of magnetically-labeled biomolecules using on-chip microfabricated structures. This approach has shown advantages not only in increasing biomolecular recognition reaction rates but also on overcoming the large difference between sensor size and probe area. Consequently, this approach promises increased biological sensitivities together with fast responses (Sheehan and Whitman, 2005). A description of the evolution and other design guidelines is followed.

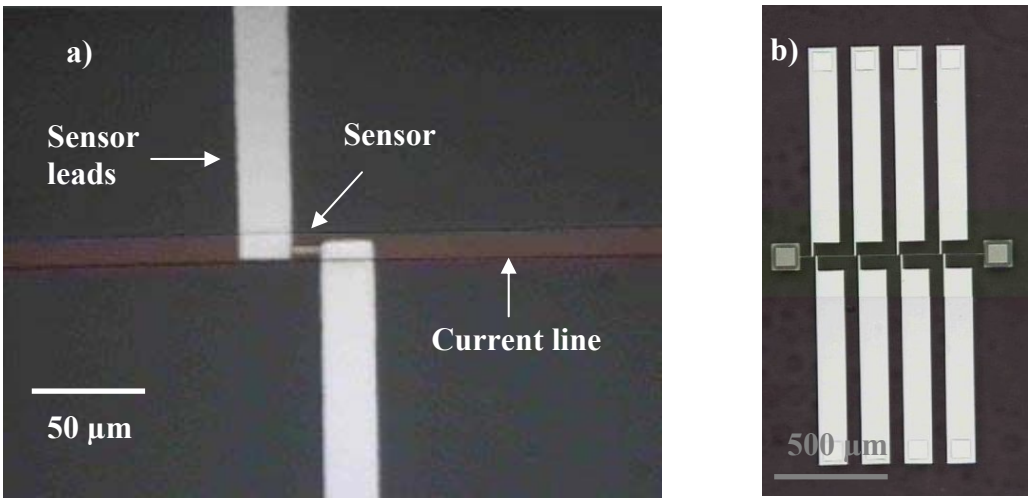


Fig. 4.5: First biochip, design “Nanomag”, comprising a single aluminum current line and four 2 µm × 6 µm spin valve sensors.

The fist biochip was developed within the scope of the Microtechnologies course during the Physics degree and comprised a simple aluminum current line (0.8 mm length, 10 µm wide and 3000 Å thick) over which 4 spin valve sensors of dimensions of 2 µm × 6 µm were fabricated (fig. 4.5; Ferreira, 2000). The combination of transport and detection was then introduced but the design included other novel aspects. Until then, no magnetic sensing applications required the sensors to operate in fluid. Here, an oxide passivation layer for protecting the sensor structure and the lines was used and long

leads for the sensors were introduced, such that wirebonds would be made at the periphery of the die and would not contact with the fluid. Later on, after experimentation, it was observed that the aluminum wirebonds were corroded by the fluid and a silicon gel covering the bond was used to avoid it (see section 5.2).

At the time, and during the duration of the course, it was observed that magnetic particles were attracted to the full length of the line, covering also the transducers. An experimental sample of 400 nm dextran magnetic particles (Nanomag-D, Micromod) was used then (see section 2.2).

The next design took into account those results and was comprised of step-like current lines adjacent to the same 2 μm × 6 μm spin valve sensors. The current lines were thinner (5 μm wide) in the area immediately adjacent to the sensor (4 μm away), such that a higher current density and a higher magnetic field would be achieved at that site (see fig. 4.6 and Wirix-Speetjens, 2000). The idea was to focus particles just near the sensor and not over the full line, like in the previous design. At the time it was observed that particles preferred to stay at the step corners, which were regions of higher current density as well. Furthermore, it was observed that sensors were quite sensitive to temperature, and only temperature changes from dispensing liquid over the chip or removing it completely were observed.

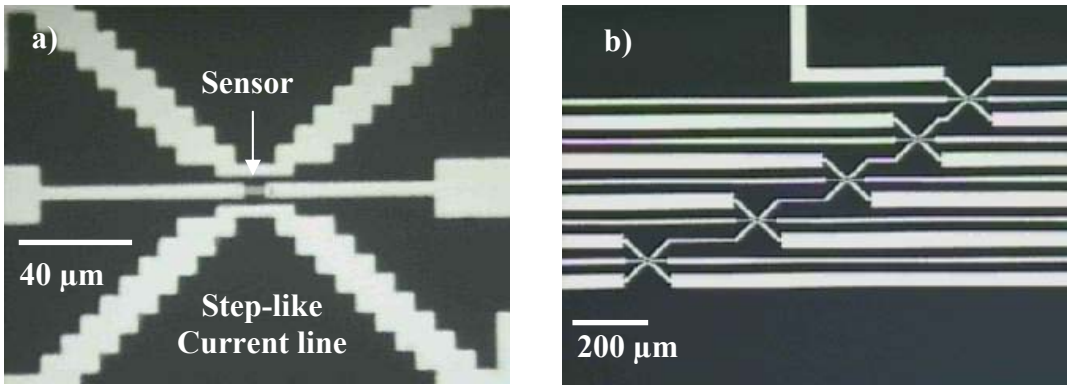


Fig. 4.6. a) “Biosensor” design comprising step-like current lines adjacent to a 2 μm × 6 μm spin valve sensor. b) Designed system for moving magnetic labels from one sensing unit to the next.

In order to avoid, particle trapping at the corners of the step-like current line, a tapered current line design was developed at the senior student project (see fig. 4.7a). The idea for this design was to use the dip the chip in a solution, as schematized in fig 4.7b. For

that the chip was fabricated using a glass substrate, such that it would not be corroded by the experimental solution, whereas a silicon substrate might have been. All the contacts were also designed to be away from sensing site, such that they would not be contact with fluid.

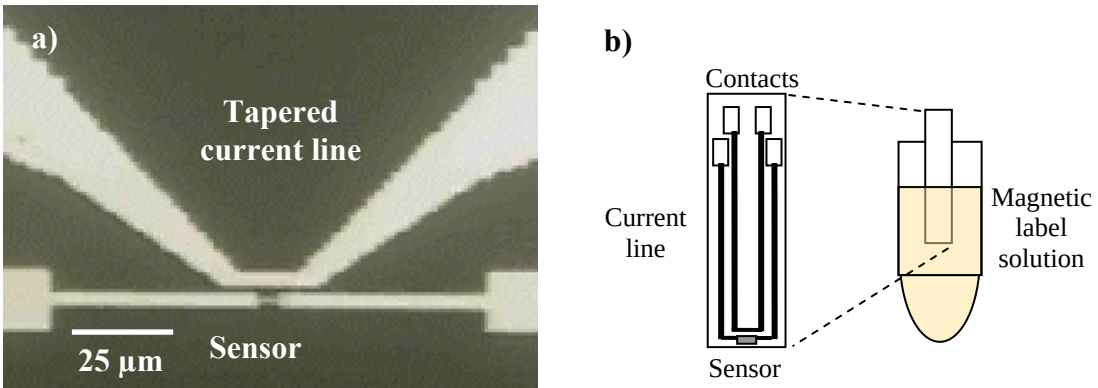


Fig. 4.7: Biochip "Snsdiver" design comprising a single tapered current line adjacent to a 2 µm × 6 µm spin valve sensor. a) Fabricated chip. b) Usage of the chip in the bulk solution.

This design was discontinued at the time, but later on it was thought that a similar design could be used for scanning a magnetically labeled biological surface, in a conception of a biological credit card-or hard-disk (see discussion further below).

The following design, also developed during the senior thesis project, was to be used in the traditional way, where biomolecules are functionalized to the sensor surface and the magnetic label solution is dispensed over the chip.

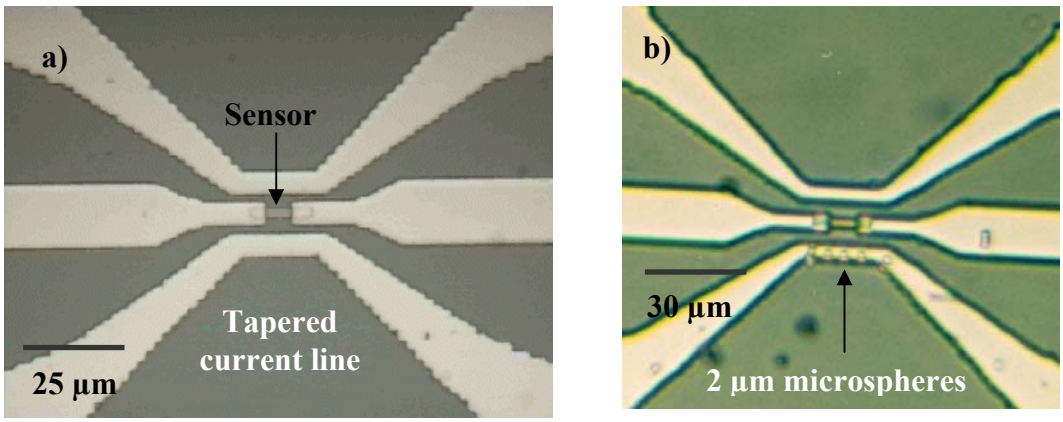


Fig. 4.8: Biochip "Spider" design comprising 2 tapered current lines and a 2 µm × 6 µm spin valve sensor, for controlled placement, manipulation and detection of single magnetic labels. Each "Spider" was comprised of 6 sensor/ tapered current line units.

This design included two tapered current lines adjacent to a 2 μm × 6 μm spin valve sensor, and targeted for the controlled placement, manipulation and detection of magnetic labels (fig. 4.8). Using this system, detection of magnetically labeled enzymes was achieved, together with the detection of single 2 μm microspheres (Graham *et al*., 2002). In addition, it was a starting point for experiments concerning magnetic field assisted hybridization (see chapter 7 and Graham *et al*., 2005).

These small size sensors have a small dynamic range of ~200 nanoparticles of 250 nm in diameter (Graham *et al*., 2005), which seems reasonable for applications where it is necessary to distinguish between a yes or no answer more than a quantitative value. Examples of such assays are the distinction between different mutations in the same gene, including single nucleotide polymorphisms (SNPs) or the assessment of differences in the splicing of mRNA (splice-site mutations), or even the detection of a single pathogenic microoganism.

The platform is then suitable for the detection of few number of nano and micron sized particles and, therefore, has the potential to detect single biomolecular recognition events (Graham *et al*., 2004). In particular it could be an interesting tool for studying molecular motors (see chapter 8).

Before, further developing the concept of magnetic field hybridization, a set of chips was developed which were based on the post-hybridization detection scheme, which does not use magnetic field focusing of bio-functionalized labels at probe sites.

The first of those chips being developed comprised 24 sensors grouped in pairs. Each pair had a common contact lead and an independent lead for each sensor, such that they could be individually measured. Again, 2 μm × 6 μm spin valve sensors were used, but were separated by 75 μm in the pair. This architecture was used for differential and sensor pair measurement, in a manner to avoid sensor drift with temperature and to distinguish between an “active” sensor, over which biomolecular recognition was detected, and a reference sensor (see section 6.2 and fig. 4.9).

With this platform the first results on the detection of biomolecular recognition were obtained using the biotin-streptavidin model (see chapter 3 and 7, and Graham *et al*.,

2003). Furthermore, this chip was the first to be used by National Microelectronics Research Centre (NMRC), now called Tyndall Institute, in Ireland, for spotting. The distance of 75 µm between the sensors in the pair was found to be suitable for the spotting of ~100 µm diameter regions of probe DNA (fig. 4.9b). Finally, this same design served as an inspiration to the test chip made by the Korean Institute of Technology, which was tested at INESC-MN.

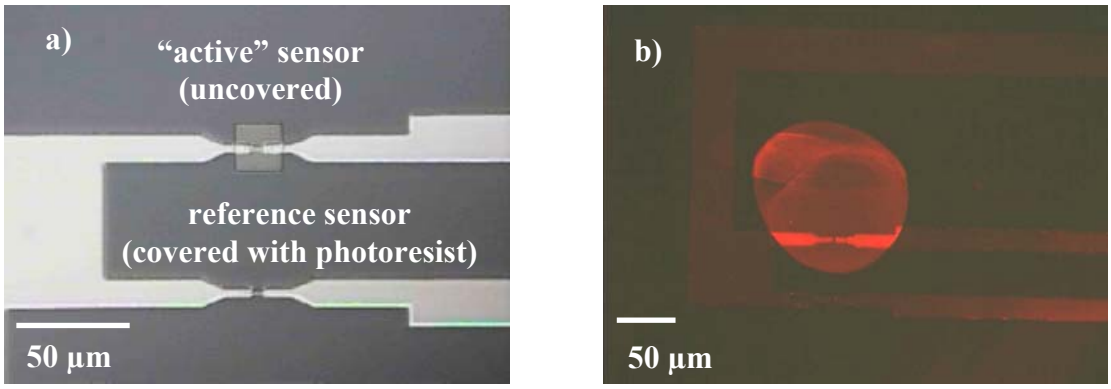


Fig. 4.9. a) Photograph of the "Dragonfly" chip design, comprised of sensor pairs with a common and two independent leads; sensors are 2 µm × 6 µm and are separated by 75 µm. b) Fluorescently (Cy3) labeled oligos patterned and immobilized over the active sensor of the pair.

In the meantime, the same sensor pair unit was used in a chip specially designed for use with the PDMS microchannels (see section 2.3 and next chapters). In this chip, the sensing units were fabricated in a row in the middle of the chip and incorporated also a tapered current line. The sensor and current line pads were located in just two of the sides of the die, such that the microchannels were bonded along the die and did not cross over the wirebond pads (see fig. 4.10).

Next, the concept of a common contact for different individual sensors evolved together with the need to fit the size of a probe spot to the sensing size, such that the biological sensitivity of the system would increase. Here the post-hybridization detection scheme was considered. Two chips were designed were a common contact fed 7 "active" sensors and 1 reference sensor (without spotting). These sensors were also of the spin valve type with dimensions 2 µm × 82 µm, and the distance between the reference sensor and the set of "active" sensors was ~100 µm (see fig. 4.11). This chip was designed according to the requirements for the detection of cystic fibrosis related targets

but had a number of drawbacks. Although, having 7 long sensors within a 100 µm diameter spot, the sensing area was only ~15% of the probed area, and the number of contacts was very large, a 9 probe chip accounted for 81 pins alone. This design then was not suitable for scalability, and was discontinued.

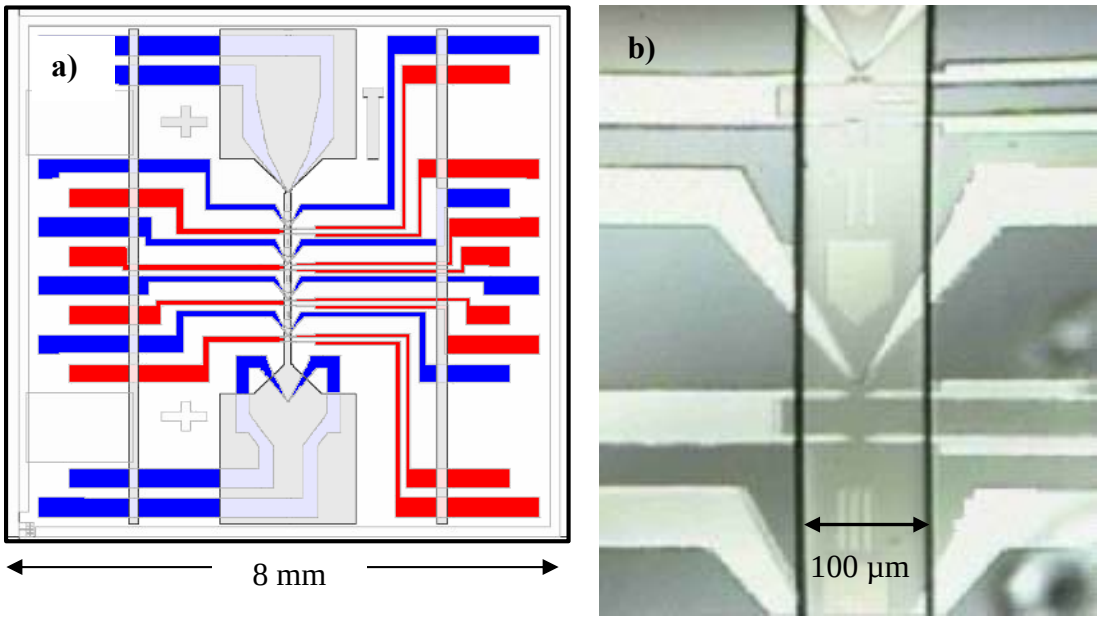


Fig. 4.10. a) "Dragonfly" design, using 2 µm × 6 µm sensors pairs and integrated with an adjacent tapered current line. Contact pads were located in the sides of the die, such that a polymer channel could be easily bonded to the chip. b) Photograph of a 100 µm wide and 25 µm height PDMS channel mounted on the "dragonfly" chip.

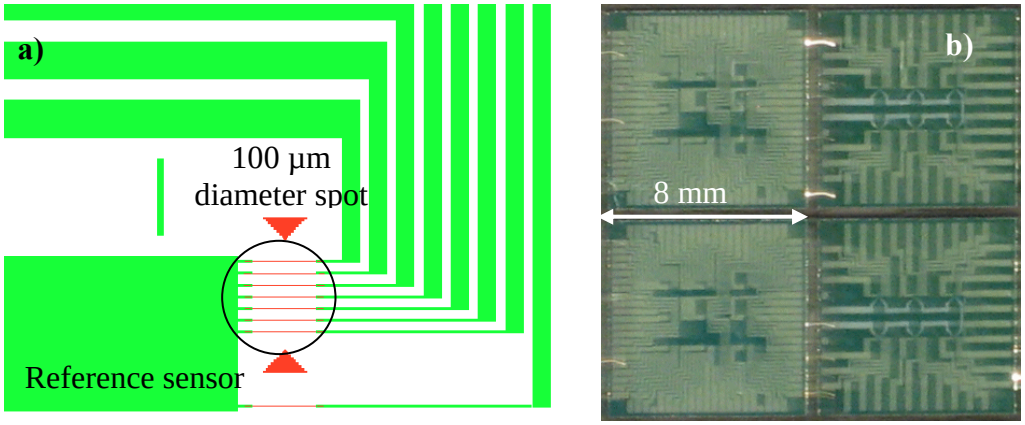


Fig. 4.11. a) "Centipede" design comprised of 2 µm × 82 µm sensors arrays, suitable for the detection of 9 different analytes only. b) Photograph of "Centipede" (left) and "Ladybug" (right) chips of a diced wafer.

A simpler die using 40 contacts was designed though, having 6 sensing units of five 2 µm × 82 µm spin valves with a common contact, without a reference sensor but with an

adjacent current line. This design was eventually used for chip temperature characterization (see figures 4.11 and 5.19 and section 5.5).

At the same time, a chip was developed with collaboration with MIC, using planar Hall sensors instead. The die was comprised of five 10 µm × 10 µm and another five 20 µm × 20 µm transducers (see fig. 4.12). Both 2 µm microspheres and 250 nm nanoparticles were detected using these transducers (Ejsing *et al.*, 2004, 2005). Later on at INESC-MN, recognition between a biotin immobilized on the sensor surface and streptavidin coated labels was demonstrated. At the time, the design of the chip was modified for magnetic manipulation of biomolecules and to enable the automatic characterization of the sensors (see fig. 4.12, chapter 6 and Carias, 2004).

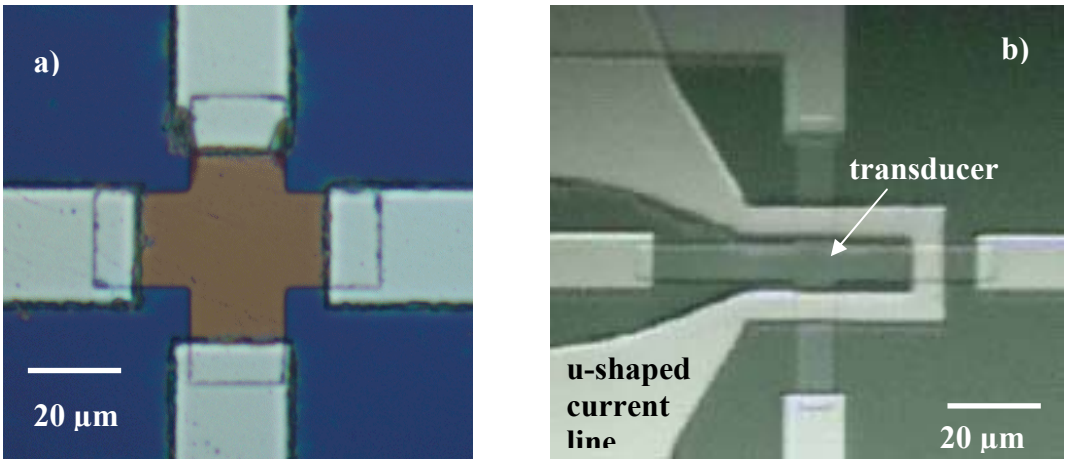


Fig. 4.12. a) Photograph of a 20 µm × 20 µm planar Hall transducer and b) a 10 µm × 10 µm planar Hall sensor with and integrated u-shaped line.

Planar Hall sensors have the advantage of being easier to fabricate than other sensors and of having larger areas than other magnetoresistive sensors, while keeping a linear response. The potential of having larger and continuous sensing areas, given by a square or round geometry of the sensor, make these sensors more suitable for fitting the sensing area to a DNA probe spot. The other magnetoresistive sensors are based on array, serpentine or spiral shaped sensors and always leave an empty space between or within the sensors that is not sensitive (see fig. 4.4b, and the discussion above concerning design on fig. 4.11).

Nevertheless, planar Hall sensors have a lower sensitivity and signal to noise ratio at high frequencies than the other types of magnetoresistive sensors, and consequently their sensitivity towards the magnetic labels is smaller.

In 2004, a renewed interest was given to magnetically labeled biomolecule on-chip transport and placement, as a consequence of having already demonstrated the detection of biomolecular recognition with several models and of recognizing the limitations of the post-hybridization detection scheme (Graham *et al*., 2004; Freitas *et al*., 2004).

The chip design encompassing 2 µm × 6 µm spin valve sensors with adjacent tapered current lines was again used (see fig. 4.8), but this time for magnetic field assisted hybridization experiments. Hybridization between cystic fibrosis related targets and probes was demonstrated to occur in 3 to 5 minutes only, using this method, unlike the previous post-hybridization detection scheme methodology where hybridization alone took at least 3 hours but usually, overnight time scales (Graham *et al*., 2005).

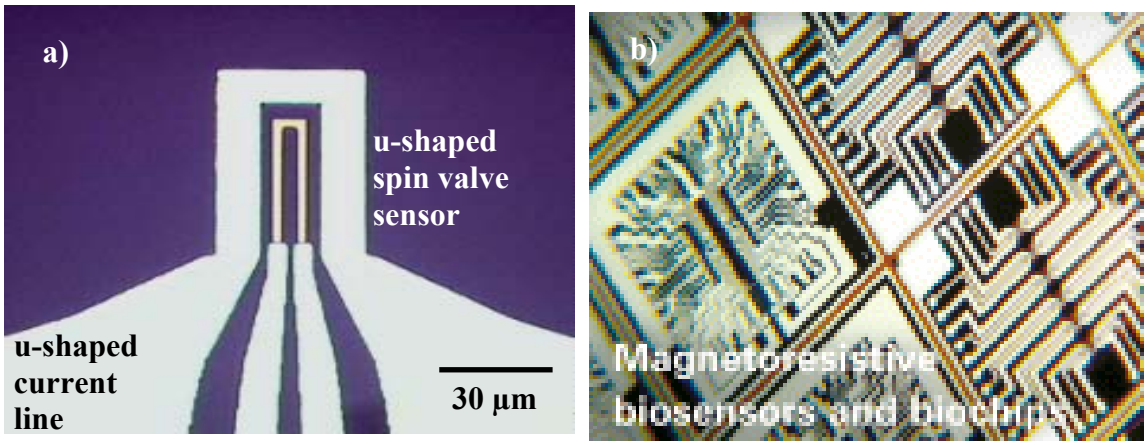


Fig. 4.13. a) "Usensor" sensing unit comprised of a 2.5 µm × 80 µm u-shaped spin valve sensor and a u-shaped current line. b) "Usensor" and "Spider" chips from cover of Trends in Biotechnology 22 issue (Graham *et al*., 2004).

At a later stage a chip was designed to quantify differences in gene expression of an ill tissue versus a healthy one (see chapters 3 and 7). In this case, a larger dynamic range was necessary and as a consequence larger 2.5 µm × 80 µm u-shaped spin valve sensors were fabricated (24 sensors per chip). These sensors allowed the detection up to a maximum of ~3200 nanoparticles of 250 nm in diameter. Each sensing unit was further

comprised by a u-shaped current line, which enabled the focusing of magnetic labels over these larger sensors, and consequently, enabled magnetic field assisted hybridization (see fig. 4.13 and Ferreira *et al*, 2005b, 2005c).

These sensors still have a very small sensing region when comparing to a typical probe spot size of 100 µm, whereas the comparison is even more unfavorable when considering the previous smaller 2 µm × 6 µm spin valves. Nevertheless, these limitations are overcome by the use of on-chip biomolecular transport and focusing systems, as discussed before in section 2.4.

Also, with respect to chip architecture, it is a fact that both single sensor proof-of-concept studies and more advanced biochip platforms show a design limitation. These platforms comprise a small number of sensing elements: INESC-MN, 24 sensors (Ferreira *et al*., 2005c); NRL, 64 serpentines (Rife *et al*., 2003); and University of Bielefeld, 200 spiral-shaped transducers (Schotter *et al*., 2004). A further increase in the number of sensing elements is accompanied by a prohibitively large number of contacts and an increasingly complex off-chip multiplexing circuitry. These designs limit then the number of different probes that can be immobilized and, consequently, the number of different analytes that can be detected in a single sample.

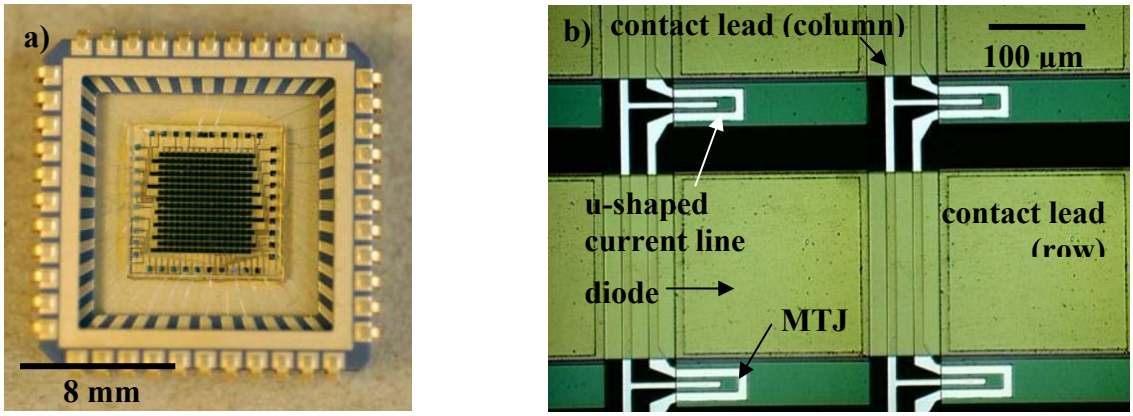


Fig. 4.14. a) Matrix of 256 magnetic tunnel junction (MTJ) sensing elements fabricated at INESC-MN (chip mounted on a chip carrier). b) Photograph showing four sensing elements of the matrix. Each sensing element is addressed using thin-film diodes of amorphous-silicon. Also shown are the row and column contacts and u-shaped current lines for the focusing of magnetically labeled targets.

Recently though, a fully scalable biosensing platform was proposed and fabricated at INESC-MN, based on a structure of a switching element and a magnetic transducer

previously studied for MRAM applications (Sousa *et al.*, 1999). A first prototype of a 16 × 16 matrix was fabricated, comprising as a sensing unit, a hydrogenated amorphous silicon (a-Si:H) thin-film diode (TFD) in series with a magnetic tunnel junction with a linear response (see fig. 4.14 and Cardoso, 2005; Cardoso *et al.*, 2006). This system can potentially be expanded to 10,000 or more sensing elements, and consequently, thousands of analytes could be screened simultaneously.

The architectures mentioned above are based on the concept of an array of sensors on a substrate or chip that is functionalized with biomolecules of interest. In this "Memory" type biochip (because the sensor arrangement in an array is similar to that of a semiconducting or magnetic memory), sensing units are comprised of sub-arrays of sensors that are functionalized with a single probe biomolecule or where each probe zone is comprised by a single sensor (see fig. 4.4b).

Nevertheless, other magnetic biosensing architectures are envisioned for the same surface detection bioassays (see fig. 1.3). These include "Credit-card" and "Hard-disk" type biochips (see fig. 4.15).

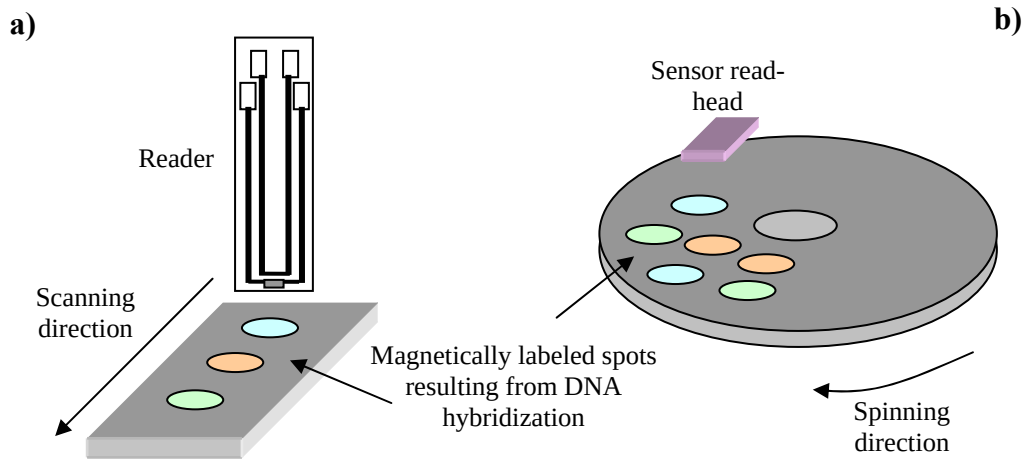


Fig. 4.15. Alternative way to measure biomolecular recognition, credit-card (a) or hard-disk (b) conception.

Both of these systems are based on the fact that the magnetic field sensor is not on the bio-functionalized substrate, but instead it scans over the functionalized and target analyte tested regions. These bioassays have then the advantage of only requiring the fabrication of a sensor or an array of sensors that is mounted as a read-head, and that functionalization and testing could be made on standard substrates using standard

procedures, apart from the required magnetic labelling. These alternatives seem to be simpler and potentially much lower cost. Nevertheless, they have the disadvantage of the magnetic reporters or tags being further away from the sensing elements, this can then limit the sensitivity of these systems and require a more complex detection apparatus.

“Memory” type biochip platforms have then the advantage of being, in principle, more sensitive and a more integrated and robust system, and can potentially be more suited for stand-alone and mobile applications. The drawbacks are then to guaranty the complementary between chip processing and surface chemistry and molecular biology, and the potential higher cost.

# 5. Magnetoresistive Biochip

## 5.1. Design

In the previous chapter several architectures and designs were discussed regarding the evolution of the work, which is related to suiting the device for the intended application.

The design starts off with issues like: the number of sensing sites required; the type of sensor to use and their size, sensitivity and dynamic range; the use of transport systems, either microchannels, current lines or both; the microfabrication process; the chip or die size; the outside world contacts; the biochemical functionalization; the detection scheme and the measurement apparatus. Frequently, a compromise has to be reached between all of these requirements.

The chip or die design is made using computer assisted drawing (CAD) software tools. During this work both the Cadence and Autocad software programs were used. The design of a chip is based on masks or layers, which correspond to steps in the microfabrication process, as it will be referred in the next section.

An example of the different masks used for the fabrication of a spintronic biochip are shown in the figure below, separately and the ensemble of them all.

Following design, the masks are converted into direct write laser (DWL) machine language. This is accomplished by converting then directly from gdsii files into lic files, in the case of using the Cadence software, or converting first dxf files generated from Autocad into gdsii files using a software package like Lasi7. The convertion itself into lic files (DWL files) is made using a specific program. Lic files correspond to 200 μm wide stripes of the exposed laser area, and the length of stripes correspond to the length of the die of the chip. There will be then a rounded up integer number of lic files that correspond to the width of the chip divided by 200 μm. This has further important consequences, as during mask design care must be taken to guaranty that features of

small sizes (example the sensors) are not placed at multiples of 200 μm. If they are there is the risk of the structures not being well exposed.

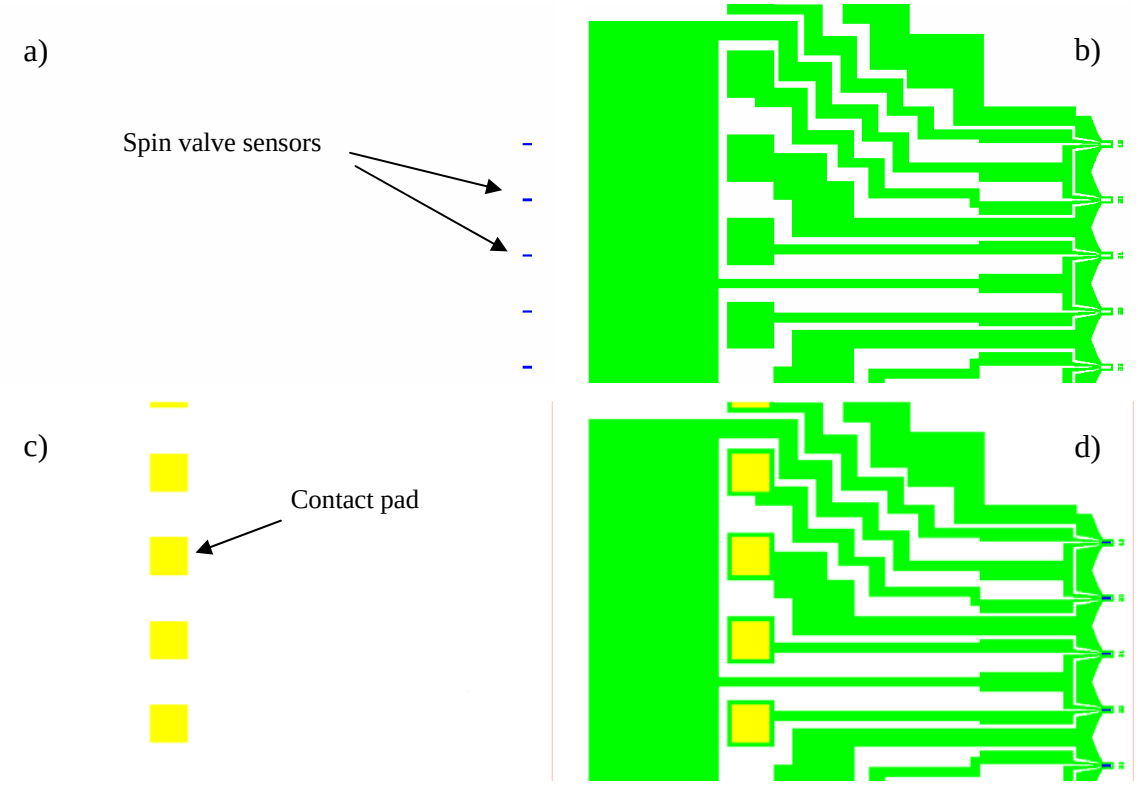


Fig. 5.1. Detail of uchip layout (spin valves) and the different layers or masks. a) sensor mask; b) sensor leads and u-shaped current lines; c) opening vias; d) ensemble of all layers.

Convertion must also take into account the photoresist or photosensitive polymer used for soft mask fabrication. If a positive photoresist is used then bonds between atoms of the polymer are broken where the polymer is exposed to light; the region then becomes soluble to a suited developer. In the case that a negative photoresist is used the reticulation of the polymer is promoted by laser light exposure and the structure is hardest to remove. In INESC-MN's standard chip processing a positive photoresist is used. In this regard and depending on the process of the wafer the mask layouts must be converted either to hold the masks or its background. The mask is said to be inverted or non-inverted (fig. 5.2)

Finally, depending on sample size, a map is made for multiple die exposure. Figure 5.3 shows an example for ~50 die exposure in a 3" Si wafer, the standard susbtrate.


Fig. 5.2. A mask layout can be converted to hold the mask itself or its background. A set of squares in the layout can result in a set of squared “mesas” in photoresist or a set of squared holes in a photoresist layer.

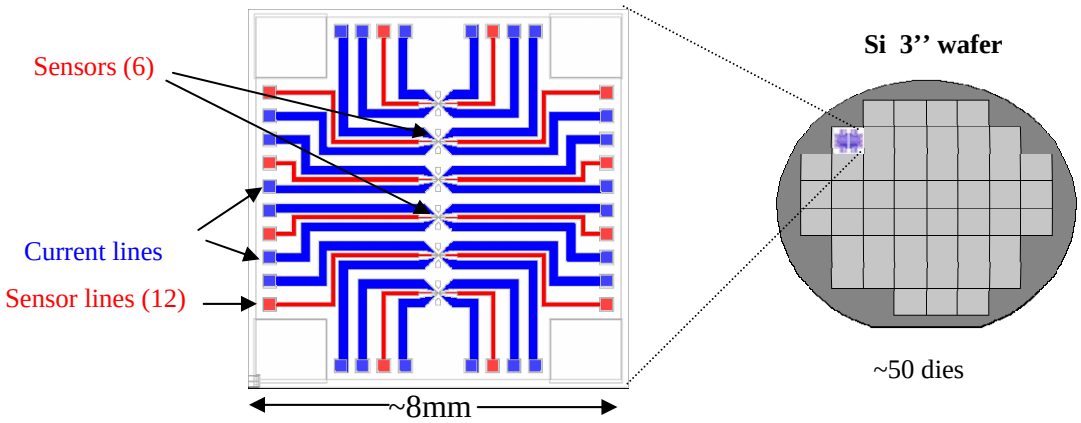


Fig. 5.3. The “Spider” layout design, where the sensor lines are shown in red and the associated current lines in blue and the sensors are located in the chip’s central region. There are ~50 chips per 3” wafer.

## 5.2. Fabrication

All chip processing is done at the clean-room 10, 100 and 10 000 class facilities in order to avoid particle contamination of the chips (fig. 5.4). Together with an air conditioning system that blows downwards to carry particles to the ground, human operators are required to use special garments and gloves in order not to contaminate chips and dirt the clean-room with skin remains and hair. Finally, security protocols and behaviors should be strictly followed when using equipment and chemicals.

Here, the standard processes for spintronic chips and poly-dimethylsiloxane (PDMS) microchannels fabrication in succinctly discussed, while thorough process run-sheets for various spintronic biochips based either on planar Hall, spin valves or MTJ sensors are presented in the appendix section at the end of the document. The core of the work

done in this thesis is using spin valve sensors, so the next subsection on spintronic chip fabrication is referred to this type of sensor.

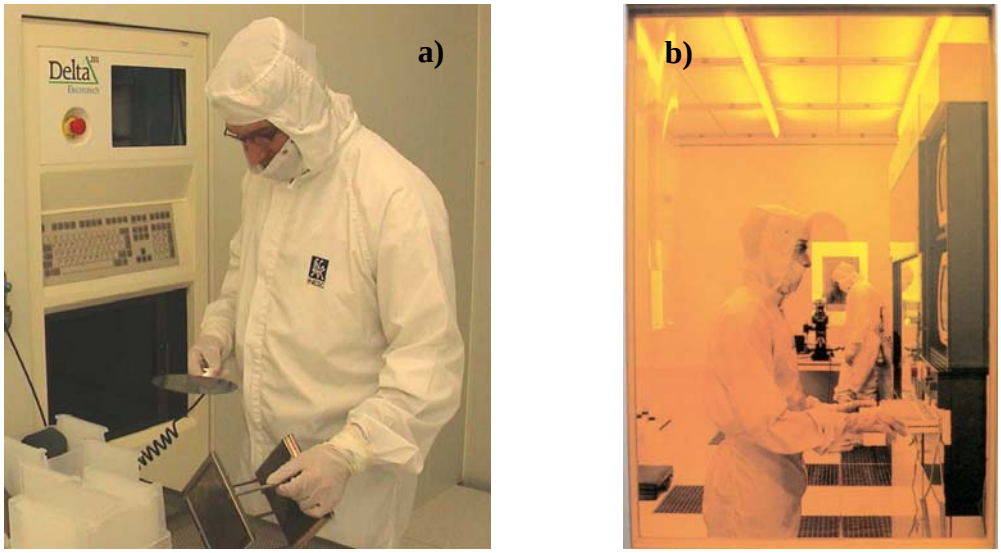


Fig. 5.4. Clean-room facilities: a) detail on clean-room garments; b) yellow room for circuit masking.

### 5.2.1. Spintronic Chip Fabrication

Spintronic chip fabrication comprises a number of steps, which are referred below (see also accompanying process pictures at the appendix after the process run-sheets).

**STEP 1:** Substrate cleaning

In this step, a 3" Si wafer (<100> orientation, 350 to 400 μm thick, 1 to 2 Ω cm, International Wafer Service) or another Si or glass sample, is washed with IPA (isopropyl alcohol) and rinsed with DI (deionised) water to remove any grease and/or particles from the substrate surface. Clean-room paper embedded in IPA can also be used. After washing, the sample is dried with a nitrogen gun and the substrate is heated in an oven at 130ºC for 30' to remove all remaining water. Alternatively, this step can be avoided if the substrate surface as obtained from the supplier. This process is done in the wet bench.

**STEP 2:** Alumina deposition

The cleaned substrate wafer or sample is passivated with 500 Å thick $Al_2O_3$ (alumina or aluminium oxide) layer in order to prevent current leakage from the sensor or current line structures into the substrate, shorting these elements. This step can be avoided if

low resistivity substrates are used and metal features on the wafer are far apart. This process is done by sputtering or physical vapour deposition (PVD) at the in-house made UHV2 machine.

**STEP 3:** Spin-valve test deposition

Before the deposition of the spin-valve material in the substrate, a 5 mm × 2.5 cm glass strip is deposited in order to check for the properties of the material. This is made in an in-house measurement setup that makes a measurement of the resistance in function of the applied magnetic field, resulting in a hysteresis loop (see section 5.3).

As seen in section 2.1 on magnetoresistive sensors, spin valves are comprised of a metallic multilayer and the standard structure is Ta/NiFe/CoFe/Cu/CoFe/MnIr/Ta. The thicknesses of the several layers vary slightly with the deposition equipment used and the machine conditions. Two machines were used, both Nordiko 2000, a sputtering tool, and Nordiko 3000, an ion-beam deposition system.

**STEP 4:** Spin-valve deposition

After the right properties are obtained, the spin-valve material is finally deposited over the cleaned $Si/Al_2O_3$ substrate.

**STEP 5:** TiW($N_2$) deposition

In this step a TiW($N_2$) 150Å layer is deposited over the spin-valve material. This layer is used to protect the spin-valve material from corrosion and damage, but also is used as an anti-reflective layer for a good mask exposure. The titanium-tungsten nitrate layer is deposited in a sputtering machine: Nordiko 7000, present in the INESC-MN's clean-room.

**STEP 6:** Resist coating

The wafer or sample is then spin coated with an organic compound called photoresist (JSR Micro PFR 7790G-27cP, positive photoresist). The polymer final thickness is 1.5 μm for a coating at 3200 rpm in the SVG tracks. The photoresist is used to make a soft mask by exposure to laser light (see previous section). Always before resist coating, the wafer or sample is deposited with an organic compound (HMDS, hexamethyldisilane,

$C_6H_{18}Si_2$) to improve the adhesion of the resist to the substrate. This previous step results in a better mask exposure.

**STEP 7:** Mask exposure (sensor mask)

The photoresist layer is exposed in a direct write laser machine (DWL 2.0, Heidelberg Instruments) using a 422 nm wavelength laser (near ultra-violet light), thus creating the required pattern (the mask). This chip layout exposure is repeated all-over the substrate surface according to a die map as in fig. 5.3.

**STEP 8:** Mask development

Bonds between atoms of the polymer are broken during exposure, making those regions more soluble to a suitable developer (JSR Micro PTH70EG solvent). The development is also done in the SVG tracks, which are located in a room illuminated with yellow light such that the photoresist does not get exposed. After development a soft mask containing the sensor patterns is obtained. Masking procedures are indeed analogous to the photography systems: a photosensitive film, exposure to light and development.

**STEP 9:** Spin-valve + TiW($N_2$) etch

The sensor structure is, finally, obtained by the "eating away" the material through the mask, in a process called etch. The spin-valve material/TiW($N_2$) which is not protected by the soft photoresist mask is etched away by an ion milling process in Nordiko 3000 or Nordiko 3600 machines, leaving the sensor shape structures well defined.

**STEP 10:** Resist stripping

After the last step, the remaining resist material on top of sensor structure is removed. This is done by putting the sample on a special organic solvent for removing the photoresist (Microstrip 2001 photoresist stripper, Fujifilm) at 80ºC, for the necessary time, and, eventually, applying ultrasounds that make the removal easier. The sample is then washed with IPA and then rinsed with DI water. This protocol is necessary because the Microstrip 2001 solution when in contact with water becomes corrosive. After rinsing, the sample is blown dried with a nitrogen gun.

Alternatively, instead of Microstrip solution, acetone can be used. This solvent is particularly suited for materials that have lower adhesion towards the substrate and tend

to peel off or materials and processes that are incompatible with the standard resist removal. Both this methods are done in the wet bench.

**STEP 11:** Resist coating

The definition of the sensor leads and current lines for magnetic transport starts, as in STEP 6, with the coating of the sample with the photoresist polymer, such that a soft mask can be made.

**STEP 12:** Mask exposure (sensor leads and current lines mask)

In the standard process both sensor leads and current lines are patterned at the same time using a single mask. Alternatively, different masks are used for sensor leads and current lines when different metal thicknesses are required for improved sensor signals and magnetic field generation.

**STEP 13:** Mask development

The mask is then developed in the SVG developer track as in STEP 8.

**STEP 14:** Al 3000Å deposition

In this step a 3000 Å thick layer of Aluminum is deposited over the photoresist mask. The Al structures comprise the metal contacts for the sensors and at the same time the associated current lines for focusing the particles at sensing sites. The Al is deposited in the Nordiko 7000 machine.

**STEP 15:** Al liftoff

To obtain the required structures for the sensor and current lines the excess Al is removed from the top of the mask using a process called lift-off. The remaining structures are those that do not have photoresist underneath. Lift-off is done by putting the sample in a Microstrip®2001 solution at 80ºC and, like in resist stripping, ultrasounds can be applied to facilitate the resist and Al removal.

**STEP 16:** Resist coating

The sample is then coated again with photoresist such that a mask for leaving opened vias to contact with sensor and current line leads is made. This is needed since oxide

layers are deposited over these structures to protect them from corrosion due to liquids and also to provide a suitable surface for biochemistry (see chapter 3).

**STEP 17:** Mask exposure (opening contact vias)
The mask is then exposed with the laser as before (see also schematics after run-sheet).

**STEP 18:** Mask development
This step is the same as before.

**STEP 19:** $Al_2O_3$ 1000Å deposition
A layer of alumina, 1000Å thick, is deposited over the surface in order to prevent corrosion of sensing and transport structures during surface functionalization and experimentation with liquid samples. This was found to be a good solution for harsh surface functionalization chemical methods such as those used by NMRC over INESC-MN's chips. The reason for this is thought to be the fact that alumina is a denser oxide than silicon dioxide ($SiO_2$), and consequently less prone to etch or damage from chemical solution, which can have high or low pH values and reasonable salt concentrations. Alumina deposition is as before done in the magnetron sputtering machine UHV2.

**STEP 20:** $SiO_2$ 2000Å deposition
A 2000Å thick layer of $SiO_2$ is subsequently deposited over the sample, not only for protection against corrosion and damage but specially to provide a suitable surface for bio-functionalization. Nevertheless, some evidences suggest that the alumina material alone is capable of being functionalized. The deposition is done in the Alcatel SCM 450 machine, also a sputtering device.

**STEP 21:** Oxide liftoff
In this step the double oxide layer is liftoff leaving opened vias for outside contact to the sensors and current lines to be made. The procedure is like of STEP 15. This is the last step of the microfabrication protocol. The wafer is now ready to be tested and subsequently diced.

Alternatively, when the extra alumina layer is not required the protocol can have some differences and following the aluminum liftoff in STEP 15, the 2000Å thick layer of $SiO_2$ can already be deposited. In this case, a soft mask is subsequently defined for opening contact vias on the oxide (the mask is reciprocal to that of previous protocol), and the oxide is etched away. This etch is done at a LAM Research machine and is is called a reactive ion etch since it uses, besides the ion's physical etch, chemical etch with $O_2$ and $CF_4$. The process ends with resist stripping in the wet bench, just like in STEP 10 (see appendix and Ferreira, 2001).

In the alternative protocol, the Delta201 (Electrotech) can be used for silicon dioxide deposition. The deposition is made by a method called chemical vapour deposition (CVD) and requires high temperatures, which in the previous microfabrication process for oxide lift-off would result in the burning of the photoresist. Consequently, the removal of the mask would be much harder.

The time-scale for spin valve biochip process is typically 1,5 to 2 weeks.

After control testing of the sensors in an home-made setup using probe needles (see next section), the wafer is diced in a Disco DAD 321 machine into its several dies (fig. 5.5). Previously the wafer is coated with photoresist such that the dirt created during the dicing does not contaminate the chips. After dicing, individual chips are washed with acetone or put in a bath of Microstrip 2001 at 80ºC for a couple of minutes and are then rinsed with IPA and DI water.

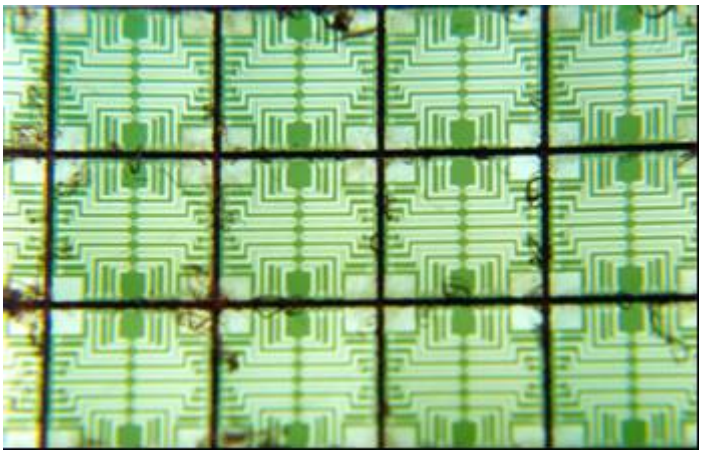

Fig. 5.5. Final manufactured chips cut using a dicing saw.

Finally, chips are mounted on chip carriers or designed print circuit boards (PCBs). Chips are glued into the recess or cavity of the chip carrier using an acrylate-based glue (super-glue) and aluminum wirebonds (18 to 25 μm in diameter) are made from the carrier metal pads to the chips sensor and current line pads. The wirebonds are then covered with a silicon polymer (Elastosil E41, Wacker) for mechanical resistance and protection from corrosion. The silicon layer further creates a chamber in the carrier where the experiments are made (fig. 5.6).

Run-sheets and processing details for planar Hall and magnetic tunnel junction based biochips can be found elsewhere (Carias, 2004; Cardoso, 2005).

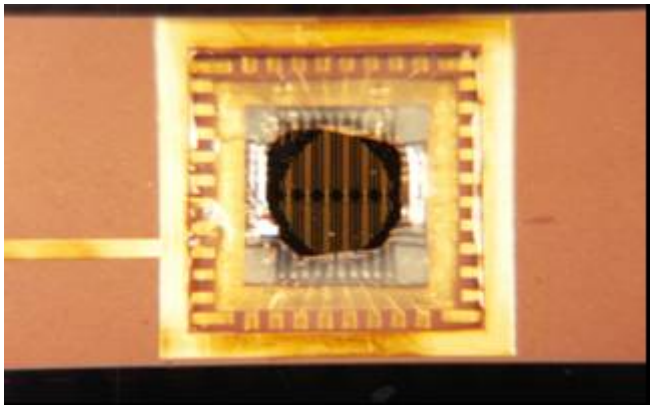

Fig. 5.6: Picture showing wirebonds between the contact pads of the chip and those of the chip carrier. A silicon gel layer covers the wirebonds for mechanical resistance and protection from corrosion.

### 5.2.2. PDMS Microchannel Fabrication

The standard process for microchannel fabrication is by molding, which involves casting of the polymer over a thick photoresist mould. The mould itself is defined by ultra-violet (UV) light exposure of the resist through a quartz mask. Therefore polydimethylsiloxane (PDMS, Sylgard 184, Dow Corning) microchannel fabrication involves three different processes: the fabrication of the quartz mask; the preparation of the polymer and the fabrication of the mold.

Here below, the process steps will be described and at the appendix run-sheets can be found, which includes bonding of the microchannel to the biochip. A more complete and thorough description along with different fabrication process can be found elsewhere (Parracho, 2002).

*Quartz mask*

**STEP 1:** Substrate cleaning

A 1”×1” quartz substrate is washed using a detergent solution (Alconox) and ultrasounds for 30 min. This is followed by rinse with DI water and drying with nitrogen gun. This is done in the wet bench

**STEP 2:** Metal deposition

In this step, 1500 Å thick aluminum followed by 150 Å thick TiW($N_2$) layers are deposited in Nordiko 7000, a sputtering machine.

**STEP 3:** Resist coating

A 1.5 µm thick layer of photoresist (JSR Micro PFR 7790G-27cP) is deposited over the sample at 3200 rpm, preceded by HMDS deposition or priming in order to promoted the resist adhesion.

**STEP 4:** Mask exposure (microfluidic structure)

The mask for the microfluidic structure, including channels and reservoirs is exposed as mentioned in the previous subsection.

**STEP 5:** Mask development

The development of the mask also proceeds as before.

**STEP 6:** Metal etch

The aluminum/ titanium tungsten nitrate bilayer is etched using an ion beam deposition system such as Nordiko 3000 or Nordiko 3600.

**STEP 7:** Resist stripping

The final step of the quartz mask fabrication is the removal of the remaining photoresist. The procedure mentioned in the previous subsection is used.

*Polymer preparation*

**STEP 1:** Weighting

The PDMS polymer preparation consists of adding a base and a curing agent. The amount to add of each of the substances depends on the application and desired material properties. Here, a ratio of 10:1 base to curing agent ratio was considered.

**STEP 2:** Mixing

The base and curing agent in the desired proportion are then added and mixed gently to prevent air to be incorporated in the mixture.

**STEP 3:** Degassing

The mixture is left to rest for 1 to 2h for degassing. Nevertheless, this time can be reduced to ~15 min if the PDMS mixture is put in primary vacuum.

*Mold fabrication*

**STEP 1:** Substrate cleaning

In this step, a 6" Si wafer is washed with IPA and rinsed with DI water to remove any grease and/or particles from the substrate surface. Clean-room paper embedded in IPA can also be used. After washing, the sample is dried with a nitrogen gun and the substrate is heated in an oven at 130ºC for 30' to remove all remaining water. Alternatively, this step can be avoided if the substrate surface as obtained from the supplier. This process is done in the wet bench.

**STEP 2:** Thick resist coating

Before resist coating, the wafer or sample is covered or primed with HMDS to improve the adhesion of the resist to the substrate. The wafer or sample is then spin coated with a thick photoresist (AZ4562 positive resist, Clariant). Before baking, the resist is left to degas for 15 min. The polymer final thickness is ~20 μm, but extra coating can be done for thickness up to 50 μm.

**STEP 3:** Mask exposure (microfluidic structure)

The thick resist is then used to make a mold by exposure to ultra-violet (UV) light, using a 250W UV Flood Lamp (UV Light Technology) and the quartz mask mentioned above.

**STEP 4:** Mask development

The thick resist mask is developed in AZ 351B developer. The sample is then rinsed in DI and dried with a nitrogen gun.

*Microfluidic fabrication and assembly*

**STEP 1:** Polymer pouring

The PDMS material can then be cast or poured over the thick photoresist mold. This can be done using a spinner or manually. In the latter case, time must be given to achieve a flat surface. At this step, metal tubes can be placed over the reservoir mold in order to define an open chamber for outside contact to macroscopic tubing.

**STEP 2:** Polymer curing

The polymer mixture is then cured at an oven for 1h at 65ºC. In alternative it can be left for 48 hours at room temperature to solidify.

**STEP 3:** Master removal

The microfluidic structure is then removed from the mold by cutting the right size with a razor blade, for example, and then peeling it off.

**STEP4:** Assembly

The final step is the assembly of the microfluidic structure with the spintronic biochip. In that regard both the microchannel and the chip are exposed to oxygen ($O_2$) plasma (PlasmaTherm In-Line WaferEtch), which increases the adhesion of the PDMS towards the $SiO_2$ surface. After the $O_2$ treatment both surfaces are put into contact, applying pressure, such that a permanent sealing can be made.

A picture of the final magnetoresistive chip with a bound microchannel structure is shown in fig. 5.7.

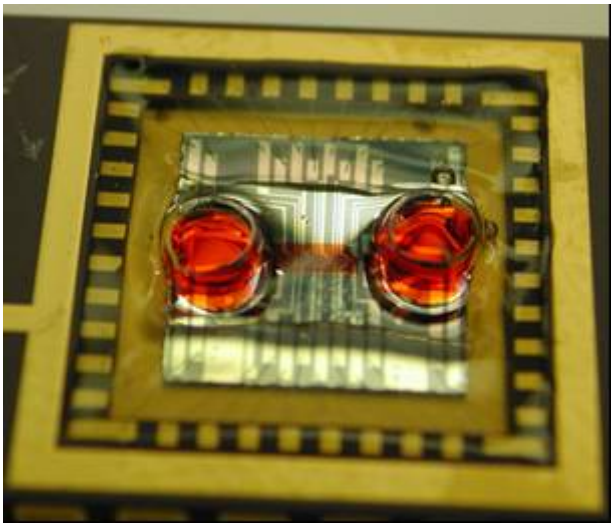

Fig. 5.7. Magnetoresistive biochip with bound microchannel assembled onto a chip carrier.

## 5.3. Electrical and Magnetic Characterization

As discussed in the previous section for the spintronic biochip fabrication, the sensor material is first tested for evaluation of the right properties. A 5 mm × 2.5 cm glass strip is used for that effect. The glass strip is deposited with the sensor multilayer under an external magnetic field in order to define an easy axis for the magnetization of the ferromagnetic layers. A hysteretic loop measured along this direction results in a square shaped loop response.

The measurement setup is shown below in figure 5.8, where the easy axis direction is referred to as well.

Typical bulk sample response to the applied magnetic field is shown in the figure 5.9 for major and minor hysteresis loops.

In the major loop, $H_{ex}$ represents the exchange field, which is the magnetic field required for rotating the pinned layer and results from exchange coupling between an antiferromagnetic and a ferromagnetic layer. In the minor loop, $H_c$ represents the coercive field necessary to rotate the free layer along the applied field, and $H_f$ represents the ferromagnetic coupling field, and is related to coupling between the ferromagnetic

layers due to stray fields produced by interface roughness. This effect is also called orange peel or Néel coupling.

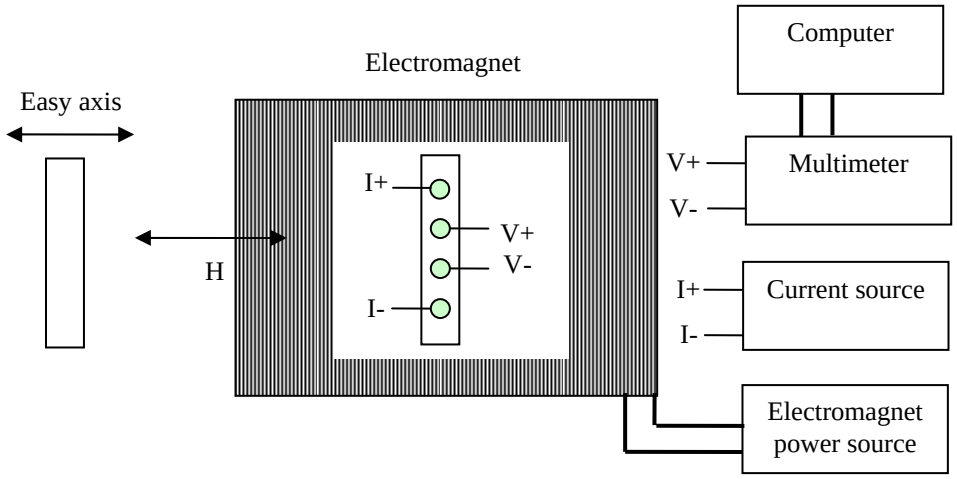


Fig. 5.8. Four-point probe measurement setup for electrical and magnetic characterization of bulk samples of spin valve material. H indicates the direction of the generated magnetic field.

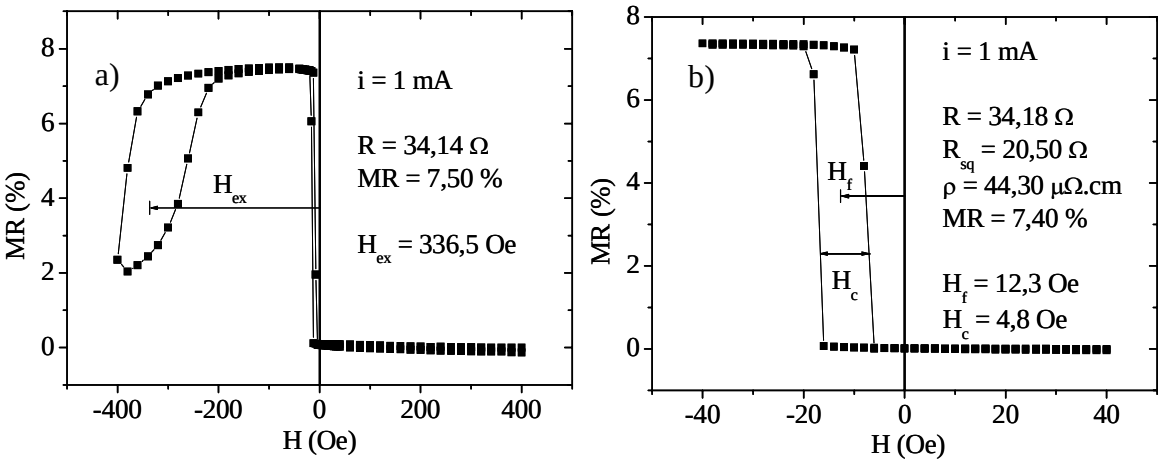


Fig. 5.9. Spin valve coupon sample transfer curve measured with the field applied in the easy axis direction a) major loop; b) minor loop. R is the resistance of the sample, $R_{sq}$ is the square resistance, ρ is the electrical resistivity, MR is the magnetoresistance ratio and I is the sense current (see text for more details).

Typical parameter values for working sensors are: magnetoresistance ratios (MR) >6%; $H_c$ < 6 Oe; $H_f$ < 10-12 Oe; and $H_{ex}$ > 250 Oe. Also typical square resistances for spin valves range between 15 to 20 Ω/ sq. If the test sample do not comply with this requisites, process conditions are fined tuned and new samples are deposited.

When the sensor material characterization is not as straightforward as is in the case of spin valves or some more in-depth characterization is required, the Vibrating Sample Magnetometry (VSM) device (DMS system) is used instead. In this case the glass coupon sample is put to vibrate under a magnetic applied field. The magnetization or the magnetic moment of the different ferromagnetic layers creates a magnetic field that excites a pick-up coil at a particular frequency. This signal is then measured and probes the magnetic properties of the sensor materials. Contrary to the other measurement setup, the VSM apparatus does not enable an electrical characterization of the sensor. A typical measurement for a planar Hall test sample is shown below.

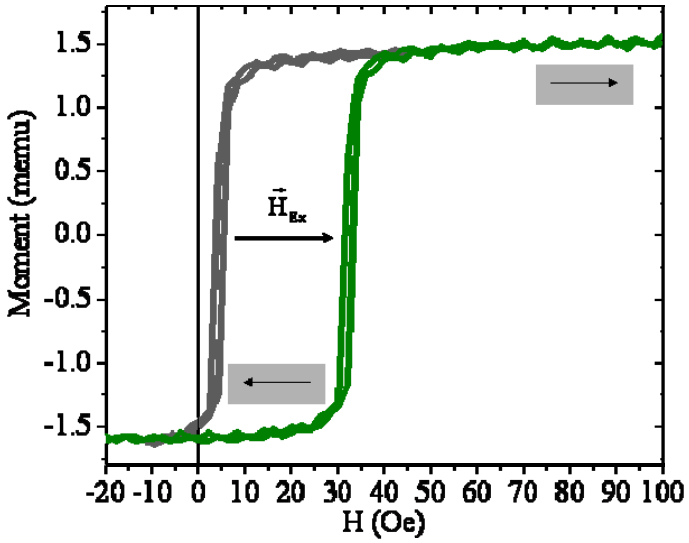


Fig. 5.10. Vibrating Sample Magnetometry measurements of a planar Hall sensor test samples with the structures Ta30Å/NiFe300Å/Ta30Å (black curve) and Ta30Å/NiFe300Å/MnIr200Å/Ta30Å (green curve), respectively. The shift in the green curve ($H_{ex}$, exchange field) is due to the extra exchange coupling between the MnIr antiferromagnetic layer and the soft permalloy layer. Here, NiFe stands for $Ni_{80}Fe_{20}$ and MnIr stands for $Mn_{76}Ir_{24}$). Arrows enclosed in the grey squares indicate the direction of the magnetization or magnetic moment of the thin film multilayer (See Carias, 2004 for details).

After patterning, the sensor response is distinct from the one presented above for the bulk or coupon sample. Due to shape anisotropy the magnetic moment of the free layer is roughly perpendicular to the magnetization of the pinned layer, and as was discussed in chapter 2, the sensor response is linear around zero applied field. This holds for both spin valve and magnetic tunnel junction sensors, while for planar Hall sensors the requirement for linearity is that the direction of the magnetization and that of the current are perpendicular at zero magnetic field.

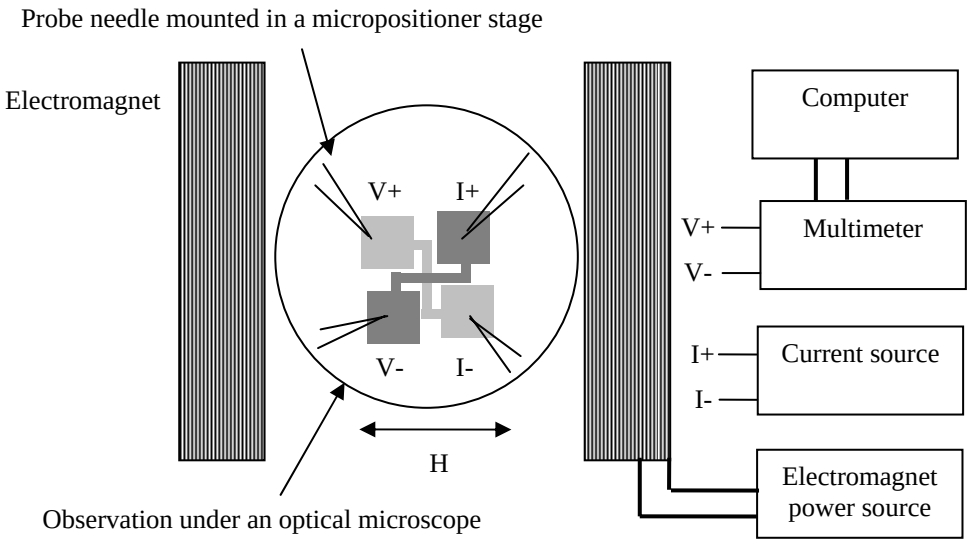


Fig. 5.11. Measurement setup for patterned sensors. 4-point probe needles are used for measuring MTJ test sensor structures. H indicates the direction of the generated magnetic field (Drawings not to scale).

The electrical characterization and transfer curve of the patterned sensors are done in a setup similar to the one of Fig. 5.8 but contact to sensors is made using either 2 or 4 probe needles, depending on the sensor and whether measurements are made 2 or 4 point, respectively, and the field is generated by two separated electromagnets (see fig. 5.11).

A typical transfer curve for a spin valve sensor is shown in fig. 5.12 below.

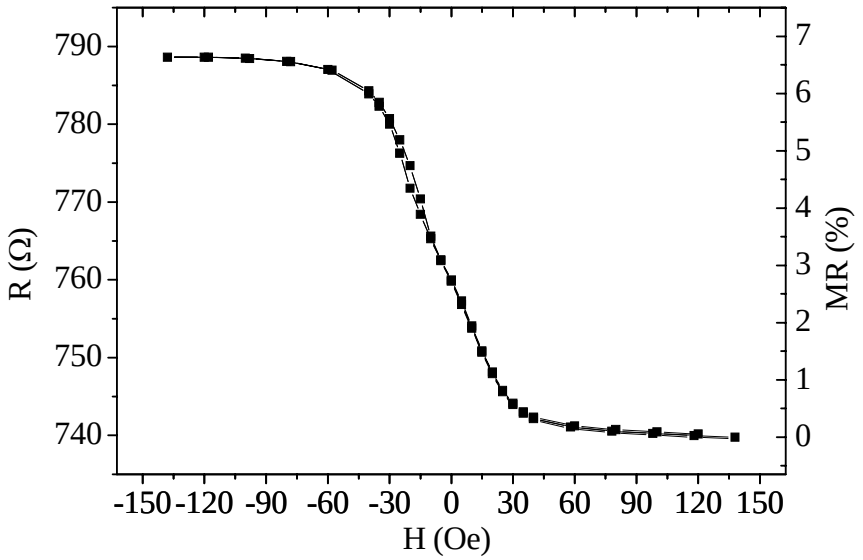


Fig. 5.12. Typical transfer curve for a 2.5 µm × 80 µm u-shaped spin valve sensor (see previous subsection on spintronic biochip fabrication and related run-sheets for the structure of the transducer).

All the referred measurement setups are semi-automatic in the sense that, although magnetic field looping and data acquisition and is done automatically, different sensing structures are manually probed for measurement. This can be a quite time-consuming process, especially when a single die can have tens or hundredths of transducers.
In order to have a higher sensor characterization throughput an automatic measurement setup (KLA 1007E, KLA Instruments) can be used (see fig. 5.13). The latter consists of a series of probe needles in a dual line arrangement. After a first stage of aligning the sensor die with the needles the data acquisition and the commutation between different sensing structures is done automatically. Usually sensor die test structures are used for testing and evaluating material and process properties, but it can also be adapted to biochips (Carias, 2004).

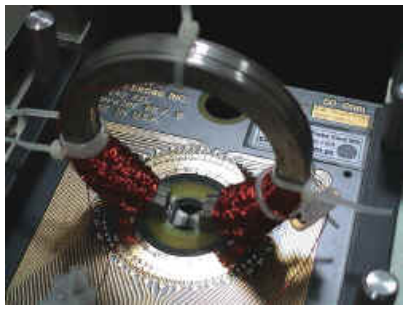

Fig. 5.13. Photograph of the KLA automatic measurement setup.

## 5.4. Noise Characterization

Sensor noise was already introduced back in chapter two as a measure of figure of merit of sensor performance. This section is thus devoted to the methodology followed and apparatus used in the characterization of sensor noise.

In a first study of sensor noise properties, noise was measured using the lock-in setup used for bioassay experiments (see next chapter). The background sensor ac response was measured at the typical operating conditions for magnetic label detection, including 30 Hz excitation magnetic field and a lock-in time constant of 0.3 s, and magnetic field amplitudes and sense currents depending on sensor type and transfer-curve. Signals from different sensors were averaged for about 2 min, the time above which the average value remains relatively constant.

This approach had some drawbacks as measurements were quite time consuming, depended on the time constant time and sensitivity range of the lock-in amplifier and was specific for a single frequency. In addition the used setup was not perfectly shielded. Nevertheless, it was possible to make a comparison between the different sensor types and geometries and assess which were the best sensors to use for a particular set of conditions (see section 2.1 and Freitas et al., 2004).

In a second, more recent approach, a chip-carrier, with an assembled magnetoresistive chip, was mounted in a bread-board inside a µ-metal shielded box and was connected through a low frequency voltage amplifier (DLPV-100-BLN-S, Femto), using a gain of 60 dB, to a real-time spectrum analyzer (Model RSA 3308A, Tektronix) (see figure 5.14 and also R. Ferreira *et al*., in press).

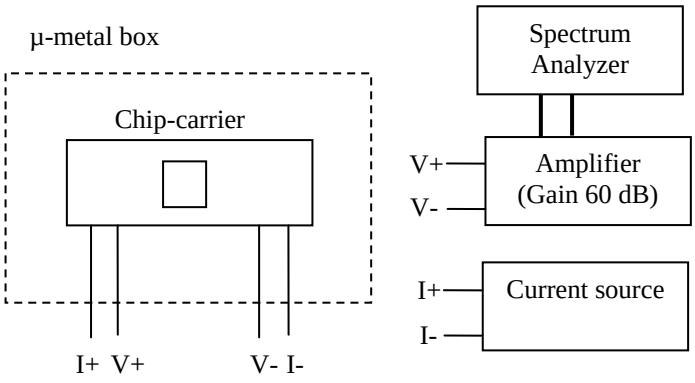


Fig. 5.14. Experimental setup for noise power spectra measurements.

Power noise spectra from spin valves were then measured from dc up to 100 kHz for sense currents of 0.1 mA within the linear regime of the sensor where no external magnetic bias field was applied.

Figure 5.15 shows a noise power spectrum obtained for a u-shaped 2.5 µm × 80 µm spin valve sensor, together with a power noise fit comprising the 1/f and thermal noise:

$$S_V^N = \left(V_{rms}^N\right)^2 = \frac{R^2 I^2}{N_C}\frac{\gamma}{f^\alpha} + 4k_B TR \qquad (32)$$

Here the left hand side term is the 1/f noise and the right hand side term is the thermal noise, given as in equation 15 on section 2.1. R is also the resistance of the transducer and I is the sense current. $N_C$ is the number of charge carriers, assumed to be one noise carrier per atom and incorporating the free, spacer and pinned layers (Raquet, 2001). Finally, the fitting parameters $\gamma$ ~1 (Hooge's constant) and $\alpha$ ~1 were estimated from the fit.

The calculated thermal background is also shown ($1.1\times10^{-17}$ V/Hz), and agrees well with the measured value (~$1.4\times10^{-17}$ V/Hz). The observed difference may be due to a parasitic noise, but most probably can be due to a contribution from magnetic noise (Almeida *et al*., in press).

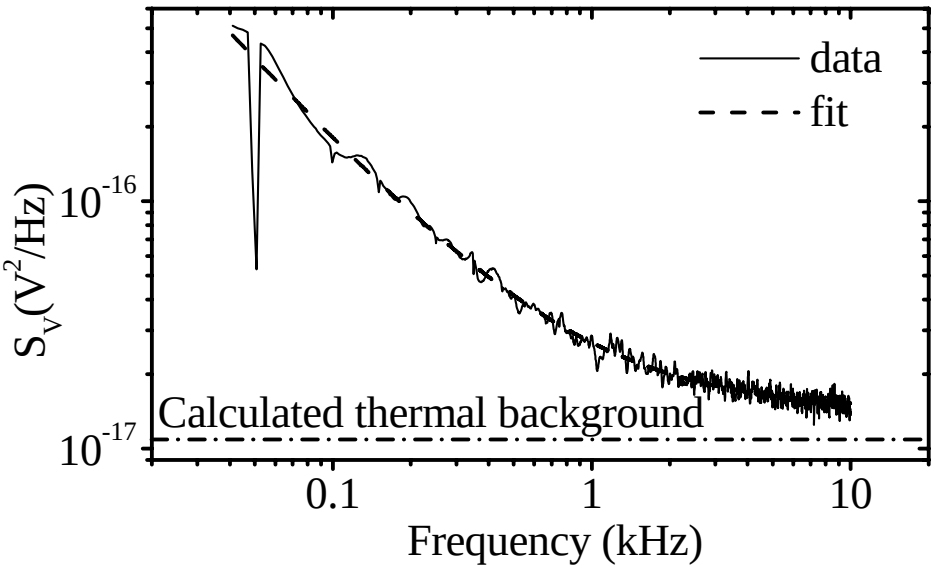


Fig. 5.15. Noise spectrum for a a u-shaped 2.5 µm × 80 µm spin valve sensor, together with a fit comprising the 1/f and thermal noise. The sense current was 0.1 mA due to amplifier current limitations.

The 1/f knee was observed at ~1 kHz for a sense current 0.1 mA. Nevertheless, the measuring sense current in bioassay applications is 1 mA. The use of 0.1 mA current is a limitation of the amplifier. For 1 mA the 1/f knee was estimated at 50 kHz, given the fitting parameters.

In addition, given the u-shaped spin valves typical sensitivities, the sensor noise was calculated to be of ~0.2 $nT/Hz^{0.5}$ in the thermal noise regime, while at 30 Hz (the

frequency typically used in bioassay measurements, see next chapter) it was estimated to be ~11 nT/Hz$^{0.5}$. This value of noise corresponds to about 250 nV rms, which is considerably smaller than the experimental setup measured noise (see also next chapter and Ferreira *et al*., 2006).

Finally, even given the limitations stated for the first approach, the parameters obtained from the spectrum analyzer result in noise values in the same order of magnitude estimated for similar sized spin valve sensors. This means that the first setup already provided a good indication of the noise characteristics.

## 5.5. Temperature Characterization

Besides performing electrical and magnetic characterization, temperature response of the sensors was also studied. Temperature is an utmost important parameter when doing biological assays. Biomolecules are sensitive to temperature, and as was mentioned previously temperature may be used to promote or hinder biomolecular recognition. Furthermore it can be used as a stringency method for discriminating complementary from non-complementary or unspecific binding. It is therefore necessary to measure and control on-chip temperature.

Spin valve sensors were tested for the response to temperature, and two different experimental setups were used for that purpose.

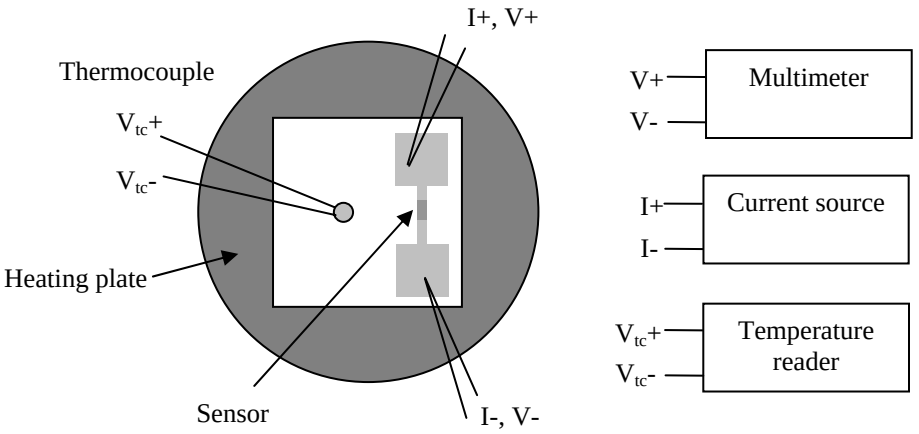


Fig. 5.16. Experimental setup for measuring spin valve sensor response to temperature.

A first setup was used where a spin-valve sensor resistance was measured while varying its temperature. The resistance was measured using probe needles, while the temperature was recorded using a chromel-alumel type K thermocouple (Omega), which was glued to the chip using a silver-based epoxy. The calibration of the sensor response was done by heating the chip from room-temperature up to about 100 ºC. Then, the system was left to cold down back to room temperature, while both sensor resistance and temperature was recorded at the same time. It was found that it results were more reliable when measuring during cold down, than heating up, because the heating plate changed increased the temperature quite rapidly, while its value also was not very stable.

A second setup was used where the chip was already mounted in a chip carrier, as discussed above. In addition, the chip-carrier was mounted on a bread-board to where connections to the sensor where made via BNC cables. These fed also to a multimeter. The bread-board was placed inside an oven which was heated up to 100 ºC. The resistance measurements were also done the same way as before during cool down. The temperature was measured again with the thermocouple in contact with the chip surface (see also Vidal, 2005).

Both approaches held the same results. A typical temperature response is shown in Fig. 5.17.

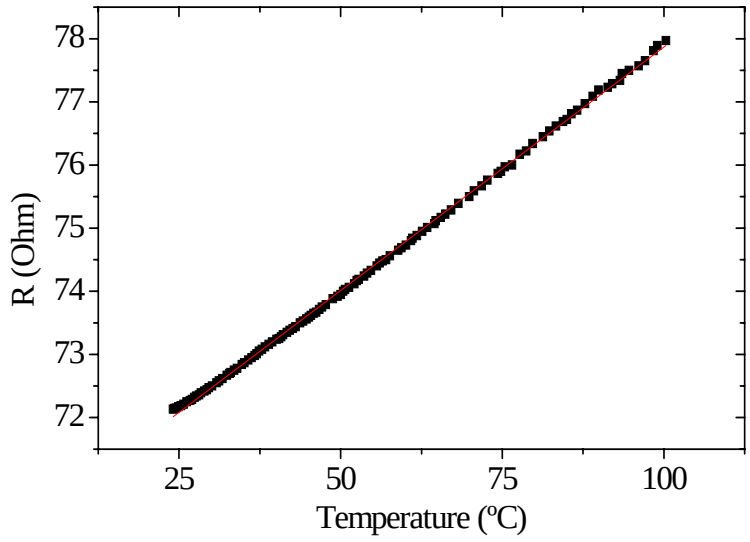


Fig. 5.17. Spin valve sensor response to temperature.

The spintronic transducer response was observed to be linear and its slope normalized to the resistance was shown to be independent of the sensors resistance and size, $1/R_0$ $\Delta R/\Delta T \sim 10^{-3}$, as the response with the temperature is characteristic of the spin valve multilayer materials. In the previous relation $R_0$ is the sensors' resistance at room temperature, R is the resistance and T, the temperature.

These results show that spin valve sensors are good temperature sensors provided that they are shielded from external magnetic fields. In fact, these sensors show a thermal drift response that can be explained due to the fact that the sensor is reaching thermal equilibrium with the surrounding environment (see discussion on the next chapter).

When combining solid-state transducers and chips and biological assays, it matters to know whether the heat dissipation from on-chip structures hinders or promotes biomolecular recognition processes (see previous chapters).

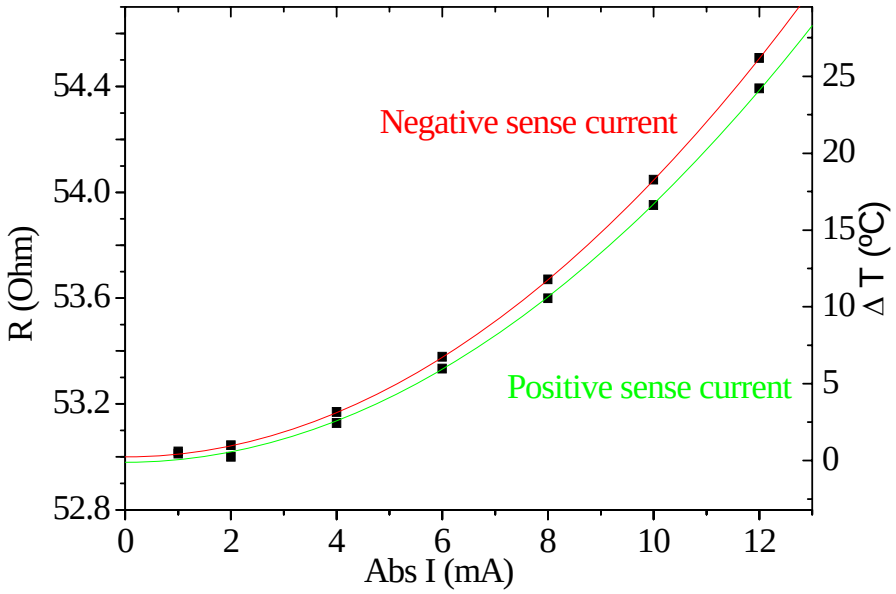

Fig. 5.18. Spin valve sensor response to different sensing currents.

In that regard, the temperature of the sensor due to Joule heating was measured by applying increasing currents and measuring the transducer resistance immediately after applying the current. The spin valves where saturated in the low resistance state while measuring such that they would not be sensitive to the bias field created by the sense current itself. Figure 5.18 show a parabolic behaviour of the resistance in function of the

applied current obtained for a 2 µm × 6 µm spin valve sensor. This is consistent with Joule heating.

The difference observed between positive and negative sense currents is due to a small response of the transducer to the bias magnetic field created by the current. It is also observed that, for typical sense currents of 8 mA used in small spin valve sensors, the transducer itself increases its temperature around 10ºC. This results in a temperature at the sensor surface (above the oxide passivate layers) close to 35ºC, which is closer to the optimum for hybridization conditions (between 37 to 42ºC) and well below the melting point of target-probe pairing DNA strands used in experiments (Graham *et al*., 2005).

Larger u-shaped 2.5 µm × 80 µm spin valve sensors are usually operated with 1 mA sense currents, resulting in an increase of temperature of only a few degrees.

Nevertheless much larger currents are applied to the on-chip magnetic transport structures, which could heat up the chip and in particular, the biological probe sites. For typical currents of 20 to 60 mA through the tapered conductors the temperature increase of the sensor was less than 3 to 6ºC over a period of 10 min (Graham *et al*., 2005).

A further study was done with a test chip, where five 2 µm × 80 µm spin valve sensors with a common contact where measured over time while applying current through a tapered conductor, adjacent to one of the sensors. The sensors were located at about 20, 40, 60, 80 and 100 µm away from the current line (see also fig. on chapter 4).

In figure 5.19 the sensor temperature in function of the distance to the current line is shown. Sense currents of 0.1 mA, such that the sensors did not heat due to the sense currents themselves; currents of 60 mA were applied through the tapered current line.

More recently, a temperature actuator was introduced in chip design for temperature control. This has the possibility of improving biomolecular recognition processes by using a suitable temperature (e.g. 37 to 42ºC) and of improving assay specificity by using heating as a stringent method to discriminate between perfect matching from unspecific binding. On-chip temperature control potentially enables the use of

polymerase chain reaction for amplification of nucleic acids, fully integrated with in the chip.

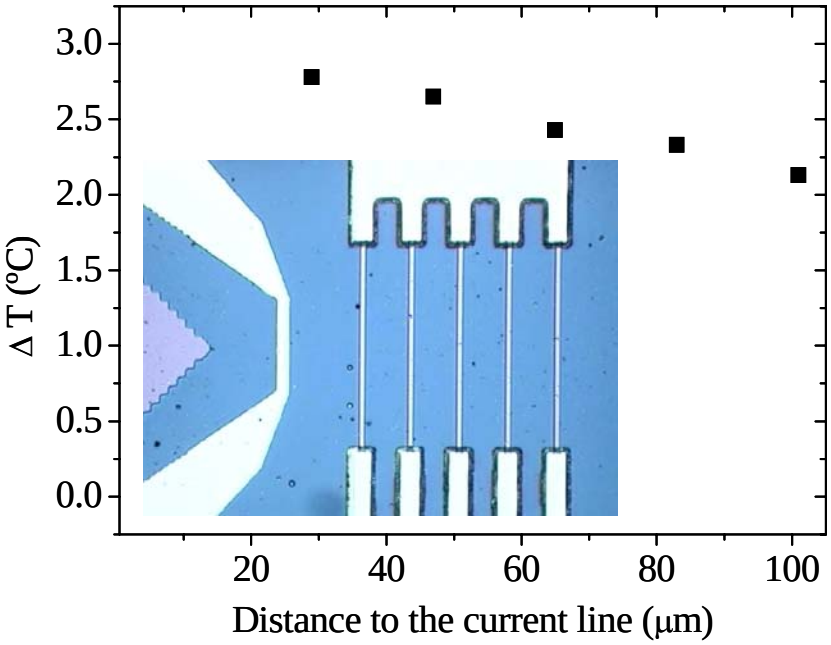


Fig. 5.19. Sensor temperature in function of the distance to the heat source.

The fabricated temperature actuator is a simple metallic serpentine fabricated of aluminum at the same time as the sensor leads and transport current lines (see fig. 5.20). In alternative, the heater lines can be made of a higher resistivity material such as TiW($N_2$) for improved Joule heat dissipation, but at the expense of a more complex fabrication process (Vidal, 2005).

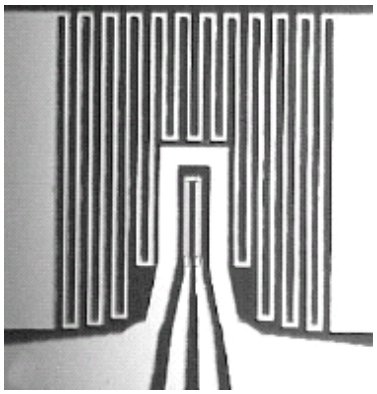

Fig. 5.20. U-shaped spin valve sensor chip with integrated serpentine heater lines.

Using heater lines temperatures above 100ºC could be easily obtained in open air or liquid environment (see fig. 5.21). Nevertheless, in liquid environment it was observed that aluminum lines corroded after a couple of minutes of heating for even low applied currents. This was the case where tap or DI water was used, and most probably resulted from pH local changes due to large on-chip voltages across the heater structures (see also related discussion in section 5.1). This fact is further confirmed by use of a phosphate buffer solution (keeps pH nearly constant at values of 7.0), which enabled the application of higher currents for longer periods of time with no corrosion observed (Vidal, 2005).

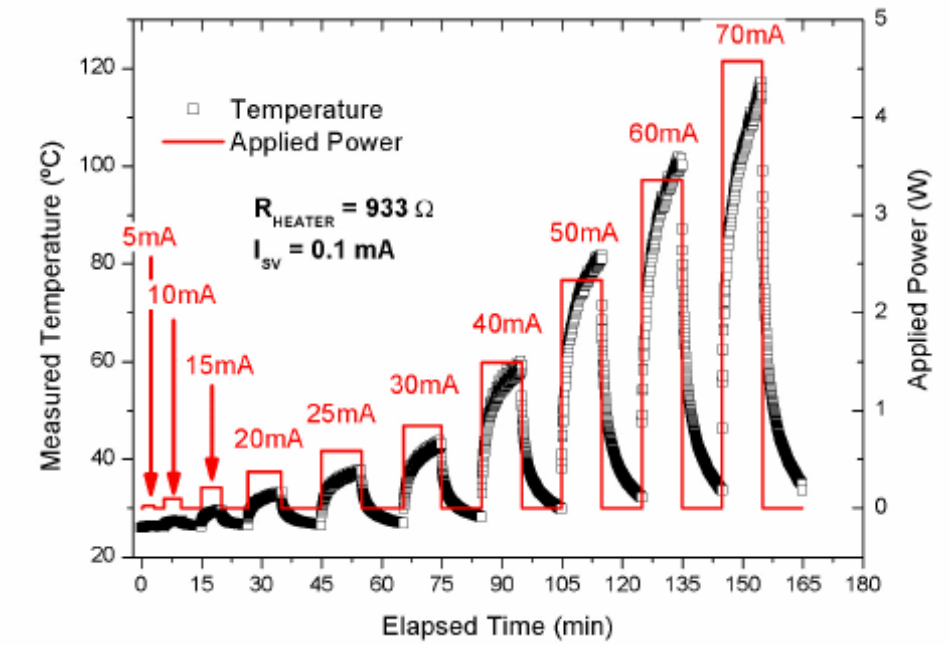


Fig. 5.21. Heating of biochip using serpentine heater lines. Current applied on the heater lines is indicated as well as the corresponding power. The temperature was measured using u-shaped spin valve sensors (Vidal, 2005).

During chip development a number of parameters have been identified which are important for heat generation and control. Such parameters include the substrate and the passivation materials, as well as the fluid used (see above and next chapter), which impose constraints on the design of the chip and limit the range of current/ voltage that can be applied and the time of operation.

From early experiments, it was noticed that the use of a glass substrate resulted in a large heating and frequently in the destruction of on-chip structures, especially when using the transport current lines. When the goal is to generate large magnetic fields and magnetic field gradients then silicon substrates are a best choice, since the heat dissipates much better to silicon than through glass. In fact, it was observed that the material and the thickness of the oxide layers for passivating the substrate and the chip are quite important.

As discussed in section 5.1, typically thin layers of alumina oxide (500 Å) were used. These layers were observed to conduct heat well to the silicon substrate. In an experiment done with a similar chip from the Korean Institute of Technology (KIST), which had a 2000 Å thick oxide layer as a substrate, boiling of testing fluid was observed for similar currents. This can be explained by a lower thermal conductivity of $SiO_2$ (1.38 W $m^{-1}$ $K^{-1}$) relatively to $Al_2O_3$ (36 W $m^{-1}$ $K^{-1}$), and by the increased thickness of the first case (see details in Vidal, 2005).

Consequently, is also important to take into account the thicknesses of the layers that passivate the chip structures (sensors, magnetic transport current lines and heater lines) in order for the heat to be correctly dissipated either to the substrate or to the sample fluid, as desired.

All these parameters are associated with heating time constants that can be studied from the curves shown above in figure 5.21 (see details in Vidal, 2005).

# 6. Experimental Setup

## 6.1 Design and Operation Constraints

The experimental setup has, as the chip design itself, evolved over time, together with the chip and the detection schemes as discussed in previous chapters.

The experimental setup shows also some design and operation constraints and these include sensor, transport system, chip design, bioassay, security and power consumption issues, which are all interconnected.

Depending on sensor type, either planar Hall, spin-valves or MTJs then different voltage/ current limitations exist in order not to degrade sensor performance and transfer curve linearity or even to destroy the sensor. For the fabricated devices, currents up to 10 mA and above could be fed into planar Hall sensors and spin-valves, whilst applying voltages above 1 to 2 V would be sufficient to destroy the MTJ oxide barrier.

Current maximum depends on sensor resistance and chip fabrication but also on the assay. Since these magnetoresistive devices are used in liquid environment, heating effects limit the current maximum that can be applied. Heating effects can lead to protein denaturation or melting of double stranded DNA, which are undesired effects if not under control (see previous chapter). Furthermore, heating may lead to bubble formation, turning the assay unviable.

Joule heating is related to sensor resistance, as the higher the resistance the higher the power dissipated in the form of heat (see previous chapter). So for instance for smaller 2 μm × 6 μm spin valve sensors, currents up to 10 mA were used, while for larger 2.5 μm × 80 μm transducers current was limited to 2 mA in liquid to prevent bubble formation. The heating considerations above also hold for the on-chip magnetic transport structures, as they also behave as resistors.

It was also observed that chip fabrication is important for heating, as for instance if thicker oxide layers or glass are used as a substrate, heat dissipation is larger to the liquid sample, thus preventing the use of larger currents either for sensing or transport. In fact, all the layers and materials have to be taken into account when designing the chip and the application (see fig. 6.1 and discussion in previous chapter).

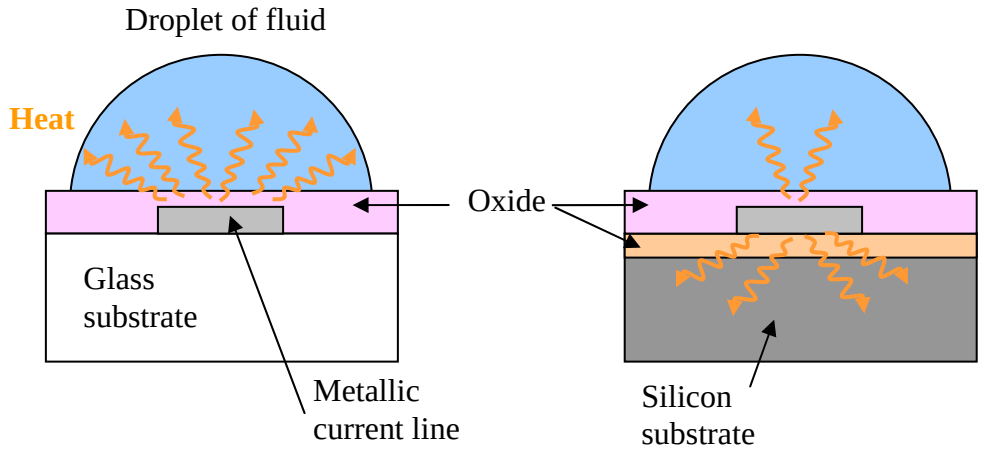


Fig. 6.1. Substrate and oxide materials used and their thickness determine where Joule heating dissipates preferably. This fact imposes constraints on chip design and operation.

Current limitation is also related to the voltage applied across the sensing structures. In fact large on-chip voltages of >3 to 4 V seem to be associated with the chemical damaging of the oxide passivating layer and the destruction of the covered metal lines used as sensor leads or current conductors for magnetic transport (see previous chapter). These high dc voltages over time give rise to local pH changes and electrolysis. It is thought that pH changes result from the attraction of hydroxyl anions and other charged species to the higher voltages sites. Then these chemical species promote the etching of the oxide and subsequently of the metal lines (see Fig. 6.2).

Finally, the setup should also be designed taking into account security constraints, like having system low voltages (< 5V) and correct wiring and grounding between devices, and also power consumption constraints, which must be keep as low as possible to comply with the development of a portable biosensing system, the end goal for this project.

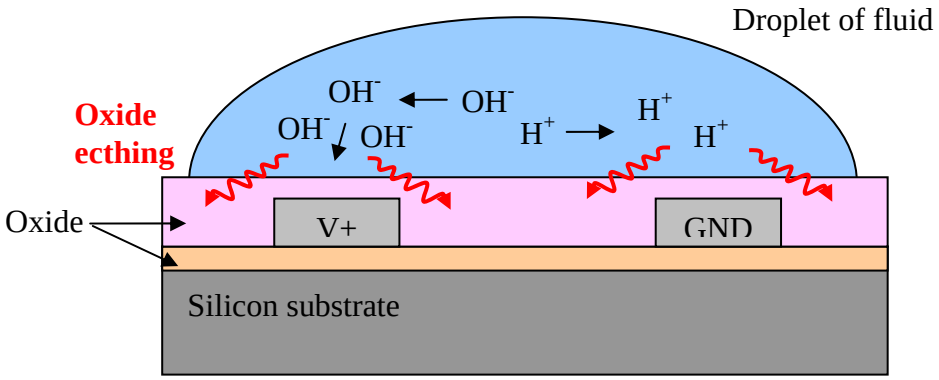


Fig. 6.2. Large voltages across on-chip structures result in local pH changes that promote oxide etching and, consequently, the corrosion of metallic lines.

## 6.2 Direct Current Measurements

The first setup built was simple direct current (dc) resistance measurement (fig. 6.3a).

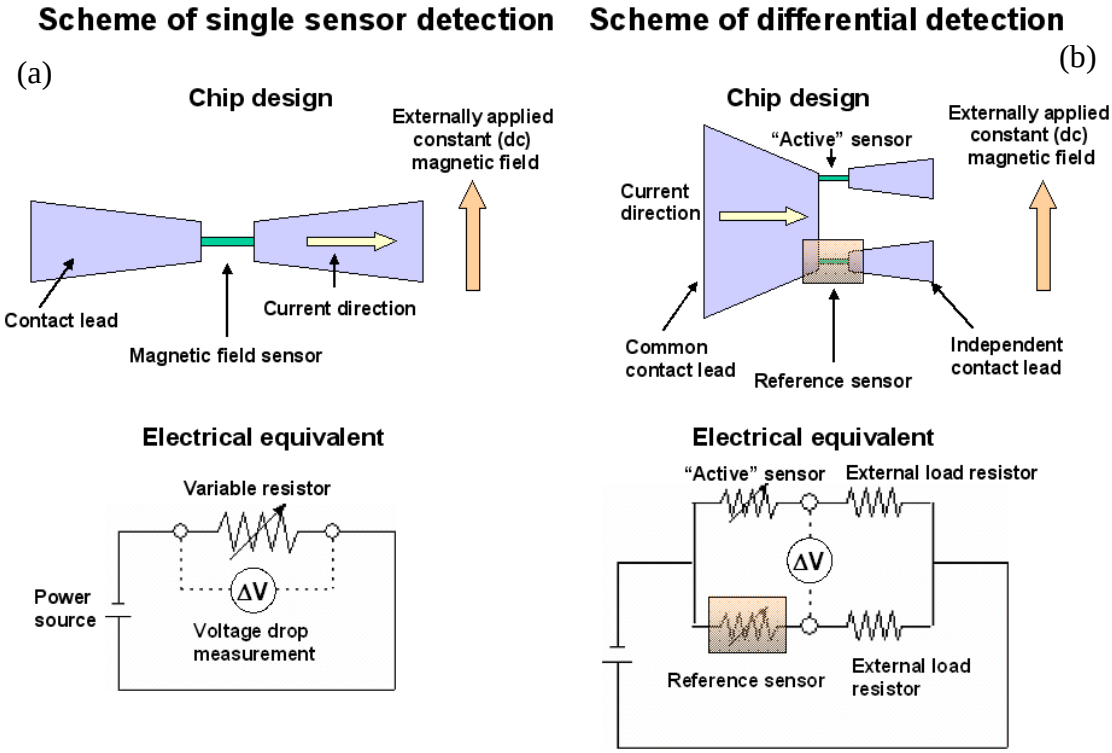


Fig. 6.3. Schemes for single (a) or differential (b) sensor measurements, together with electrical equivalents and emphasizing on the direction of the external magnetizing field.

The apparatus was comprised of breadboard that established the connections between the biochip, mounted in a 40-pin dual side braze chip carrier (CSB04057, Spectrum

Semiconductor Materials), and a dc current power source (HP 6236B Triple Output Power Supply or Keithley 220 programmable current source) that fed a sensor, and two dc power sources (HP E3612A DC power supply) that could be used to excite the current lines adjacent to the sensor.

An additional power source (HP E3612A DC power supply) was used to feed a custom-made horseshoe electromagnet that was placed above the chip carrier. The electromagnet had a $Ni_{80}Fe_{20}$ soft magnetic core made from old 5 cm diameter sputtering targets and a 0.25 mm diameter copper winding was made around the full structure. The electromagnet generated an uniform dc magnetic field in the plane of the chip and in the sensing direction of the transducer (see fig. 6.3 and chapter 2). The field was used both to magnetize the superparamagnetic labels and to bias the sensor curve. Typically 150 mA were used to feed the magnet, which correspond to about 15 Oe (1.2 kA/m) at the chip surface (see magnet calibration in Ferreira, 2001).

A multimeter (HP 34401A) was used to measure the voltage drop across the sensor. Data was fed to a computer by a general purpose interface bus (GPIB) connection (Agilent GPIB PCI board) and the acquisition was controlled using a VisualBasic (Microsoft) program developed in-house. All electrical connections between instruments and components were made using co-axial cables (fig. 6.4).

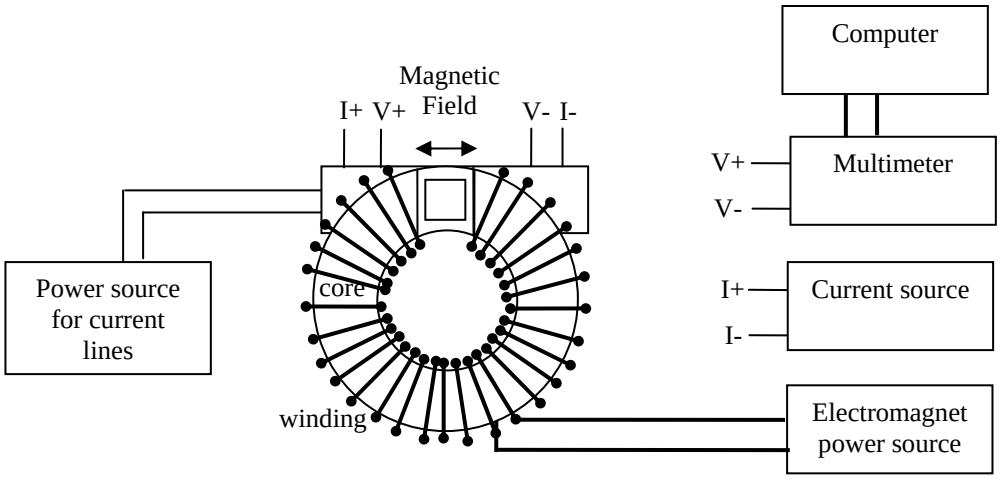


Fig. 6.4. Experimental setup for single sensor and differential measurements.

The breadboard, the chip carrier and the electromagnet could further be housed in an aluminum noise shielding box or placed under a high focal distance objective of an

optical microscope (Leica LMDM) for simultaneous detection experiment and photo/video capture (JVC 3-CCD KY-F55B video camera and FlashBus MV Pro Frame Grabber, Integral Technologies).

This setup was used in early experiments for single sensor measurement and magnetic label control using tapered current conductors (Graham *et al*., 2002; Ferreira *et al*., 2003). It was observed though, that the system was quite sensitive to temperature changes in the environment, and furthermore a temperature drift was observed. As a consequence, the system was generally left for an hour or two to stabilize and reach equilibrium temperature with the surroundings. In addition, and as mentioned previously in the section concerning magnetic labels, the noise of the experimental setup was measured to be 10 to 20 μV.

In magnetic label movement and controlled placement experiments, tapered conductors were typically fed with 20 to 40 mA. This corresponded to ~ 0.6 to 1.2 Oe (~0.05 to 0.1 kA/m) created at the sensor, which is located 5 μm away from the adjacent current lines (see section 2.4).

The setup was further adapted for differential measurements (Fig. 6.3b), where a half-wheastone bridge arrangement was used. A sensor pair with a common contact comprised half of the bridge that was completed with two external load resistors (~1 kΩ). The idea behind this setup was to measure a differential signal between an "active" sensor and a reference sensor, such that temperature drift effects were canceled. The "active" sensor detected biomolecular recognition whilst the reference sensor was covered with a photoresist layer to prevent sensor surface functionalization. In fact, the full chip was covered with photoresist except a 20 μm × 20 μm area on top of the "active" sensor. This area further defined the biological sensing area (see discussion on chapter 4).

The signal $\Delta V_{diff}$ obtained from the differential measurement was proportional to the difference in signal between the two sensors:

$$\Delta \mathbf{V_{diff}} = \frac{(R_A - R_R)R_L}{R_A + R_R + 2R_L} I \qquad (33)$$

Where $R_A$ is the electrical resistance of the "active" sensor and changes due the presence of magnetic labels in the vicinity, $R_R$ is the resistance of the reference sensor, and $R_L$ is the resistance of the off-chip load resistors that complete the bridge (assumed to be equal for both arms of the bridge). Finally, I is the current that feeds the bridge arrangement.

From the above expression, it can be seen that for the signal to be related only to the difference between the two sensors and not significantly to the effect of the "active" sensor resistance change in the denominator, the load resistors resistance should be around 5 to 10 times larger than the resistance of the sensors. Ideally, for $R_L >> R_A, R_R$ comes that $\Delta V_{diff} = I(R_A\text{-}R_R)/2$, but in order to comply with sensor voltage/current limitations, heating effects, security and power consumption guidelines, smaller current have to be used, and consequently smaller signals are obtained.

The trade-off here was that to diminish temperature drift effects, a smaller signal was obtained. Nevertheless, it was observed that temperature drift were not significantly canceled as sensors had distinct resistances, which resulted over the time of the experiment in a considerable resistance change.

Instead, sensor pair measurements were done. Using the same half-wheatstone bridge arrangement, each sensor in the pair was measured using an independent GPIB-controlled multimeter (HP 34401A), and the differential signal was obtained in the end (Graham *et al*., 2003). Apart from the extra load resistors for the bridge and the extra multimeter and the software change, the experimental apparatus remained the same as for the single sensor measurements.

Sensor pair measurements were also done in fluid flow velocity experiments (see section 2.3). In this case though, two different current sources were used to feed two 2 μm × 6 μm spin-valve sensors, one located near the inlet and the other located near the outlet of a microfluidic PDMS structure bonded to the chip. Here, two multimeters

controlled by a personal computer were also used for measuring each transducer (see fig. 6.5).

Sequential measurements from each of the sensors was obtained using a variation of the VisualBasic program mentioned above, and velocities were then calculated from the time difference of the signal rises and the distance between the sensors (~1.65 mm) (see section on results and Ferreira *et al*., 2004).

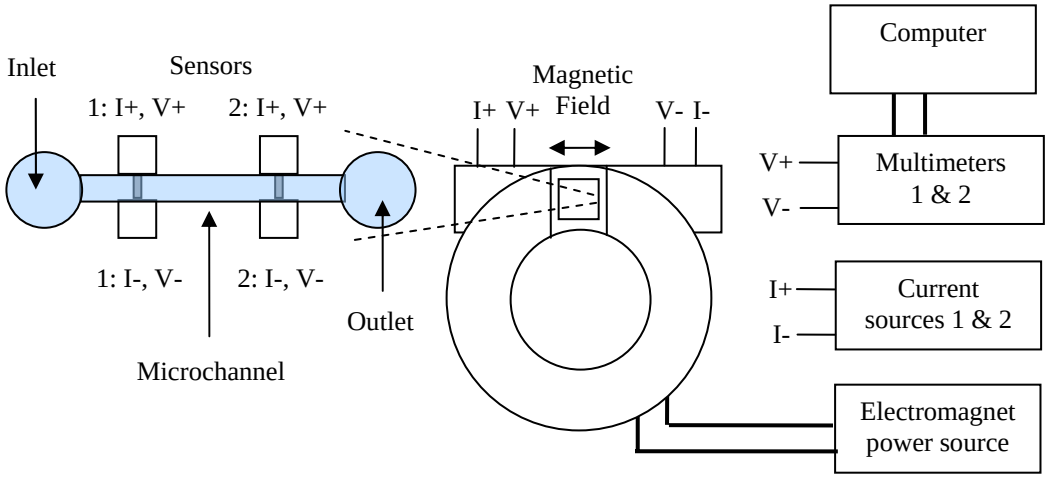


Fig. 6.5. Experimental setup for fluid velocity measurements (no electromagnet copper winding visible for simplicity of schematic).

## 6.3 Alternate Current Measurements

In order to avoid the thermal drift, and consequently, the hour long times for sensor stabilization, an alternate current (ac) measuring setup was built. The apparatus was similar to the one used for dc measurements, but in this case the multimeter was replaced by a lock-in amplifier (EG&G Princeton Applied Research 5209 Lock-in Amplifier) and an ac current was supplied to the horse-shoe electromagnet in order to excite the spintronic transducers at a specific frequency. A Philips PM 5132 function generator was used for that effect, and more recently it was used instead a HP 3220A function generator, which as improved features.

In addition, when using the focusing of magnetically labeled biomolecules (see chapter 2), an extra Philips PM 5132 function generator was used (see fig. 6.6).

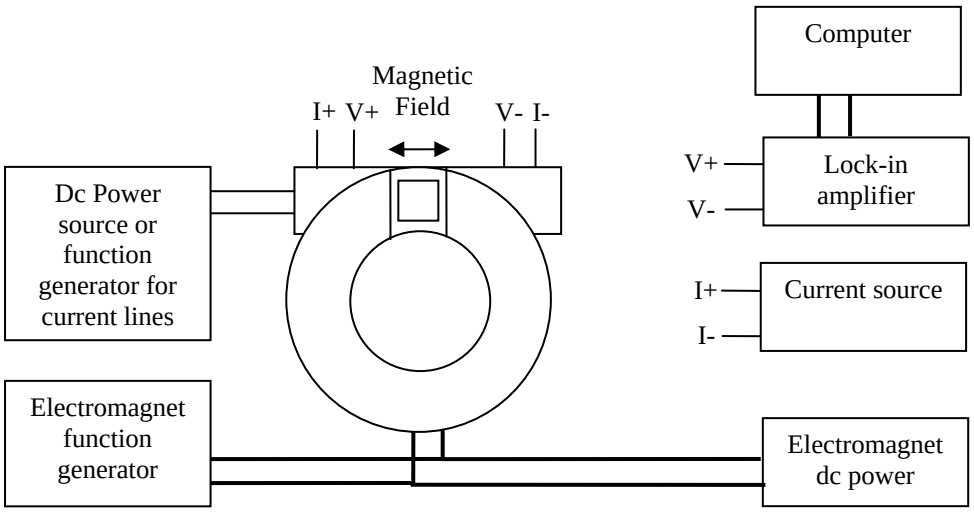


Fig. 6.6. Experimental setup for alternate current measurements.

Data acquisition and apparatus control was achieved using a custom adapted LabView (National Instruments) program.

Although, sensor noise is reduced at higher excitation frequencies, as discussed in chapter 5, ac measurements were done at 30 Hz. This low frequency was chosen because the initially used function generator, the PM 5132 instrument, had an output that diminished reasonably with the increase in frequency. So, in order to supply the highest current possible such that magnetic labels acquire a high magnetic moment, a compromised between frequency and current output was achieved.

In addition, the operating frequency was chosen such that it did not correspond to 50 Hz or multiples of that frequency, in order to avoid these noise sources generated from the laboratory electrical cabling.

As observed in fig. 6.6, a dc power source was set in parallel with a function generator to feed the electromagnet. This arrangement was used for both biasing the sensors' transfer curve and exciting at 30 Hz measuring frequency (Ferreira *et al*., 2005c, 2006). Typical dc currents used were between 150 to 250 mA depending on sensor size and transfer curve characteristics. The field created was 15 Oe (1.2 kA/m) and 25 Oe (~2.0 kA/m), respectively, and was chosen such that the ac sensor response was maximum (see discussion on chapter 2.)

The dc magnetic field created by the electromagnet was also used for focusing magnetic labels at sensor sites and for magnetic field assisted hybridization. In this case the extra function generator was used to feed the u-shaped current lines with 20 to 40 mA rms (0.3 to 0.6 Oe rms at 10 µm away) at frequencies ranging 0.2 to 20 Hz (Ferreira *et al.*, 2005c).

Alternatively, when performing magnetic focusing experiments without simultaneous magnetic label measurements, the function generator was used to feed the electromagnet at currents of 130 to 170 mA rms and the same frequency range as mentioned above. A dc current (from 20 to 40 mA) was then applied to the u-shaped current lines (see section 2.4 and Ferreira *et al*., 2005b).

Finally, the noise of the setup alone was about 1 to 3 µV rms for the typical operating conditions of 10 mV lock-in resolution and 300 ms time constant. This noise was observed to be the limit for detection of single 250 nm magnetic labels using the 2 µm × 6 µm spin-valve sensors (see chapter 2).

## 6.4 Multiplexing

The above mentioned setups were used for single or dual/differential sensor measurements. This limited the chip to be tested with few sensors at a time. In particular, when performing biomolecular recognition assay, only a sensor per chip was used, as after the first assay is done, the surface of the chip would be covered already with magnetic labels (for a complementary target and probe case).

In order to be able to measure more than one sensor in a bioassay, a setup for ac measurements was developed that enables the automatic switching and monitoring of an array of sensors. This was achieved using a complementary metal-oxide semiconductor (CMOS) analog multiplexer (Maxim DG406DJ 16-Channel integrated circuit). The IC (integrated circuit) was powered with ± 5 V using a GW GPC-3020 DC power supply and the switching was done using a National Instruments board, NI DAQ PCI6024E (see multiplexer and DAQ connection in appendix E).

The switching between sensors was achieved using a common contact at ground and the IC switching port at a positive voltage. The ac sensor responses were measured also at these points, and although the multiplexer on-resistances are ~100 Ω, only the sensing elements are responsive to an ac exciting magnetic field. The apparatus is then similar to the one for ac measurements, as presented above, and was controlled using a custom made LabView program with switching capabilities (see fig. 6.7 and also Appendix E).

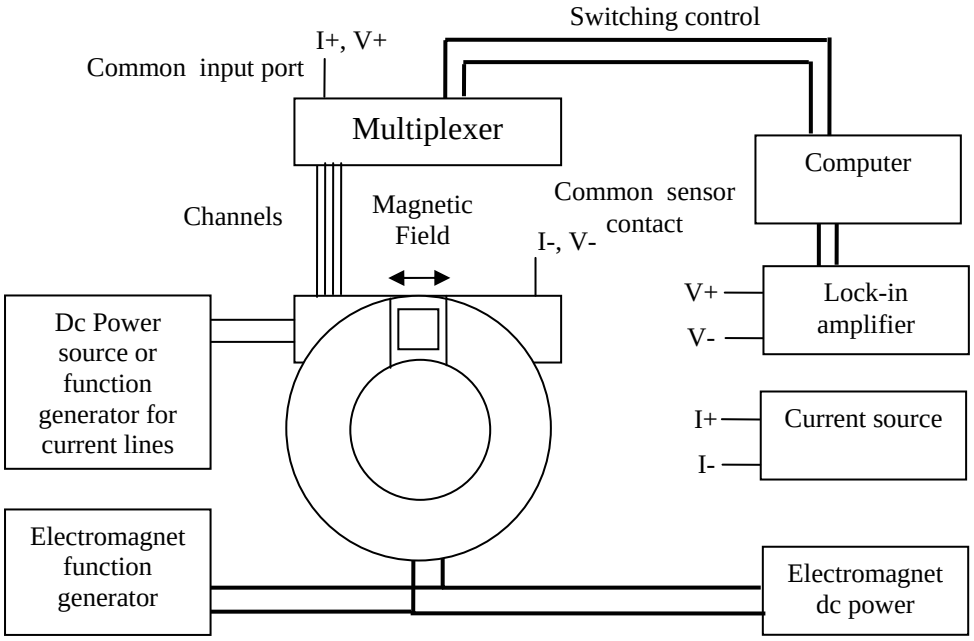


Fig. 6.7. Experimental setup for multiplexing sensor alternate current measurements.

This experimental setup resulted in statistical data, which provided much richer information regarding the dynamics and variability of magnetic label detection and biomolecular recognition (see chapter 7 and Ferreira *et al*., 2005c, 2006).

Furthermore, during bioassay experiments and taking into account the response of reference sensors the noise was estimated to be ~10 μV rms over 1 hour experiment time (see chapter 2 and Ferreira *et al.*, 2006).

The experimental setups shown here are the ones used for mainly spin-valve based biochips, but were also used with planar Hall sensors and magnetic tunnel junctions by introducing slight changes in the apparatus (e.g. 4 point measurements in the case of planar Hall transducers) and in operation (e.g. different currents and biasing magnetic

fields in the case of magnetic tunnel junctions). Details can be found elsewhere for planar Hall sensors (Carias, 2004) and magnetic tunnel junctions (Cardoso, 2005).

## 6.5 Fluid Handling

With respect to fluid handling operation, all experiments, dc, ac and multiplexing assays for the detection of magnetic labels only or for the detection of biomolecular recognition, where done in open chamber, which is defined by the chip-carrier recess and the silicon gel (see fig. 5.6). Fluid handling was achieved using micropipettes (Pipetman, Gilson), including buffer and sample dispensing and washing steps.

This method of fluid handling is not ideal, since it lacks control and depends on the operator. For instance during washing steps more or less fluid pressure can be applied and it can be applied differently across the chip, consequently the washing may not be uniform. This indeed may be one of the factors responsible for the variability found in multiplexing bioassay experiments (see chapter 8 and Ferreira *et al*., 2005, 2006).

In fluid velocity experiments, instead syringes coupled to the PDMS reservoirs of the microfluidic structures (see fig. 5.7 and 6.5) were used instead. Nevertheless, the system was operated manually and was hard to operate alone. This system also lacked some control (Ferreira *et al*., 2004).

More recent efforts though are resulting in the development of fully integrated system that comprises a fluid handling system (S0-05-28-010 Micropump, Bartel Microtechnik), a credit card sized electronics board for data acquisition, and a blue-tooth module for communicating wirelessly with a portable computer or personal digital assistant (see chapter 8 for more details). The idea is to build a system were fluid handling can be done automatically, and consequently have much more control on sample dispensing and washing steps, in an effort to reduce some of the variability found in experimental results.

# 7. Results and Discussion

The bioassays that have been developed so far concern the detection of oligonucleotides (short DNA strands) or of structural antigens from pathogenic microorganisms.

The BARC chip, mentioned before, was used in the detection of biological warfare agents such as: *Bacillus anthracis*; *Yersinia pestis*, *Brucella suis*, *Francisella tularensis*, *Vibrio cholarae*, *Clostridium botulinum*, and *Campylobacter jejuni*. Here, DNA strands 30 nucleotides (or bases) long that represent specific bacterium, were immobilized on gold pads fabricated on top of the sensitive areas, and the chip was interrogated with a particular complementary DNA target (Edelstein *et al*., 2000; Miller *et al*., 2001).

The biochip from the University of Bielefeld, on the other hand, used polymerase chain reaction (PCR) amplified probe DNA sequences 1kb (kilo-bases) long. The chip was immobilized with probes that were complimentary or not to a particular DNA target. The non-complimentary probe was used to assess the background signals. In this work, a comparison with traditional fluorescence methods was made, showing that the magnetoresistive platform was more sensitive at low probe DNA concentrations (Schotter *et al*., 2004).

At INESC-MN, work started by detecting ensembles of magnetic labels, down to the single microsphere and nanoparticle level. In addition, the combination of the fabricated magnetoresistive chips with microfluidic structures enabled, later on, the determination of the flow velocity passing through a microchannel.

After demonstrating the feasibility of the system to detect magnetic particles, a series of experiments were done using model biomolecular interactions: biotin-streptavidin; proteinA-Immunoglobulin G; and DNA-DNA hybridization. Finally, magnetoresistive biochip assays started to be developed for the diagnostics of cystic fibrosis and the detection of pathogens in water samples. The results concerning the detection of cells are not though reported here (see section 3.3.4).

## 7.1. Magnetic Label Detection

At INESC-MN, the first system that demonstrated detection of magnetic labels was the one comprised of a 2 μm × 6 μm spin valve sensor with two adjacent tapered current lines (see fig. 4.9 and Graham *et al*., 2002). For this device, a simple direct current (dc) measurement setup was used (see fig. 6.4), together with 8 mA sense currents and 15 Oe (1.2 kA/m) dc external magnetizing fields created by a NiFe core horseshoe electromagnet.

In addition, 20 mA were passed through the tapered current lines to control and manipulate magnetic labels back and forth across and over the sensor (see section 2.4 and fig. 2.29).

Finally, the chip was placed under an optical microscope while detection data was acquired.

The real-time data of the detection and manipulation of 2 μm microspheres functionalized with horseradish peroxidase (HRP) enzyme or coated with streptavidin is shown in figs. 7.1 and 7.2, respectively (see section 3.2.1, and Ferreira, 2001).

In these figures the sensor is represented by a green rectangle and the magnetic beads correspond to red spheres. The relative distribution of labels over the sensor and the corresponding detection signals are shown.

These measurements were done as follows. First the chip was incubated with a buffer solution (100 mM phosphate buffer, pH of 7) and thermal equilibrium was reached before starting data acquisition (see chapter 6). Subsequently, one or two current lines adjacent to a spin valve sensor were turn on by passing current of about 20 mA, and solutions (same phosphate buffer, see chapter 3) containing magnetic labels were introduced next. The presence of labels in solution and over the sensor results then in an increase in voltage drop, with respect to the initial state. This increase in signal corresponds in fact to a decrease in sensor resistance when a positive sense current is used, and depends not only on the number of particles being detected but also on the

external applied field, the field created by the sense current and the magnetostatic fields created by the magnetic layers of the sensor itself (see section 2.1.6 and Ferreira *et al.*, 2005a).

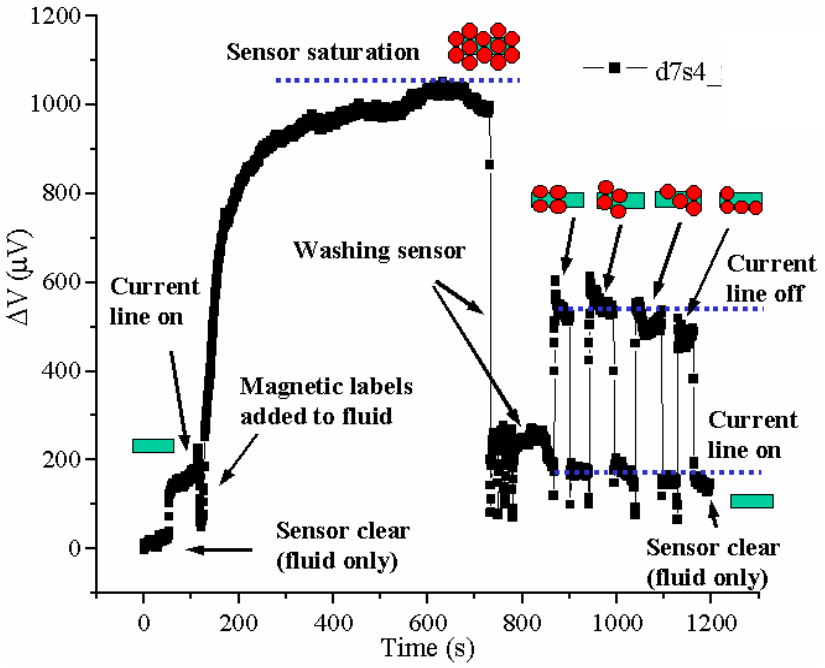


Fig. 7.1. Real-time data for the movement and detection of Micromer-M labels with immobilized horseradish peroxidase. Shown also the relative position of the labels to the sensor.

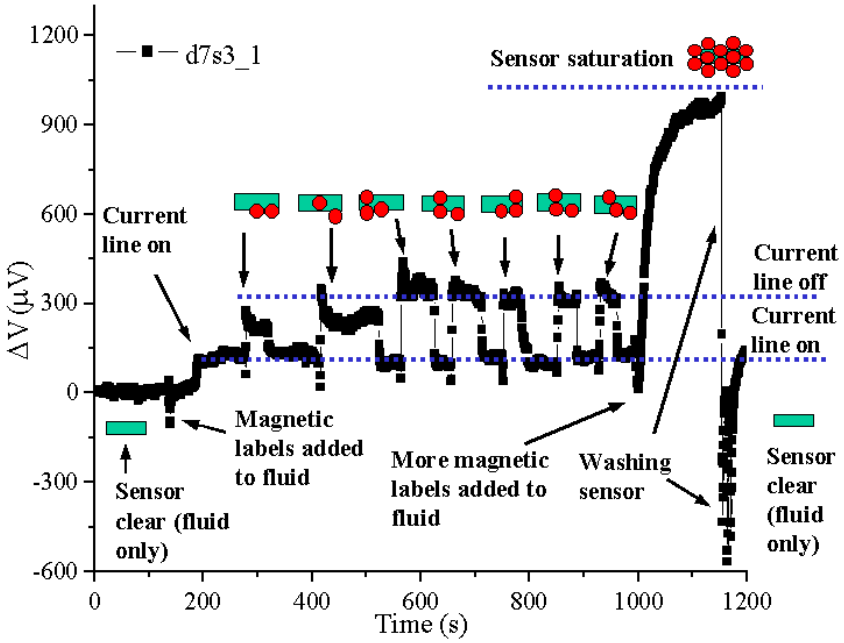


Fig. 7.2. Real-time data for the movement and detection of Micromer-M labels with immobilized streptavidin. Shown also the relative position of the labels to the sensor.

The accumulation of particles over the sensor results in a steady increase in measured voltage drop, and when high concentration magnetic label solutions are used a sharp increase is observed, until it reaches a plateau when the signal no longer increases or increases very slightly. This corresponds to a "saturation signal" where labels accumulating over the sensor contribute very little to the overall signal, as they are increasingly further away from the sensor (see section 2.1.6).

When washing, a buffer solution is introduced in the chip using a pipette (see chapter 6) and some pressure is applied to remove the labels.

Finally, the current lines enable the movement of magnetic particles to and from the sensor by sequentially turning off and on the current through these structures, respectively. By initially turning on the tapered current lines, the attraction and focusing of the labels is promoted toward these structures and when turning off, the carriers are then attracted to the sensor, which is also transversed by current. In addition, by using one current line (top or down, see fig. 4.9) on and the other off and then the opposite, enabled the movement of the magnetic markers between them.

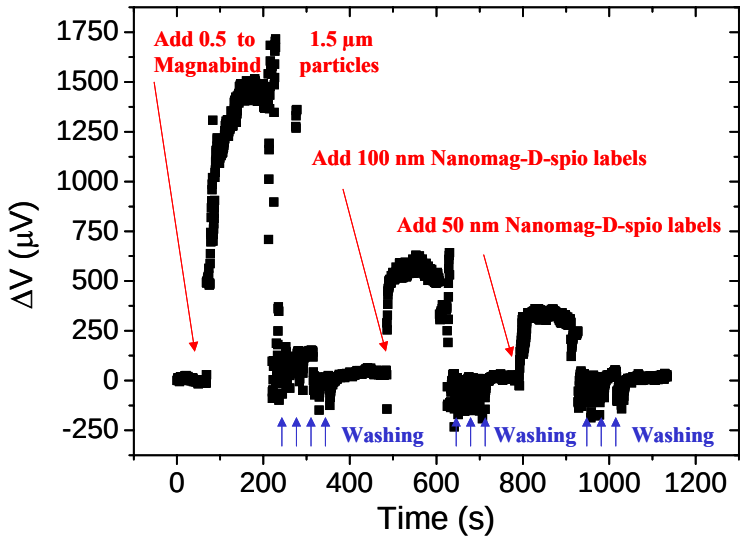


Fig. 7.3. Real-time detection data for saturation signals obtained with 5 µL solutions of 0.5 to 1.5 µm diameter range Magnabind particles (~7.5 × $10^9$ labels/mL); 100 nm diameter Nanomag-D-spio particles (~7.5 × $10^{13}$ labels/mL); and 100 nm diameter Nanomag-D-spio particles (~5.5 × $10^{14}$ labels/mL) (Ferreira *et al*., 2003).

This device was also used to detect ensembles of several micron-sized and nanometer-sized magnetic labels, with dimensions ranging from 50 nm up to 2.8 μm (see fig. 7.3; Ferreira *et al*., 2003; Lagae *et al*., 2002).

The mentioned experimental procedure was also used in subsequent experiments for simply detecting other magnetic labels or for the detection of biomolecular recognition. Furthermore, adapted protocols were used for detecting labels using alternate current (ac), ac attraction and multiplex acquisition setups (see chapter 6), as shown below.

Finally, other sensor types such as planar Hall transducers and magnetic tunnel junctions were used to detect magnetic labels as well (see Ejsing *et al*., 2004, 2005; Carias, 2004; Cardoso, 2005, Cardoso *et al*., 2006).

## 7.2. Single Label Detection

### 7.2.1 Detection of Single Microspheres

The same device referred above was used to manipulate and detect single microspheres. Figure 7.4 shows the detection of single beads of 2 μm in diameter. While measuring, the chip was observed under an optical microscope and a picture taken for a single bead standing over the sensor is shown as well.

From the data obtained it can be seen that the signal for each particle is about 150 to 200 μV for this sensor and operating conditions (8 mA sense current and 15 Oe externally applied magnetic field). These are consistent with what is expected from the sensor model and magnetic label properties (see section 2.1 and chapter 2; Freitas *et al*., 2004).

A study on the response of a typical spin valve sensor to the number of particles and distribution of the labels over the sensor is shown in the figure below (see Ferreira, 2001).

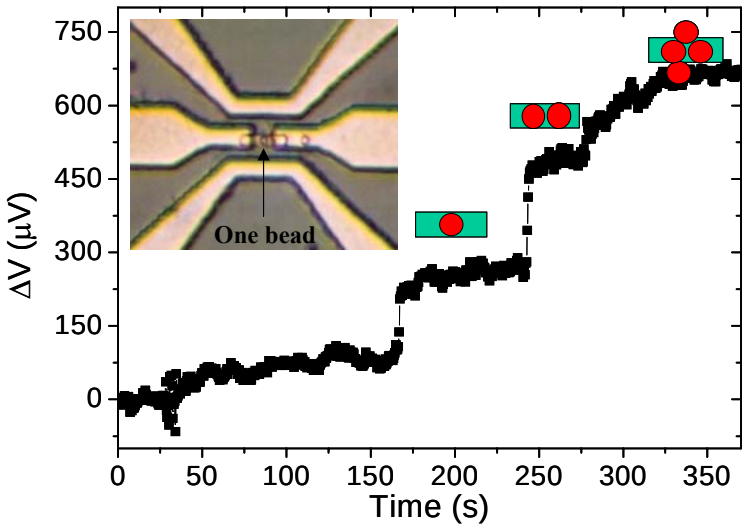


Fig. 7.4. Real-time data for the detection of a single micrometer-sized magnetic label. The relative position of the labels with respect to the sensor is shown as observed by optical microscopy. The inlet shows an optical photography of a single bead over the sensor, taken during experimentation. In this experiment a dc measurement setup was used with 8 mA sense current and 15 Oe external magnetic field.

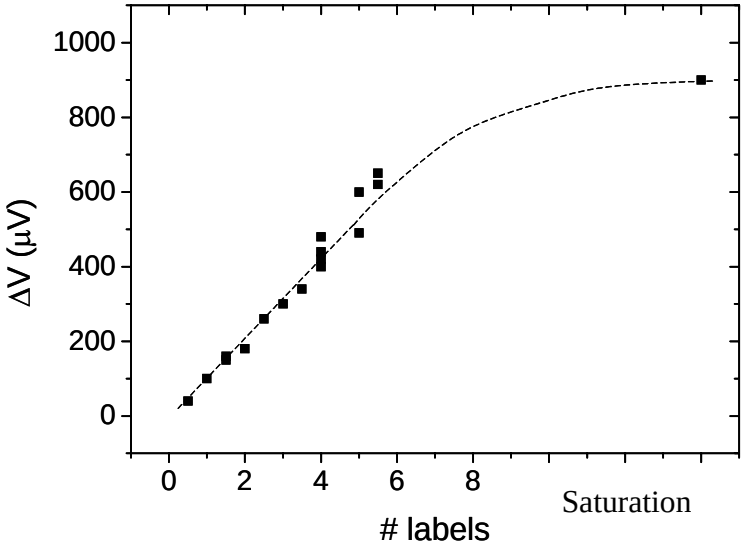


Fig. 7.5. Experimental 2 μm × 6 μm spin valve sensor output with respect to the number of 2 μm diameter particles over the sensor. Half-integer numbers of particles correspond to labels at the edges, touching the sensor. Saturation signals correspond to more than one monolayer of particles over the sensor. The number of particles was counted using an optical microscope while measuring the sensor.

In figure 7.5, half-integer particle numbers correspond to particles at the edges of the sensor, superimposing the sensor. This was considered since in fig. 2.14b shows that particle at the edges of the sensor structure (at 1 μm away from the centre of the sensor) contribute to the sensor signal with roughly half the magnetic field created by a label

located at its centre. Figure 7.5 further shows that the response of the sensor is approximately linear up to 5 - 6 microspheres over the sensor.

Above this value, magnetic labels are either further above the sensor and contribute with ever-small increasing fields or are further away to the sides and contribute with much smaller decreases in signal. The fields created by these latter particles at the sensing layer are opposite to the ones created by labels directly above the sensor (see fig. 2.14b and its discussion).

Thus, the resulting signal of a large number of labels being detected by the sensor is a signal plateau called saturation signal.

### 7.2.2 Detection of Single Nanoparticles

The same sized spin valve sensors (2 μm × 6 μm) were used to detect smaller 250 nm diameter magnetic particles (Nanomag-D, Micromod). In this case though, the particle size is too small for labels to be counted using a conventional optical microscope. Consequently, a statistical analysis of sensor readout signals was made to determine the signal per nanoparticle and confirm the detection of a single carrier.

In a set of experiments different nanoparticle solutions with decreasing dilutions was used and dispensed over the chip. Detection of labels was done, in this case, using an ac measurement setup (see fig. 6.6), using 8 mA sense currents and an excitation field of frequency 30 Hz and amplitude of 10.5 Oe (0.8 kA/m) rms (see fig. 7.6).

The tested samples corresponded to 1:1, 1:200, 1:400, 1:800 and 1:1600 dilutions of a 250 nm magnetic particle solution in phosphate buffer, and 5 μL volumes were used. The stock sample nanoparticle concentration corresponds to about $3\times10^{11}$ particles/mL.

The signal curve obtained for the 1:1 dilution corresponds to a saturation signal, as described above. Nevertheless, for diluted samples the obtained curves have a different and step-like shape (see fig. 7.7). Whereas in the former case a great number of particles settles over the sensor almost at the same time, in the latter cases only occasionally a

particle or cluster of particles is attracted and detected by the sensor. In fact, and as mentioned previously in section 2.4, the sensor itself creates a local magnetic field gradient that attracts the labels.

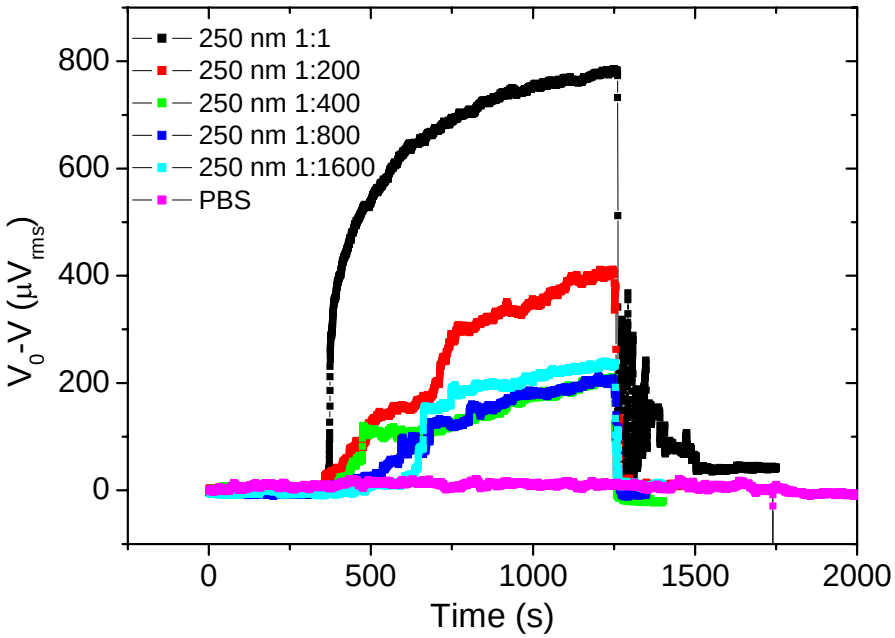


Fig. 7.6. Response of a 2 μm × 6 μm spin valve sensor to increasing dilutions of a 250 nm diameter magnetic label solution. The detection was done using an ac measurement setup, and the signal is taken as the difference between an initial voltage drop signal without labels $V_0$ and with labels V. PBS represents a blank or negative control testing.

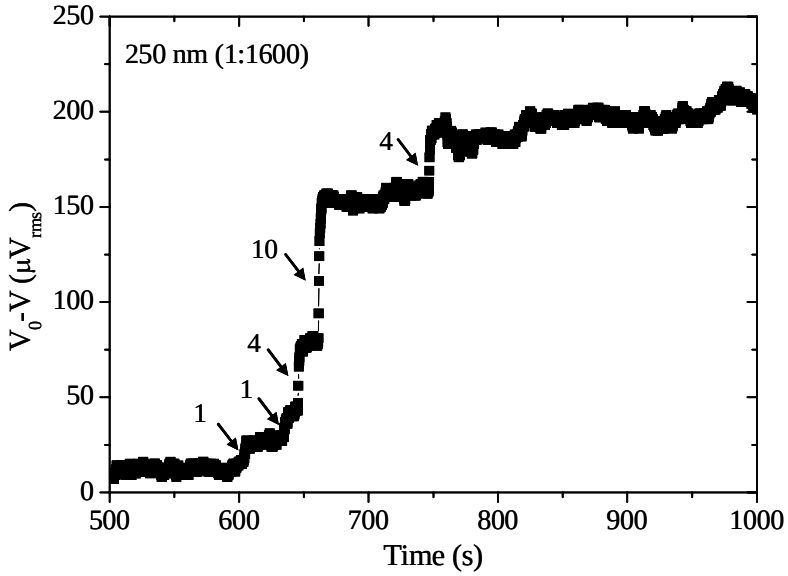


Fig. 7.7. Detail on sensor response to the 1:1600 solution of 250 nm labels, show in fig. 7.6. The number of detected nanoparticles is indicated.

In order to verify and quantify the signal obtained from a single 250 nm label, a statistical study was made, where a sharp transition in signal with amplitude above a defined off-set was considered as nanoparticle signature. In fact, it was observed under the microscope, that beads move towards the sensor for a few seconds before landing over it, generating a step-like signal response. The off-set was defined as the signal amplitude of sharp signals obtained with a phosphate buffer saline solution, which reflects the background noise of the system.

Figure 7.8 shows the relative frequency of signals with different amplitudes occurring in a control sample and in diluted samples of nanoparticles. The criterion for identifying a signal is that it should happen as a transition in less than 5 s. In addition, a 300 s time interval was analysed for each curve. In particular for diluted samples of magnetic labels the 300 s are analysed after dispensing the solution over the chip.

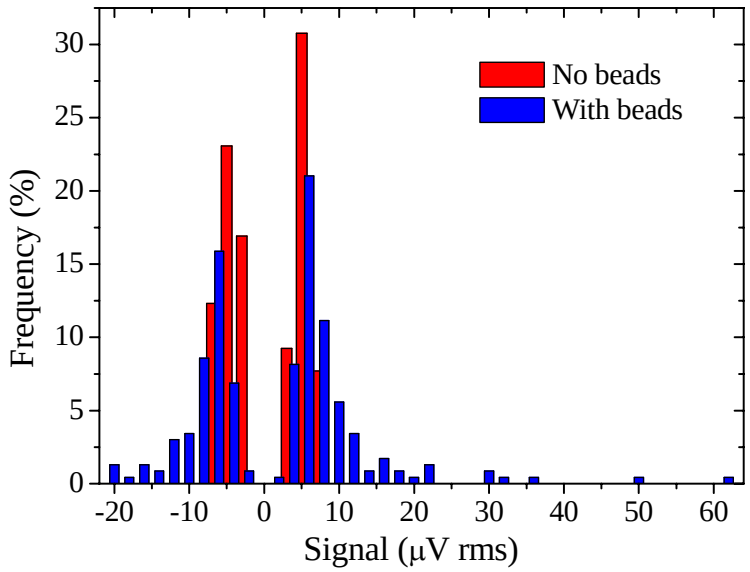


Fig. 7.8. Signal statistics obtained from the analysis of curves of fig. 7.6, in response to nanobead diluted samples or blank solution. The bar chart represents the relative frequency that a sharp transition of particular amplitude occurs in 300 s analysis time interval.

It is observed that in the absence of particles, both positive and negative transition signals are measured, as expected from a noise background. Furthermore, maximum counts are obtained for transitions between 4 and 5 µV rms, and the average absolute value for noise was determined to be ~4.5 ± 1.2 µV rms. In fact this value is close to the lock-in amplifier resolution alone (~3 µV rms for the sensitivity range and time constant

of 300 ms). The extra noise is most probably due to cabling to the chip and other instruments.

As a note, similar noise statistics were obtained after washing the chip following an experiment with magnetic nanobeads. This indicates that the washing steps were efficient.

When, adding diluted 250 nm magnetic label solutions, the statistics is different. It comprises sensor responses to the presence of particles superimposed with the background noise. In this case larger amplitude signals are obtained coming from the labels. In fact, the largest signals were found to correspond to multiples of a signal, determined to be ~7 ± 1 μV rms, which corresponds to the higher frequency obtained signals. According to the model given in section 2.1.6 and the spin valve sensor equation (10), this value corresponds to a particle of a magnetic moment of $\sim 1 \times 10^{-13}$ emu. This is consistent with what was obtained for a single 250 nm nanoparticle from vibrating sample magnetometer measurements using the same field conditions (see section 2.2 and Freitas *et al*., 2004).

The multiples of the mentioned quantum signal correspond then to cluster of nanoparticles in solution being detected.

Another thing that is observed though, is negative signals corresponding to particles, whereas it could be expected to obtain only positive signals. This can be explained from the interplay of magnetic forces acting upon the particles. As mentioned in sections 2.1. and 2.4., both magnetostatic fields from the sensor layers and the sense current, contribute, together with the external magnetic fields, to the local magnetic energy landscape of the sensor (Ferreira *et al.*, 2005a). This may result in repulsion of labels from the sensor under the ac excitation, much similarly to the mechanism of label focusing using the u-shaped current lines (see section 2.4).

Finally, although almost within the noise of the system, the detection and quantification of single 250 nm diameter magnetic particles was possible using a small 2 μm × 6 μm spin valve sensor and an ac measurement setup (see also fig. 7.6). Even smaller 130 nm diameter beads can in principle be detected, as the intrinsic 1/f noise of the sensor is

considerably smaller than the present system (electronics and cabling) noise (see fig. 2.24).

## 7.3. Fluid Velocity Measurements

Small 2 μm × 6 μm spin valve sensor, where used in the meantime for the measurement of flow velocities within microfluidic structures. A new chip and polydimethylsiloxane (PDMS) microchannels 25 μm high, 100 μm wide and 3 cm long were developed for that effect (see figs. 4.10, 5.7 and Parracho, 2002).

For this measurement an adapted dc experimental setup was used, where the responses of spin valve sensors located near the inlet and outlet were simultaneously recorded, using GPIB-controlled multimeters (see fig. 6.5 and Ferreira *et al.*, 2004).

Using standard syringes, different pressures were applied to the inlet and outlet of a microchannel, resulting in the flow of a solution containing 250 nm magnetic particles with distinct velocities. Figures 7.9 and 7.10 show the signals measured with the two magnetoresistive sensors.

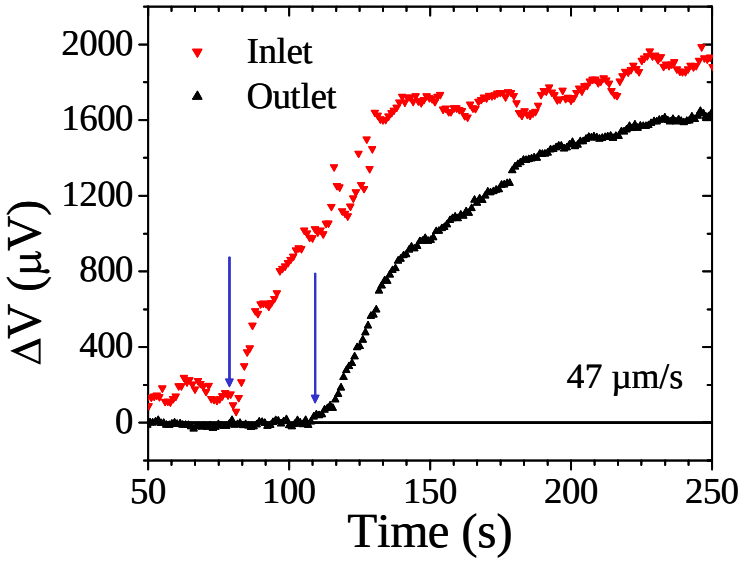


Fig. 7.9. Real-time detection signals for the passage of ensembles of 250 nm magnetic labels over spin valve sensors and estimation of the flow velocity. Signal rise is indicated with arrows for both inlet and outlet sensors.

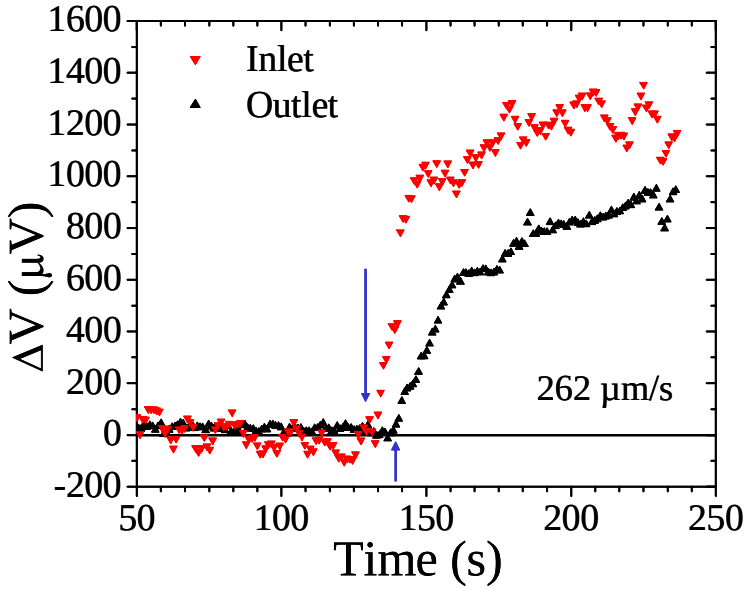


Fig. 7.10. Estimation of the flow velocity using a magnetoresistive chip. Signal rise is indicated with arrows.

The flow velocity was determined from the time difference between the passage of ensembles of nanoparticles over each sensor, and from the distance that separates the two sensors (1.65 mm).

In particular, it was considered the detection signal rise for the velocity estimation, as this corresponds to the first particles moving over the sensor. Given the parabolic flow profile resulting from hydrodynamic pumping (see fig. 2.26), the calculated response should correspond to the maximum flow velocity.

As observed in figs. 7.9 and 7.10, flow velocities of ~50 and 250 µm $s^{-1}$ were obtained, corresponding to Reynolds numbers of ~$10^{-3}$ (see equation 21). This value is typical of a laminar flow regime, as expected for microfluidic structures.

The use of magnetoresistive sensors and superparamagnetic particles for measuring flow velocities was quite innovative and has a number of advantages over conventional optical methods (Ferreira *et al.*, 2004). These latter ones, can provide micrometer resolution but at the expense of complex optical systems. The fabricated device offers a simple and low-cost method, where flow velocities are directly translated into electrical signals enabling an almost real-time control of fluid flow on microfluidic chips.

The technique was also proposed to be developed as an imaging system for fluids, using arrays of sensors. Furthermore, these devices should be suitable for studying fluid properties such as viscosity, and complex fluids such as blood or plant sap.

## 7.4. Biotin-Streptavidin Binding Model

Biotin-streptavidin was the first biomolecular recognition model to be studied at INESC-MN. These studies started on simple glass and $Si/SiO_2$ substrates to investigate the suitability of the surface chemistry. One of such tests was to fabricate arrays of magnetic labels bound to the substrate through this high affinity bond, as illustrated in fig. 3.9 (see also Ferreira, 2001).

The same principle was applied to the magnetoresistive chips, where a half-wheatstone bridge arrangement was used for a sensor pair chip (see fig. 4.9). Here one of the sensors was covered with photoresist, and consequently, was not functionalized with biotin and worked as a reference sensors, whilst the other sensor had an exposed $SiO_2$ surface that could be biotinylated and bound to streptavidin coated magnetic particles. This latter sensor worked thus as an active sensor (see fig. 7.11 and Graham *et al.*, 2003).

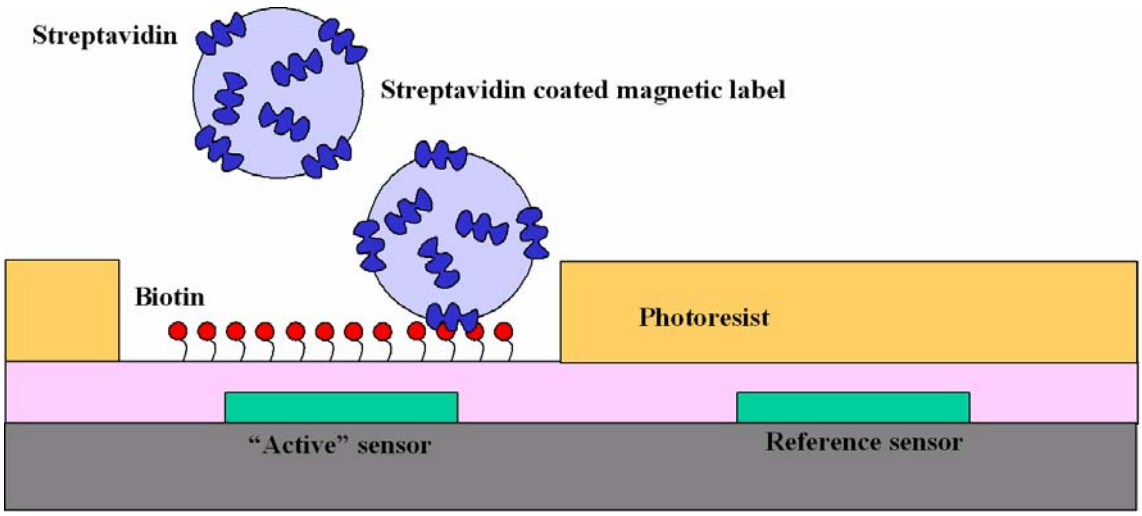


Fig. 7.11. Schematic for the detection of biotin-streptavidin binding using a half-wheatstone bridge arrangement (drawings not to scale).

Figure 7.12 shows the real-time signals obtained from incubating a streptavidin-coated magnetic label solution with a biotinylated chip, with a sensor pair, just as described.

After dispensing particles over the chip a saturation signal is observed, as mentioned in previous sections. This signal is smaller for the reference sensor (in red) because, due to the photoresist layer, particles are further away from the sensor, and contribute with a smaller magnetic field for the transducer response. Otherwise, response is similar.

After washing, the signal of the reference sensor returns to the baseline, as photoresist was not functionalized with biotin, and magnetic labels were washed away. On the contrary, the active sensor, with a silicon dioxide exposed surface, was biotinylated and bound streptavidin-coated microspheres, resulting in a residual signal.

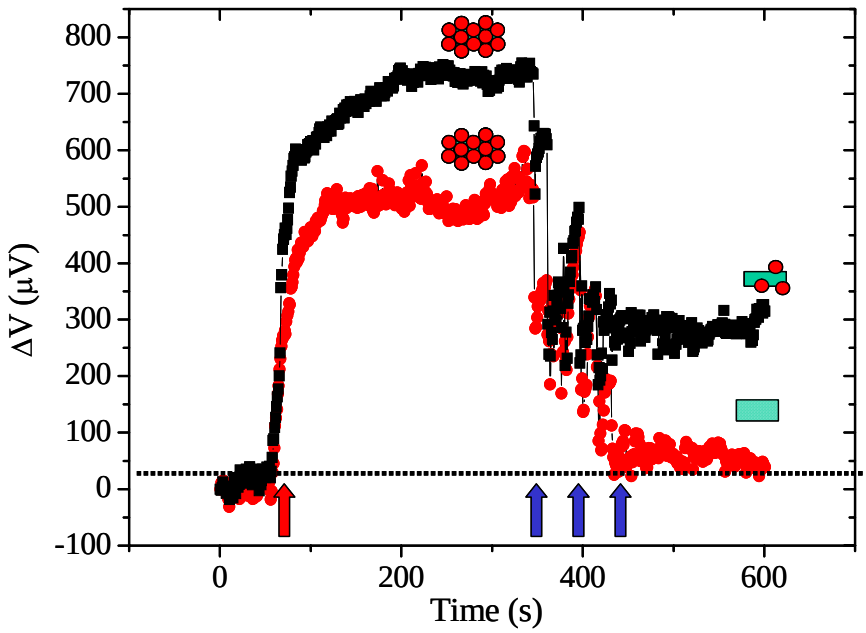


Fig. 7.12. Real-time sensing data of biotin-streptavidin binding using the sensor pair arrangement of fig. 7.11. The black and red signals represents the active and reference sensor resposnses, respectively. The red arrow indicates addition of 2 μm microspheres coated with streptavidin to the biotinylated sensor surface. The blue arrows indicate washing of the chip. Saturation signals are represented by a cluster of labels and the sensor is represented as a green rectangle. A baseline is represented in dash.

This experiment was made using 8 mA sense currents through the sensors and 15 Oe (1.2 kA/m) in-plane magnetizing field. Microspheres of 2 μm in diameter coated in streptavidin (Micromer-M) in a phosphate buffer solution, pH of 7, were used.

An optical micrograph of the resulting chip, after removal of photoresist with acetone is shown in the figure below.

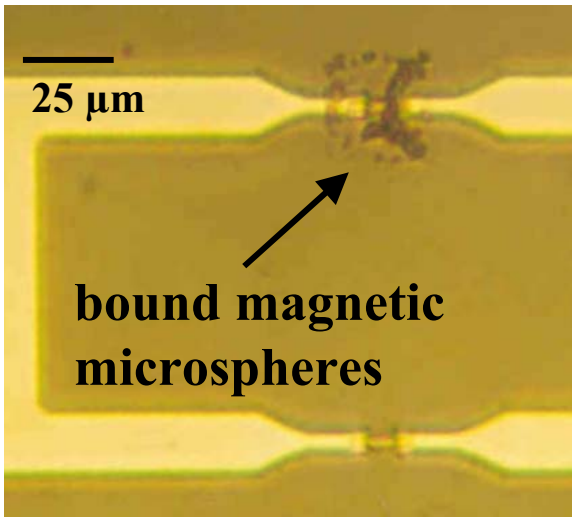


Fig. 7.13. Photograph of biotin-streptavidin binding experiment, after removing the photoresist layer.

Similar experiments were also made using a single sensor only and both streptavidin-coated microspheres (Graham *et al.*, 2003) or nanoparticles (see fig. 7.14 and Ferreira *et al.*, 2003).

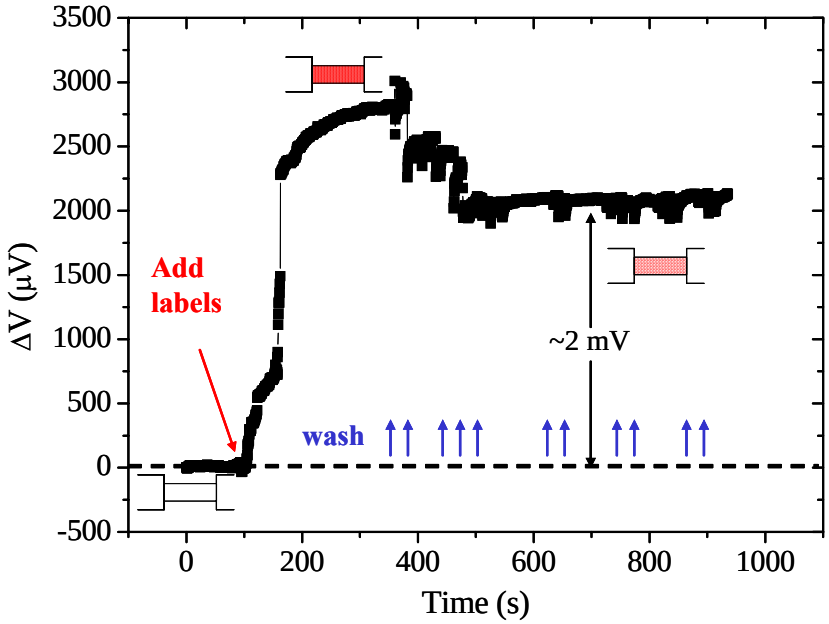


Fig. 7.14. Real-time data for binding detection of 250 nm streptavidin-functionalized magnetic beads (Nanomag-D) to a biotinylated silicon dioxide surface. A volume of 5 µL of labels was used together with 8 mA sense currents and 18 Oe applied field.

Finally, the biomolecular recognition between biotin and streptavidin was further demonstrated with planar Hall sensors, using an adapted ac measurement setup (see fig. 7.15 and Carias, 2004).

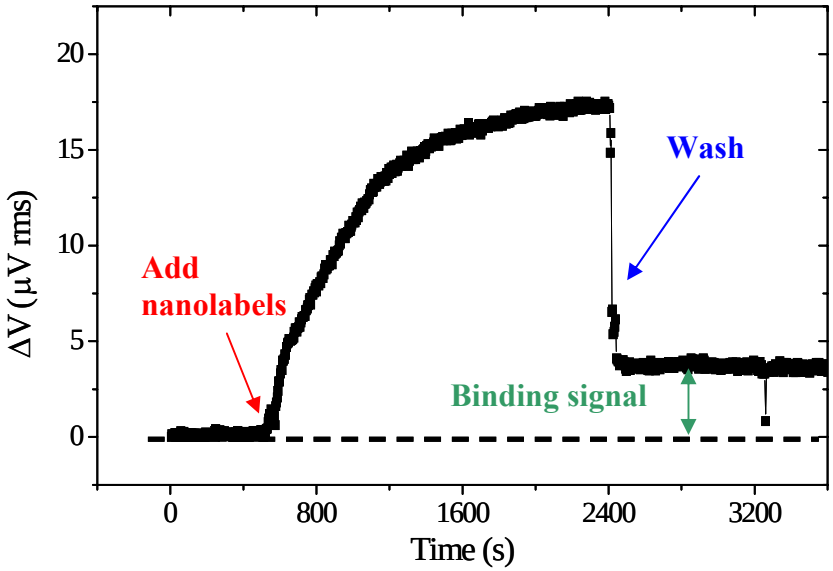


Fig. 7.15. Real-time detection signal of biotin-streptavidin binding using planar Hall sensors.

## 7.5. Protein A-IgG Recognition

The spin valve biochip platform was also tested for the detection of proteinA-IgG recognition as a model for future magnetic protein chips and immunoassays.

The detection strategy is illustrated in fig. 3.10. Immunoglobulin G antibodies are first immobilized on the chip surface, which is later interrogated with protein A functionalized magnetic labels. The antibodies then bind to protein A through their Fc regions.

Chip functionalization is done as follows. First goat anti-mouse whole (heavy + light chains) IgG antibodies are reduced to produce free thiol groups that can react with a cross-linking reagent. Subsequently, the reduced antibodies are desalted using a minicolumn, and antibody fractions are collected.

In the meantime, the silicon dioxide passivated chip is silanized using APTES (similarly to what was described in section 3.1), and is reacted with a hetero-bifunctional cross-

linker (sulfo-SMCC, Pierce). The reduced antibody is then immobilized to the surface, and finally, detection experiments are performed using protein A functionalized magnetic labels.

Figure 7.16 shows the real-time detection data for a negative control experiment, where the immunochip was interrogated with 250 nm diameter streptavidin-coated particles (Nanomag-D). After washing the chip with a high salt alcaline buffer the signal returns to the base line indicating that there was no non-specific binding. This experiment, as well as all the others in this section, was done using 2 µm × 6 µm spin valve sensors, 8 mA sense currents, external magnetizing fields of 18 Oe in amplitude, and room temperature.

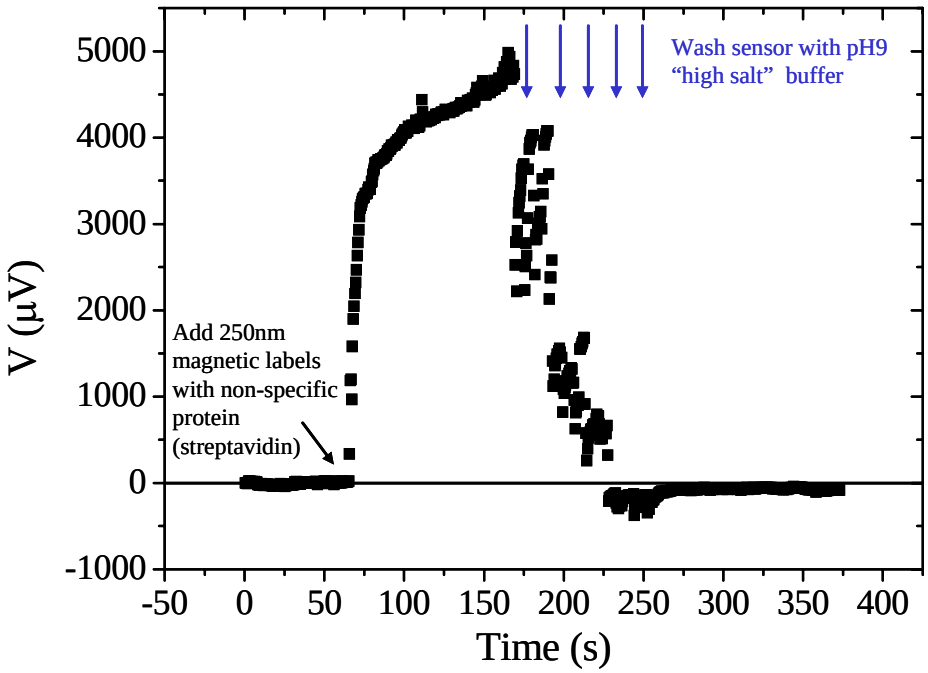


Fig. 7.16. Real-time detection for immunoassay negative control experiment: the IgG antibody functionalized surface was incubated with streptavidin coated magnetic labels.

Figure 7.17 also show detection signal for a negative control, but in this case an untreated chip (no antibody was immobilized) was incubated with a 250 nm protein A functionalized beads (Nanomag-D). Here the resulting signal is also negligible.

Finally, figures 7.18 and 7.19 show positive control experiments were IgG immobilized chips surfaces were interrogated with protein A nanoparticles. These experiments

resulted in residual signals due to binding of labels to the surface through the antibody-ligand recognition.

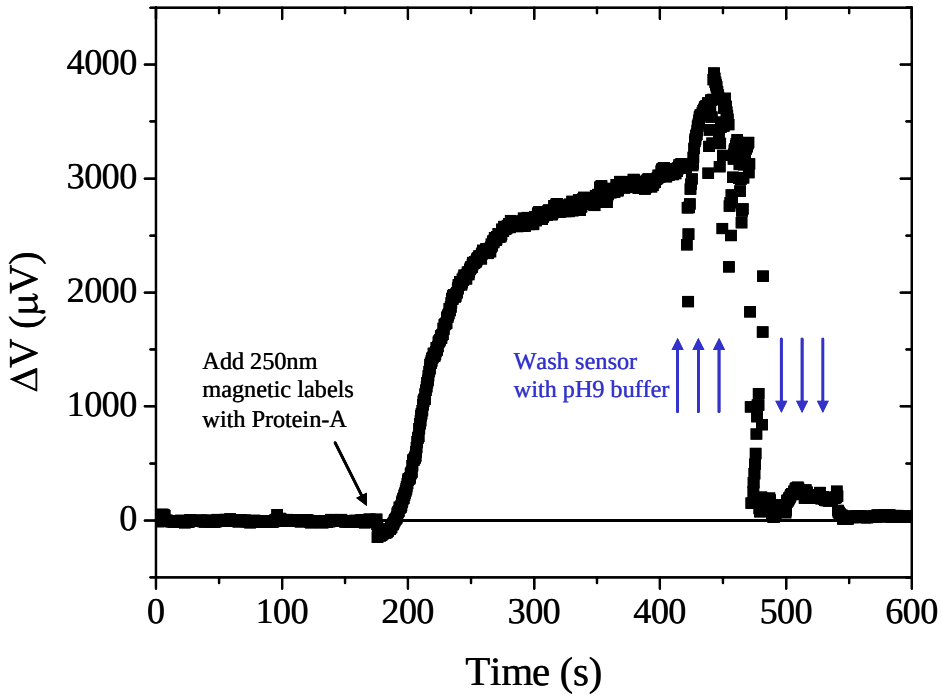


Fig. 7.17. Real-time detection for immunoassay negative control experiment: an untreated chip was interrogated with protein A coated magnetic labels to assess for unspecific binding of the protein to the surface.

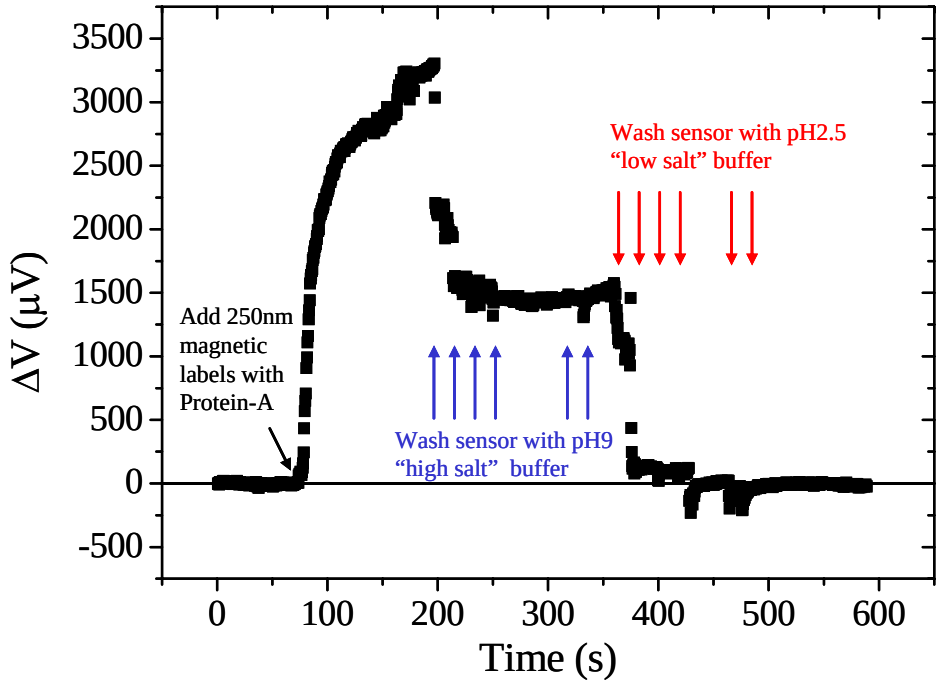


Fig. 7.18. Detection of binding and elution of magnetically labeled protein A to surface immobilized antibody (goat anti-mouse IgG).

Both these experiments also show the elution of the bound magnetic labels by washing the chip with different salt concentration and pH buffers. The use of these buffers results in the weakening of the electrostatic bonds, salt-bridges and Van der Waals forces between the antibody and proteins. In fact, this method is typically used in immuno-separation processes.

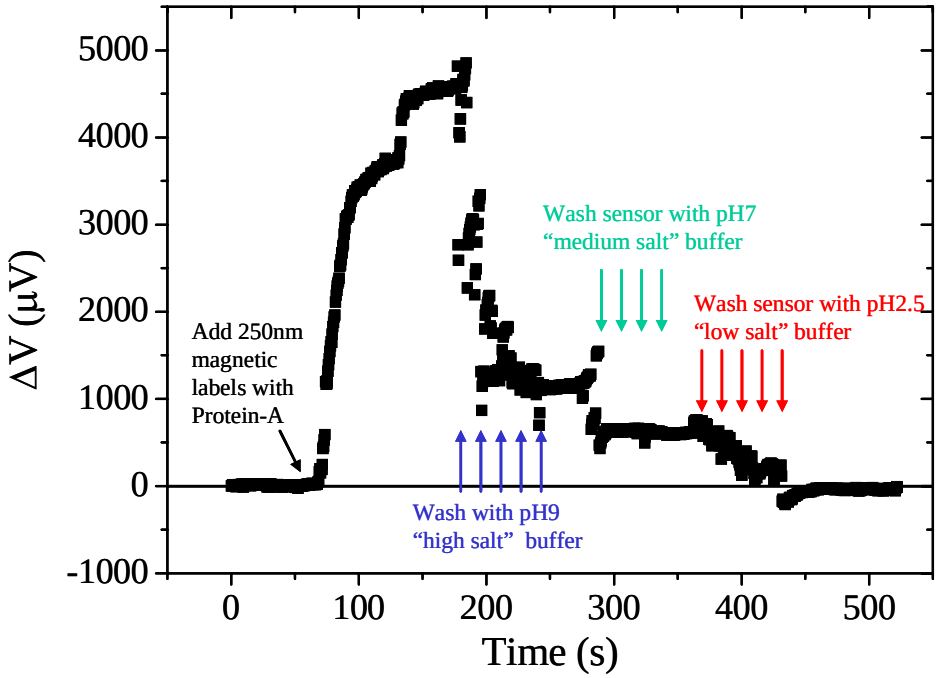


Fig. 7.19. Detection of binding magnetically labeled protein A to surface immobilized antibody and elution of labels using different salt concentrations and pH buffers.

In the fig. 7.18, after washing the chip with a low salt acidic buffer the signal returns to the base line indicating that no magnetic labels remained bound to the spintronic transducer surface.

In addition, the chip of fig. 7.19 was washed with a medium salt, pH 7, buffer prior to the wash with the low salt acidic buffer. This results in the partial elution of magnetic labels, as the weaker bonds are first removed with the neutral buffer. The use of the acid buffer results then in the complete elution as before.

Finally, the above results demonstrate that the magnetoresistive system can be used for immunoassays, and that by changing the salt concentrations and pH's of the washing buffers, the chips could eventually be reutilized in some applications.

## 7.6. DNA Hybridization of PCR Products: Cystic Fibrosis

The same sized spin valve sensors were also used to demonstrated the feasibility of the magnetic sensing platform to be used as DNA chips and DNA hybridization interaction studies.

### 7.6.1 Immobilization and Hybridization Testing

Cystic fibrosis and proto-oncogene related DNA probe and targets were used for testing both immobilization and hybridization procedures. The magnetoresistive chips were functionalized with oligonucleotides, 50 bases long, in single strand using a protocol as described in chapter 3 and in appendix C.

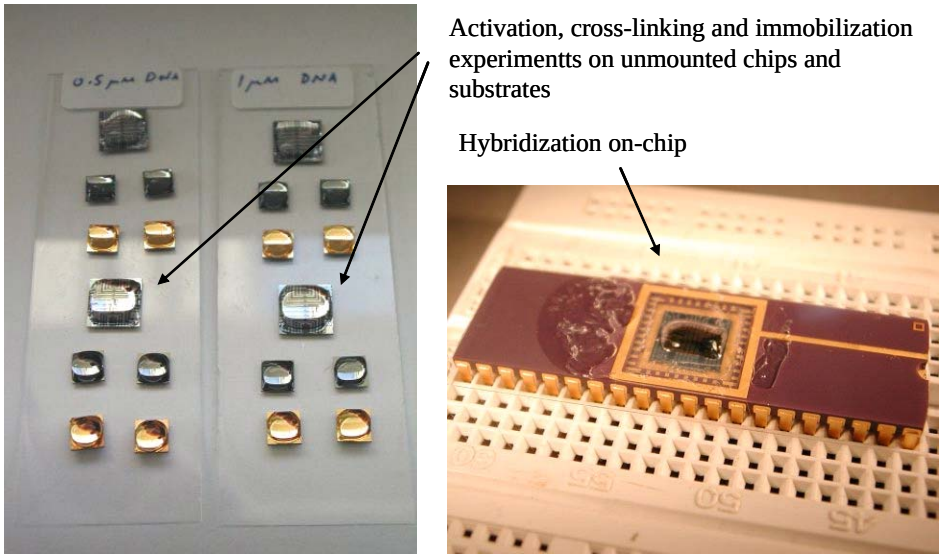


Fig. 7.20. Samples and substrates for both DNA immobilization and hybridization. Immobilization tests were made in open chamber and at room-temperature. Hybridization tests, on the other hand, were done in a chamber formed the chip carrier recess and covered with a glass slip glued to the chip carrier with a temperature curing epoxy. Hybridizations were further done in overnight time scales and in a humid chamber, at a temperature of 37 to 42ºC.

The probe used was designed such that corresponds to the antisense strand of the cystic fibrosis transmembrane conductance regulator (CFTR) gene, exon 10, nucleotides 1626-1675. It therefore spans the region where the most common cystic fibrosis mutation, F508del, occurs. Also, as mentioned in section 3.3.3, the probe was fabricated with a thiolated 3'-end and with or without a fluorescein label in the 5'-end for immobilization

tests. These were done in both plain substrates, chip surfaces and mounted chips (see fig. 7.20 and fig. 3.12 for fluorescence image results).

As mentioned also in section 3.3.3 targets are PCR products obtained from the reverse transcription of mRNA of CFTR and Rac1 genes. The complementary target are 96 bp long corresponding to CFTR nucleotide positions 1613-1708 in exon 10, and thus matches the wild-type CFTR probe. The non-complementary target is a 75 bp PCR product corresponding to Rac1 nucleotide positions x-y across exons 4-5 and has a 80% mismatch with the CFTR probe (80% of bases between probe and target do not result in Watson-Crick pairs).

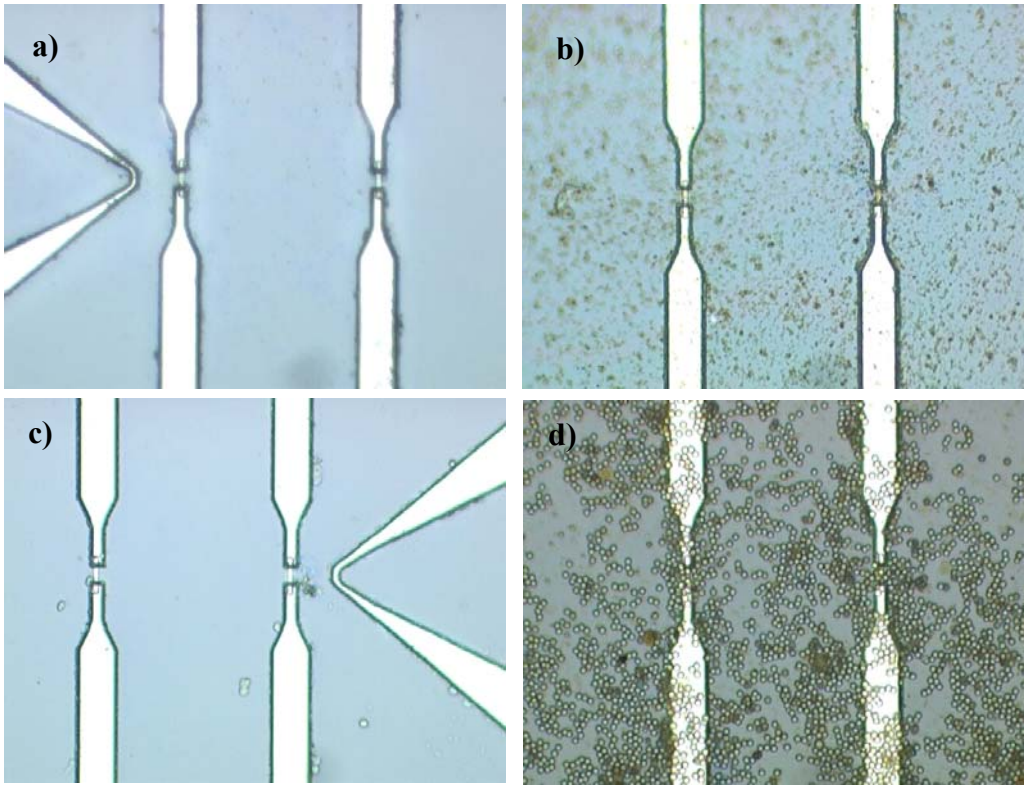


Fig. 7.21. Optical photographs of CFTR probe immobilized chips incubated with either non-complementary, a) and c), or complementary, b) and d), targets; and later on interrogated with streptavidin coated 250 nm particles, a) and b), or 2 µm microspheres, c) and d).

Both complementary and non-complementary targets were biotinylated at the 3' end and were incubated overnight with probe functionalized chips (see fig. 7.20), washed to remove unbound molecules and subsequently incubated with streptavidin-coated

magnetic labels. Only when complementary base-pairing occurred thus labels remain bound to the chip surface (see fig. 7.21).

Figure 7.21 shows that there is little unspecific binding of magnetic carriers when the chip was incubated with the non-complimentary probe, whereas for the complementary case the binding degree is considerably high.

As a note, this hybridization results were also confirmed using conventional hybridization detection via fluorescence.

Also, from these pictures it can be seen that this system can be used as an optical bioassay as well, as there is a clear difference between the matching and un-matching cases. Furthermore, by counting the number of labels bound to the surface is possible to extract some quantitative information on the target concentration present on the sample. In fact, this is a method that was also suggest and is being followed by the Naval Research Laboratory as an alternative to conventional bioassay systems (Baselt *et al*., 1998).

Nevertheless, on-chip integrated magnetoresistive sensors offer the advantage of not requiring a bulky optical system and a specific software tool for magnetic label identification and counting, besides being much more sensitive to smaller labels.

### 7.6.2 Post Hybridization Detection

The experiments just described were then tested onto spintronic biochips, corresponding to a post-hybridization detection strategy as referred in chapter 4 and fig. 4.1 specifically.

Incubation with functionalized chips was then left overnight for hybridization reactions to take place; where biotinylated target molecules movement and interaction are limited by diffusion rates.

Figures 7.22 and 7.23 then show the result of such experiments for non-complementary and CFTR target incubation. As expected, when the Rac1 cDNA targets were used no

residual signal was obtained after washing the chip, whereas with the complementary targets a residual signal remained after extensive wash (Graham *et al*., 2004; Freitas *et al*., 2004).

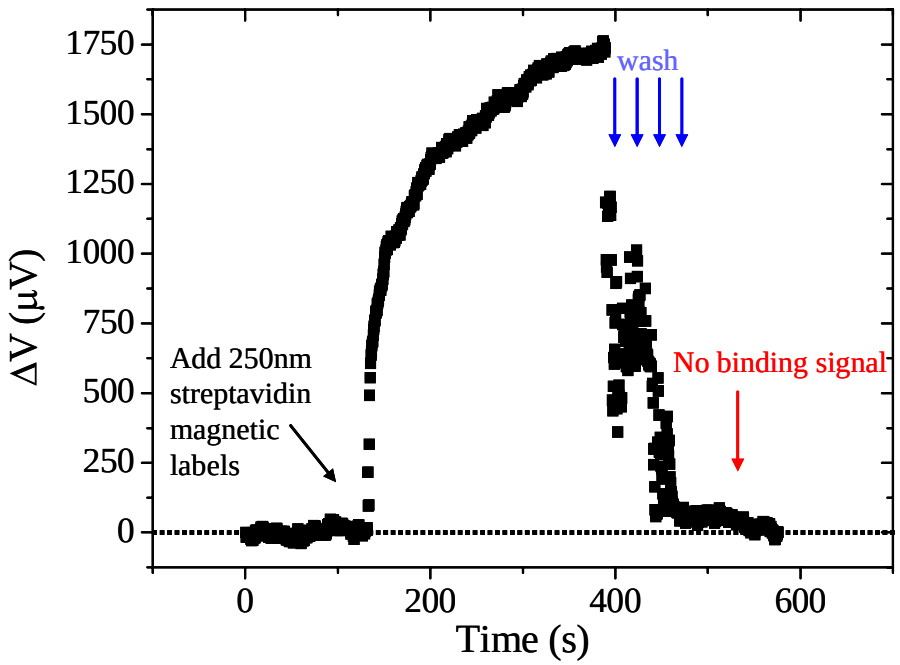


Fig. 7.22. Post-hybridization detection experiment. A CFTR related probe immobilized chip was incubated with Rac1 related cDNA biotinylated targets and then tested with 250 nm streptavidin coated magnetic particles.

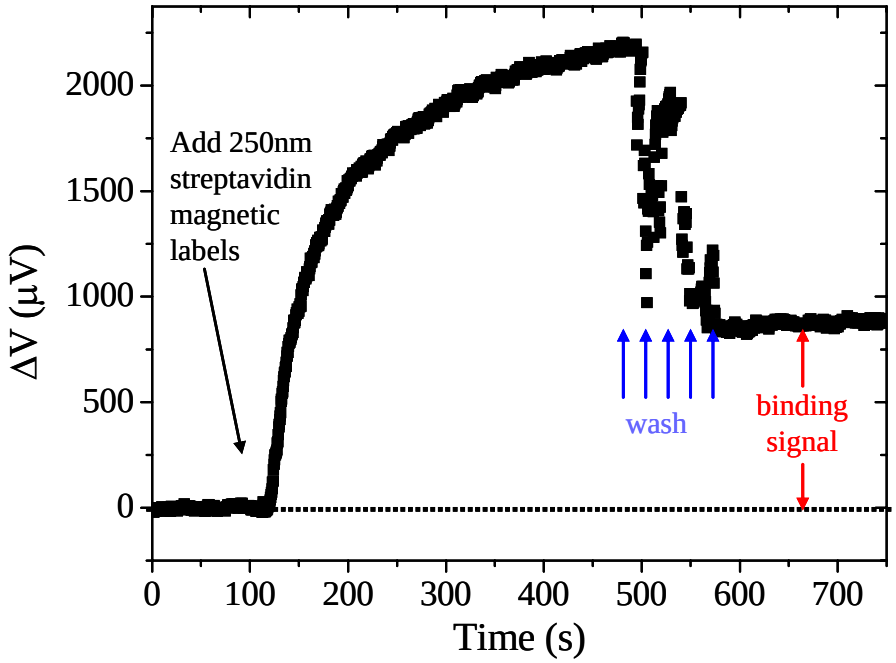


Fig. 7.23. A chip immobilized with CFTR related probes was incubated with biotinylated complementary targets and interrogated with streptavidin coated labels.

Here 2 μm × 6 μm spin valve sensors were used with 8 mA sense currents and 15 Oe magnetizing fields in a dc measurement setup (see fig. 6.4).

The chips were incubated with 5 μL volumes of 200 nM target DNA in 100 mM phosphate buffer, pH of 7.2. Later on, chips were interrogated with 250 nm streptavidin-coated labels dispersed in the same phosphate buffer and using the same volume. Washing was done again with the same buffer.

Given the operating conditions and the model described on section 2.1, then the obtained residual signal of 0.9 mV corresponds to about 100 nanoparticles or 50% of sensor coverage (a full monolayer over the sensor is about 200 beads) (see Graham *et al.*, 2004).

Note, that in this case, although the detection of the binding of magnetic tags to the chip surface can be achieved in ~ 5 min, the hybridization of biotinylated targets takes several hours (usually overnight time scales), such that a considerable degree of DNA-DNA hybridization is obtained.

### 7.6.3 Magnetic Field Assisted Hybridization and Detection

In order to surpass this above mentioned limitation, an innovative approach was undertaken at INESC-MN, which consisted on combining on-chip magnetic label manipulation structures with the sensing of biomolecular recognition. This method was dubbed magnetic field assisted hybridization and detection and is depicted in figure 4.2.

Here, magnetically-labeled target biomolecules are focused onto probe-immobilized sensing sites using current line microstructures. The proximity between probe and target molecules promotes biomolecular recognition, overcoming this way the passive diffusion limitations that conventional bioassays possess.

Consequently, the same DNA-cDNA hybridization model was used with the tapered current lines and sensor based chip (see fig. 4.8). In these experiments chips were immobilized with a CFTR probe as before, but PCR targets (both complementary,

CFTR related, and non-complementary, Rac1 related) were labeled with magnetic particles prior to incubation with the chip (see section 3.2.3 and appendix D).

Figures 7.24 and 7.25 show the real-time detection signals for magnetic field hybridization and simultaneous detection, using magnetically labeled cDNA targets non-complementary and complementary to the immobilized probe.

In these experiments single 2 μm × 6 μm spin valve sensors were used again with 8 mA sense currents and 15 Oe magnetizing fields in a dc measurement setup and at room temperature.

The experimental protocol was as follows. An aliquot of 2 to 4 μL of DNA target functionalized magnetic nanoparticles (250 nm in diameter) was added to a histidine buffer on-chip resulting in a 10 to 20 μL volumes. Subsequently, a current of 20 to 40 mA was applied to one or both tapered current lines associated with the spin valve, until the narrower regions of the line became saturated with magnetic labels (see fig. 2.30).

Afterwards, the current is turn off resulting in the movement of the labels towards and above the sensor, as it also attracts the labels (see section 2.4). Finally, the chip was washed with 1× sodium saline citrate (SSC) containing 0.1% sodium dodecyl sulphate (SDS) followed by a further wash with 1× SSC to remove weakly or unspecifically bound magnetically labeled DNA (Graham *et al*., 2005).

Eventually, this cycle of steps was repeated in the same experiments (as in the figures below), to improve hybridization degree. Each cycle last about 10 min with focusing and saturation times of about 5 min, and another 5 min for washing.

In figure 7.24 it is observed that even performing two cycles of focusing, saturation and washing, the signal returns to the baseline, which is consistent with the fact that the magnetically-labeled targets are not complementary to the immobilized probes.

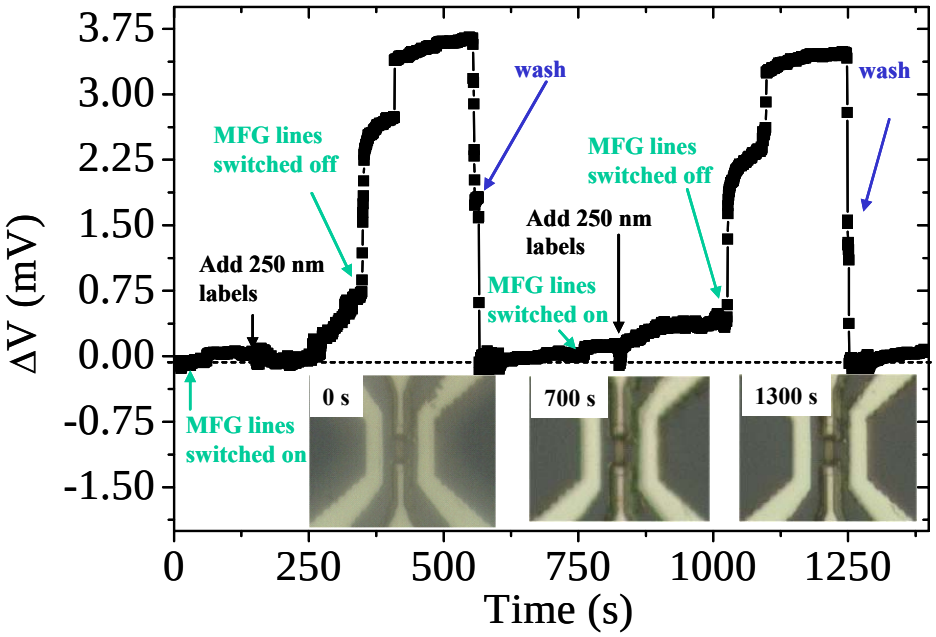


Fig. 7.24. Magnetic field assisted hybridization experiment where magnetically-labeled Rac1 related targets were incubated with a non-complementary probe surface. Here MFG stands for magnetic field generating lines. Inset: pictures show the surface of the measured sensor in the beginning of the experiment, after a first focusing, saturation and washing, and in the end of the experiment.

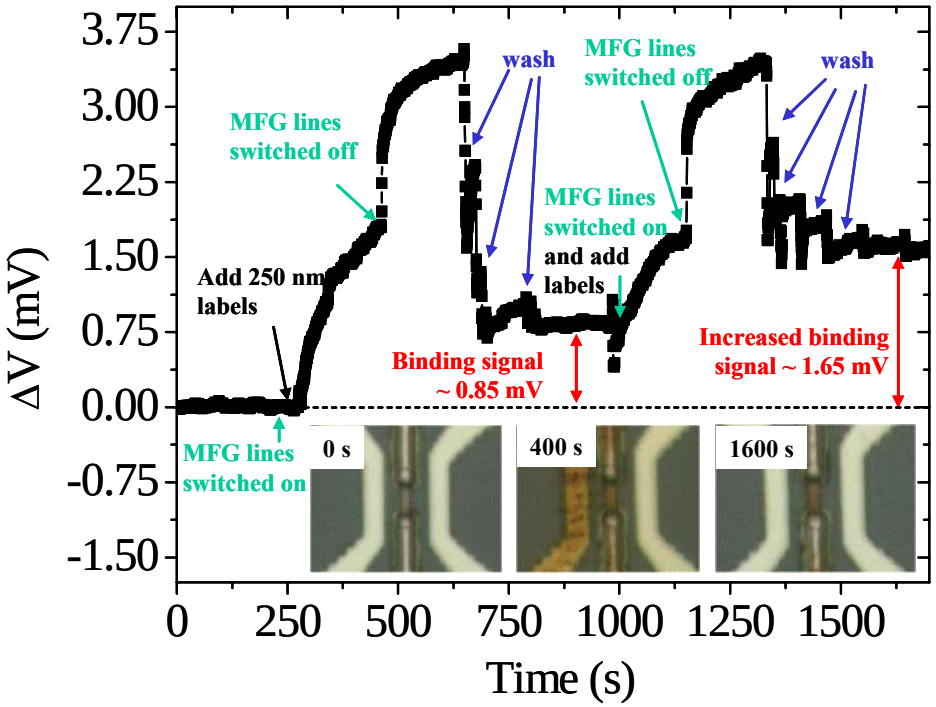


Fig. 7.25. Real-time data resulting from incubating magnetically-labeled CFTR DNA targets with complementary DNA probes, using the magnetic field assisted hybridization method. MFG stands for magnetic field generating lines. Inset: pictures show the surface of measured sensor in the beginning of the experiment, while focusing, saturation and after two hybridization cycles. A third cycle and resulting increase in binding signal is shown elsewhere (Graham *et al.*, 2005).

On the hand, figure 7.25 for shows that after the first cycle a residual signal of ~0.85 mV is obtained, and for a second one an increased binding signal of 1.65 mV results. A third cycle (not shown) further increased the binding signal to 1.85 mV (Graham *et al*., 2005). These values translate an increase in hybridization degree, as more magnetically-labeled DNA molecules interact and hybridize with the probes on the sensor surface.

Also, both figures 7.24 and 7.25 show as inlets pictures taken during experimentation for the times mentioned. These frames encompass initial, focusing, and after washing times. A clear difference is observed on the sensor surfaces of non-complementary and complementary binding experiments.

The sensor detection model mentioned in chapter 2, and the considerations on the quantification of biomolecular interactions discussed specifically in section 2.1.7 (see also Graham *et al*., 2004), enabled the estimation of the maximum density of DNA molecules detected. For this estimation a 1 biotinylated DNA target per streptavidin molecule on the label surface was considered, which correspond to a relative concentration of 1 nanoparticle per 500 target molecules in the magnetic labelling protocol. The DNA surface densities are shown in fig. 7.26 below.

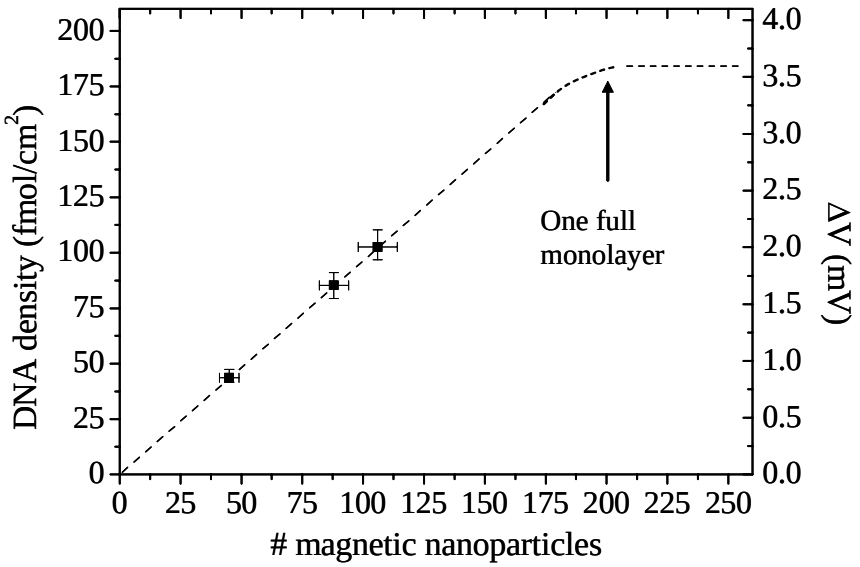


Fig. 7.26. Sensitivity and dynamic range of a single 2 μm × 6 μm spin valve sensor with respect to binding of 250 nm magnetic particles during magnetic field assisted hybridization experiments. The number of magnetic nanoparticles detected and the corresponding DNA surface density were calculated from previously described model. The three binding signals of fig. 7.27 are also shown.

The picture above shows that the sensor response is almost linear up to a full monolayer of 250 nm diameter nanoparticles. In addition, the maximum detected DNA densities are comparable with other improved bio-techniques. Nevertheless, smaller densities are possible if, for instance, the ratio of DNA strands per label is smaller, and even down to 1:1. In this latter case though, hybridization could be less efficient as, the nanoparticles and target would have to be in a correct position to bind the surface immobilized probes. Nevertheless, 10 to 50 DNA target molecules per label may be sufficient for high hybridization performance, and consequently it would be possible to analyse femto-molar concentrations on-chip.

Magnetic field assisted hybridization experiments showed that detection of biomolecular recognition was possible for hybridization times of 5 min or less, and with target concentrations smaller than 10 pM (see figures above and other data in Graham *et al.*, 2005), which is a considerable improvement over the post-hybridization detection scheme.

Nevertheless, the magnetic field assisted hybridization includes an extra step of labelling of the targets. This step presently takes about 3 hours (see appendix D), although it has not yet been fully studied and optimized. It is expected that this time can be reduced to minutes by using on-chip mixing for the labelling of targets. In spite of this, the present methodology enables the reduction in assay time (hybridization and detection) from overnight time scales to about 3 hours, which is already advantageous over other conventional techniques.

The system has shown that it can distinguish between unrelated DNA strands. Nevertheless, it is still necessary, and is suggested, to study the degree of dissimilarity between the strands that the magnetic biosensing device is able to discriminate, either 3 or 2 nucleotide differences or even single nucleotide changes, for example. In fact, the goal of a recently started European project where INESC-MN is to build a magnetic sensing platform that is able to detect single nucleotide polymorphism (SNP), using again cystic fibrosis as a disease model.

## 7.7. DNA Hybridization for Gene Expression: Cystic Fibrosis

The magnetoresistive platform at INESC-MN was further developed to be used for diagnostics of cystic fibrosis through gene expression. As mentioned in section 3.3.3, in this application, the goal is to quantify the expression of certain genes that are found to be either up or down regulated in cystic fibrosis tissues in relation to healthy ones. In order to achieve a higher dynamic range for quantification of gene expression, longer transducers were developed and with that a novel magnetic label focusing system.

### 7.7.1 Ac Field Focusing of Magnetically Labeled Target DNA

Based on initial studies on a metal ring structure, a u-shaped structure for on-chip magnetic label manipulation was developed (see fig. 2.32 and Feliciano, 2003; Ferreira *et al*., 2005a).

As was thoroughly described in section 2.4, ac field focusing of magnetic labels results from the creation of on-chip local alternating magnetic field gradients. These magnetic fields attract particles alternatively to one or the other arm of the u-shaped current line, and over time result in the accumulation of the carriers in the inter-arm region (see fig. 2.34).

Furthermore, it was explained that the movement and the efficiency in focusing depended on the frequency of the applied magnetizing fields, and for the system studied it was observed that low frequencies between 0.1 to 10 Hz resulted in considerable focusing of particles (Ferreira *et al*., 2005a).

This dependency of the focusing efficiency on the frequency of the applied fields further resulted in a modulation of biomolecular recognition efficiency. This was shown for both the biotin-streptavidin model, using a biotinylated chip surface and streptavidin-coated labels (Feliciano, 2003) and for the hybridization of cystic fibrosis related DNA targets (Ferreira *et al*., 2005a).

Figure 7.27 shows the results of a frequency dependent magnetic field assisted hybridization experiment using the ac field focusing method.

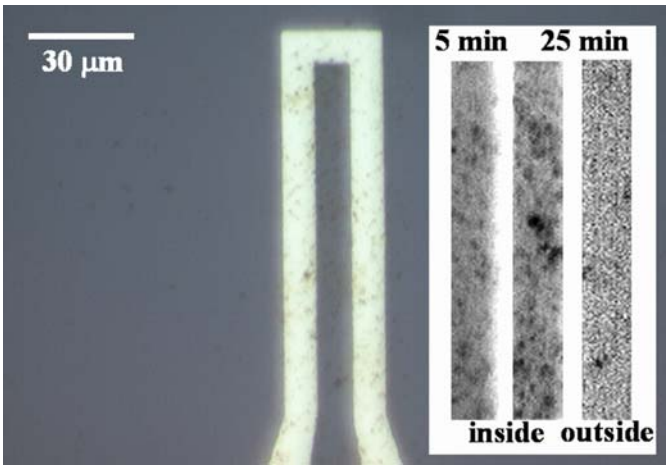


Fig. 7.27. Optical microscope images showing DNA hybridization (through nanoparticle binding) using ac field focusing of magnetically-labeled targets for 5 min. Insets: comparisons of contrast-enhanced amplified pictures of 10 μm wide regions inside the u-shaped line structure after 5 and 25 min focusing time and a region 100 μm away from the structure. A dc current of 40 mA was passed through the line and an ac field of amplitude of 1.4 kA/m rms at a frequency of 0.2 Hz, was applied in-plane, by an external electromagnet to generate an alternating magnetic field gradient.

The experiments were made as follows. The chip surface was functionalized with the same 50-mer CFTR related probe as discussed in the previous section. In addition, both PCR targets, complementary or not to the probe, were labeled magnetically using the same protocol as before.

Typically, 40 mA current were passed through the current lines and oscillating magnetic fields of 1.4 kA/m rms at frequencies ranging between 0.1 Hz and 20 Hz were created by an external NiFe core electromagnet.

Magnetic labeled target solution volumes of 5 μL with a DNA concentration of 100 pM were dispensed over the chip surface using a pipette, and focusing was set for 5 or 20 min before washing to remove unbound labels. In fact, in the experiment of fig. 7.27, after a first focusing of 5 min, a second one followed for another 20 min for investigating increased hybridization degree, just like in the previous section.

In figure 7.27 it can be seen that after 5 minutes only, there is a considerable number of magnetic labels bound to the inside region of the u-shaped line structure. A grey scale improved contrast image of the inside region is also shown in the inlet (left panel). Here, nanoparticles or nanoparticle clusters are the darkened spots.

After 25 min total focusing time, the degree of hybridization improved as shown by an increased number of labels bound to the inside region (middle panel in the inlet).

At the same time a picture of a region 100 μm away from the current line structure shows negligible nanobead binding (right panel in the inlet). This indicates that, not only the focusing results in increased hybridization degree, but also those labels near the u-shaped structure are efficiently attracted towards the line. This result demonstrates that although the chip may be functionalized with probe in a region larger than that of the u-shaped element, the effective sensing region is defined by the line itself due to focusing. This is advantageous with respect to conventional diffusion based systems, as the biological sensitive region is tailored to the size of the sensor (see fig. 4.4 and accompanying discussion).

Another advantage of the ac field focusing with respect to other on-chip magnetic field attraction systems is that cluster of particles have the tendency to disaggregate, due to the back and forth movement. This was clearly observed during experimentation.

Finally, control experiments, using non-complementary targets resulted in negligible binding to the chip surface.

### 7.7.2 Detection of Magnetic Labels Using Ac Field Focusing

The u-shaped line system was further integrated with a u-shaped 2.5 μm × 80 μm spin valve sensor defined inside the structure (see fig. 4.13). This sensing element enabled both the focusing and detection of magnetic labels.

Figure 7.28 shows the real-time data for a single sensor measured with the ac setup while using the ac field focusing method (see fig. 6.6). It is observed that the rise in

signal oscillates due to the movement of labels over the sensor, which is a direct consequence of the focusing mechanism (see section 2.4)

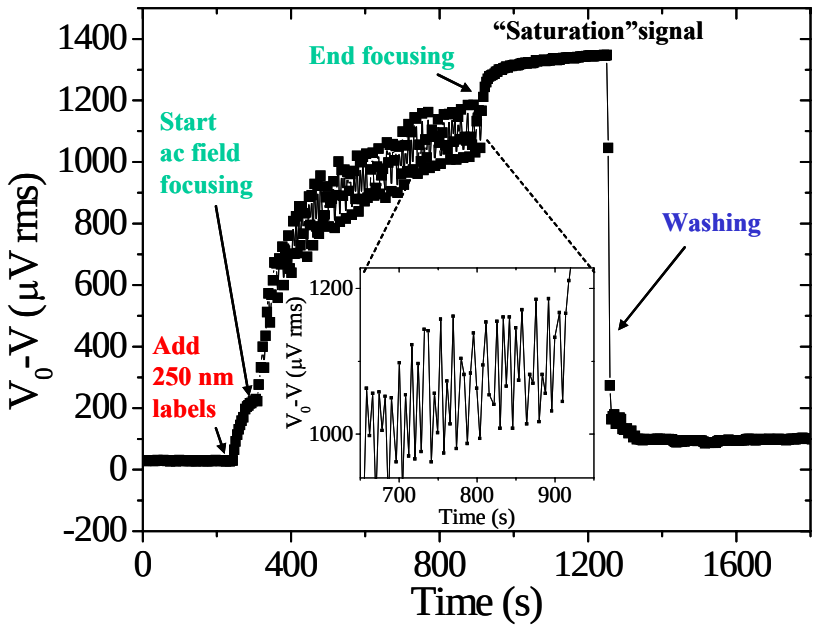


Fig. 7.28. Real-time data of the detection of 250 nm labels by a single 2.5 μm × 80 μm u-shaped spin valve sensor using the ac field focusing method. Inset shows an enlargement of the signal rise while focusing is applied.

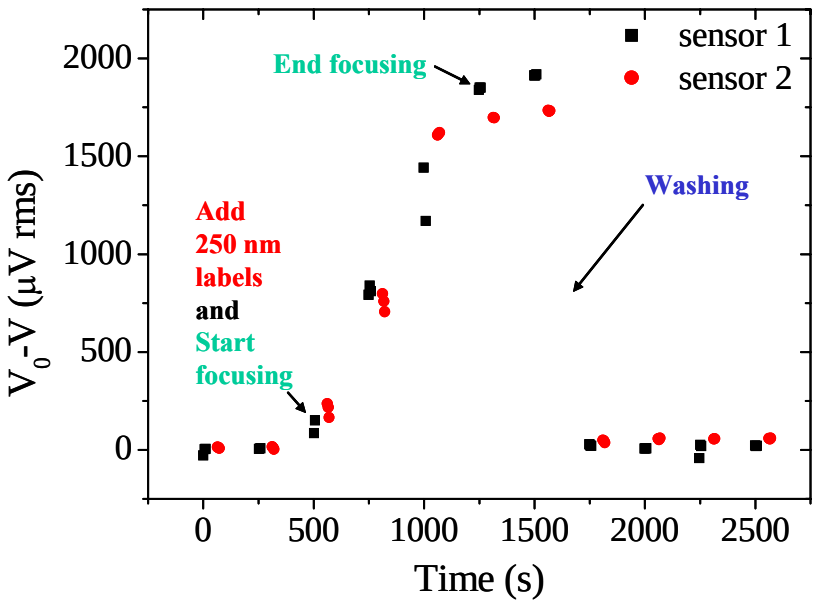


Fig. 7.29. Data obtained for the detection of 250 nm labels by measuring two 2.5 μm × 80 μm spin valves sequencially using the multiplexing setup of figure 6.7.

When using multiplexed measurements (see fig. 6.7 and Appendix E), every sensor in an array is sequencially monitored for a certain period of time (typically 5 seconds or

less). Consequently, the obtained data corresponds to different time intervals of a real-time data curve obtained for a single sensor, as can be seen in figure 7.29 for two different u-shaped spin valve sensors measured sequentially over time. In a typical experiment the data is further analysed to obtain the average signals, standard variations and the noise, as is shown below.

A recent study was then made on the sensitivity of this magnetoresistive platform, within the scope of the development of a diagnostics tool for cystic fibrosis based on gene expression (Ferreira *et al*., 2005c, 2006).

In this study an ac experimental setup for multiplexing measurements was used (see fig. 6.7), and the response of an array of sensors (11 sensors) was evaluated in function of increasing concentrations of 250 nm and 2 μm magnetic labels. In addition, 5 sensors were covered with a silicon gel (Elastosil E41), to assess the background noise of the system.

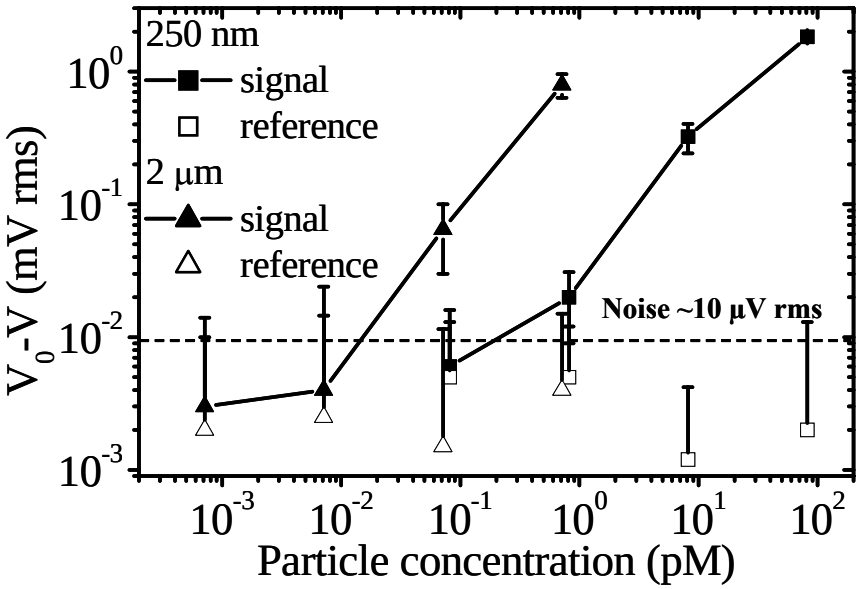


Fig. 7.30. Detection signals of 250 nm particles (squares) and 2 μm microspheres (triangles), using an array of 2.5 μm × 80 μm spin valve sensors. Outputs are shown for saturation (11 sensors; filled symbols) and background signals (5 reference sensors; open symbols). Points correspond to average signals and error bars correspond to standard deviations.

The experiments were made as follows, similarly to what is described in Appendix E. Sensors were transversed by a 1 mA sense current and an ac external magnetizing field of ~1 kA/m rms amplitude at a frequency of 30 Hz was applied in-plane in the

transducers's sensing direction together with a dc bias field of 0.8 kA/m. Sensor response was measured at 30 Hz with a time constant of 300 rms. The same dc bias field was used together with an ac field created by the u-shaped structures for magnetic label focusing. The u-shaped lines were transversed by a current of amplitude 30 mA rms and frequency of 0.2 Hz. Finally, the frequency was chosen as the one for which there is a considerable hybridization degree, as discussed previously. The results are shown in fig. 7.30 above (see also Ferreira *et al*., 2006).

The figure shows that output signals increase linearly above a noise background threshold for both 250 nm and 2 μm beads. Thus the detection limit for the smaller labels is below 1 pM and for the larger labels is about 10 fM, and both their dynamic range is at least two orders of magnitude.

Considering the magnetic labeling protocol of 1 DNA target per streptavidin molecule on the bead surface (see previous section 7.6 and appendix D), then the DNA detection limits are below 500 pM (or 0.5 fmol/μL) for the nanoparticles and about 770 pM for the microsphere. Both these concentrations are similar, as the lower limit for the larger labels also corresponds to a higher number of proteins on the particle surface (see table II in subsection 2.1.7).

The model described in section 2.1.6 which considers external magnetizing fields and sense current and magnetostatic fields as intervenient in the label-sensor system (Ferreira *et al*., 2005b), was used to estimate the number of detected labels (see fig. 7.31).

Figure 7.31 shows that the sensor platform responds linearly to almost the full sensor coverage (3200 nanoparticles and 80 micron-sized beads) and that it has a dynamic range of ~2.5 orders of magnitude for the smaller labels and almost of 2 orders of magnitude for the larger ones. The detection limits for device is about 12 nanoparticles and one 2 μm microsphere, which according to the considered magnetic labeling protocol correspond to a detected hybridized DNA surface density of 4.2 and 6.5 DNA molecules/$\mu m^2$, respectively.

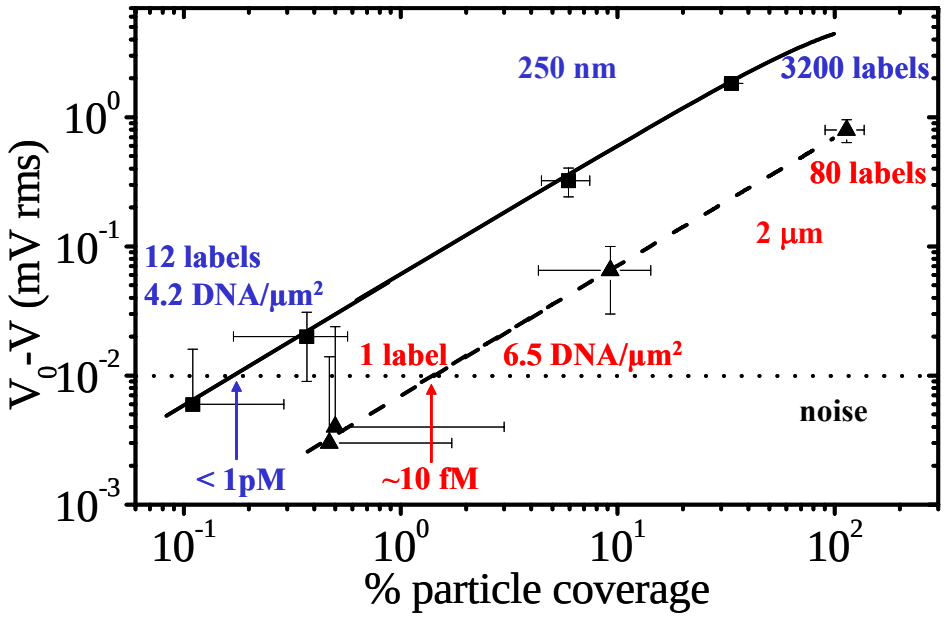


Fig. 7.31. Output in function of the percentage of coverage of the sensor surface with 250 nm particles (squares) and 2 µm microspheres (triangles). The continuous and dashed curves result from a model described in this thesis for the sensor output. The dotted line translates the present system detection limit. Error bars correspond to standard deviations from experimental data and the resulting estimation of particle numbers. Also shown, the detection limit in terms of particle numbers, concentrations and DNA surface densities.

The noise evaluation considered the output of the reference sensors and the variation within this group. The noise of 10 µV rms, in fact does not correspond to the noise of the sensors, as for the measuring frequency of 30 Hz, the intrinsic noise was evaluated to be 250 nV rms (see fig. 5.15 and accompanying discussion). The source of noise is instead the measuring instruments; cablings and the multiplexing system (see fig. 6.7 and details in Ferreira *et al.*, 2006).

Consequently, by improving the measurement apparatus are eliminating some of the extraneous noise sources than, detection limits can be improved at least 10 fold. In addition, if the sensor operates above the 1/f noise regime, then these limits can be further be taken down by two orders of magnitude. At this point, smaller sized labels below 50 nm could be detected individually, as well as single DNA hybridization events (see Graham *et al.*, 2004; Ferreira *et al.*, 2006). Nevertheless, the present referred dynamic range and detection limits of this biosensing platform already make it suitable for gene expression assays (see next subsection).

### 7.7.3 DNA Hybridization Detection Using Ac Field Focusing

This ac field focusing based magnetic sensing platform was applied for the detection of gene expression related DNA targets. These targets were 50 nucleotides long and corresponded to genes that were found to be wither up-regulated (*rpl29*) or down-regulated (*asah*) in cystic fibrosis cell lines with respect to normal tissues (see section 3.3.3). Targets were synthesized with 3'-end biotin functionality and were labeled with 250 nm streptavidin-coated magnetic particles, using a 1 label: 500 DNA molecules ratio (see appendix D). Complementary 50-mer probes were also synthesized and immobilized on chip surfaces for either single or multiprobe experiments, using a protocol described in appendix C (Ferreira *et al*., 2005c).

Experimental conditions similar to the ones described above were used. Currents of 1 mA in amplitude was passed through the sensors and an in-plane ac excitation field of 13.5 Oe rms at a frequency of 30 Hz was applied together with a dc bias field of 24 Oe along the spin valve sensing direction. Sensor outputs were measured at 30 Hz with a constant time of 300 ms. The focusing of labels used the same dc bias field together with 25 to 40 mA rms currents through the u-shaped line structures at a frequency of 0.2 Hz. The multiplexing ac measurement setup depicted in fig. 6.7 was also used.

Small volumes of 20 µL of magnetically labeled target solutions with a target concentration of ~80 fmol/µL (or ~1.3 pg/µL) were dispensed over the chip surfaces. Ac field focusing was applied for 10 to 20 min and the particles were left to completely settle over the sensor for another 5 to 10 min (saturation signals were measured at this time). Subsequently, chips were washed with 100 mM phosphate buffer, pH of 7, to remove unbound labels and were washed again with again with a higher stringency phosphate buffer containing 150 mM NaCl, to further remove weakly and unspecifically bound nanoparticles.

Figure 7.32 shows two single probe experiments where chips functionalized with *rpl29* related probes were interrogated with complementary (*rpl29*) and non-complementary (*asah*) magnetically-labeled targets.

Here, results account for the average signal values of 6 sensors and error bars correspond to the associated standard deviation. Also, pictures of sensing elements surfaces after the end of the experiments are shown as insets. Whilst the in complementary case there is extensive nanolabel binding, in the non-complementary case the surface appears clean of particles.

Figure 7.33, on the other hand, shows a multiprobe experiment were both *rpl29* and *asah* related probes were immobilized onto 7 and 6 sensors, respectively, using a manual spotting method with a pipette. In addition, 3 sensors were left unspotted for assessing the background or unspecific binding signals.

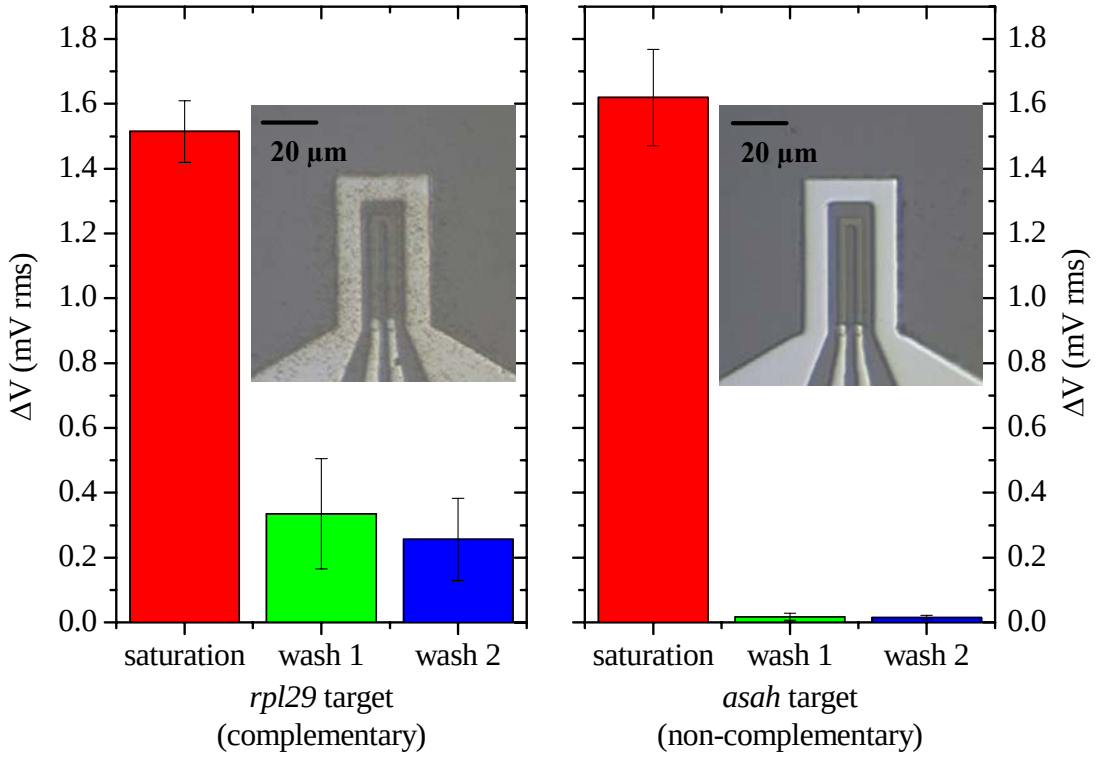


Fig. 7.32. Magnetic field assisted hybridization and simultaneous detection experiments using the ac field focusing method. Spintronic biochips functionalized with *rpl29* related probe were interrogated with complementary (*rpl29*) and non-complementary (*asah*) magnetically labeled targets. Targets were focused using 40 mA currents for ~15 min before washing. A second wash was done with a more stringent buffer solution to further remove weakly or unspecific bound labels. Statistical data is presented for 6 monitored sensors. Insets show pictures for complementary and non-complementary experiments.

Both figures 7.32 and 7.33 show complementary/ non-complementary signal ratios of 7 to 10. The same ratio is found for the complementary/background signals of fig. 7.33 (details on these signals can be found in Ferreira *et al.*, 2005c). Furthermore, both non-complementary and background signals are almost within the system noise level discussed in the previous subsection. These results mean that there is a very small unspecific binding of labels to the surface.

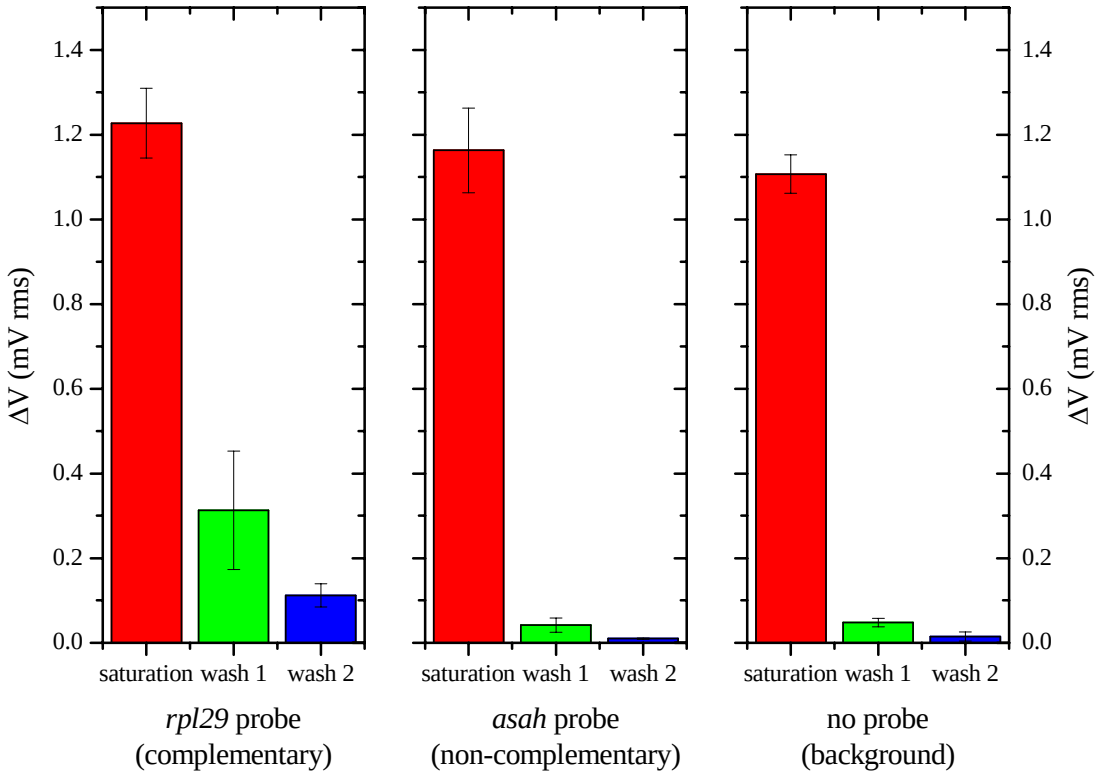


Fig. 7.33. Multiprobe experiment using the ac field focusing method. Chips were functionalized with both DNA probes corresponding to up-regulated (*rpl29*) and down-regulated (*asah*) genes and tested with *rpl29* related magnetically labeled targets. Focusing occured for about 30 min at 25 mA rms focusing current. In these charts saturation represents the sensor responses to labels just before washing.

In addition, these ratios are shown to be sufficient for discriminating between genes that are over expressed or sub-expressed, as in conventional microarray gene expression analysis, a fluorescence signal (coming from a hybridized DNA spot) of intensity < 0.5× or >2× that of a signal obtained from a control sample, represents a down- or an up-regulated gene, respectively.

Another aspect that is also observed is that signals have a considerable variation from sensor to sensor, about 10% in saturation signals and ~50% in hybridization signals. Whereas this variation cannot be explained by slightly different sensor resistances and sensitivities it should be more related to a number of cumulative effects such as: distinct probe density at the chip surface, non-uniform dispensing of labels onto the chip, focusing, hybridization efficiencies and washing steps and even non-uniform particle size, magnetic content, and label clustering.

It can be reasoned that, since saturation signals have smaller deviations of about 10% than the remaining 40% observed in hybridization signals would be due to other effects than focusing or target dispensing onto the chip. In addition, non-complementary and background signals show small variations, this might indicate that the washing is uniform, although that may not be true for partially hybridized strands.

Nevertheless, efforts are on-going to determine the sources of and minimize the variations. These include controlled fluid dispensing and washing, using an automated fluid handling system (see chapter 8), a different chip and focusing design that improves uniformity of fluid distribution over the sensors and is suitable for spotting using automatic robotic systems (see also chapter 8). This latter aspect can also improve probe density uniformity. All these aspects should translate in more uniform hybridization efficiencies. With respect to label size and magnetic content variation and clustering some work is being done worldwide to achieve more uniform and less clustering particles, as mentioned in chapter 2.

In spite of the 50% hybridization signal variation though, the complementary to non-complementary or background ratios are presently sufficient for the use of the system for analysis of the expression of a few genes of diagnostic interest.

Finally, conventional fluorescence based DNA microarrays have comparable dynamic ranges and sensitivities. These systems though, require overnight time scales for hybridization and use expensive instrumentation, turning them unsuitable for high throughput population screening.

In contrast, the present magnetic sensing platform has fast response times, with hybridization times of 5 to 30 minutes, is inexpensive to fabricate at a large scale and have the potential of portability. These systems then show the potential to become powerful tools in mobile biosensing applications.

# 8. Conclusions and Future Perspectives

The work presented in this thesis covered the development of a spintronic biochip platform in its multitude and inter-connected aspects such as sensor physics and materials; magnetic particles and transport; data acquisition and control electronics, signal processing and data analysis; and finally surface chemistries and biological models. All these issues and fields of knowledge were important for the development of the biosensing system, and consequently required the expertise of a number of persons with distinct backgrounds.

As shown, the interdisciplinary effort of the team, which I am proud to belong to, resulted in the demonstration of a novel platform for the detection of biomolecular recognition, using biological models such as biotin-streptavidin binding, antibody-ligand interaction and DNA-DNA hybridization. Furthermore, efforts were taken and proof-of-concepts were obtained from the development of this platform for applications in diagnostics of genetic diseases (cystic fibrosis) and detection of pathogens in water samples (*Salmonella*).

INESC-MN's unique approach comprised the integration of spintronic sensors with on-chip manipulation of magnetically labeled biomolecules, which enabled an almost real-time detection of biomolecular recognition events.

The final fabricated and tested devices already show that magnetic biosensing could be a good alternative to conventional fluorescence based microarray techniques. The combination of features such as fast response, high sensitivity, simple transduction mechanism, parallel analysis capabilities, potential portability and low-cost, show that magnetoresistive biosensors would be useful for the detection of few 10's to 100's of different analytes in point-of-care applications or mobile settings. In fact, these needs are still largely unmet by conventional and some novel biosensing devices.

As a result, an ever increasing number of research groups and companies worldwide are studying and developing magnetoresistive biochips. Targeted applications include veterinary diagnostics and screening for bioterrorism agents (Naval Research

Laboratory), the detection of drugs and proteins of medical interest (Philips), and diagnostics of genetic diseases and detection of pathogens in drinking water (INESC-MN), to name a few.

As for INESC-MN, the road lies ahead and current efforts are focused on increasing the system sensitivity, demonstrating the detection of single nucleotide polymorphisms and on integrating the detection device onto a portable platform, with the ultimate goal of developing a lab-on-a-chip system for complete sample analysis (Ahn *et al*., 2004).

Recent advances and on-going work include the development of novel chip architectures for spin valves and magnetic tunnel junctions (see fig. 8.1). The new designs have some advantageous over its predecessors. They include dual line arrangements of 32 active sensors and 2 references for increased number of sensing sites; metallic pads for use in the automatic sensor electric/magnetic characterization setup (see section 5.3); alignment marks for automatic spotting of biomolecules; and a heater line for on-chip temperature actuation, which may enable the use of optimum assay temperatures, stringencies or target amplification on-chip (see section 5.5).

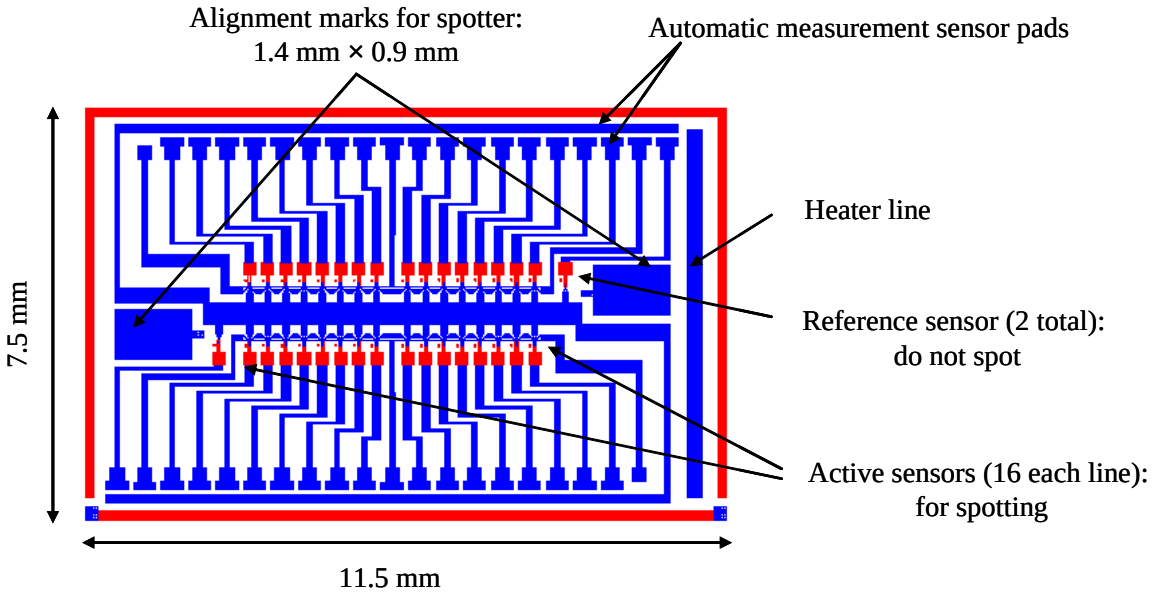


Fig. 8.1. Novel magnetoresistive biochip design for automatic sensor characterization and sensor spotting. The chip comprises a dual line arrangement of 32 active sensors and 2 references, metallic pads designed for used with an automatic measurement setup system (see fig. 5.13). It further includes alignment marks for automatic spotting and heater lines for on-chip temperature actuation.

These novel chips together with the matrix-based platform (see fig. 4.14) are further being integrated in a portable system which comprises a fluid handling system and an electronics control board for data acquisition, fluid and temperature control and communications with a personal computer (PC) or a personal digital assistant (PDA) (see Piedade *et al*., 2005 and Germano, 2006).

Figure 8.2 shows the fabricated new fluid handling system, which is based on hydrodynamic pumping using a piezoresistive micro-element. The system was machined in acrylic and contains a manual valve that allows the commutation between two inlet reservoirs for sample and washing buffers. It further includes a reaction chamber of dimensions of ~1 mm × 5 mm × 5 mm, which is defined by a home-made polydimethylsiloxane (PDMS) squared ring and the chip surface.

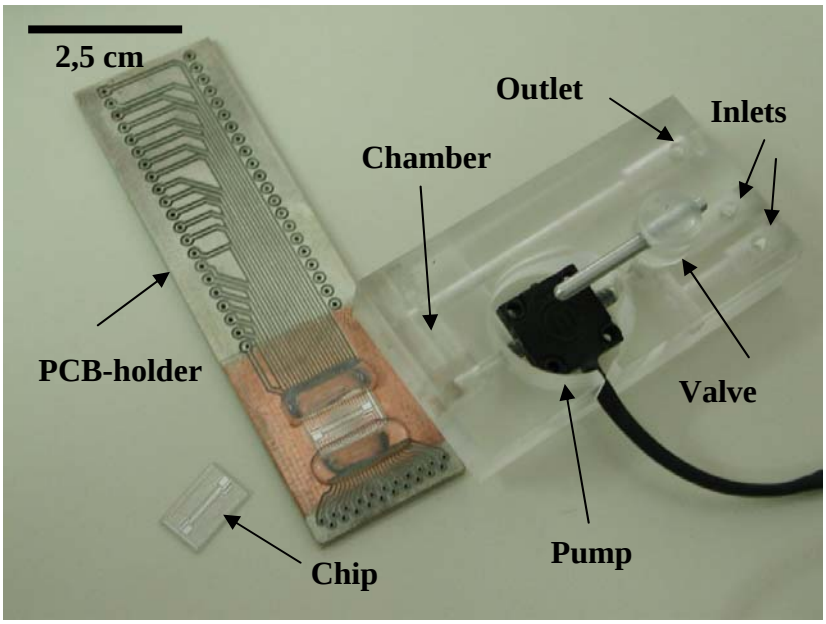


Fig. 8.2. New fluid handling system and PCB holder for chip mounting.

The chip itself is now assembled onto a print circuit board (PCB) for electric connections replacing the much more expensive ceramic chip carrier (see fig. 5.6). The mounted chip is place beneath the ring structure to define the reaction chamber.

Figure 8.3 shows then the electronics board which is being developed for data acquisition from both the novel designs and the 256 sensing element chip of fig. 4.41,

for control of the piezoresistive pump and for other various functions. In fact, the electronics board is about 5.5 cm × 5.5 cm and will replace the full detection setup shown on figures E1 and E2 of appendix E.

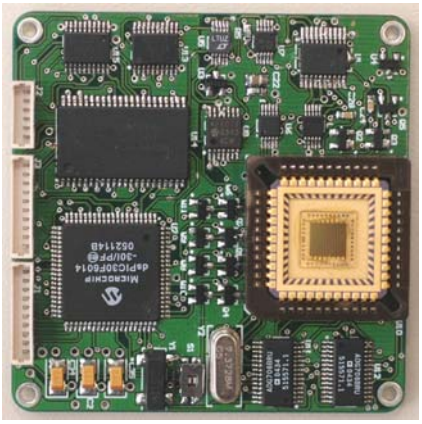

Fig. 8.3. Electronics board for data acquisition, fluid and temperature control and communications with a personal computer (PC) or a personal digital assistant (PDA). The photograph is the actual board size.

Apart from these advances and on-going studies, the biosensing platform can find other uses beyond the applications just mentioned, but also in combination with microbioreactor systems (Ferreira, 2006). Furthermore, the highly sensitive sensors and the potential for single biomolecular recognition detection (see section 2.1.7 and Graham *et al.*, 2004) make this system interesting as a biomolecular research tool for single molecule studies. In fact, the system was already proposed to be used in the study of a molecular motor (Ferreira, 2005).

As a concluding remark, and as a personal opinion, I firmly believe that the upcoming years will see the rise of magnetic biosensing platforms into the market for various applications. As far as I am concerned I would like to be a driving force behind that. With the collaboration of INESC-MN and other research groups and companies, and within a spin-off company environment I will try my best to make these systems succeed and help the community. In resume, magnetoresistive biochips are here to stay!

# References


Ahn, C.H., Choi, J.-W., Beaucage, G., Nevin, J.H., Lee, J.-B., Puntambekar, A., and Lee, J.Y. (2004). Disposable smart lab on a chip for point-of-care clinical diagnostics. *Proceedings of the IEEE*, **92**, 154-173.

Almeida, J.M., Ferreira, R., Freitas, P.P., Langer, J., Ocker, B., and Maass, W. (2006). 1/f noise in linearized low resistance MgO magnetic tunnel junctions. *Journal of Applied Physics*, **99**, 08B314.

Anguelouch, A., Reich, D.H., Chien, C.L., and Tondra, M. (2004). Detection of ferromagnetic nanowires using GMR sensors. *IEEE Transactions on Magnetics*, **40**, 2997-2999.

Astalan, A.P., Ahrentorp, F., Johansson, C., Larsson, K., and Krozer, A. (2004). Biomolecular reactions studied using changes in Brownian rotation dynamics of magnetic particles. *Biosensors and Bioelectronics*, **19**, 945-951.

Baibich, M. N., Broto, J. M., Fert, A., van Dau, F. N., and Petroff, F. (1988). Giant magnetoresistance of (001)Fe/ (001)Cr magnetic superlattices. *Physical Review Letters*, **61**, 2472-2475.

Ball, J.C., Puckett, L.G., and Bachas, L.G. (2003). Covalent immobilization of beta-galactosidase onto a gold-coated magnetoelastic transducer via a self-assembled monolayer: toward a magnetoelastic biosensor. *Analytical Chemistry*, **75**, 6932-6939.

Bamdad, C. (1998). A DNA self-assembled monolayer for the specific attachment of unmodified double- or single-stranded DNA. *Biophysical Journal*, **75**, 1997-2003.

Bao, Y., and Krishan, K.M. (2005). Preparation of functionalized and gold-coated cobalt nanocrystals for biomedical applications. *Journal of Magnetism and Magnetic Materials*, **293**, 15-19.

Baselt, D.R., Lee, G.U., Natesan, M., Metzger, S.W., Sheehan, P.E., and Colton, R.J. (1998). A biosensor based on magnetoresistance technology. *Biosensors and Bioelectronics*, **13**, 731-739.

Berry, C. C., and Curtis, A. S. G. (2003). Functionalization of magnetic nanoparticles for applications in biomedicine. *Journal of Physics D: Applied Physics*, **36**, R198-R206.

Berthier, J., and Silberzan, P. (2006). *Microfluidics for biotechnology*,: Artech House, Boston.

Bertram, H.N. (1994). *Theory of Magnetic Recording*,: Cambridge University Press, Boston.

Besse, P.-A.., Boero, G., Demierre, M., Pott, V., and Popovic, R. (2002). Detection of single magnetic microbead using a miniaturized silicon Hall sensor. *Applied Physics Letters*, **80**, 4199-4201.

Binasch, G., Grünberg, P., Saurenbach, F., and Zinn, E. (1989). Enhanced magnetoresistance in layered magnetic structures with antiferromagnetic interlayer exchange. *Physical Review B*, **39**, 4828-4830.

Blohm, D. H., and Guiseppi-Elie, A. (2001). New developments in microarray technology. *Current Opinion in Biotechnology*, **12**, 41-47.

Bobadilla, J. L., Macek Jr., M., Fine, J. P., and Farrell, P. M. (2002). Cystic fibrosis: a worldwide analysis of CFTR mutations: correlation with incidence data and application to screening. *Human Mutation*, **19**, 575-606.

Brzeska, M., Panhorst, M., Kamp, P. B., Schotter, J., Reiss, G., Pühler, A., Becker, A., and Brückl, H. (2004). Detection and manipulation of biomolecules by magnetic carriers. *Journal of Biotechnology*, **112**, 25-33.

Brown, W.F. Jr., (1963). Thermal fluctuations of a single-domain particle. *Physical Review*, **130**, 1677-1686.

Bürgler, D., and Grünberg, P. (2003). Magnetoelectronics – Magnetism and Magneto-transport in Layered Structures. In *Nanoelectronics and Information Technology*. Waser, R. (Ed.), Wiley-VCH,: Weinheim, Germany.

Cardoso, F. (2005). Magnetic tunnel junction maxtrix-based biochip. Senior student project thesis, Physics Department, Instituto Superior Técnico.

Cardoso, F.A., Ferreira, H.A., Conde, J.P., Chu, V., Freitas, P.P., Vidal, D., Germano, J., Sousa, L., Piedade, M.S., Andrade, B., and Lemos, J.M. (2006). Diode/magnetic tunnel junction for fully scalable matrix-based biochip. *Journal of Applied Physics*, **99**, 08B307.

Carias, C. (2004). Biochips com sensores de efeito Hall planar. Senior student project thesis, Physics Department, Instituto Superior Técnico.

Chemla, Y. R., Grossman, H.L., Poon, Y., McDermott, R., Stevens, R., Alper, M.D., and Clarke, J. (2000). Ultrasensitive magnetic biosensor for homogeneous immunoassay. *Proceedings of the National Academy of Sciences*, **19**, 14268-14272.

Chiriac, H., Tibu, M., Moga, A.E., and Hera, D.D., (2005). Magnetic GMI sensor for detection of biomolecules. *Journal of Magnetism and Magnetic Materials*, **293**, 671-676.

Choi, J.-W., Ahn, C. H., Bhansali, S., and Henderson, H. T. (2000). A new magnetic bead-based filterless bio-separator with planar electromagnet surfaces for integrated bio-detection. *Sensors and Actuators B: Chemical*, **68**, 34-39.

Choi, J.-W., Oh, K. W., Thomas, J. H., Heineman, W. R., Halsall, H. B., Nevin, J. H., Heimicki, A. J., Henderson, H. T., and Ahn, C. H. (2002). An integrated microfluidic biochemical detection system for protein analysis with magnetic bead-based sampling capabilities. *Lab on a Chip*, **2**, 27-30.

Chován, T., and Guttman, A. (2002). Microfabricated devices in biotechnology and biochemical processing. *Trends in Biotechnology*, **20**, 116-122.

Chrisey, L.A., Lee, G.U., and O'Ferrall, C.E. (1996). Covalent attachment of synthetic DNA self-assembled monolayer films. *Nucleic Acids Research*, **24**, 3031-3039.

Chung, S.H., Hoffmann, A., Bader, S.D, Liu, C., Kay, B., Makowski, and Chen, L. (2004). Biological sensors based on Brownian relaxation of magnetic nanoparticles. *Applied Physics Letters*, **85**, 2971-2973.

Cirino, N.M., Musser, K.A., and Egan, C. (2004). Multiplex diagnostic platforms for detection of biothreat agents. *Expert Review of Molecular Diagnostics*, **4**, 841-857.

Clarke, L.A., Braz, C., and Amaral, M.D. (2004). Cystic fibrosis-related patterns of gene expression: a genome-wide microarray approach. *Pediatric Pulmonology*, **38**, supplement 27, 219.

Collins, F.S. (1992). Cystic fibrosis – molecular biology and therapeutic implications. *Science*, **256**, 1149-1156.

Connolly, J., and St. Pierre, T. (2001). Proposed biosensors based on time-dependent properties of magnetic fluids. *Journal of Magnetism and Magnetic Materials*, **225**, 156-160.

Cooper, G..M. (2000). *The Cell – a Molecular Approach, Second Edition*, ASM Press: Washington, D.C..

Cras, J.J., Rowe-Taitt, C.A., Nivens, D.A., and Ligler, F.S. (1999). Comparison of chemical cleaning methods of glass in preparation for silanization. *Biosensors and Bioelectronics*, **14**, 683-688.

Debye, P. (1929). *Polar Molecules*, Chemical Catalog Company,: New York.

del Campo, A., Sen, T., Lellouche, J.-P., and Bruce, I.J. (2005). Multifunctional magnetite and silica-magnetite nanoparticles: synthesis, surface activation and applications in life sciences. *Journal of Magnetism and Magnetic Materials*, **293**, 33-40.

Demers, L.M., Ginger, D.S., Park, S.-J., Li, Z., S.-W., Chung, and Mirkin, C.A. (2002). Direct patterning of modified oligonucleotides on metals and insulators by dip-pen nanolithography. *Science*, **296**, 1836-1838.

Deng, T., Whitesides, G. M., Radhakrishnan, M., Zabow, G., and Prentiss, M. (2001). Manipulation of magnetic microbeads in suspension using micromagnetic systems fabricated with soft lithography. *Applied Physics Letters*, **78**, 1775-1777.

Dieny, B., Speriosu, V.S., Metin, S., Parkin, S.S., Gurney, B.A., Baumgart, P., and Wilhoit, D.R. (1991). Magnetotransport properties of magnetically soft spin-valve structures. *Journal of Applied Physics*, **69**, 4774-4779.

Duffy, D. C., Cooper, J. C., Scheller, J. A. O, and Whitesides, G. M. (1998). Rapid prototyping of microfluidic systems in poly(dimethylsiloxane). *Analytical Chemistry*, **70**, 4974-4984.

Edelstein, R.L., Tamanha, C.R., Sheehan, P.E., Miller, M.M., Baselt, D.R., Whitman, L.J., and Colton, R.J. (2000). The BARC biosensor applied to the detection of biological warfare agents. *Biosensors and Bioelectronics*, **14**, 805-813.

Ejsing, L., Hansen, M.F., and Menon, A.K. (2003). Planar Hall effect magnetic sensor for micro-bead detection. *Proceedings of the* 17$^{th}$ *European Conference on Solid-State Transducers, Eurosensors* 2003, 21-24 *September* 2003, *Guimarães, Portugal*, 1095-1098.

Ejsing, L., Hansen, M.F., Menon, A.K., Ferreira, H.A., Graham, D.L., and Freitas, P.P. (2004). Planar Hall effect sensor for magnetic micro- and nanobead detection. *Applied Physics Letters*, **84**, 4729-4731.

Ejsing, L., Hansen, M.F., Menon, A.K., Ferreira, H.A., Graham, D.L., and Freitas, P.P. (2005). Magnetic microbead detection using the planar Hall effect. *Journal of Magnetism and Magnetic Materials*, **293**, 677-684.

Enpuku, K., Minotani, T., Gima, T., Kuroki, Y., Itoh, Y., Yamashita, M., Katakura, Y., and Kuhara S. (1999). Detection of magnetic nanoparticles with Superconducting Quantum Interference Device (SQUID) magnetometer and application to immunoassays. *Japanese Journal of Applied Physics*, **38**, L1102-L1105.

Erickson, D., and Li, D. (2004). Integrated microfluidic devices. *Analytica Chimica Acta*, **507**, 11-26.

Feliciano, N. (2003). Transporte de biomoléculas com marcadores magnéticos utilizando campos locais num chip. Senior student project thesis, Physics Department, Instituto Superior Técnico.

Ferreira, H. (2000). Partículas nano-magnéticas. Microtechnologies course report. INESC – Microsystems and Nanotechnologies.

Ferreira, H. (2001). Application of magnetic reading technology in new biochip development. Senior student project thesis, Physics Department, Instituto Superior Técnico.

Ferreira, H. A. (2005). Rotary molecular motors: $F_1$-ATPase. Celular and Biomolecular Engineering course report. Chemistry Department, Instituto Superior Técnico.

Ferreira, H. A. (2006). Essay on micro-bioreactors: a miniaturized packed-bed reactor. Enzymatic Technology course report. Chemistry Department, Instituto Superior Técnico.

Ferreira, H.A., Graham, D.L., Freitas, P.P., and Cabral, J.M.S. (2003). Biodetection using magnetically labeled biomolecules and arrays of spin valve sensors. *Journal of Applied Physics*, **93**, 7281-7286.

Ferreira, H.A., Graham, D.L., Parracho, P., Soares, V., and Freitas, P.P. (2004). Flow velocity measurement in microchannels using magnetoresistive chips. *IEEE Transactions on Magnetics*, **40**, 2652-2654.

Ferreira, H.A., Feliciano, N., Graham, D.L., and Freitas, P.P. (2005a). Effect of spin-valve sensor magnetostatic fields on nanobead detection for biochip applications. *Journal of Applied Physics*, **97**, 10Q904.

Ferreira, H. A., Feliciano, N., Graham, D. L., Clarke, L. A., Amaral, M. D., and Freitas, P. P. (2005b). Rapid DNA hybridization based on AC field focusing of magnetically-labeled target DNA. *Applied Physics Letters*, **87**, 013901.

Ferreira, H.A., Graham, D.L., Feliciano, N., Clarke, L.A., Amaral, M.D., and Freitas, P.P. (2005c). Detection of cystic fibrosis related DNA targets using AC field focusing of magnetic labels and spin-valve sensors. *IEEE Transactions on Magnetics*, **41**, 4140-4142.

Ferreira, H. A., Cardoso, F. A., Ferreira, R., Cardoso, S., and Freitas, P. P. (2006). Magnetoresistive DNA-chips based on ac field focusing of magnetic labels. *Journal of Applied Physics*, **99**, 08P105.

Fixe, F., Cabeça, R., Chu, V., Prazeres, D.M.F., Ferreira, G.N.M., and Conde, J.P. (2003). Electric-field-pulse-assisted covalent immobilization of DNA in the nanosecond time scale. *Applied Physics Letters*, **83**, 1465-1467.

Fixe, F., Dufva, M., Telleman, P., and Christensen, C.B.V. (2004a). Functionalization of poly(methyl methacrylate) (PMMA) as a substrate for DNA microarrays. *Nucleic Acids Research*, **32**, e9.

Fixe, F., Dufva, M., Telleman, P., and Christensen, C.B.V. (2004b). One-step immobilization of aminated and thiolated DNA onto poly(methylmethacrylate) (PMMA) substrates. *Lab Chip*, **4**, 191-195.

Fixe, F., Branz, H. M., Louro, N., Chu, V., Prazeres, D. M. F., and Conde, J. P. (2004c). Immobilization and hybridization by single sub-millisecond electric field pulses, for pixel-addressed DNA microarrays. *Biosensors and Bioelectronics*, **19**, 1591-1597.

Fixe, F., V. Chu, Prazeres, D. M., and Conde, J. P. (2004d). An on-chip thin-film photodetector for the quantification of DNA probes and targets in microarrays. *Nucleic Acids Research,* **32**, e70.

Fixe, F., V. Chu, Prazeres, D. M. F., and Conde, J. P. (2005a). Single base mismatch detection by microsecond voltage pulses. *Biosensors and Bioelectronics,* **21**, 888-893.

Fixe, F., Branz, H. M., Louro, N., Chu, V., Prazeres, D. M. F., and Conde, J. P. (2005b). Electric-field assisted immobilization and hybridization of DNA oligomers on thin-film microchips. *Nanotechnology*, **16**, 2061-2071.

Florin, E.-L., Moy, V. T., and Gaub, H. E. (1994). Adhesion forces between individual ligand-receptor pairs. *Science*, **264**, 415-417.

Freitas, P.P., Silva, F., Oliveira, N.J., Melo, L.V., Costa, L., and Almeida, N. (2000). Spin-valve sensors. *Sensors and Actuators A*, **81**, 2-8.

Freitas, P. P., and Ferreira, H. A. (in press). Spintronic biochips for the detection of biomolecular recognition. In *The Handbook of Magnetism and Advanced Magnetic Materials*. Kronmüller, H., and Parkin, S. (Eds.), Wiley,: New York.

Freitas, P.P., Ferreira, H.A., Graham, D.L., Clarke, L.A., Amaral, M.D., Martins, V., Fonseca, L., and Cabral, J.S. (2004). Magnetoresistive DNA chips. In *Magnetoelectronics*, Johnson, M. (Ed.), Academic Press,: New York, pp. 332-373.

Freitas, P. P., Ferreira, H. A., Ferreira, R., Cardoso, S., van Dijken, S., and Gregg, J. (2006). Nanostructures for spin electronics. In *Advanced Magnetic Nanostructures*, Sellmyer, D., and Skomski, R. (Eds.), Springer,: Berlin, pp. 403-460.

Freitas Jr., R. A. (1999). *Nanomedicine, Volume I: Basic Capabilities*. Landes Bioscience,: Georgetown.

Fritz, J., Baller, M. K., Lang, H. P., Rothuizen, H., Vettiger, P., Meyer, E., Güntherodt, Gerber, C., and Gimzewski, J. K. (2000). Translating biomolecular recognition into nanomechanics. *Science*, **288**, 316-318.

Galvin, P., Clarke, L. A., Harvey, S., and Amaral, M. D. (2004). Microarray analysis in cystic fibrosis. *Journal of Cystic Fibrosis*, **3S2**, 29-33.

Germano, J. (2006). Portable system for DNA analysis based on a biochip. Master thesis, Electronics Computer Engineering Department, Instituto Superior Técnico.

Geschke, O., Klank, H., and Tellemann, P. (Eds.) (2004). *Microsystem engineering of Lab-on-a-Chip devices*. Wiley-VCH Verlag,: Weiham.

Gijs, M. A. M. (2004). Magnetic bead handling on-chip: new opportunities for analytical applications. *Microfluid Nanofluid*, **1**, 22-40.

Gould, P. (2004). Nanoparticles probe biosystems. *Materials Today*, **7** (2), 36-43.

Graham, D. L., Ferreira, H., Bernardo, J., Freitas, P. P., and Cabral, J. M. S. (2002). Single magnetic microsphere placement and detection on-chip using current line designs with integrated spin valve sensors: biotechnological applications. *Journal of Applied Physics*, **91**, 7786-7788.

Graham, D.L., Ferreira, H.A., Freitas, P.P., and Cabral, J.M.S. (2003). High sensitivity detection of molecular recognition using magnetically labelled biomolecules and magnetoresistive sensors. *Biosensors and Bioelectronics*, **18**, 483-488.

Graham, D.L., Ferreira, H.A., and Freitas, P.P. (2004). Magnetoresistance-based biosensors and biochips. *Trends in Biotechnology*, **22**, 455-462.

Graham, D.L., Ferreira, H.A., Feliciano, N., Freitas, P.P., Clarke, L.A., and Amaral, M.D. (2005). Magnetic field-assisted DNA hybridisation and simultaneous detection using mícron-sized spin-valve sensors and magnetic nanoparticles. *Sensors and Actuators B*, **107**, 936-944.

Grancharov, S. G., Zeng, H., Sun, S., Wang, S. X., O' Brien, S., Murray, C. B., Kirtley, J. R., and Held, G. A. (2005). Bio-functionalization of monodisperse magnetic nanoparticles and their use as biomolecular labels in a magnetic tunnel junction based sensor. *Journal of Physical Chemistry B*, **109**, 13030-13035.

Grünberg, P., Schreiber, R., Pang, Y., Brodsky, M. B., and Showers, H. (1986). Layered magnetic structures: evidence for antiferromagnetic coupling of Fe layers across Cr interlayers. Physical Review Letters, **57**, 2442-2445.

Guedes, A., Mendes, M.J., Freitas, P.P., and Martins, J.L. (2006). Study of synthetic ferromagnet-synthetic antiferromagnet structures for magnetic sensor application. *Journal of Applied Physics*, **99**, 08B703.

Häfeli, U., Schutt, W., Teller, J., and Zborowski, M. (Eds.) (1997). *Scientific and Clinical Applications of Magnetic Carriers*, Plenum Press,: New York.

Heim, D. E., Fontana, R. E., Tsang, C., Speriosu, V. S., Gurney, B. A., and Williams, M. L. (1994). Design and operation of spin-valve sensors. *IEEE Transactions on Magnetics*, **30**, 316-321.

Heller, M.J. (1996). An active microelectronics device for multiplex DNA analysis. *IEEE Engineering in Medicine and Biology*, **15**, 100-104.

Jackson, J. D. (1975). *Classical Electrodynamics, 2nd Edition*. John Wiley and Sons,: New York.

Joos, B., Kuster, H., and Cone, R. (1997). Covalent attachment of hybridisable oligonucleotides to glass supports. *Analytical Biochemistry*, **247**, 96-101.

Jordan, P., Brazão, R., Boavida, M. G., Gespach, C., and Chastre, E. (1999). Cloning of a novel Rac1b splice variant with increased expression in colorectal tumors. *Oncogene*, **18**, 6835-6839.

Joshi, V., Li, G., Wang, S.X., and Sun, S. (2004). Biochemical stability of components for use in a DNA detection system. *IEEE Transactions on Magnetics*, **40**, 3012-3014.

Jullière, M. (1975). Tunneling between ferromagnetic films. *Physics Letters* A **54**, 225-226.

Katsura, S., Yasuda, T., Hirano, K., Mizuno, A., and Tanaka, S. (2001). Development of a new detection method for DNA molecules. *Superconductor Science and Technology*, **14**, 1131-1134.

Katz, E., and Willner, I. (2004). Integrated nanoparticle-biomolecule hybrid systems: synthesis, properties and applications. *Angewandte Chemie International Edition*, **43**, 6042-6108.

Kiselev, S. I., Sankey, J. C., Krivorotov, I. N., Emley, N. C., Schoelkopf, R. J., Buhrman, R. A., and Ralph, D. C. (2003). Microwave oscillations of a nanomagnet driven by a spin-polarized current. *Nature*, **425**, 380-383.

Kittel, C. (1996). *Introduction to Solid State Physics, Seventh Edition*, John Wiley and Sons, Inc.: New York., pp. 441-484.

Klem, M. T., Willits, D., Solis, D. J., Belcher, A. M., Young, M., and Douglas, T. (2005). Bio-inspired synthesis of protein encapsulated CoPt nanoparticles. *Advanced Functional Materials*, **15**, 1489-1494.

Kötitz, R., Matz, H., Trahms, L., Koch, H., Weitschies, W., Rheinländer, T., Semmler, W., and Bunte, T. (1997). SQUID based remanence measurements for immunoassays. *IEEE Transactions on Applied Superconductivity*, **7**, 3678-3681.

Kriz, C.B., Radevik, K., and Kriz, D. (1996). Magnetic permeability measurements in bioanalysis and biosensors. *Analytical Chemistry*, **68**, 1966-1970.

Kriz, K., Gehrke, J., and Kriz, D. (1998). Advances toward magneto immunoassays. *Biosensors and Bioelectronics*, **13**, 817-823.

Kurlyandskaya,, G., and Levit, V. (2005). Magnetic Dynabeads detection by sensitive element based on giant magnetoimpedance. *Biosensors and Bioelectronics*, **20**, 1611-1616.

Kurlyandskaya, G.V., Sánchez, M.L., Hernando, B., Prida, V.M., Gorria, P., and Tejedor, M. (2003). Giant-magnetoimpedance-based sensitive element as a model for biosensors. *Applied Physics Letters*, **82**, 3053-3055.

Lagae, L., Wirix-Speetjens, R., Das, J., Graham, D., Ferreira, H., Freitas, P. P., Borghs, G., and de Boeck, J. (2002). On-chip manipulation and magnetization assessment of magnetic bead ensembles by integrated spin-valve sensors. *Journal of Applied Physics*, **91**, 7445-7447.

Lagae, L., Wirix-Speetjens, R., Liu, C.-X., Laureyn, W., de Boeck, J., Borghs, G., Harvey, S., Galvin, P., Graham, D.L., Ferreira, H.A., Freitas, P.P., Clarke, L.A., and Amaral, M.D. (2005). Magnetic biosensors for genetic screening of cystic fibrosis. *IEE Proceedings on Circuits, Devices & Systems*, **152**, 393-400.

Landry, G., Miller, M.M., Bennett, B.R., Johnson, M., and Smolyaninova, V. (2004). Characterization of single magnetic particles with InAs quantum-well Hall devices. *Applied Physics Letters*, **85**, 4693-4695.

Lee, C. S., Lee, H., and Westervelt, R. M. (2001). Microelectromagnets for the control of magnetic nanoparticles. *Applied Physics Letters*, **79**, 3308-3310.

Lee, G. U., Metzger, S., Natesan, M., Yanavich, C., and Dufrene, Y.F. (2000). Implementation of force differentiation in the immunoassay. *Analytical Biochemistry*, **286**, 261-271.

Li, G., Joshi, V., White, R.L., Wang, S.X., Kemp, J.T., Webb, C., Davis, R.W., and Sun, S. (2003). Detection of single micron-sized magnetic bead and magnetic nanoparticles using spin valve sensors for biological applications. *Journal of Applied Physics*, **93**, 7557-7559.

Li, G., and Wang, S.X. (2003). Analytical and micromagnetic modeling for detection of a single magnetic microbead or nanobead by spin valve sensors. *IEEE Transactions on Magnetics*, **39**, 3313-3315.

Li, G., Wang, S.X., and Sun, S. (2004). Model and experiment of detecting multiple magnetic nanoparticles as biomolecular labels by spin valve sensors. *IEEE Transactions on Magnetics*, **40**, 3000-3002.

Liu, C., Yang, F., Chung, S. H., Jin, Q., Han, Z., Hoffmann, A., Kay, B., Bader, S. D., Makowski, L., Chen, L. (unpublished)

Martins, V. C. B., Fonseca, L. P., Ferreira, H. A., Graham, D. L., Freitas, P. P., and Cabral J. M. S. (2005). Use of magnetoresistive biochips for monitoring of pathogenic microorganisms in water through bioprobes: oligonucleotides and antibodies. *Technical Proceedings of the* 2005 *NSTI Nanotechnology Conference and Trade Show*, 8-12 *May* 2005, *Anaheim, California, USA*, **1**, chapter 8: Bio Micro Sensors, 493-496.

Martins, V. C. B., Fonseca, L.P., Ferreira, H. A., Cardoso, F. A., Loureiro, J., Germano, J., Sousa, L., Piedade, M. S., Costa, B. A., Lemos, J. L., Freitas, P. P., and Cabral, J. M. S. (submitted). A magnetoresistive biochip for microbial analysis of water samples.

Miller, M.M., Sheehan, P.E., Edelstein, R.L., Tamanaha, C.R., Zhong, L., Bounnak, S., Whitman, L.J., and Colton, R.J. (2001). A DNA array sensor utilizing magnetic microbeads and magnetoelectronic detection. *Journal of Magnetism and Magnetic Materials*, **225**, 138-144.

Miller, M.M., Prinz, G.A., Cheng, S.-F., and Bounnak, S. (2002). Detection of a micron-sized magnetic sphere using a ring-shaped anisotropic magnetoresistance-based

sensor: a model for a magnetoresistance-based biosensor. *Applied Physics Letters*, **81**, 2211-2213.

Moodera, J.S., Kinder, L.R., Wong, T.M., Meservey, R. (1995). Large magnetoresistance at room temperature in ferromagnetic thin film tunnel junctions. *Physical Review Letters*, **74**, 3273-3276.

Moy, V. T., Florin, E.-L., and Gaub, H. E. (1994). Intermolecular forces and energies between ligand and receptors. *Science*, **266**, 257-259.

Nishibiraki, H., Kuroda, C.S., Maeda, M., Matsushita, N., Abe, M., and Handa, H. (2005). Preparation of medical magnetic nanobeads with ferrite particles encapsulated in a polyglycidyl methacrylate (GMA) for bioscreening. *Journal of Applied Physics*, **97**, 10Q919.

Néel, L. (1955). Some theoretical aspects of rock magnetism. *Advances in Physics*, **4**, 191-243.

Okamoto, T., Suzuki, T., and Yamamoto, N. (2000). Microarray fabrication with covalent attachment of DNA using bubble jet technology. *Nature Biotechnology*, **18**, 438-441.

Pamme, N. (2006). Magnetism and microfluidics. *Lab on a Chip*, **6**, 24-38.

Pankhurst, Q.A., Connolly, J., Jones, S.K., and Dobson, J. (2003). Applications of magnetic nanoparticles in biomedicine. *Journal of Physics D: Applied Physics*, **36**, R167-R181.

Pappaert, K., Van Hummelen, P., Vanderhoeven, J., Baron, G. V., and Desmet, G. (2003). Diffusion-reaction modeling of DNA hybridization kinetics on biochips. *Chemical Engineering Science*, **58**, 4921-4930.

Parracho, P. G. F. (2002). Microfluidic devices for biochip applications. Senior student project thesis, Physics Department, Instituto Superior Técnico.

Parkin, S. S. P., Kaiser, C., Panchula, A., Rice, P. M., Hughes, B., Samant, M., and Yang, S.-H. (2004). Giant tunneling magnetoresistance at room temperature with MgO (100) tunnel barriers. *Nature Materials*, **3**, 862-866.

Patolsky, F., and Lieber, C. M. (2005) Nanowire nanosensors. *Materials Today*, **8** (4), 20-28.

Pease, A.C., Solas, D., Sullivan, E.J., Cronin, M.T., Holmes, C.P., and Fodor, S.P. (1994). Light generated oligonucleotides arrays for rapid DNA sequence analysis. *Proceedings of the National Academy of Sciences USA,* **91**, 5022-5026.

Pekas, N., Porter, M. D., Tondra, M., Popple, A., and Jander, A. (2004). Giant magnetoresistance monitoring of magnetic picodroplets in an integrated microfluidic system. *Applied Physics Letters*, **85**, 4783-4785.

Peruski, A.H., and Peruski, L.F. Jr. (2003). Immunologic methods for detection and identification of infectious disease and biological warfare agents. *Clinical and Diagnostic Laboratory Immunology*, **10**, 506-513.

Piedade, M., Sousa, L., Germano, J., Lemos, J., Costa, B., Freitas, P., Ferreira, H., Cardoso, F., and Vidal, D. (2005). Architecture of a portable system based on a biochip for DNA recognition. *Proceedings of the* XX *Conference on Design of Circuits and Integrated Systems (DCIS),* 23-25 *November, Lisboa, Portugal*.

Prinz, G.A. (1998). Device physics – magnetoelectronics. *Science*, **282**, 1660-1663.

Ramalho, A. S., Beck, S., Meyer, M., Penque, D., Cutting, G. R., and Amaral, M. D. (2002). Five percent of normal CFTR mRNA ameliorates the severity of pulmonary disease in cystic fibrosis. *American Journal of Respiratory Molecular Biology*, **27**, 619-627.

Ramsay, G. (1998). DNA-chips: state-of-the-art. *Nature Biotechnology*, **16**, 40-44.

Raquet, B. (2001). Electronic noise in magnetic materials and devices. In *Spin Electronics*, Lecture Notes in Physics, Ziese, M., and Thorton, M.J. (Eds.), Springer,: Berlin, pp. 232-273.

Reich, D.H., Tanase, M., Hultgren, A., Bauer, L.A., Chen, C.S., and Meyer, G.J. (2003). Biological applications of multifunctional magnetic nanowires. *Journal of Applied Physics*, 7275-7280.

Resnick, D., Gilmore, K., Klem, M. T., Smith, E., Douglas, T., and Idzerda, Y. U. (2005). Modeling of magnetic behaviour of $\gamma$-$Fe_2O_3$ nanoparticles mineralized in ferritin. *Journal of Applied Physics*, **95**, 7127-7129.

Richardson, J., Hawkins, P, and Luxton, R. (2001). The use of coated paramagnetic particles as a physical label in a magneto-immunoassay. *Biosensors and Bioelectronics*, **16**, 989-993.

Richardson, J., Hill, A., Luxton, R., and Hawkins, P. (2001). A novel measuring system for the determination of paramagnetic particles for use in magneto-immunoassays. *Biosensors and Bioelectronics*, **16**, 1127-1132.

Rife, J.C., Miller, M.M., Sheehan, P.E., Tamanaha, C.R., Tondra, M., and Whitman, L.J. (2003). Design and performance of GMR sensors for the detection of magnetic microbeads in biosensors. *Sensors and Actuators A*, **107**, 209-218.

Ruan, C., Zeng, K., Varghese, O.K., and Grimes, C.A. (2003). Magnetoelastic immunosensors: amplified mass immunosorbent assay for detection of *Escherichia coli* O157:H7. *Analytical Chemistry*, **75**, 6494-6498.

Ryan, O., Smyth, M. R., and Fágáin, C. O. (1994). Horseradish peroxidase: the analyst's friend. *Essays in Biochemistry*, **28**, 129-146.

Salgado, J. D., Horiuchi, K., and Dutta, P. (2006). A conductivity-based interface tracking method for microfluidic application. *Journal of Micromechanics and Microengineering*, **16**, 920-928.

Sandhu, A., and Handa, H. (2005). Practical Hall effect sensors for biomedical instrumentation. *IEEE Transactions on Magnetics*, , in press.

Sandhu, A., Sanbonsugi, H., Shibasaki, I., Abe, M., and Handa, H. (2004*)*. High sensitivity InSb ultra-thin film micro-hall sensors for bioscreening applications. *Japanese Journal of Applied Physics*, **43**, L868-L870.

Schepper, W., Schotter, J., Brückl, H., and Reiss, G. (2004). Single molecule detection with magnetic beads – computer simulation. *Journal of Magnetism and Magnetic Materials*, **272-276**, e1695-e1696.

Schotter, J., Kamp, P.B., Becker, A., Pühler, A., Brinkmann, D., Schepper, W., Brückl, H., and Reiss, G. (2002). A biochip based on magnetoresistive sensors. *IEEE Transactions on Magnetics*, **38**, 3365-3367.

Schotter, J., Kamp, P.B., Becker, A., Pühler, A., Reiss, G., and Brückl, H. (2004). Comparison of a prototype magnetoresistive biosensor to standard fluorescent DNA detection. *Biosensors and Bioelectronics*, **19**, 1149-1156.

Shen, W., Liu, X., Mazumdar, D., and Xiao, G. (2005). *In situ* detection of single micron-sized magnetic beads using magnetic tunnel junctions sensors. *Applied Physics Letters*, **86**, 253901.

Smistrup, K., Hansen, O., Bruus, H., and Hansen, M. F. (2005). Magnetic separation in microfluidic systems using microfabricated electromagnets – experiments and simulations. *Journal of Magnetism and Magnetic Materials*, **293**, 597-604.

Solin, S. A. (2004). Magnetic field nanosensors. *Scientific American*, **291** (1), 44-51.

Sousa, R.C., Freitas, P.P., Chu, V., and Conde, J.P. (1999). Vertical integration of a spin dependent tunnel junction with an amorphous Si diode for MRAM application. *IEEE Transactions on Magnetics*, **35**, 2832-2834.

Southern, E.M., Mir, K., and Shchepinov, M. (1999). Molecular interactions on microarrays. *Nature Genetics*, **21**, 5-9.

Stoner, E.C., and Wohlfarth, E.P. (1948). A mechanism of magnetic hysterisis in heterogenous alloys. *Phylosophical Transactions of the Royal Society of London*, series A, **240**, 599-642.

Sun, S., Anders, S., Hamann, H.F., Thiele, J.U., Baglin, J.E., Thomson, T., Fullerton, E.E., Murray, C.B., and Terris, B.D. (2002). Polymer mediated self-assembly of magnetic nanoparticles. *Journal of the American Chemical Society*, **124**, 2884-2885.

Sun, S., and Zeng, H. (2002). Size-controlled synthesis of magnetite nanoparticles. *Journal of the American Chemical Society*, **124**, 8204-8205.

Tamanaha, C.R., Whitman, L.J., and Colton, R.J. (2002). Hybrid macro-micro fluidics system for a chip-based biosensor. *Journal of Micromechanics and Microengineering*, **12**, N7-N17.

Tansil, N. C., and Gao, Z. (2006). Nanoparticles in biomolecular detection. *Nanotoday*, **1** (1), 28-37.

Tondra, M., Granger, M., Fuerst, R., Porter, M., Nordman, C., Taylor, J., and Akou, S. (2001). Design of integrated microfluidic device for sorting magnetic beads in biological assays. *IEEE Transactions on Magnetics*, **37**, 2621-2623.

Tondra, M., Porter, M., and Lipert, R.J. (2000). Model for detection of immobilized superparamagnetic nanosphere assay labels using giant magnetoresistive sensors. *Journal of Vacuum Science and Technology A*, **18**, 1125-1129.

Voet, D., Voet, J.G. and Pratt, C.W. (1999). *Fundamentals of Biochemistry*, John Wiley & Sons Inc,: New York.

Wang, S.X., Bae, S.-Y., Li., G., Sun, S., White, R.L., Kemp, J.T., and Webb, C.D. (2005). Towards a magnetic microarray for sensitive diagnostics. *Journal of Magnetism and Magnetic Materials*, **293**, 731-736.

Weetall, H.H. (1976). Covalent coupling methods for inorganic support materials. *Methods in Enzymology*, **44**, 134-148.

Wirix-Speetjens, R. (2000). Magnetic beads and spin-valves, a step forward in DNA analysis. Summer internship report. INESC – Microsystems and Nanotechnologies.

Wirix-Speetjens, R., and de Boeck, J. (2004). On-chip magnetic particle transport by alternating magnetic field gradients. *IEEE Transactions on Magnetics*, **40**, 1944-1946.

Wirix-Speetjens, R., Fyen, W., Xu, K., de Boeck, J., and Borghs, G. (2005). A force study of on-chip magnetic particle transport based on tapered conductors. *IEEE Transactions on Magnetics*, **41**, 4128-4133.

White, F. M. (1974). *Viscous Fluid Flow*. MacGraw-Hill,: New York, pp. 119-125.

Wood, D. K., Ni, K. K., Schmidt, D. R., and Cleland, A. N. (2005). Submicron giant magnetoresistive sensors for biological applications. *Sensors and Actuators A: Physical*, **120**, 1-6.

Yang, L., Biswas, M. E., and Chen, P. (2003). Study of binding between Protein A and Immunoglobulin G using a surface tension probe. *Biophysical Journal*, **84**, 509-522.

Yellen, B. B., Hovorka, O., and Friedman, G. (2005). Arranging matter by magnetic nanoparticle assemblers. *Proceedings of the National Academy of Sciences USA*, **102**, 8860-8864.

Yu, A.A., Savas, T.A., Taylor, G.S., Guiseppe-Elie, A., Smith, H.I., and Stellacci, F. (2005). Supramolecular nanostamping: using DNA as movable type. *Nano Letters*, **5**, 1061-1064.

Yuasa, S., Nagahama, T., Fukushima, A., Suzuki, Y., and Ando, K. (2004). Giant room-temperature magnetoresistance in single-crystal Fe/MgO/Fe magnetic tunnel junctions. *Nature Materials*, **3**, 868-871.

Zhu, H., Bilgin, M., Bangham, R., Hall, D., Casamayor, A., Bertone, P., Lan, N., Jansen, R., Bidlingmaier, S., Houfek, T., Mitchell, T., Miller, P., Dean, R. A., Gerstein, M., and Snyder, M. (2001). Global analysis of protein activities using proteome chips. *Science*, **293**, 2101-2105.

O Sopro de Vénus

E assim …
Talhei as formas que são tuas
com o suor do meu ser…
E limei as arestas do teu colo nuas
com a minha alma sem a ter…
De matizados de lágrimas e de sangue
colori o teu corpo de rosa …
E para o profundo dos teus olhos grandes
dei-te os sonhos de sempre e de agora …
Tornaste-te, sem eu saber parte de mim …

E com o Sopro de Vénus despertaste ….
e no corpo, na luz e na noite ….
um teu doce beijo …
um suspiro…
um fechar de olhos …
Tomaste-me então com a tua gentil mão …
no meu coração
um sonho sem fim …

# Appendix A. Magnetoresistive Chip Run-Sheet

## Usensor

**Responsible:** Hugo Ferreira
**Sample ID:** Usensor #

**STEP 1: Substrate Cleaning in Wet Bench**

**Substrate**
3" diameter Si wafer <100> from International Wafer Service
thickness: 356 - 406 $\mu$m
resistivity: 1.0 - 2.0 Ωcm

**Date:**
**Operator:**
**Pre-Treatment:** No
**Conditions:**
Blow dry


**Observations:**

**STEP 2: $Al_2O_3$ 500 Å Deposition in UHV2**

**Date:**
**Operator:**
**Pre-Treatment:** No
**Conditions:**
200 W/ 45 sccm Ar/ 5 mT/ 40' (~500 Å)


**Observations:**

**STEP 3: Spin-Valve Test Deposition in Nordiko 3000**

**Date:**
**Operator:**
**Pre-Treatment:** No
**Conditions:**
B.P.: $1\times10^{-7}$ Torr $T_{cryo}$ = 17 K

Spin-valve structure
Ta20Å/NiFe30Å/CoFe24Å/Cu22Å/CoFe20Å/MnIr80Å/Ta20Å

Chamber pressure before deposition: $\times10^{-}$ Torr

Deposition conditions:
95W, +1450/-300V, 33 mA, 1.5 sccm Xe, 50% rot, 80º pan

Recipe: Sv20

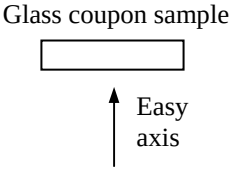


**Observations:**
Wafer and glass test sample deposited at the same time.

SV IBD #:
Test measurements between [-400, 400] Oe:
$R_{min}$ = Ω MR ~ % $R_{sq}$ = Ω ρ = μΩ.cm
$H_f$ ~ Oe $H_c$ ~ Oe $H_{ex}$ > Oe

**STEP 4: Spin-Valve Deposition in Nordiko 3000**

**Date:**
**Operator:**
**Pre-Treatment:** No
**Conditions:**
**Same as in step 3**

**Observations:**

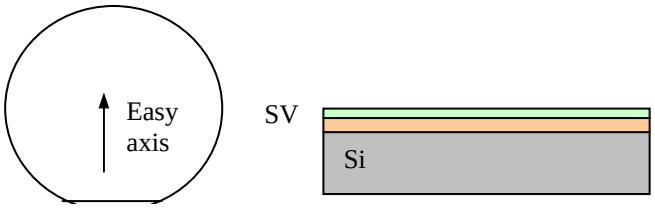


Easy axis perpendicular to the flat of the wafer.

**STEP 5: TiW($N_2$) 150 Å Deposition in Nordiko 7000**

**Date:**
**Operator:**
**Pre-Treatment:** No
**Conditions:**
Run #
Seq. 17 svpassiv
Mod3 F19 TiW_protective_layer
27" 0,5 $kW_{DC}$ 3,0 mT 50,0 sccm Ar + 10 sccm $N_2$

**Read**

**Observations:**

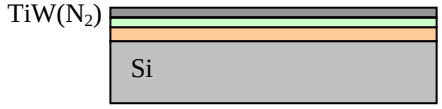


**STEP 6: Resist Coating (PR+) in SVG Tracks – sv sensors definitions**

**Date:**
**Operator:**
**Pre-Treatment:** Vapour – prime (5')
**Conditions:**
Coater 6/2 speed =3500 rpm

**Observations:** The Vapour – prime step (HDMS for 5') comprises a total time of 30'.

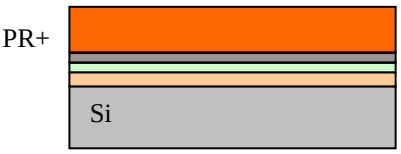


**STEP 7: Mask Exposure in DWL – sv sensors definitions**

**Date:**
**Operator:**
**Pre-Treatment:** No
**Conditions:**
Mask : usensors (inverted)
Map: hugo4.map
E: F: Power: mW
start : finish : (Total time ~ h )
Die dimensions: [X: 8000.000 Y: 8000.000]
Alignment masks usensor:

| | | |
|---|---|---|
| usensors: | X: 168.00 | Y: 173.79 |
| usensorl: | X: 168.00 | Y: 55.76 |
| usensorp: | X: 168.00 | Y: 293.00 |

**Observations:**

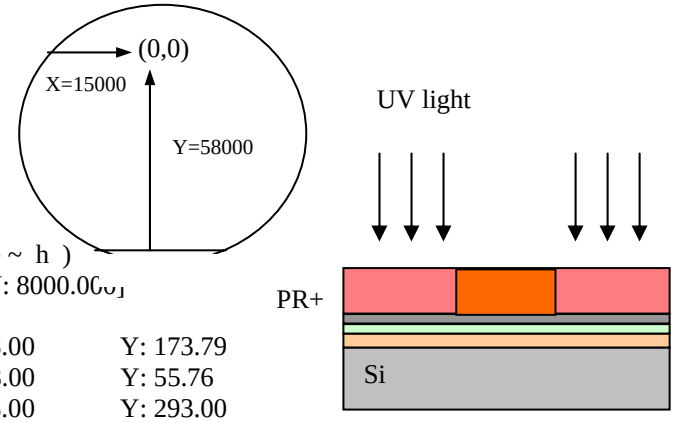

**STEP 8: Mask Development in SVG Tracks – sv sensors definitions**

**Date:**
**Operator:**
**Pre-Treatment:** No
**Conditions:**
Developer 5/2

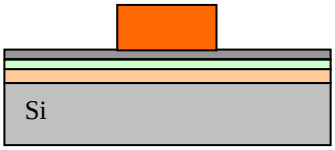


**Observations:**

**STEP 9: Spin-Valve Etch in Nordiko 3600 (IBD)**

**Date:**
**Operator:**
**Pre-Treatment:** No
**Conditions:**
B.P.:
**Batch**: junction_etch
wafer #1: etch_junction_stack: junction etch 70 degrees/ end junction

Etch rate: 0.44 Å/s
Etch time: 1100" (with slight over-etch)

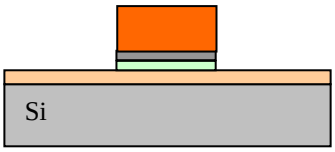


**Setpoint**
Assit Gun: 140 W +500/ -250 V 12 sccm Ar
Assist Neutraliser: 90 mA 3 sccm Ar
Etch time: 1100" ?
Target #6 (NiFeCr)

**Read**

Assist Gun: W + V/ – V + mA
– mA sccm Ar
Assist Neutraliser: mA V sccm Ar
Subst Rotn % Subs Pan º
Chamber pressure : torr
Target #6 (NiFeCr)

**Observations:**
Total thickness to etch: sv + TiW($N_2$) = 302Å + 150Å = 452Å

**STEP 10: Resist Stripping in Wet Bench – sv sensors definition**

**Date:**
**Operator:**
**Pre-Treatment:** No
**Conditions:**
Microstrip 2001 @ 80 ºC + ultrasounds


**Observations:**
The heater is set on 4 scale temperature.
Pictures for each mask!

**STEP 11: Resist Coating (PR+) in SVG tracks – sensor contacts and lines**

**Date:**
**Operator:**
**Pre-Treatment:** Vapour – prime (5')

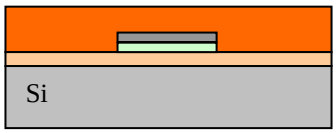


**Conditions:**
Coater 6/2 speed =3500 rpm

**Observations:**

**STEP 12: Mask Exposure in DWL – sensor contacts and lines**

**Date:**
**Operator:**
**Pre-Treatment:** Should be used pre-development
**Conditions:**
Mask : usensorl2ninv (non-inverted)
Map: hugo4.map
E: F: Power: mW
start : finish : (Total time ~ h )
Alignment masks usensor:
usensors: X: 168.00 Y: 173.79

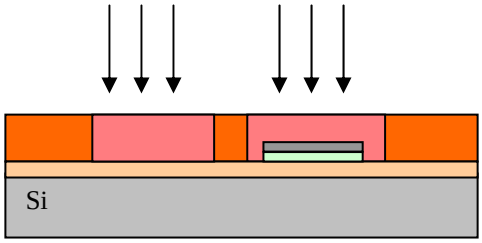


**Observations:**

**STEP 13: Mask Development in SVG tracks**

**Date:**
**Operator:**
**Pre-Treatment:** No
**Conditions:**
Developer 5/2

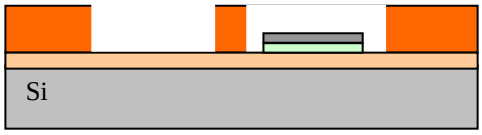


**Observations:**

**STEP 14: Al 3000 Å Deposition in Nordiko 7000**

**Date:**
**Operator:**
**Pre-Treatment:** No
**Conditions:**
B.P.: torr
Run #
Seq. 33 svpadnoetch
Mod2 F9 contetch 30" 50,0 sccm 3,0 mT RF1: 70 W RF2: 40 W
Mod4 F1 metalization 1'20" 50,0 sccm 3,0 mT DC: 2,00 kW

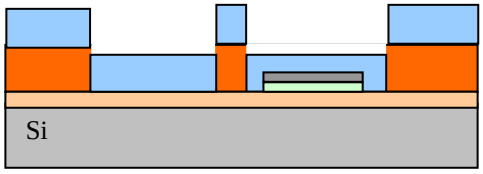


**Observations:**
Leave the exposed wafer at least one day before depositing the Al. It makes the Al lift-off easier!

**STEP 15: Al Liftoff in Wet Bench**

**Date:**
**Operator:**
**Pre-Treatment:** No
**Conditions:**
Microstrip 2001 @ 80 ºC + ultrasounds

**Observations:**
Be careful about rabbit ears!!
Pictures for each mask!

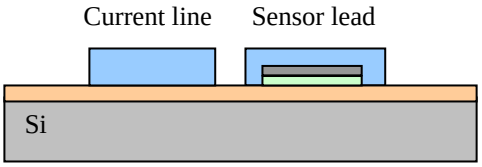


**STEP 16: Resist Coating (PR+) in SVG tracks – opening contacts**

**Date:**
**Operator:**
**Pre-Treatment:** Vapour – prime (5')
**Conditions:**
Coater 6/2 speed =3500 rpm

**Observations:**

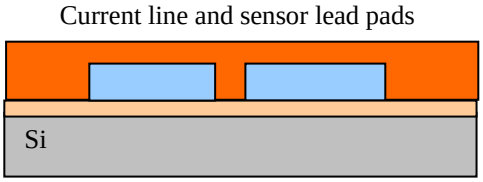


**STEP 17: Mask Exposure in DWL – opening contacts**

**Date:**
**Operator:**
**Pre-Treatment:** No
**Conditions:**
Mask : usensorp (inverted)
Map: hugo4.map
E: F: Power: mW
start : finish : (Total time ~ h )
Alignment masks usensor:
usensors: X: 168.00 Y: 173.79

**Observations:**

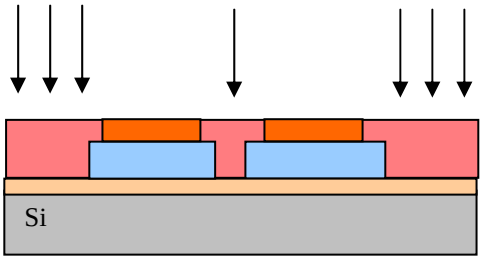


**STEP 18: Mask Development in SVG tracks – opening contacts**

**Date:**
**Operator:**
**Pre-Treatment:** No
**Conditions:**
Developer 5/2

**Observations:**

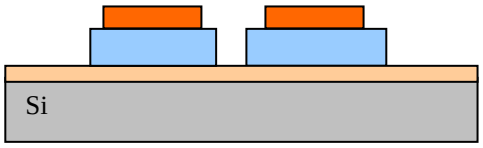


**STEP 19: $Al_2O_3$ 1000 Å Deposition in UHV2**

**Date:**
**Operator:**
**Pre-Treatment:** No
**Conditions:**
200 W/ 45 sccm Ar/ 5 mT/ 80' (~1000 Å)

**Observations:**

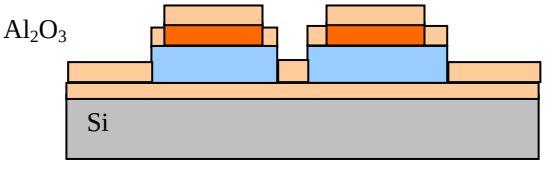

**STEP 20: $SiO_2$ 2000 Å Deposition in Alcatel SCM 450**

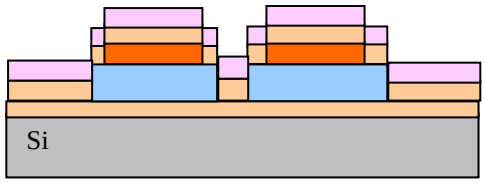


**Date:**
**Operator:**
**Pre-Treatment:** No
**Conditions:**

Deposition started @ : finished @ : ( 3 hours)
4 rpm / 2,0 mb / 140 W / 20 sccm Ar / $V_{bias}$ = V

**Observations:** Calibration with a glass piece gives a deposition rate of ~ Å/h.

**STEP 21: $Al_2O_3$ and $SiO_2$ Lift-Off**

**Date:**
**Operator:**
**Pre-Treatment:** No
**Conditions:**

Microstrip 2001 @ 80 ºC + ultrasounds

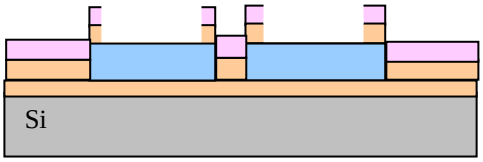


**Observations:**

The heater is set on 4 scale temperature.

**STEP 22: Wafer Dicing in Disco DAD 321**

**Date:**
**Operator:**
**Pre-Treatment:** No
**Conditions:**

Coat photoresist to protect the wafer.

Recipe #201

Work thickness = 0,33 mm
Tape thickness = 0,150 mm
Blade height = 50 µm
Speed = 20 mm/s
Kerf width = 400 µm

index
CH1 = 8,2 mm
CH2 = 8,2 mm

**Observations:**

Process Time : days

**Process Completed!**

# Appendix B. Microchannels Run-Sheet

## Waterstrider

**Responsible:** Hugo Ferreira
**Sample ID:** Waterstrider channel #

*Quartz mask*

**STEP 1: Substrate Cleaning in Wet Bench**

**Substrate**
1"×1" quartz substrate

**Date:**
**Operator:**
**Pre-Treatment:** No
**Conditions:**
Alconox + ultrasounds for at least 30 min
Blow dry

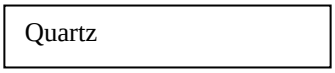


**Observations:**

**STEP 2: Al 1500 Å + TiW($N_2$) 150 Å Deposition in Nordiko 7000**

**Date:**
**Operator:**
**Pre-Treatment:** No
**Conditions:**
B.P.: torr
Run #
Seq. 33 svpadnoetch
Mod4 F1 metalization 40" 50,0 sccm 3,0 mT DC: 2,00 kW
Run #
Seq. 17 svpassiv
Mod3 F19 TiW_protective_layer
27" 0,5 $kW_{DC}$ 3,0 mT 50,0 sccm Ar + 10 sccm $N_2$

**Read**

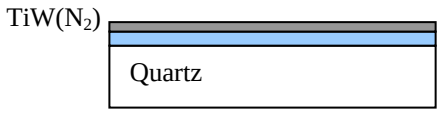


**Observations:**

**STEP 3: Resist Coating (PR+) in SVG Tracks – microchannel mask definition**

**Date:**
**Operator:**
**Pre-Treatment:** Vapour – prime (5')
**Conditions:**
Resist JSR Micro PFR 7790G-27cP
Coater 6/2 speed =3500 rpm

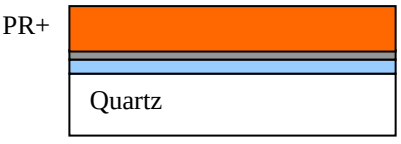


**Observations:** The Vapour – prime step (HDMS for 5') comprises a total time of 30'.

**STEP 4: Mask Exposure in DWL – microchannel mask definition**

**Date:**
**Operator:**
**Pre-Treatment:** No
**Conditions:**

Mask : wsl4 (inverted)
Map: hugo4.map
E: F: Power: mW
start : finish : (Total time ~ h )
Die dimensions: [X: 8000.000 Y: 8000.000]

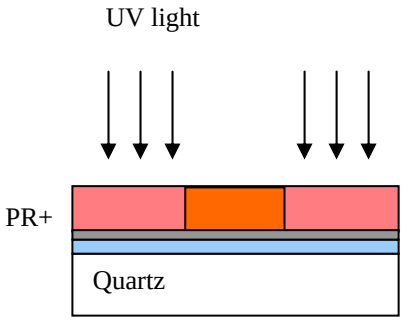


**Observations:**

**STEP 5: Mask Development in SVG Tracks – microchannel mask definition**

**Date:**
**Operator:**
**Pre-Treatment:** No
**Conditions:**

Solvent JSR Micro PTH70EG
Developer 5/2

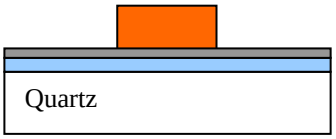


**Observations:**

**STEP 6: Al + TiW($N_2$) Etch in Nordiko 3600 (IBD)**

**Date:**
**Operator:**
**Pre-Treatment:** No
**Conditions:**

B.P.:
**Batch**: junction_etch
wafer #1: etch_junction_stack: junction etch 70 degrees/ end junction

Etch rate: 0.44 Å/s
Etch time: 3800" (with slight over-etch)

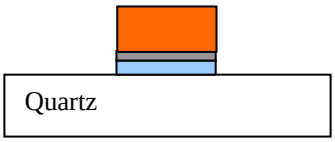


**Setpoint**

Assit Gun: 140 W +500/ -250 V 12 sccm Ar
Assist Neutraliser: 90 mA 3 sccm Ar
Etch time: 3800" ?
Target #6 (NiFeCr)

**Read**

Assist Gun: W + V/ – V + mA
– mA sccm Ar
Assist Neutraliser: mA V sccm Ar
Subst Rotn % Subs Pan º
Chamber pressure : torr
Target #6 (NiFeCr)

**Observations:**

Total thickness to etch: Al + TiW($N_2$) = 1500Å + 150Å = 1650Å

**STEP 7: Resist Stripping in Wet Bench – microchannel mask definition**

**Date:**
**Operator:**
**Pre-Treatment:** No
**Conditions:**
Microstrip 2001 @ 80 ºC + ultrasounds


**Observations:**
The heater is set on 4 scale temperature.
Pictures for each mask!

*Polymer preparation*

**STEP 1: Weighting of PDMS base and curing agent**

**Date:**
**Operator:**
**Pre-Treatment:**

**Conditions:**
PDMS, Sylgard 184, Dow Corning
1:10 base to curing agent

**Observations:**

**STEP 2: Mixing of PDMS base and curing agent**

**Date:**
**Operator:**
**Pre-Treatment:**
**Conditions:**
Mix gently to prevent incorporation of air into the mixture

**Observations:**

**STEP 3: Mixing of PDMS material**

**Date:**
**Operator:**
**Pre-Treatment:** No
**Conditions:**
Remove bubbles by leaving mixture at open air for at least an hour
Alternatively remove bubbles at primary vacuum

**Observations:**

*Mold fabrication*

**STEP 1: Substrate Cleaning in Wet Bench**

**Substrate**
6” diameter Si wafer

**Date:**
**Operator:**
**Pre-Treatment:** No
**Conditions:**
IPA + rinse with de-ionised water
Blow dry
Heat substrate in oven at 130ºC for 30’


**Observations:**

**STEP 2: Thick Resist Coating (PR+) in SVG Tracks – microchannel mold definition**

**Date:**
**Operator:**
**Pre-Treatment:** Vapour – prime (5’)
**Conditions:**
Resist Clariant AZ4562
Coater 4/4


**Observations:**
The Vapour – prime step (HDMS for 5’) comprises a total time of 30’.
The thick photoresist is dispensed manually over the Si substrate using a glass pipette.
Before backing, the photoresist is left at room-temperature for 15 min in order for the solvent to evaporate.

**STEP 3: Mask Exposure in 250 W UV Flood Lamp – microchannel mold definition**

**Date:**
**Operator:**
**Pre-Treatment:** No
**Conditions:**
Quartz mask in contact with the thick photoresist layer
2 steps of 10 s with 120 s cooling time in between

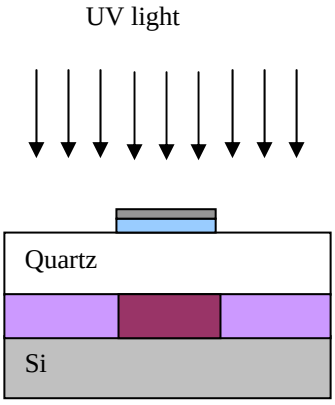


**Observations:**

**STEP 4: Mask Development in SVG tracks – microchannel mold definition**

**Date:**
**Operator:**
**Pre-Treatment:** No
**Conditions:**
Solvent Clariant AZ 351B, 1:4 dilution
Development for 7 to 8 min with agitation


**Observations:** Sample rinsed with DI and blow dried in the end.

*Microfluidic fabrication and assembly*

**STEP 1: Polymer Pouring**

**Date:**
**Operator:**
**Pre-Treatment:** No
**Conditions:**
PDMS polymer dispensed manually over the mold

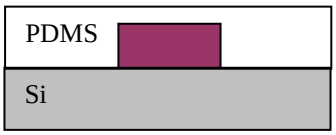


**Observations:**
Metallic or teflon pins may be placed over the thick photoresist mold at reservoir sites to leave channel connections open (see Parracho, 2002).

**STEP 2: Polymer Curing**

**Date:**
**Operator:**
**Pre-Treatment:** No
**Conditions:**
PDMS polymer cured at an oven at 65ºC for 1 hour

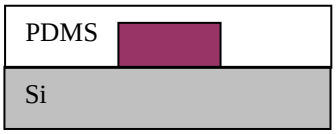


**Observations:**
The polymer also cures at room-temperature for overnight time-scales.

**STEP 3: Master removal**

**Date:**
**Operator:**
**Pre-Treatment:** No
**Conditions:**
PDMS polymer is peeled-off from the mold
PDMS layer cut to the required sized

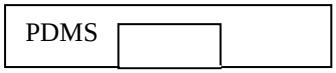


**Observations:**

**STEP 4: Assembly**

**Date:**
**Operator:**
**Pre-Treatment:** Both microchannel and magnetoresistive chip subjected to $O_2$ Plasma (PlasmaTherm)
Setpoint: 300 mTorr 25 W 25 ºC 100 sccm $O_2$ 30”

**Conditions:**
Both surfaces are put in contact as soon as possible
Pressure can be applied to promote bonding

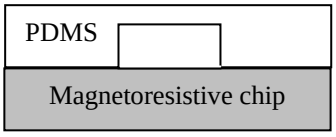


**Observations:**

**Process Time: hours**

# Appendix C. Surface Chemistry Run-Sheet

## Probe DNA immobilization

**Responsible:** Hugo Ferreira
**Sample ID:** Chip/plain surface sample #

**STEP 1: Surface Cleaning**

**Substrate**

Magnetoresistive chip passivated with 2000 Å $SiO_2$ or plain $Si/SiO_2$ 2000 Å sample.

**Date:**
**Operator:**
**Pre-Treatment:** No
**Conditions:**

Wash with acetone + IPA and rinse with $dH_2O$
Blow dry

Available functional groups

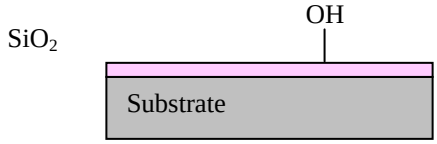


**Observations:**

Alternatively, a photoresist solvent (Microstrip 2001 photoresist stripper, Fujifilm) at 80ºC can be used instead of acetone.

**STEP 2: Activation**

**Date:**
**Operator:**
**Pre-Treatment:** No
**Conditions:**

Treat chip with cholic acid 2% (w/v) for overnight times at room-temperature
Wash extensively with $dH_2O$

Available functional groups

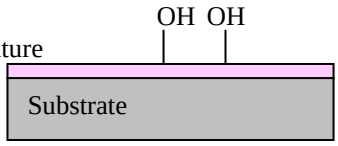


**Observations:**

Optional. This step may be necessary if there are not enough hydroxyl groups at the silicon dioxide surface. Most frequently this step is not required.

**STEP 3: Silanization**

**Date:**
**Operator:**
**Pre-Treatment:** No
**Conditions:**

Treat chip with APTES 15%(v/v) aqueous solution for 30 min at RT
Wash extensively with $dH_2O$

Available functional groups

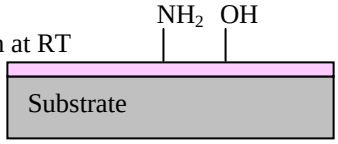


**Observations:** Other protocols can be used (see chapter 3).

**STEP 4: Cross-Linking**

**Date:**
**Operator:**
**Pre-Treatment:** No
**Conditions:**

Treat chip with a solution of 0.7 mg/ml sulfo-EMCS in 100 mM borate buffer, pH of 8.5, containing 150 mM NaCl, for 2 hours. at RT
Wash with same borate buffer and with 100 mM phosphate buffer, pH of 7.0, containing 150 mM NaCl.

Available functional groups

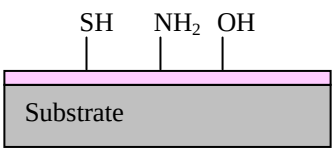


**Observations:**

**STEP 5: DNA Probe Immobilization**

**Date:**
**Operator:**
**Pre-Treatment:** No
**Conditions:**

Treat chip with a solution 3'-end thiolated single-stranded DNA probes as 3 µM solution in the same phosphate buffer, for 3 hours at RT.
Wash with 100 mM phosphate buffer, pH of 7.0, containing 1 M NaCl.
Wash again with previous phosphate buffer.

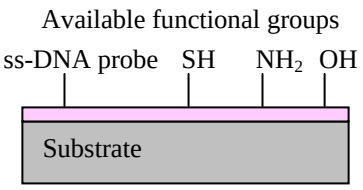


**Observations:**

The higher salt concentration buffer was used to remove unbound DNA probes.

**STEP 6: Pre-Hybridization**

**Date:**
**Operator:**
**Pre-Treatment:** No
**Conditions:**

Treat chip with a 2.0% (w/v) BSA solution in same phosphate buffer for 2 hours at room-temperature.
Wash with previous phosphate buffer.
Leave chip with phosphate buffer for subsequent hybridization experiments.

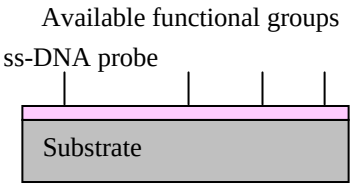


**Observations:**

Bovine serum albumin proteins block the unreacted functional groups at the chip surface, which are native to the surface OH or were left from previous surface treatments ($NH_2$ and SH groups). The blocking prevents or reduces unspecific binding during the assays.

**Process Time: hours**

# Appendix D. Magnetic Labeling Run-Sheet

## Target PCR products

**Responsible:** Hugo Ferreira
**Sample ID:** Sample #

**STEP 1: Biotinylation**

**Date:**
**Operator:**
**Pre-Treatment:** No
**Conditions:**

Use 3'-end biotinylation kit (Pierce) to biotinylate target PCR products at the 3'-end.

**Observations:**

**STEP 2: Magnetic Label Washing**

**Date:**
**Operator:**
**Pre-Treatment:** No
**Conditions:**

Wash streptavidin-coated magnetic particles from stock solution in 100 mM phosphate buffer, pH of 7, at least 3 times.

Each wash comprises precipitation of particles with a permanent magnet, removal of the supernatant, addition of phosphate buffer solution, and elution by vortexing.

In the final wash leave particles in the same phosphate buffer.

**Observations:**

The washing and the final volume of magnetic label solution is adjusted according to the desired particle concentration or dilution.

**STEP 3: Magnetic Labeling of Targets**

**Date:**
**Operator:**
**Pre-Treatment:** No
**Conditions:**

Incubate biotinylated target solution with streptavidin-coated magnetic particles in phosphate buffer for 3 hours with gentle mixing.

Target and magnetic label concentrations are chosen such that the target to streptavidin ratio is 1:1, although different ratios can be used.

The magnetically labeled target solution is then centrifuged at 10,000 rpm and the supernatant is removed.

The pellet is then re-suspended in the same phosphate buffer.

The process is repeated 2 more times.

The final re-suspension is done in the hybridization buffer.

**Observations:**

Pay attention to the validity of the magnetic particle solution as if it is out-of date the labeling may be compromised.

**STEP 4: Preparation for Hybridization**

**Date:**
**Operator:**
**Pre-Treatment:** No
**Conditions:**

Prior to incubation with DNA probe functionalized chips the magnetically labeled double-stranded target DNA samples are denatured at 95ºC for 5 min and cooled immediately on ice. This produces single-stranded target molecules

**Observations:**

In the case that single-stranded DNA targets (like synthesized oligos) this step is not required.

**Process Time: hours**

# Appendix E. Magnetic Label Detection Procedure

## Usensor

**Responsible:** Hugo Ferreira
**Sample ID:** Sample #
**Date:**

This protocol can be used to measure, in almost real-time, the response of an array of sensors from the U-chip layout. The latest required or suggested instrumentation is depicted in the figures E1 and E2 below (connections between instruments are schematically shown in fig. 6.7 of this thesis).

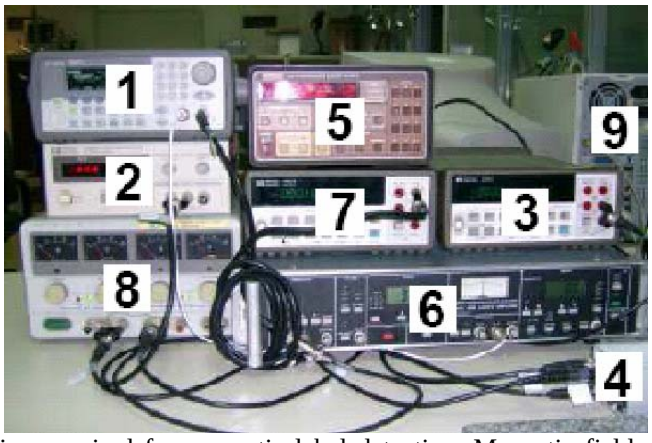


Fig. E1. Instrumentation required for magnetic label detection. Magnetic field excitation: 1, function generator (HP 3220A); 2, dc power source (HP E3612A DC); 3, amperometer (HP 34401A); and 4, Current control box (custom-made). Sensor power supply and readout: 5, dc power source (Keithley 220); 6, lock-in amplifier (EG&G Princeton Applied Research 5209); and 7, voltmeter (HP 34401A). Multiplexing power supply: 8, dc voltage supply (GW GPC-3020 DC). Control and data acquisition: 9, PC with Agilent GPIB card and NI DAQ PCI6024E. An additional function generator (PM 5132) is also used as a power supply for current lines. Also, BNC and GPIB cables are required for connections between instruments and control boards.

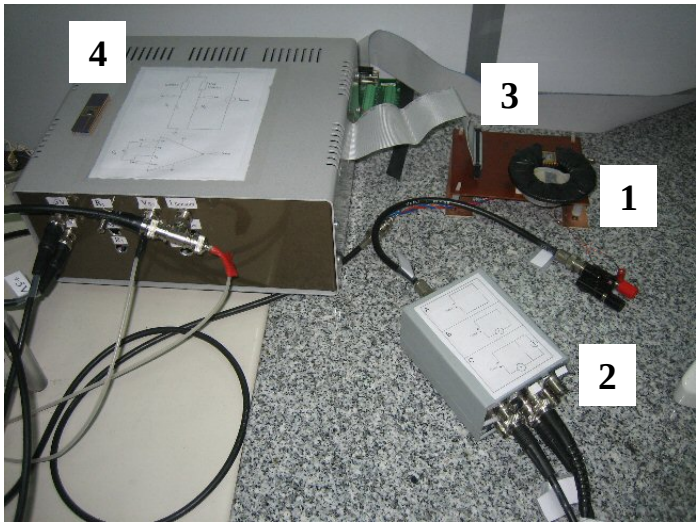


Fig. E2. Custom instrumentation required for magnetic label detection: 1, horse-shoe electromagnet; 2, electromagnet current control box; 2, chip interface; and 4, multiplexing control board.

The connections between usensor chips, the analog multiplexer (Maxim DG406DJ 16-Channel integrated circuit) and the data acquisition board NI DAQ PCI6024E, are on the other hand shown in fig. E3.

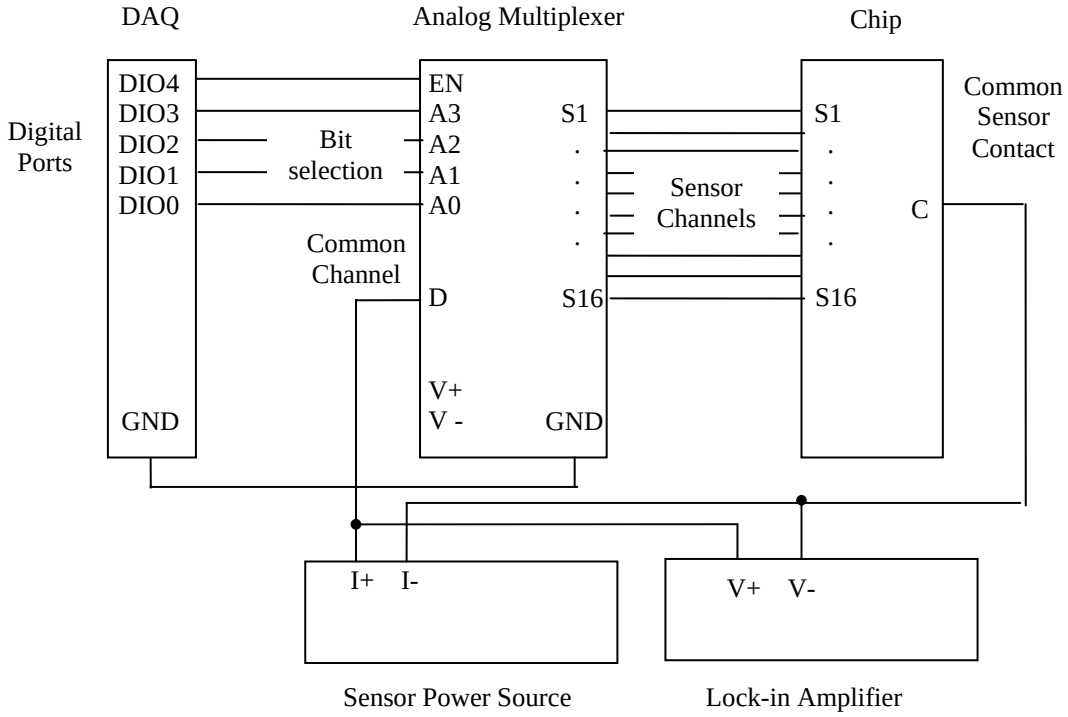


Fig. E3. Connections between chip, analog multiplexer and switching board.

Finally, a LabView program (**biomeas_1.vi**) is used for sensor switching, through a DAQ board and a custom-designed print-circuit board (**biomeas_1**), and for data acquisition through the GPIB-controlled multimeters and lock-in amplifier.

## Instrument Setup

**STEP 1:** Set all the instruments on.

**STEP 2:** Set sense current to 1 mA.

**STEP 3:** Set electromagnet to create in-plane excitation fields in the spin valves sensing directions

- Ac excitation frequency of 31 Hz and amplitude 13.5 Oe rms (123 mA rms)
- Dc bias field of 24 Oe (240 mA) or other such that the transfer curve of the transducer is entering the saturated minimum resistance (see section 2.1.6 of this thesis)

**STEP 4:** Set lock-in amplifier to measure sensor response

- Measuring frequency of 31 Hz (TTL signal fed by the function generator)
- Time constant of 300 ms (or frequency bandwidth of 1/300 ms ~ 0.83 Hz)

**STEP 5:** Set magnetic label focusing parameter

- Ac current of frequency of 0.2 Hz and amplitude of 25 to 40 mA rms
- Ac focusing works in combination with the dc bias field above

## Experiments

**STEP 1:** Start acquisition without focusing and with buffer solution

**STEP 2:** Leave sensors acquiring for 5 to 10 min (1 or 2 cycles of measurements for each sensor) to get a baseline

**STEP 3:** Remove buffer solution from chip (leave a thin film of buffer on)

**STEP 4:** Add small volumes from 5 to 20 µL of sample solutions

- Before hand is recommended to vortex the magnetic label solution
- After adding is recommend to mix the sample solution with remaining thin film of buffer

**STEP 5:** Focus labels for 5 to 20 min

**STEP 6:** Measure all sensors at least 1 cycle after focusing and before washing to get saturation signals

**STEP 7:** Wash chip thoroughly (recommended 5 min)

**STEP 8:** Measure all sensors at least 1 cycle after washing to get binding signals

**Total hybridization time:** 10 to 30 min

- 5 to 20 min focus + 5 to 10 min saturation signal measurement

**Total experiment time:** 25 to 55 min

- 5 to 10 min baseline + hybridization time + 5 min wash + 5 to 10 min binding signal measurement

# Curriculum Vitae

**Hugo Alexandre Teixeira Duarte Ferreira**

June 2006

**Contents**

## 1. Synopsis

I see myself as a curious and multidisciplinary person, with a huge will to learn and to teach, and with a particular liking for challenges. Since I know myself, I have always felt fascinated by science and technology with its broader range of knowledge. Naturally, I ended up finishing a degree in 2002 on Physics Engineering in Instituto Superior Técnico (IST), Technical University of Lisbon. In addition, I am presently finishing my doctoral studies in Physics Engineering in the same institution.

I have always liked Physics and Life Science in a special way. As such, during my degree and doctoral studies I set my learning path in order to combine a major in Physics and Engineering with Biology and Biomedicine. Fortunately, I had the opportunity to develop my senior student project and my graduated studies in a fantastic field that encompasses several sciences altogether: Nanotechnologies.

My work, for a couple of years now, consisted in the development of DNA and protein chips for the detection of genetic diseases and pathogenic microorganisms. This work was done at INESC – Microsystems and Nanotechnologies in collaboration with the Bioengineering Research Group of the Centre for Biological and Chemical Engineering of IST and the Chemistry and Biochemistry Department of the Faculty of Sciences, University of Lisbon, as well as other scientific institutions in the scope of national and European projects.

The developed biosystems were based on the use of magnetoresistive sensors for the biomolecular recognition, whereas traditionally these transducers are used in the read-heads of hard-disk drives. This work further introduced a worldwide novelty: the combination of on-chip manipulation of magnetically labeled biomolecules with the sensing of biomolecular interactions. Consequently, a patent was submitted, and book chapters and more than a dozen of papers in scientific journals have been published. The work was also presented in a dozen of international scientific conferences by myself, and at least as many times by other co-authors. The quality of my work has been recognized both nationally and internationally, which resulted in the attribution of a number of prizes and honors.

My interest in science and technology also finds place in the teaching of Physics to several courses at IST. This is something I particular enjoy: contacting with students, to witnessing their evolution and learning with and through them.

More recently, and in parallel to a deeper dedication in Nanomedicine and Nanobiotechnology fields (which encompasses editorial activity in a scientific journal), I have been investing in Entrepreneurship and in Management and Economic Valorization of Science and Technology. In particular, the entrepreneurial project MagBiosense, based on my PhD work, has gathered quite favorable opinions from a diverse group of scientists, business and financing people.

In conclusion, my goal for the future is to pursuit the activities of management of research and development and the creation of value from scientific knowledge. In other words my wish is to foster innovation and to contribute to the well fare of the world.

## 2. Personal

**Full Name:** Hugo Alexandre Teixeira Duarte Ferreira
**Place of Birth:** Carnaxide – Oeiras
**Date of Birth:** 15 June 1978
**Nationality:** Portuguese
**Civil Status:** Married
**Offspring:** 1 Son
**Address:** Av. Carolina Michaëllis, nº28 2º D.to
2795-049 Linda-a-Velha
**Mobile phone:** 967387923/ 916062816
**E-mail:** hferreira@inesc-mn.pt / hatdferreira@gmail.com

## 3. Academic Education

**2002 – Present: Doctoral studies in Physics Engineering** at Instituto Superior Técnico (IST) and at Instituto de Engenharia de Sistemas e Computadores para os Micro-sistemas e as Nanotecnologias (INESC-MN).

**2001: Licenciatura em Engenharia Física Tecnológica** (5 year degree course on Technological Physics Engineering) at Instituto Superior Técnico, Universidade Técnica de Lisboa. Grade 17/20.

**1996:** High School at Escola Secundária de Linda-a-Velha. Grade 19/20.

## 4. Complementary Education

**2005:** Course on Entrepreneruship and Management of Innovation: **"Programa Avançado em Empreendedorismo e Gestão da Inovação"** (PAEGI) 2nd Edition, organized by the Faculdade de Ciências Económicas e Empresariais da Universidade Católica Portuguesa, Lisboa, 11 March – 14 July 2005.

**2005:** Course on **"Genética, Genoma e Genómica, da Clínica à Saúde Pública"**, organized by the Escola Nacional de Saúde Pública da Universidade Nova de Lisboa and by the Sociedade Portuguesa de Genética Humana, Lisboa, 17 – 19 February 2005.

**2004:** Course **"VECTOR$^{E}$ – Valorização Económica de Ciência e Tecnologia: Organização e Planeamento de Negócios para Novas Empresas"**, organized by Programa Green-Wheel, Centro de Estudos em Inovação, Tecnologia e Políticas de Desenvolvimento (IN+), Instituto Superior Técnico, Lisboa, 28 September – 14 December 2004.

**2004:** Workshop on **"Criação de Empresas com Base Tecnológica – Uma Abordagem Sistémica ao Plano de Negócios"**, organized by the Board of European Students of Technology (BEST) – Lisboa, Lisboa, 2 June 2004. Course lectured by Prof. Pedro Mendes do Departamento de Engenharia e Gestão do Instituto Superior Técnico.

**2004: "Workshop for Early Career Researchers"**, organized by Science Next Wave, Marie Curie Fellowship Association, Mobisc and ABIC, 28 February 2004.

**2003: "5th short course of the Portuguese Biophysical Society: Genomics and Proteomics – Biophysical Perspectives"**, organized by the Sociedade Portuguesa de Biofísica, Santarém, 17 – 19 October 2003.

**2003: "2º Encontro de Engenharia Biomédica"**, organized by the Instituto Superior Técnico and by the Faculdade de Medicina da Universidade de Lisboa, Lisboa, 1 October 2003.

**2002: "1º Encontro de Engenharia Biomédica"**, organized by the Instituto Superior Técnico and by the Faculdade de Medicina da Universidade de Lisboa, Lisboa, 30 October 2002.

**2002: "The MWG International Microarray Workshop"**, organized by MWG Genomic Diagnosis, Ebersberg, Germany, 24 September 2002.

**2002: "International School on Quantum Computation and Information"**, organized by the Instituto Superior Técnico, 2 – 7 September 2002.

**2001: Basic and Middle courses on IDL 5.4**, lectured by Estudio Atlas, S.L., Instituto Superior Técnico, Lisboa, 16 – 19 March 2001.

**2000:** Course on **"Astrometria com câmaras CCD – uma breve introdução"**, organized CENTRA, Instituto Superior Técnico, Lisboa, 17 – 20 October 2000. Course lectured by Dr. André Moitinho.

**2000:** BEST – Copenhagen Summer Course 2000: **"Microsystems and Nanotechnology"**, lectured by Mikroelecktronik Centret (MIC), Technical University of Denmark, Lyngby, Denmark, 6 – 19 August 2000. Learning projects: **"Investigation of Nanoparticles by Atomic Force Microscopy"**, supervised by Prof. Karsten Walzer, and **"Carbon Nanotubes as Molecular Wires"**, supervised by Prof. Niels Asger Mortensen.

**2000: Summer internship at Grupo de Tecnologia de Estado Sólido**, at INESC, Lisboa, August-September 2000. Learning project: study and development of a microchip for transport and detection of magnetic nanoparticles.

**1999: Summer internship at Grupo de Tecnologia de Estado Sólido**, at INESC, Lisboa, August-September 1999. Learning project: study and development of a thermocouple-based microchip for application in water heating devices.

**1999:** Workshop on **"Aplicações da Física em Instrumentação Médica e Biomedicina"**, organized by the Faculdade de Ciências e Tecnologia da Universidade Nova de Lisboa, Monte da Caparica, April 1999.

**1999:** Course on **"Introdução à Astronomia e à Astrofísica"**, organized by Fundação da Faculdade de Ciências de Lisboa, Lisboa, October 1998 – January 1999. Lectured by Dr. Miguel Moreira.

## 5. Honors and Awards

**2006:** 1st Prize in the **Concurso Bioempreendedor 2005**. Iniciative of the Associação Portuguesa de BioIndústrias, of ICEP Portugal (Instituto das Empresas para os Mercados Externos) and Infarmed.

**2005:** Finalist in the **Concurso Nacional de Inovação BES**. Project "**MagBiosense**" placed between the 5 best projects in the Healthcare sector. Iniciative of the Banco Espírito Santo, Fundação Ilídio Pinho and Siemens Portugal.

**2005:** Student travel award at the **"The 50th Magnetism and Magnetic Materials Conference"**, San Jose, California, U.S.A, 30 October – 3 November 2005.

**2005:** Finalist in the **Concurso Nacional de Empreendedorismo 2005**. Project **"MagBiosense"** within the top 5 Ideas and top 5 Business Plans. Iniciative of the Caixa Geral de Depósitos and Universidade Nova de Lisboa.

**2005:** 1st Prize in the **Concurso de Ideias do Programa Avançado em Empreendedorismo e Gestão da Inovação (PAEGI)** of the Faculdade de Ciências Económicas e Empresariais of the Universidade Católica Portuguesa.

**2005:** Student travel award at the **"The IEEE 2005 International Magnetics Conference"**, Nagoya, Japan, 4 - 8 April 2005.

**2005:** Technology round of the **Berkeley Nano-Opportunity Challenge 2005** – business ideas for the nano generation. Iniciative of the Berkeley Nanotechnology Club.

**2004:** 3rd Prize in the **Great Lakes Entrepreneurs Quest** 2004 Fall Edition in the category of New Business Idea at the Nort/West Michigan region.

**2004:** 1st Prize at the Business Plan competition in the entrepreneurship course **VECTOR$^{E}$ – Valorização Económica de Ciência e Tecnologia: Organização e Planeamento de Negócios para Novas Empresas**, 2004 edition. Iniciative of the Green-Wheel program, Centro de Estudos em Inovação, Tecnologia e Políticas de Desenvolvimento, IN+, Instituto Superior Técnico.

**2003: Prémio 3M à Inovação 2003 – Área das Ciências da Vida**, given by 3M Portugal and Universidade Técnica de Lisboa.

**2003: Programa Gulbenkian de Estímulo à Investigação 2003 – Área das Nanotecnologias**, given by Fundação Calouste Gulbenkian.

**2003:** Best poster prize **"A biochip based on the magnetoresistive effect: Detection of hybridisation of cystic fibrosis related oligonucleotide sequences"** at the **"Bioeng'2003 – 7th Portuguese Conference on Biomedical Engineering"**, given by Instituto de Biofísica e Engenharia Biomédica, Sociedade Portuguesa de Engenharia Biomédica and Faculdade de Ciências da Universidade de Lisboa.

**2002: Prémio Professor Luís Vidigal 2000/2001**, given by the Departamento de Engenharia Electrotécnica e de Computadores of Instituto Superior Técnico, the

Departamento de Engenharia Informática of IST and Instituto de Engenharia de Sistemas e Computadores.

**2002: Bolsa e Diploma de Mérito** 2000/2001, given by the Universidade Técnica de Lisboa.

## 6. Research

Doctoral Thesis: **"Magnetoresistive biochips: Detection of biomolecular recognition and on-chip transport of magnetically labeled biomolecules"**. Supervisor: Prof. Paulo Freitas; Co-Supervisor: Prof. Joaquim Sampaio Cabral.

Development of biochips and biosensors for the **diagnostics of genetic diseases**.

Development of biochips and biosensors for the **detection of pathogenic microorganisms**.

### 6.1 Research projects

European project NMP4-CT-2005-016833: **"Development of a complete integrated SNP analysis system"**.

National project POSC/EEA-ESE/58523/2004: **"Magnetoresistive Biochip Microarray Platform for Biomolecular Recognition"**.

European project QLK3-CT-2001-01982: **"Novel genechip technology for simplified detection of molecularly heterogeneous genetic diseases: Detection of cystic fibrosis as a model"**.

National project POCTI/BIO/34459/99: **"Detection of Biomolecular Recognition in Nanometer Sized Volumes using Magnetoresistive Sensor Arrays"**.

### 6.2 Management of research

**Preparation and writing of research projects**

**Preparation** and **writing** of **Intellectual Property Patent** documents and international submission of patent.

**Scientific support** given to undergraduate and graduate students within the scope of senior student works and research project.

### 6.3 Research scholarships

Research scholarship **INESC – Microsistemas e Nanotecnologias** (January - June 2006).

PhD scholarship **Fundação para a Ciência e Tecnologia** SFRH/ BD/ 5031/ 2001 (January 2002 - December 2005).

Scholarship **EU Access to Research Infrastructures Scheme** (RIMDAC). Scope: internship in National Microelectronics Research Centre (NMRC), Ireland (6 - 18 December 2002).

**Professional internship POCTI** in the Solid State Technology Group of INESC (March - September 2001)

**Summer internship** in the Solid State Technology Group of INESC (August - September 2000).

**Summer internship** in the Solid State Technology Group of INESC (August - September 1999).

## 7. Entrepreneurial Activity

**2006:** Founder, President and Chief-Executive Officer of **Haloris – Nanotechnologies**, a company whose focus is the development of **biosensors for the agribusiness and healthcare sectors**. It also offers services in surface chemistry, assay development and consulting on nano and biotechnologies.

**2004 – 2006:** Development of the entrepreneurial project **MagBiosense**: **development, fabrication and commercialization** of biochips and bio-sensors for **diagnostics of genetic diseases** and **detection of pathogenic microorganisms**.

## 8. Teaching

**2000 – 2003: Teaching assistant of the Physics Department of the Instituto Superior Técnico**

Física I of the Licenciatura em Engenharia Electrotécnica e de Computadores (LEEC) in the 2nd Semester of 2002/2003.

Física II of the Licenciatura em Engenharia Informática e de Computadores (LEIC – TagusPark) in the 1st Semester of 2002/2003.

Física I of the LEEC in the 2nd Semester of 2001/2002.

Física II of the Licenciatura em Engenharia Civil (LEC) and of the Licenciatura em Engenharia do Território (LET) in the 1st Semester of 2001/2002.

Física I of the LEEC in the 2nd Semester of 2000/2001.

Física Experimental of the LEIC – TagusPark, in the 1st Semestre of 2000/2001

## 9. Publications

### 9.1 Patents

**2005: "A bio-electronic device"**, D. L. Graham, H. A. Ferreira, N. Feliciano, P. P. Freitas, P. Galvin, **PCT/IB2005/052702**, 16 August 2005.

**2004: "A bio-electronic device"**, D. L. Graham, H. A. Ferreira, N. Feliciano, P. P. Freitas, P. Galvin, **IE 2004/0559**, 20 August 2004.

### 9.2 Book chapters

**In press: "Spintronic biochips for biomolecular recognition"**, P. P. Freitas, H. A. Ferreira, in The Handbook of Magnetism and Magnetic Materials, Volume 5, H. Kronmüller and S. Parkin, Eds., John Wiley and Sons, New York.

**2006: "Nanostructures for spin electronics"**, P. P. Freitas, H. A. Ferreira, R. Ferreira, S. Cardoso, S. van Dijken, J. Gregg, in Advanced Magnetic Nanostructures, Chapter 14, D. Sellmyer and R. Skomski, Eds., Springer, Berlin, 2006.

**2004: "Magnetoresistive DNA chips"**, P. P. Freitas, H. A. Ferreira, D. L. Graham, L. A. Clarke, M. D. Amaral, V. Martins, L. Fonseca, J. M. S. Cabral, in Magnetoelectronics, Chapter 7, M. Johnson, Ed., Academic Press, New York, December 2004.

### 9.3 Papers in peer-reviewed scientific journals

**Submitted: "A magnetoresistive biochip for microbial analysis of water samples"**, V. C. B. Martins, L. P. Fonseca, H. A. Ferreira, F. A. Cardoso, J. Loureiro, J. Germano, L. Sousa, M. S. Piedade, B. A. Costa, J. M. Lemos, P. P. Freitas, and J. M. S. Cabral, Journal of the Association for Laboratory Automation.

**Submitted: "A new hand held microsystem architecture for biological analysis"**, M. Piedade, L. Sousa, T. M. Almeida, J. Germano, B. A. Costa, J. M. Lemos, P. P. Freitas, H. A. Ferreira, F. A. Cardoso, D. Vidal, IEEE Transactions on Circuits and Systems.

**2006: "Diode/magnetic tunnel junction cell for fully scalable matrix based"**, F. A. Cardoso, H. A. Ferreira, J. P. Conde, V. Chu, P. P. Freitas, D. Vidal, J. Germano, L. Sousa, M. S. Piedade, B. Andrade, J. M. Lemos, J. Appl. Phys. **99**, 08B307.

**2006: "Magnetoresistive DNA-chips based on ac field focusing of magnetic labels"**, H. A. Ferreira, F. A. Cardoso, R. Ferreira, S. Cardoso, P. P. Freitas, J. Appl. Phys. **99**, 08P105. Selected for the Virtual Journal of Nanoscale Science and Technology, AIP, 1st May 2006 issue.

**2005: "Detection of cystic fibrosis related DNA targets using AC field focusing of magnetic labels and spin-valve sensors"**, H. A. Ferreira, D. L. Graham, N. Feliciano, L. A. Clarke, M. D. Amaral, P. P. Freitas, IEEE Trans. Magn. **41** (10), 4140-4142, October 2005.

**2005: "Magnetic Biosensors for genetic screening of cystic fibrosis"**, L. Lagae, R. Wirix-Speetjens, C.-X. Liu, W. Laureyn, J. De Boeck, G. Borghs, S. Harvey, P. Galvin, D. L. Graham, H. A. Ferreira, P. P. Freitas, L. A. Clarke, M. D. Amaral, IEE Proceedings on Circuits, Devices and Systems, **152**, 393-400, August 2005.

**2005: "Rapid DNA hybridisation based on AC field focusing of magnetically-labeled target DNA"**, H. A. Ferreira, N. Feliciano, D. L. Graham, L. A. Clarke, M. D. Amaral, P. P. Freitas, Appl. Phys. Lett. **87**, 013901, July 2005. Selected for the Virtual Journal of Nanoscale Science and Technology, AIP, 11th July 2005 issue and for the Virtual Journal of Biological Physics Research, AIP, July 1st 2005 issue.

**2005: "Magnetic field assisted hybridisation and simultaneous detection using micron-sized spin-valve sensors and magnetic nanoparticles**", D. L. Graham, H. A. Ferreira, N. Feliciano, P. P. Freitas, L. A. Clarke, M. D. Amaral, Sensors and Actuators B: Chemical **107**, 936-944, June 2005.

**2005: "Effect of spin-valve sensor magnetostatic fields on nanobead detection for biochip applications"**, H. A. Ferreira, N. Feliciano, D. L. Graham, P. P. Freitas, Journal of Applied Physics **97** (10), 10Q904, May 2005. Selected for the Virtual Journal of Nanoscale Science and Technology, AIP, May 30th 2005 issue and for the Virtual Journal of Biological Physics Research, AIP, June 1st 2005 issue.

**2005: "Magnetic micro-bead detection using the planar Hall effect"**, L. Ejsing, M. F. Hansen, A. K. Menon, H. A. Ferreira, D. L. Graham, P. P. Freitas, Journal of Magnetism and Magnetic Materials, vol. **293** (1), 677-684, May 2005.

**2004: "Magnetoresistive-based biosensors and biochips: a review"**, D. L. Graham, H. A. Ferreira, P. P. Freitas, Trends in Biotechnology, vol. **22** (9), 455-462, September 2004. **Magazine cover**.

**2004: "Flow velocity measurement in microchannels using magnetoresistive chips"**, H. A. Ferreira, D. L. Graham, P. Parracho, V. Soares, P. P. Freitas, IEEE Trans. Magn., vol. **40** (4), 2652-2654, July 2004.

**2004: "Planar Hall effect sensor for magnetic micro- and nanobead detection"**, L. Ejsing, M. F. Hansen, A. K. Menon, H. A. Ferreira, D. L. Graham, P. P. Freitas, Appl. Phys. Lett., vol. **84** (23), 4729-4731, June 2004. Selected for the Virtual Journal of Nanoscale Science & Technology, AIP, May 31st 2004 issue.

**2003: "Bio-detection using magnetically labeled biomolecules and arrays of spin valve sensors"**, H. A. Ferreira, D. L. Graham, P. P. Freitas, J. M. S. Cabral, J. Appl. Phys., vol. **93** (10), 7281-7286, May 2003. **Invited paper**. Selected for the Virtual Journal of Nanoscale Science and Technology, AIP, May 26th 2003 issue and for the Virtual Journal of Biological Physics Research, AIP, May 15th 2003 issue.

**2003: "High Sensitivity detection of molecular recognition using magnetically labeled biomolecules and magnetoresistive sensors"**, D. L. Graham, H. A. Ferreira, P. P. Freitas, J. M .S. Cabral, Biosensors and Bioelectronics, vol. **18** (4), 483-488, February 2003.

**2002: "Single magnetic microsphere placement and detection on chip using current line designs with integrated spin valve sensors: biotechnological applications"**, D. L. Graham, H. Ferreira, J. Bernardo, P. P. Freitas, J. M. S. Cabral, J. Appl. Phys., vol. **91** (10), 7786-7788, May 2002. Selected for the Virtual Journal of Biological Physics Research, AIP, May 15th 2002 issue.

**2002*:* "On chip manipulation and magnetization assessment of magnetic bead ensembles by integrated spin valve sensors"**, L. Lagae, R. Wirix-Speetjens, J. Das, D. Graham, H. Ferreira, P. P. Freitas, G. Borghs, J. De Boeck, J. Appl. Phys., vol. **91** (10), 7445-7447, May 2002. Selected for the Virtual Journal of Biological Physics Research, AIP, May 15th 2002 issue.

9.4 Papers in proceedings of international scientific conferences

**Submitted: "Magnetoresistive biosensor modelling for biomolecular recognition"**, T. M. Almeida, M. S. Piedade, P. C. Lopes, L. Sousa, J. Germano, F. Cardoso, H. A. Ferreira, and P. P. Freitas, Proceedings of the *XVIIIth International Measurement Confederation World Congress* (IMEKO 2006), Rio de Janeiro, Brazil, 17 – 22 September 2006.

**Submitted: "Microsystem for biological analysis based on magnetoresistive sensing"**, J. Germano, M. S. Piedade, L. Sousa, T. M. Almeida, P. Lopes, F. A. Cardoso, H. A. Ferreira, and P. P. Freitas, Proceedings of the *XVIIIth International Measurement Confederation World Congress* (IMEKO 2006), Rio de Janeiro ,Brazil, 17 – 22 September 2006.

**2006: "Characterisation and modelling of a magnetic biosensor"**, T. M. Almeida, M. S. Piedade, F. Cardoso, H. A. Ferreira, and P. P. Freitas, Proceedings of the *2006 IEEE Instrumentation and Measurement Technology Conference* (IMTC 2006), Sorento, Italy, 24 – 27 April 2006.

**2005: "Architecture of a portable system based on a biochip for DNA recognition"**, M. Piedade, L. Sousa, J. Germano, J. Lemos, B. Costa, P. Freitas, H. Ferreira, F. Cardoso, D. Vidal, Proceedings of the *XXth Conference on Design of Circuits and Integrated Systems* (DCIS 2005), Lisboa, Portugal, 23 – 25 November 2005.

**2005: "Use of magnetoresistive biochips for monitoring of pathogenic microorganisms in water through bioprobes: oligonucleotides and antibodies"**, V. C. B. Martins, L. P. Fonseca, H. A. Ferreira, D. L. Graham, P. P. Freitas, J. M. S. Cabral, Technical Proceedings of the *2005 NSTI Nanotechnology Conference and Trade Show*, Volume 1, Chapter 8: Bio Micro Sensors, 493-496, Anaheim, California, U.S.A., 8 - 12 May 2005.

**2003: "Flow velocity measurement in microchannels using spin valve sensors and superparamagnetic particles"**, H. A. Ferreira, D. L. Graham, P. Parracho, V. Soares, P. P. Freitas, Proceedings of *The 17th European Conference on Solid-State Transducers*, 1099-1102, Guimarães, Portugal, 21 - 24 September 2003.

9.5 Papers in non peer-reviewed scientific journals

**2006: "Nanotechnology and the detection of biomolecular recognition using magnetoresistive transducers"**, P. P. Freitas, H. A. Ferreira, F. Cardoso, S. Cardoso, R. Ferreira, J. Almeida, A. Guedes, V. Chu, J. P. Conde, V. Martins, L. Fonseca, J. S. Cabral, J. Germano, L. Sousa, M. Piedade, B. Silva, J. M. Lemos, L. A. Clarke, M. D. Amaral, Symposium on *Scientific Research at the Technical University of Lisbon*, Lisboa, Portugal, 2 and 3 February, 2006.

**2006: "Biossensores magnetoresistivos e nanomarcadores magnéticos – Monitorização de microorganismos patogénicos em água"**, V. Martins, H. A. Ferreira, L. P. Fonseca, P. P. Freitas, and J. M. S. Cabral, Boletim de Biotecnologia, April 2006.

**2003: "Magnetoresistive biochips"**, P. P. Freitas, H. Ferreira, D. Graham, L. Clarke, M. Amaral, V. Martins, L. Fonseca, J. S. Cabral, Europhysics News, vol. **34** (6), November/December 2003.

## 10. Communications

10.1 Scientific communications

**2006: "The 6th European Conference on Magnetic Sensors and Actuators",** Bilbao, Spain, 3 - 5 July 2006. Invited oral presentation.

**2006: "Biosensors 2006 – The 9th World Congress on Biosensors",** Toronto, Canada, 10 - 12 May 2006. Poster presentation.

**2005: "The 50th Annual Conference on Magnetism and Magnetic Materials",** San Jose, California, U.S.A., 30 October - 3 de November 2005. Oral presentation.

**2005: "The IEEE 2005 International Magnetics Conference"**, Nagoya, Japan, 4 - 8 April 2005. Oral presentation.

**2004: "The 49th Annual Conference on Magnetism and Magnetic Materials",** Jacksonville, Florida, U.S.A., 7 - 11 November 2004. Oral and poster presentations.

**2004: "The 9th Joint MMM/Intermag Conference"**, Anaheim, California, U.S.A., 5 - 9 January 2004. Oral and poster presentations.

**2003: "The 17th European Conference on Solid-State Transducers"**, Guimarães, Portugal, 21 - 24 September 2003, Two oral presentations

**2003: "Bionanotechnology – Euroconference on Biomolecular Devices",** Granada, Spain, 9 - 14 de July 2003. Poster presentation.

**2003: "Bioeng'2003 – 7th Portuguese Conference on Biomedical Engineering",** Lisboa, Portugal, 26 - 27 June 2003. Oral and poster presentations.

**2003: "The IEEE 2003 International Magnetics Conference"**, Boston, Massachusetts, U.S.A., 28 March - 3 April 2003. Invited oral presentation.

**2002: "The 47th Annual Conference on Magnetism and Magnetic Materials",** Tampa, Florida, U.S.A., 11 - 15 November 2002.

**2002: "The IEEE 2002 International Magnetics Conference"**, Amsterdam, Holland, 28 April - 2 May 2002. Oral presentation.

**2001: "The 46th Annual Conference on Magnetism and Magnetic Materials",** Seattle, Washington, U.S.A., 12 - 16 November 2001. Oral presentation.

10.2 Entrepreneurship related communications

**2006:** Presentation of the entrepreneurial project **"MagBiosense"**. Scope: **"Colóquio – Valorização Económica da Ciência"**, within **"I Feira do Conhecimento e da Inovação"**. Organization: Universidade Técnica de Lisboa and Associação Industrial Portuguesa. Centro de Congressos de Lisboa, Lisboa, 29 March 2006.

**2006:** Presentation of the entrepreneurial project **"MagBiosense"**. Scope: delegates from the **IC$^2$ Institute** and from the **University of Texas at Austin**. Organization: Centre for Innovation, Technology and Policy Research (IN+) of IST. Instituto Superior Técnico, Lisboa, 23 March 2006.

**2005:** Presentation of the entrepreneurial project **"MagBiosense"**. Scope: "**Concurso de Ideias do Programa Avançado em Empreendedorismo e Gestão da Inovação (PAEGI)"**. Organization: Faculdade de Ciências Económicas e Empresariais of the Universidade Católica Portuguesa (FCEE-UCP). FCEE-UCP, Lisboa, 28 July 2005.

**2005:** Presentation of the entrepreneurial project **"MagBiosense"**. Scope: "**Concurso Nacional de Empreendedorismo 2005"**. Organization: Caixa Geral de Depósitos and Universidade Nova de Lisboa. Culturgest, Lisboa, 7 July 2005.

**2005:** Presentation of the entrepreneurial project **"MagBiosense"**. Scope: **"Dia do Empresário – Dia Europeu do Empreendedor"**. Organization: Associação Industrial Portuguesa (AIP), Lispolis, Ambelis and Câmara Municipal de Lisboa. Centro de Congressos de Lisboa, Lisboa, 29 June 2005.

**2005:** Presentation of the entrepreneurial project **"MagBiosense"**. Scope: **"VIII Jornadas Tecnológicas de Engenharia Química 2005 – Inovação e Competitividade em Engenharia"**. Organization: Students of the 4th year of Engenharia Química of the Faculdade de Ciência e Tecnologia, Universidade Nova de Lisboa. Grande Auditório da FCT-UNL, Monte da Caparica, 11 and 12 April 2005.

**2005:** Presentation of the entrepreneurial project **"MagBiosense"**. Scope: partners of the **Atlantic Network for Business Innovation and Technology Transfer (Atlantech)**. Organization: Centro Promotor de Inovação e Negócios (CPIN) and IN+. Instituto Superior Técnico, Lisboa, 7 March 2005.

**2004:** Presentation of the entrepreneurial project **"MagBiosense"**. Scope: **Vector$^{E}$** Course 2004 Edition. Organization: IN+. Instituto Superior Técnico, Lisboa, 21 December 2004.

10.3 Seminars

**2006: "Magnetic Biochips: from hard-disk drives to biosensing devices"**, Centro de Engenharia Química e Biológica, Instituto Superior Técnico, 7 March 2006.

**2005: "Magnetoresistive Biochips and Biosensors"**, Microelectromechanical Systems (MEMS) course, Institute for Micro- and Nanotechnologies (MIC), Technical University of Denmark, Denmark, 13 October 2005.

10.4 Outreach and community service

**2006:** Divulging activity on **"Biosensores"** within the activity "Dialogues with nanoscientists" from the exposition "NanoDialogue", Pavilhão do Conhecimento – Ciência Viva, Lisboa, 8 April 2006.

## 11. Editorial Activity

**2006:** Session chair at the **"The 6$^{th}$ European Conference on Magnetic Sensors and Actuators",** Bilbao, Spain, 3 - 5 July 2006.

**2005:** Chair of the session on **"Biosensors and Bead Manipulation"** at the **"The 50$^{th}$ Annual Conference on Magnetism and Magnetic Materials",** San Jose, California, USA, 30 October - 3 November 2005.

**2005 – Present:** Member of the Editorial Board of the **Journal of Biomedical Nanotechnology**, American Scientific Publishers.

**2004 – Present:** Peer-review of scientific papers for **IEEE Transactions on Magnetics** and for **Sensors** journals within the scope of international scientific conferences.

## 12. Affiliations

**2005 – Present:** Student Member (sponsored) of the **American Association for the Advancement of Science** (AAAS).

**2005 – Present:** Student Founding Member of the **American Academy of Nanomedicine** (AANM).

**2002 – Present:** Student Member of the **Institute of Electrical and Electronics Engineers** (IEEE), including the Magnetics Society e and the Engineering in Medicine and Biology Society of the IEEE.

**2003 – Present:** Student Member of the **Sociedade Portuguesa de Biofísica**.

**1999 – 2000:** Student Member of the **Associação Portuguesa de Engenheiros Físicos**.

## 13. Relevant Works done during the Academic Education

13.1 Doctoral curricular program and works done

**Biomolecular Engineering.** Teachers: Prof.s Álvaro Tavares, Miguel Prazeres and Gabriel Monteiro. Essay: **"Rotary Molecular Motors: $F_1$ – ATPase"**.

**Functional Genomics and Bioinformatics.** Teacher: Prof.ª Isabel Sá-Correia. Essay: **"Proteomic analysis of the response of *Saccharomyces cerevisiae* to 2,4-dichloro-phenoxyacetic acid in the latency and exponential growth phases"**.

**Nanotechnologies.** Teacher: Prof. João Pedro Conde. Presentations: **"Molecular Logic"** and **"Biomimetic Nanoscale Reactors and Networks"**.

**Nanoelectronics.** Teacher: Prof. Paulo Freitas. Presentations: **"Single Electron Devices"** and **"Tactile Sensors"**.

**Enzymatic Technology.** Teacher: Prof. Joaquim Sampaio Cabral. Essay: **"Essay on microbioreactors: a miniaturized packed bed reactor"**.

13.2 Senior student project

**2001: "Application of Magnetic Recording Technology in New Biochip Development".** Scope: Design and fabrication of a device for transport and detection of magnetic nanoparticles for biological applications. Research Institute: Solid State Technology Group of INESC. Supervisor: Prof. Paulo Freitas.

13.3 Works done during undergraduate studies

**2000: "Nano-magnetic particles"**. Scope: concept and design of a device for the detection of magnetic nanoparticles. Course: Microtecnologies. Teacher: Prof. Paulo Freitas.

**2000: "Introduction to Nuclear Magnetic Resonance"**. Course: Nuclear Physics. Teacher: Prof.ª Lídia Ferreira.

**2000: "Electroencephalography – Study to Epilepsy"**. Course: Biophysics. Teacher: Prof. Eduardo Ducla Soares.

**2000: "3D Mouse"**. Course: Data Acquisition Systems. Teachers: Prof.s Pedro Brogueira e Luís Melo.

## 14. Extracurricular Activities

**2004 – Present:** Director of the Associação de Estudantes Graduados do Instituto Superior Técnico (AEGIST).

**1998 – 2001:** Delegate of Year Class of Licenciatura em Engenharia Física Tecnológica (LEFT).

**1998 – 2000:** Sub-Delegate of LEFT.

**1999 – 2000:** Effective member of the Pedagogic Council of IST

**2000:** Collaborator in the project **"Optimization of courses in Licenciatura em Engenharia Física Tecnológica"**. Project done with the support from the Serviço de Apoio Pedagógico of IST.

**1999 – 2000:** Fresh Student Mentor of LEFT

**1999:** Collaborator in the organization team of **"11ª Jobshop de Engenharia"**, promoted by the Associação de Estudantes do Instituto Superior Técnico (AEIST), 22 to 26 March 1999.

**1998 – 1999:** Collaborator of the Secção de Informação of Núcleo de Física do Instituto Superior Técnico (NFIST).

**1998:** Collaborator in the **"IIIª Semana da Física"** organized by NFIST.

**1998 – 2004:** Tutoring service on Maths, Physics, and Chemistry to high-school and college students.

## 15. Other Activities

**Musical Education:** 2nd degree in Classical Guitar, 5th degree in Musical Education, and choral practice in Escola de Música de Nossa Senhora do Cabo

**Sports:** Practice of swimming, gymnastics and Judo (**1º Dan**) in Sport Algés e Dafundo.

## 16. Languages (conversation, reading and writing)

**English:** highly skilled in conversation, reading and writing

**French:** medium skilled in conversation and reading, basic skilled in writing

**Spanish:** medium skilled in conversation and reading, basic skilled in writing

**Portuguese (native):** highly skilled in conversation, reading and writing

## 17. Programming Languages

**C/ C++:** medium skilled

**Basic:** medium skilled

**Mathematica:** medium skilled

**IDL:** medium skilled

## 18. Interests

Entrepreneurship

Management of Science and Technology

Microsystems and Nanotechnologies / Nanobiotechnology and Nanobiomedicine

Biophysics and Biomedical Engineering

Science in general

Traveling

Meet new people and new cultures

Architecture

Sports

"**W**hat I want to talk about is the problem of manipulating and controlling things on a small scale.

**A**s soon as I mention this, people tell me about miniaturization, and how far it has progressed today. They tell me about electric motors that are the size of the nail on your small finger. And there is a device on the market, they tell me, by which you can write the Lord's Prayer on the head of a pin. But that's nothing; that's the most primitive, halting step in the direction I intend to discuss. It is a staggeringly small world that is below. In the year 2000, when they look back at this age, they will wonder why it was not until the year 1960 that anybody began seriously to move in this direction."

(***Richard P. Feynman****, excerpt of the talk* ***"There's Plenty of Room at the Bottom"*** *gave on the 29th of December of 1959 at the annual meeting of the American Physical Society at the California Institute of Technology*)